Search for tachyons in cosmic rays at sea level

Hussein Farrashbashi Masdjed

SEARCH FOR TACHYONS IN COSMIC RAYS AT SEA LEVEL

by

Hussein Farrashbashi Masdjed, B.Sc. (Mashhad)

A thesis submitted to the University of Durham
for the degree of Doctor of Philosophy

Department of Physics,
Durham University, U.K.

MAY, 1986

TO MY MOTHER AND LATE FATHER

"Cosmic ray research has advanced our understanding of fundamental problems on physics, when concepts previously used are shown to have a limited range of applicability. Since cosmic rays contain information on the behaviour of matter in the smallest (elementary particles) and largest dimensions (the universe), they have been particularly valuable in testing the concepts of daily life in relation to their meaning in physics and in leading physicists to find new ones."

by

W.Heisenberg

At the opening of the 14th International Cosmic Ray Conference in Munich (1975)

"The conclusion we draw is not that it is impossible for superluminal particles to exist but that, if they were found and meaningfully identified as such, the consequences for physics would be far-reaching. Either relativity theory or basic rules of quantum mechanics would have to go by the board, or else some very fundamental assumptions of the essential controllability of events would have to be abandoned."

by

R.G.Newton

Science, Volume 167, 1970

CONTENTS

ABSTRACT

Since the advent of relativity theory, many speculations have been made as to whether any objects (tachyons) exist which travel with a velocity greater than that of light. In any method of experiment to detect tachyons, some initial assumptions concerning the properties of tachyons have to be postulated. Cosmic ray experiments can make a useful contribution to the problem since many elementry particles have been discovered in the cosmic radiation. Plastic scintillation counters are a convenient technique to use in such experiments due to their very short resolving time and the simplicity of technique. A concise discussion of the fundamental properties of scintillation counters is given in chapter three.

The design and performance of a prototype plastic scintillation counter of dimensions 80cm·50cm·5cm is described in chapter four. The response of the counter developed is such that it can give a single particle peak well resolved from the noise (thermionic electrons) when its response to the global cosmic radiation flux is displayed on a pulse height analyser. Two such scintillation counters of this type were employed as local electron density detectors to register the arrival of extensive air showers (E.A.S) in a tachyon search experiment as described in chapter five. The tachyon search experiment (chapter six) showed no conclusive evidence that tachyons are associated with extensive air showers of local electron density $\rangle 25\ m^{-2}$ at sea-level.

However , a significant flux of low energy ionising

events that arrive at sea level in the 235μsec period after the arrival of the main extensive air shower front were observed. These events are thought to be produced by low energy neutrons produced in the atmospheric hadron cascade which subsequently trail the relativistic particles as the cascade propagates through the atmosphere and are detected when they produce low energy knock on protons in the phosphor of the plastic scintillation counter.

PREFACE

This thesis describes the work performed by the author at Durham University while under the supervision of Dr.F.Ashton during the period 1979 to 1986.

During this time, the author developed a prototype plastic scintillation counter of dimensions 80cm × 50cm × 5cm of high efficiency. Subsequently nine such scintillation counters were constructed with the intention of eventually using them in other investigations. The main work carried out by the author was an experiment to search for evidence for tachyons associated with extensive air showers observed at sea-level. The experiment was operated for a period of 839.78 hours. Two scintillation counters of the type developed by the author were used as threshold electron density triggers to select extensive air showers. A further scintillation counter of dimensions 140cm × 75cm × 5cm of high efficiency was used as the tachyon detector. The author is solely responsible for calculations, analysis and interpretation of experimental data described in this thesis.

ACKNOWLEDGEMENTS

I would like to thank Professor B.H.Bransden and Professor A.W.Wolfendale for the provision of the facilities for this work and for their interest and support.

I am extremely grateful to my supervisor Dr.F.Ashton for his willing guidance , stimulating suggestions and invaluable help throughout the work.

Many members of Cosmic Ray Research Group are thanked for helpful discussions, in particular Dr.M.S.Darjazi and Mr.J.H.Madani for their friendly assistance.

The technical staff of the Physics Department, in particular Mr.K.Tindale , Mr.M.Lee , Mr.M.Davison and the late Mr.W.Leslie are thanked for their help.

The Durham Computing Unit is thanked for the provision of computing facilities as well as for advice at various times.

My thanks also are extended to Mrs.M.A.Chipchase and Miss.K.L.Gittins for their invaluable help in typing the captions and drawing the tables for this thesis.

Finally, I am extremely grateful to the members of my family, in particular to my mother, for their moral and financial support.

CHAPTER ONE

INTRODUCTION

1.1) HISTORICAL BACKGROUND

At the beginning of the present century, Elster and Geitel (1899) and, independently, Wilson (1901) suspected the existence of an ionizing extraneous radiation with strong penetration ability which affected ionization chambers operated at sea level and mountain altitudes. Gockel (1911) and Hess (1912) dispatched suitable ionization chambers up to a height of about 5Km and measured the variation of intensity of the unknown radiation as a function of altitude. Much later, in more precise experiments , it has been found that the intensity does not vary with altitude above about 50Km ($\simeq 1 g.cm^{-2}$) which corresponds quite closely to the primary intensity, with a small contribution from the albedo phenomena (see figure 1.1). Below 50Km the intensity increases rapidly to reach a maximum at an altitude of about 17.7Km and then falls off continuously down to sea level. Originally, it was concluded that the radiation came from outside the atmosphere and it was believed that the radiation consisted mostly of gamma rays. In the late 1920's after the advent of the Geiger-Muller counter, Bothe and

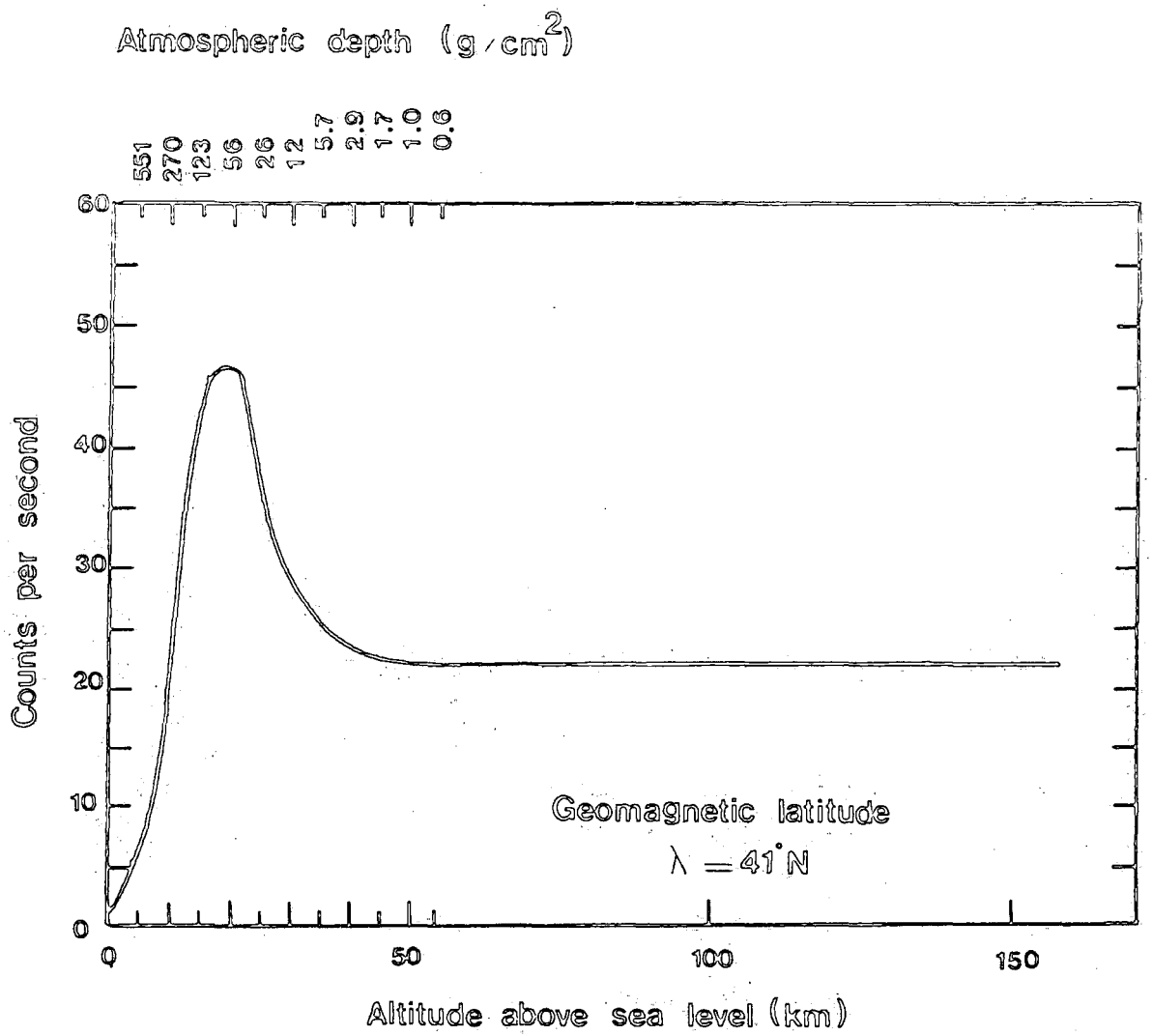

Figure 1.1 Variation of counting rate of single Geiger counter with altitude, after Van Allen et al. (1950).

Kolhorster (1928) were able to establish the corpuscular nature of the radiation. Compton (1933) found that the intensity of the radiation varied with geomagnetic latitude (λ in degree) and, consequently, it was presumed that at least some of the radiation coming near the earth are charged particles, figure 1.2. This phenomenon is called the geomagnetic latitude effect which indicates a lower intensity of radiation near the equator (i.e; $\lambda=0^{\circ}$) where the horizontal component of the earth's geomagnetic field is stronger. One of the significant subtleties in the geomagnetic latitude curve is the appearance of a knee which denotes the absence or a remarkable fall in the flux of low energy primaries. The position of the knee changes with time and this is connected with solar activity. The form of the variation of vertical intensity with geomagnetic latitude is very similar at all elevations. The magnitude of the geomagnetic latitude effect at sea level is only 14% while it changes directly in proportion to the height above sea level and becomes a factor of 10 at the top of the atmosphere. As the earth's magnetic centre is displaced from the true centre, an intensity variation along a line of constant geomagnetic latitude is observed. The magnitude of this longitude effect along the geomagnetic equator is about 4% and smaller variations are observed at higher latitudes. The fundamental relation concerning the trajectory of a charged particle (ze) and momentum p(eV/c) in a magnetic field of strength H(gauss) is:

$$\rho(\mathrm{cm}) = \frac{p.c}{300zeH} \qquad (1.1)$$

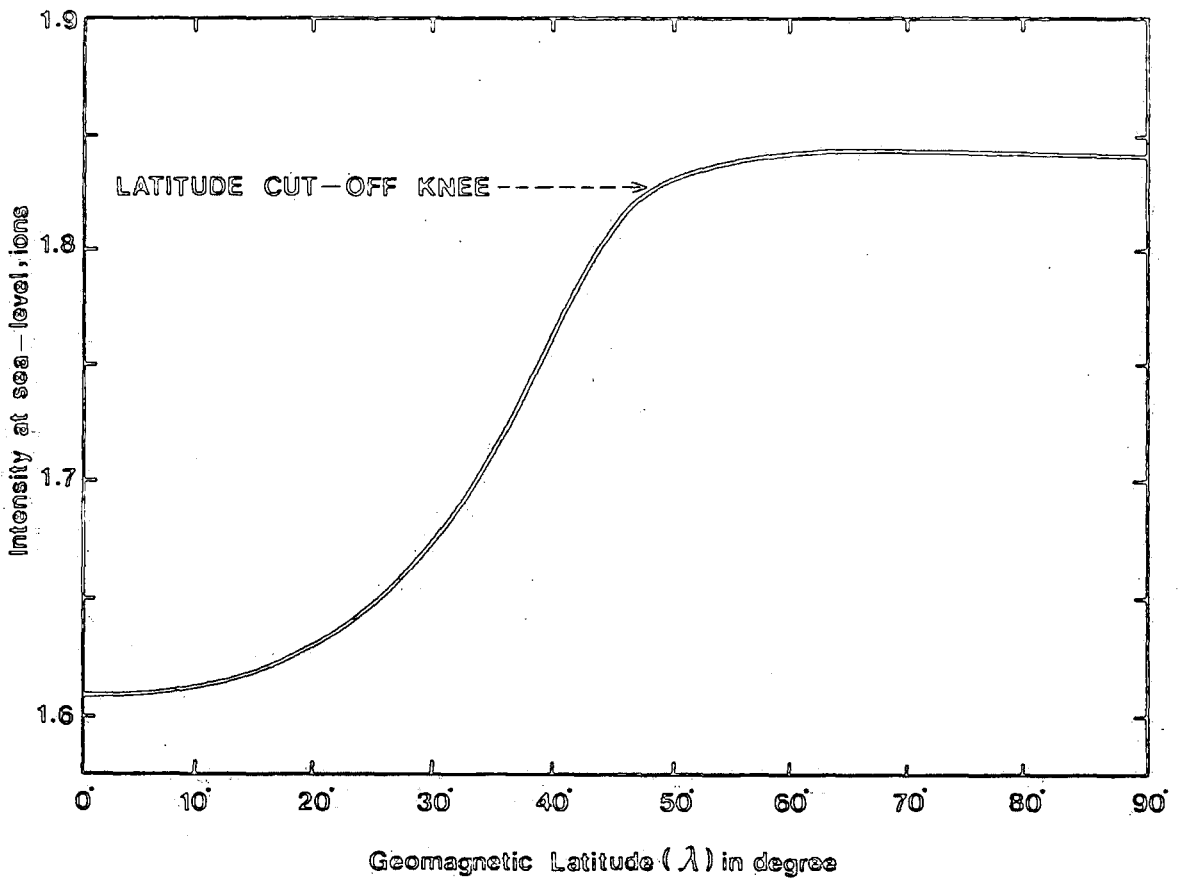

Figure 1.2 Variation of intensity with geomagnetic latitude at sea level, Compton (1933). The appearance of the latitude cut-off knee indicates the absence or serious reduction in the flux of low energy primaries, i.e. those primaries which would reach the high latitudes but not the lower latitudes.

where $\frac{p.c}{z.e}$ is the magnetic rigidity in volts. At a particular point on the earth's surface, solutions of the above equation have shown that there are allowed and forbidden directions of incidence for each magnetic rigidity considered. However, the results of calculations imply that the least permissible momentum of a charged particle (i.e; cut - off rigidity) at normal incidence on the atmosphere is a function of geomagnetic latitude. Clay (1927) and Johnson (1938) found that the intensity of the radiation arriving from the west was larger than that from the east. It was also revealed further that positively charged particles can arrive with smaller energy from the west than from the east and the reverse for negatively charged particles. This phenomenon is named the east – west effect (ϵ) and can be calculated as a function of zenith angle (θ). It was shown that ϵ increases with increasing altitude and decreasing latitude. Also, it increases with zenith angle up to around 60° (i.e; ϵ goes through a maximum value at $\theta = 60^{\circ}$), above which it falls off. Originally, it was supposed that the charged particles were electrons. Investigations were made using ionization chambers flown by means of balloons to the top of the atmosphere (Millikan and Bowen 1936). The results showed that the charged particles in the radiation were heavier than electrons and the protonic nature of the radiation was confirmed. The development of new instruments has produced visual evidence that the primary radiation contains nuclei heavier than protons , up to perhaps uranium (Fowler et al , 1967). The recent use of scintillation detectors made it

possible to measure electrons and positrons in the primary radiation which approximately constitute about 1% of the nucleonic component flux (Earl , 1961). Instruments sent in rockets led to the discovery of cosmic X-radiation (Giacconi et al, 1962) and cosmic gamma radiation (Kraushaar et al, 1968).

Essentially , the primary cosmic radiation consists of three components, nuclear (i.e; nuclei), electronic (i.e; electrons and positrons) and electromagnetic (i.e; X-rays and γ-rays). As a result of the interaction of the primary nucleonic component in the atmosphere, most of the elementary particles such as the positron and pion, which had been proposed by Dirac and Yukawa respectively, were detected. Thus, their properties were known before using accelerators to study them. The discovery of the strange particles (i.e; heavy mesons and hyperons), which were first observed in cosmic rays, led to the introduction of the quantum number of strangeness (S). These particles are produced in nuclear interactions and their number amounts to only a few percent compared with the number of pions produced. To study strange particles, cosmic ray experiments are best carried out as high as possible in the atmosphere where the flux of this component is relatively high.

1.2) CURRENT KNOWLEDGE CONCERNING COSMIC RAY FLUXES

The chemical composition of the primary cosmic rays with energy of a few GeV for elements with $Z<28$ is shown in figure 1.3. Also shown is the universal abundance of the elements determined from spectroscopic studies. The two sets of

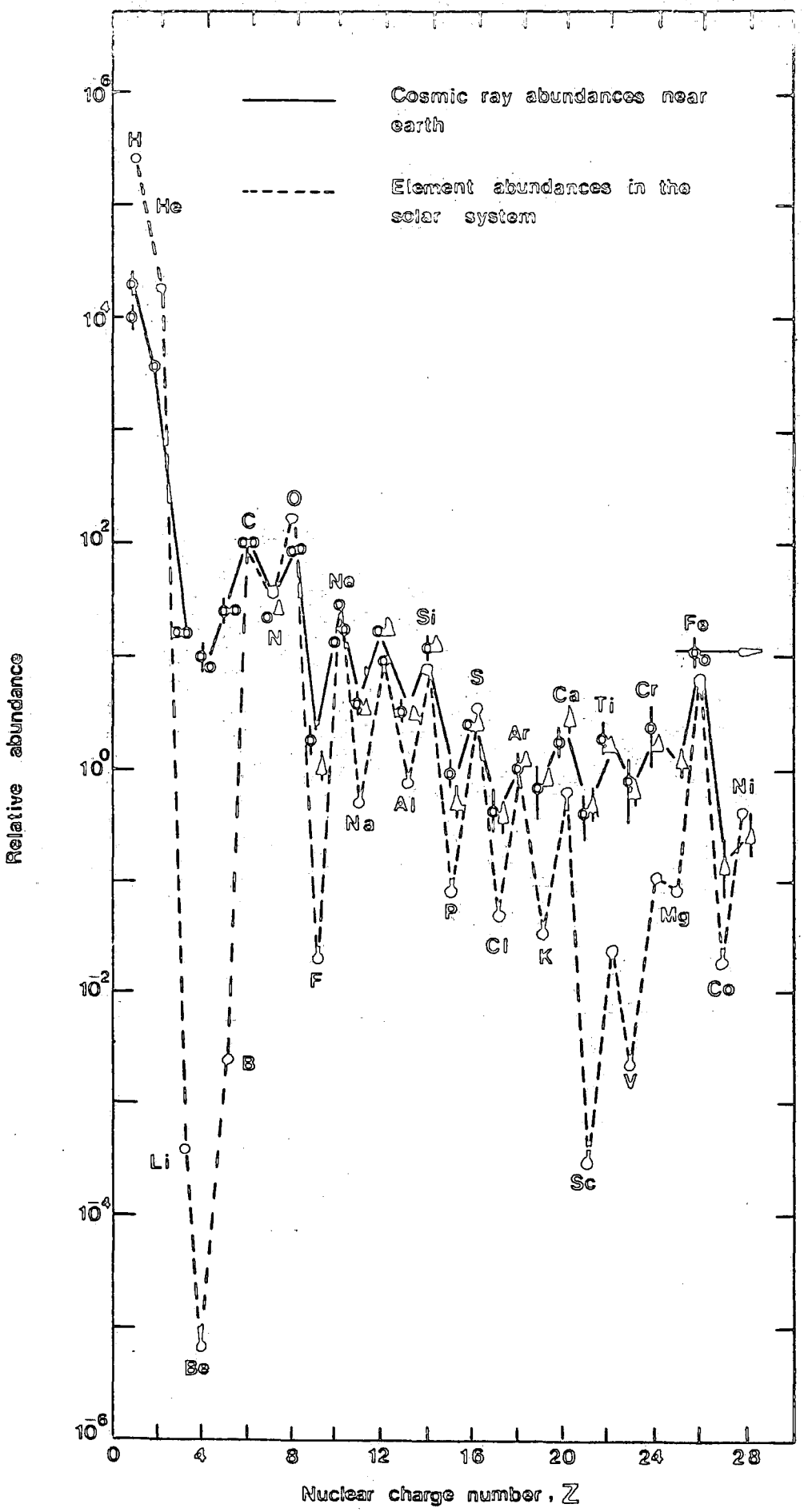

Figure 1.3 Relative abundance of the elements from Hydrogen to the iron group normalized to that of carbon (C = 100), (after Meyer et al. 1974).

abundances have been normalised to the same value for carbon. The main features of the data to be noted are:

(a) H and He are under abundant in cosmic rays compared to the universal abundance.

(b) Li, Be, B and Sc, V, Mg are over abundant in cosmic rays.

Case (a) can be understood in terms of the supernova origin of cosmic rays as, presumably, the blasted off shell of a supernova star will be rich in heavy elements relative to hydrogen and helium.

Case (b) can be understood in terms of the propogation of cosmic rays through the interstellar medium between their source and their arrival at the earth. The interstellar medium has a density of $\simeq 1$ hydrogen atom per cubic centimetre and nuclei heavier than Li , Be and B will interact with these atoms and undergo fragmentation to nuclei of Li , Be and B. In this way , even if the cosmic ray composition at the source has an abundance distribution similar to the universal abundance curve , then the dips in the universal abundance curve will be progressively more and more filled in as the cosmic ray path length in the galaxy increases. Using measured and calculated fragmentation cross sections for elements incident on protons , the mean path length traversed by cosmic rays through the interstellar medium is estimated to be $\simeq 4 g.cm^{-2}$ corresponding to a travel time of $\simeq 5.10^{6}$ years.

Table 1.1 summarises the information available on the energy dependence of the primary composition and it is seen

Atomic Number (Z)	Element	Primary kinetic energy per nucleus (eV)			
		10^{10}	10^{11}	10^{12}	10^{13}
1	Hydrogen	58 ± 5	47 ± 4	42 ± 6	24 ± 6
2	Helium	28 ± 3	25 ± 3	20 ± 3	15 ± 5
(3-5)	(Lithium-Boron) Light nuclei	1.2 ± 0.1	1.1 ± 0.1	0.6 ± 0.2	–
(6-8)	(Carbon-Oxygen) Medium nuclei	7.1 ± 0.4	12.2 ± 0.8	14 ± 2	–
(10-14)	(Neon-Silicon) Heavy nuclei	2.8 ± 0.2	6.7 ± 0.5	10 ± 1	–
(16-24)	(Sulphur-Chromium) very heavy nuclei	1.2 ± 0.2	3.6 ± 0.4	4 ± 1	–
(26-28)	(Iron-Nickel) Iron group nuclei	1.2 ± 0.2	4.5 ± 0.5	10 ± 2	24 ± 7
⩾30	(Zinc) very, very heavy nuclei		0.007±0.004		

Table 1.1 Composition of Cosmic Rays at different primary energies (after Juliusson, 1975).

that heavy nuclei of the iron group seem to be far more abundant at a primary energy of 10^{13} eV than at 10^{10} eV.

Figure 1.4 shows schematically the processes taking place between the production of primary cosmic rays at their source and their arrival at the top of the earth's atmosphere. Solar activity , with a cycle of 11 years, affects the primary cosmic ray intensity but only at energies less than 10 GeV. Hot conducting plasma ejected from the sun as the solar wind carries solar magnetic field lies with it as a frozen in field and it is this magnetic field that affects the primary cosmic rays.

Measurements of the primary cosmic ray energy spectrum now extend from $\simeq 10^{6}$ eV to $\simeq 10^{19}$ eV, figure 1.5. As shown in the figure, measurements at low energy have been made using satellites , geomagnetic effects and ballon born equipments. At energies $\gtrsim 10^{13}$ eV, the measurements are all indirect and come from studying extensive air showers (E.A.S) generated in the atmosphere by primary cosmic rays. Figures 1.6 , 1.7 and 1.8 show the estimates of the primary cosmic ray spectrum at high energies made by various authors.

On average, a high energy primary cosmic ray proton traverses a distance of $\simeq 80 g.cm^{-2}$ of air before making its first interaction at an altitude of $\simeq$ 20Km above sea level. In this interaction, the secondary particles produced are predominantly charged and neutral pions. The charged pions either go on and make a further interaction producing more pions or decay into muons which penetrate to sea level. The decay schemes of pions

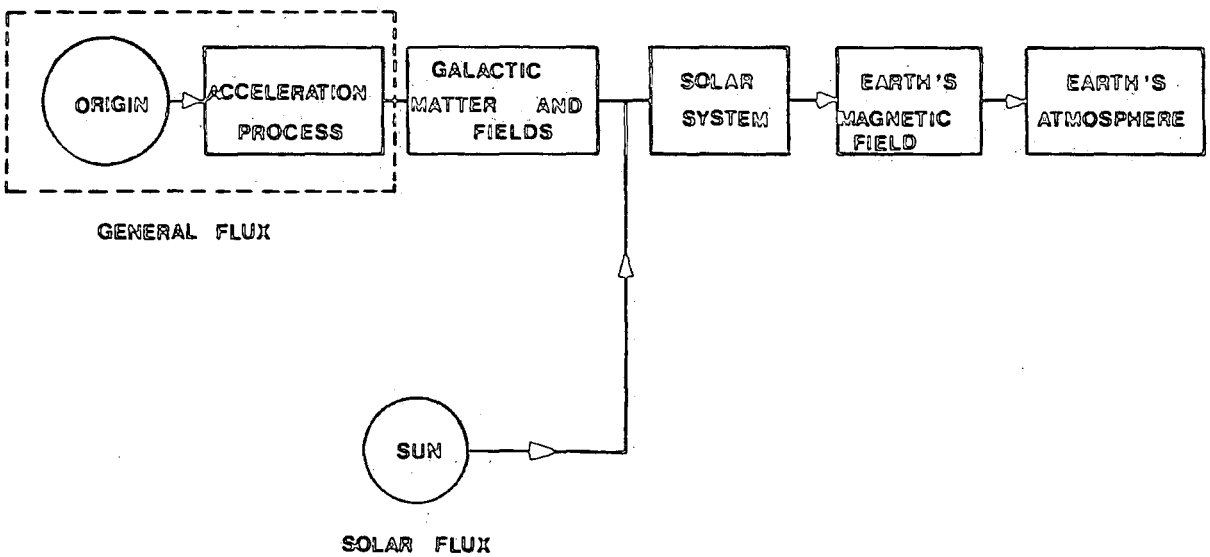

Figure 1.4 Life history of the primary Cosmic Rays. The acceleration process for the general Cosmic Rays may occur in the source itself or perhaps take place over a separate region of the Galaxy, so source and acceleration are bracketed together.

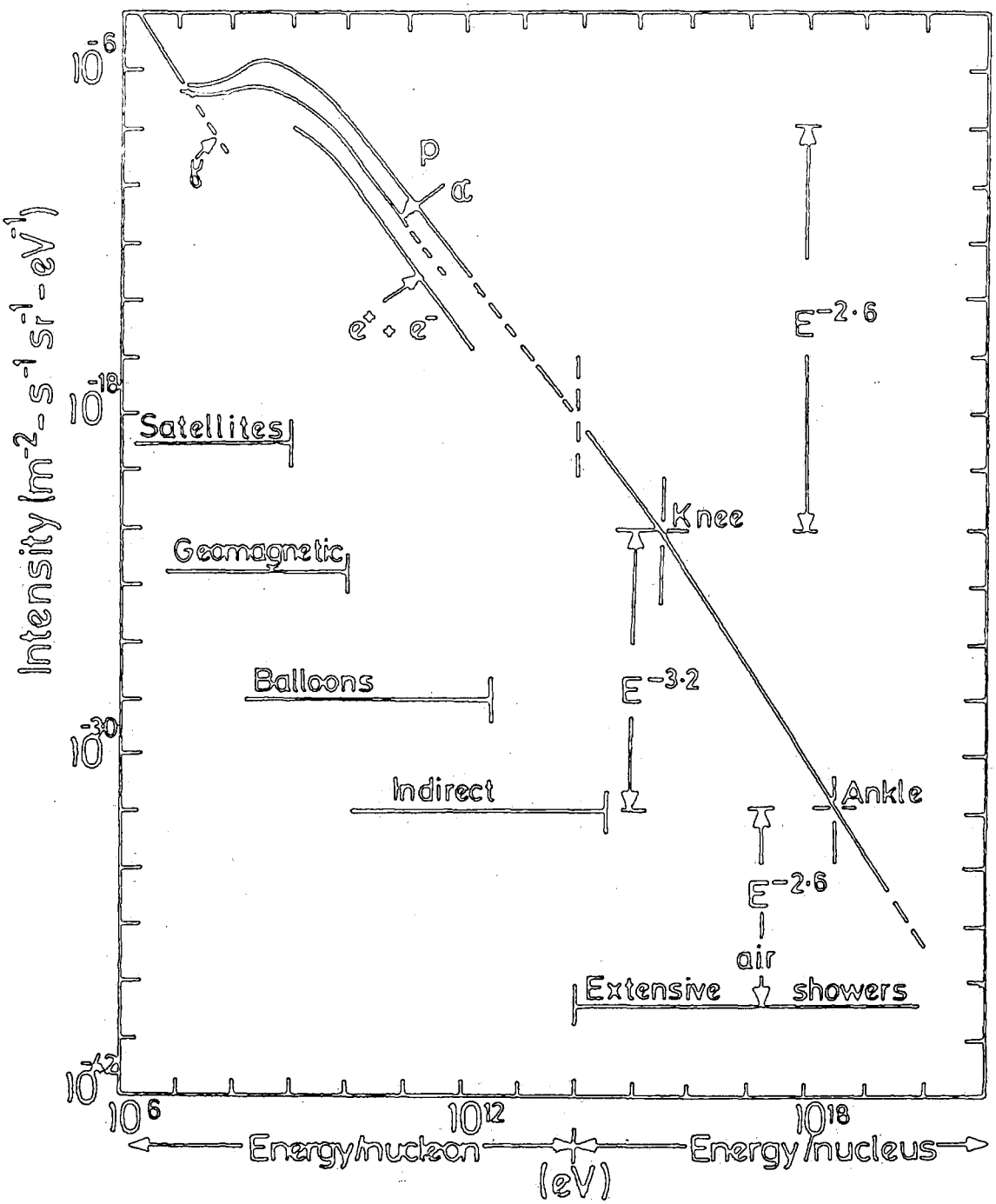

Figure 1.5 : Summary of measurements of the primary spectrum of protons and nuclei in the cosmic radiation (After Wolfendale, 1973).

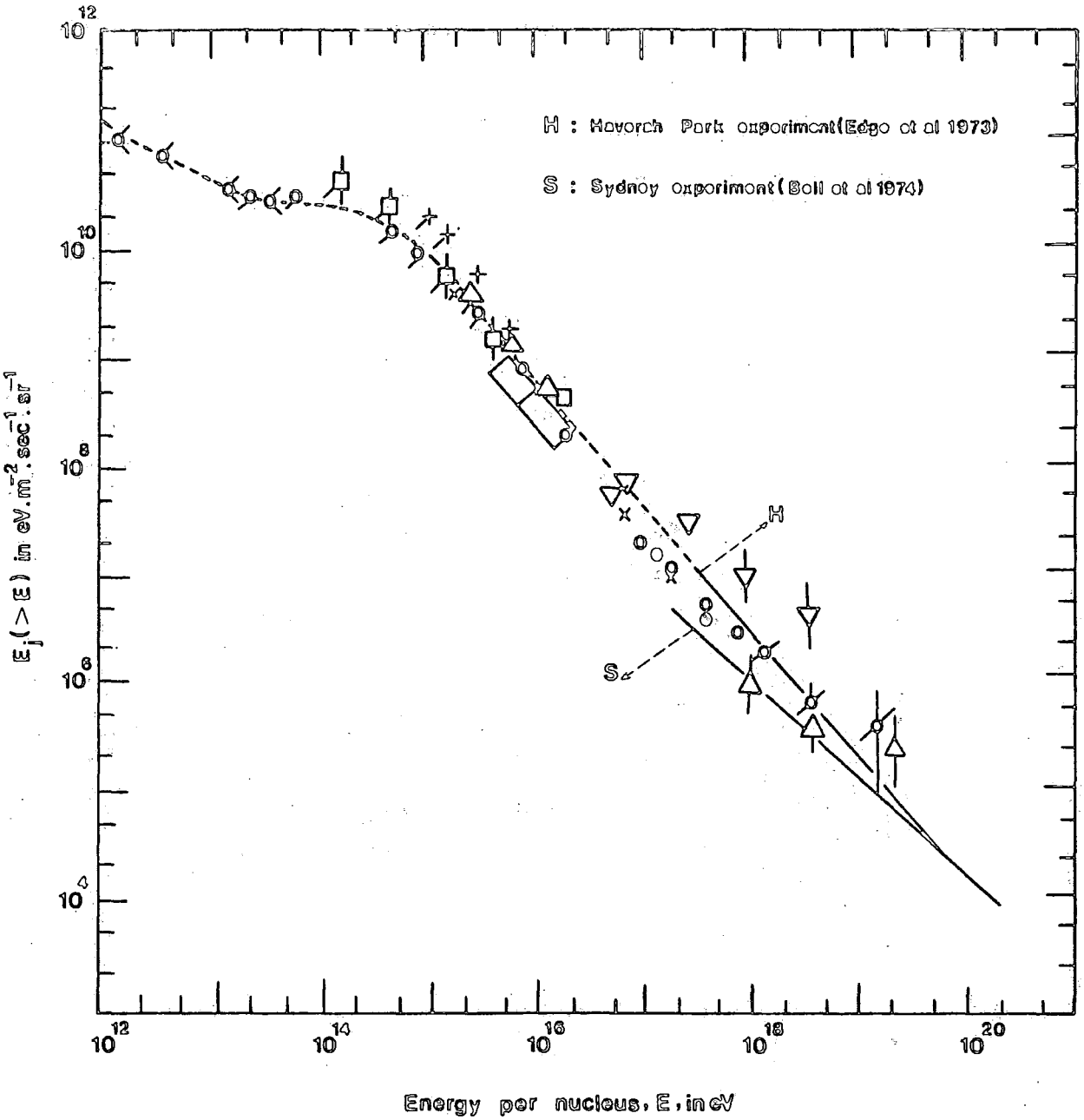

Figure 1.6 The integral primary Cosmic Ray spectrum, after Kempa et al. (1974).

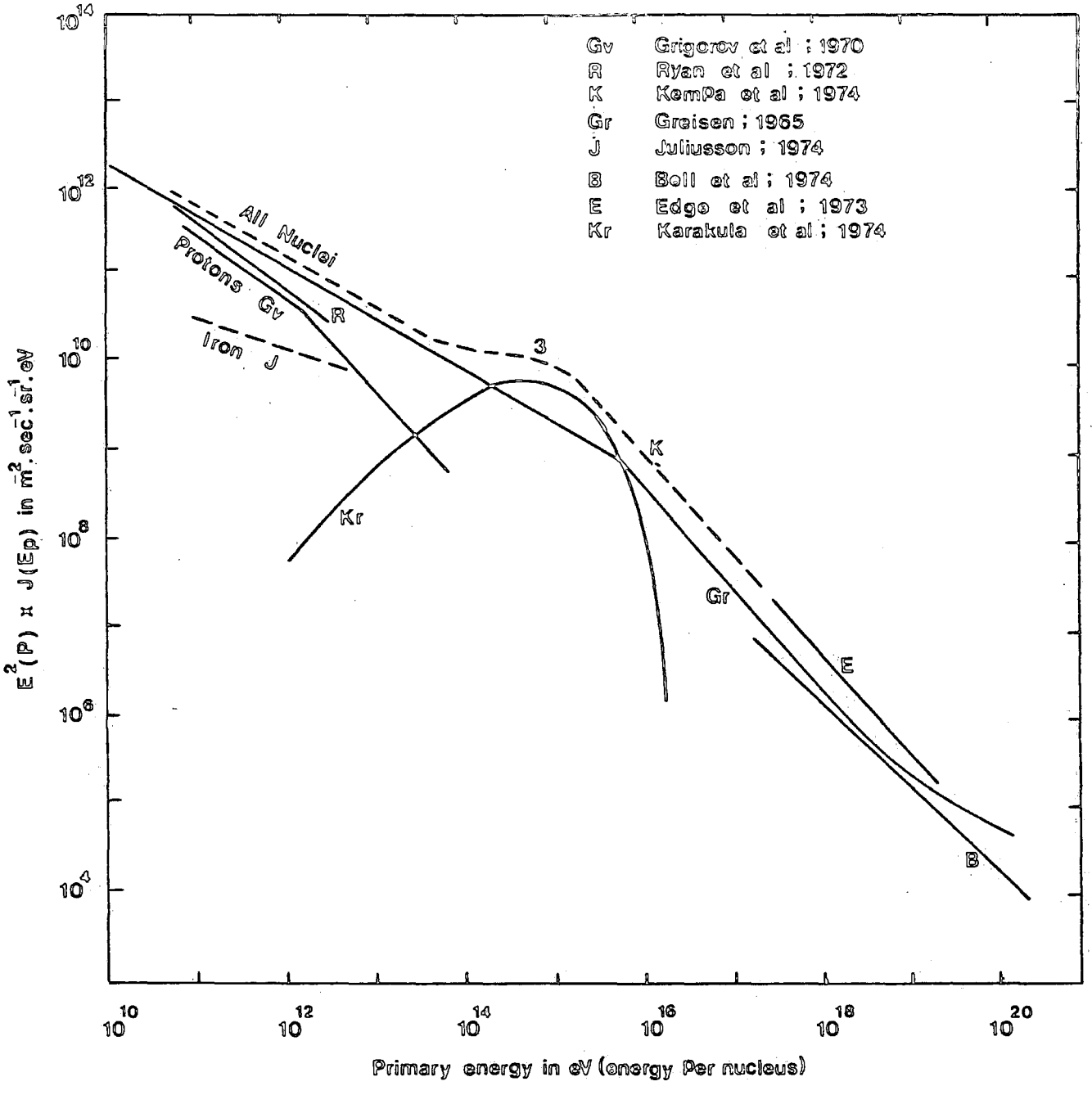

Figure 1.7 The differential energy spectrum of primary Cosmic Rays obtained from the results of various workers.

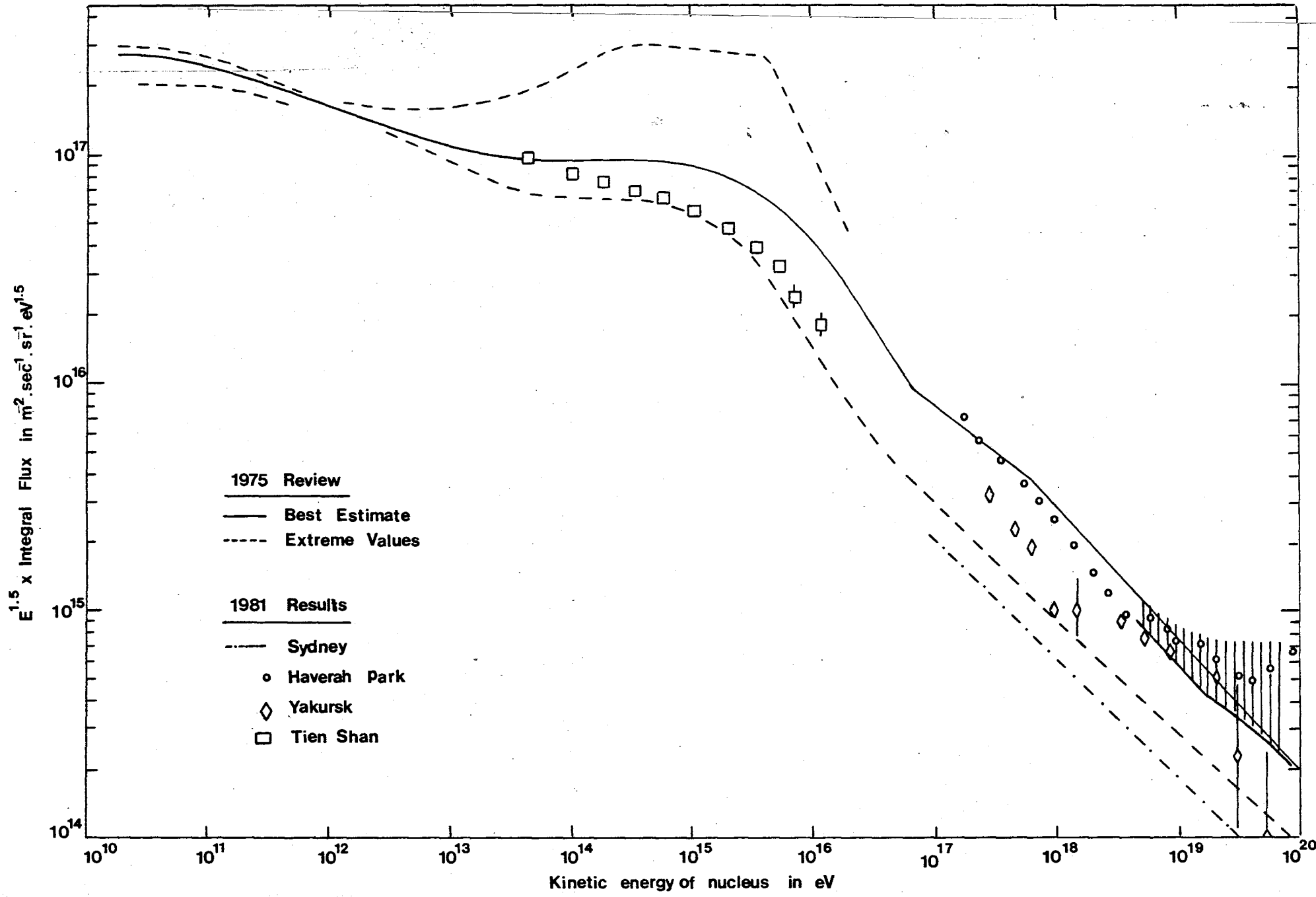

Figure 1.8 Integral energy spectrum of the primary radiation (after Hillas 1981).

and muons are shown below:

$$\pi^+ \longrightarrow \mu^+ + \nu_\mu \qquad \left.\right\} \quad \tau \simeq 1.8\times10^{-8}\ \text{sec} \qquad (1.2a)$$

$$\pi^- \longrightarrow \mu^- + \bar{\nu}_\mu \qquad \left.\right\} \qquad (1.2b)$$

$$\pi^0 \longrightarrow \gamma + \gamma \qquad \tau \simeq 10^{-16}\ \text{sec} \qquad (1.2c)$$

$$\mu^+ \longrightarrow e^+ + \nu_e + \bar{\nu}_\mu \qquad \left.\right\} \quad \tau \simeq 1.5\times10^{-6}\ \text{sec} \qquad (1.2d)$$

$$\mu^- \longrightarrow e^- + \bar{\nu}_e + \nu_\mu \qquad \left.\right\} \qquad (1.2e)$$

Because of their short lifetime, neutral pions immediately decay into two gamma rays which initiate electron-photon cascades via the processes of pair — production and bremsstrahlung in the atmosphere. Also, a primary cosmic ray nucleon only loses ≃ 50% of its energy in generating secondary particles, so that after making its first interaction, it continues to propagate through the atmosphere making a collision with an air nucleus, on average, every ≃ 80g.cm^{-2}. These processes are illustrated in figure 1.9. The result is that a primary nucleon of energy E (eV), on average, produces ≃ E/10^{10} particles at sea level consisting of 99% electrons and 1% muons with a smaller percentage of pions and other hadrons located mainly near the core of the shower.

For primary nucleons with energy $\lesssim 10^{12}$ eV, only their first few interactions are important in generating particles that subsequently penetrate to sea level and, on the whole, the electron — photon component produced via π^0 decay is absorbed in

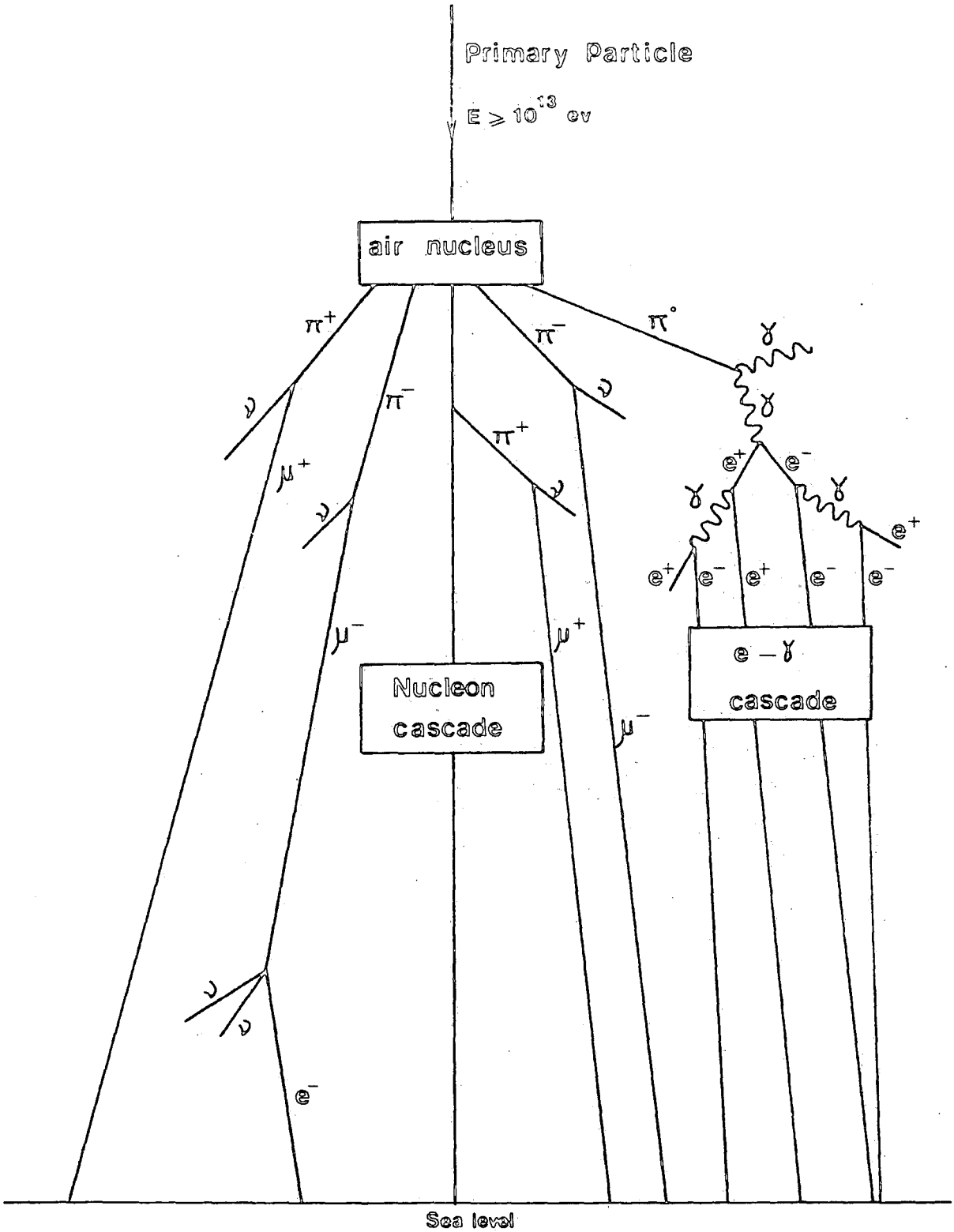

Figure 1.9 Development of an Extensive Air Shower

the high atmosphere and does not penetrate to sea level. Figures 1.10 and 1.11 show the measured muon spectrum and the energy variation of the μ^+/μ^- ratio for sea level energies up to 10^{12} eV and 10^{11} eV respectively produced in the above way. Finally, figure 1.12 shows the total flux of muons , electrons and protons measured in the atmosphere as a function of atmospheric depth. This figure refers to the total flux and the different components are produced by primary nucleons with energies down to ≃ 1 GeV and less. For comparison, the ionization loss of a relativistic particle traversing the whole of the atmosphere is ≃ 2 GeV while the threshold energy for nucleons to produce a single pion in a nucleon – nucleon collision is ≃ 300 MeV.

In the present work, the fact that cosmic rays contain higher energy particles than available from accelerators on earth is exploited. Currently, the 300GeV-300GeV $P\bar{P}$ collider at CERN is equivalent to primary nucleons of energy $1.8.10^{13}$ eV incident on nucleons at rest. Accordingly, a search has been made for tachyons associated with extensive air showers at sea level produced by primary nucleons of energy around 10^{15} eV. If they exist, tachyons are expected to be produced in nucleon – nucleon interactions via:

$$N + N \longrightarrow N + N + t + \bar{t} + \text{pions etc} \qquad (1.3)$$

Alternatively , tachyons could be present in the primary cosmic radiation itself having been produced in violent events

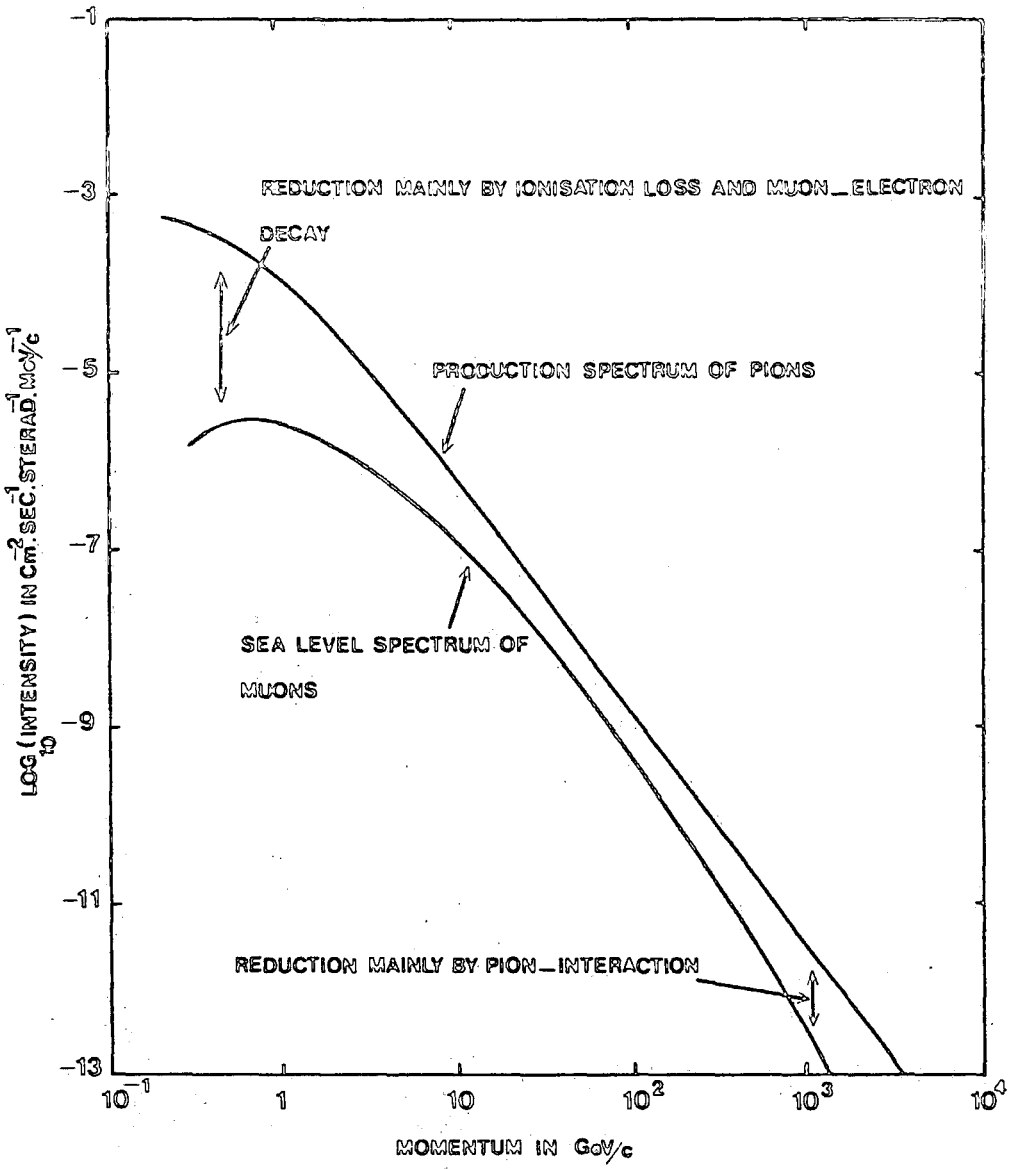

Figure 1.10 Comparison of the production spectrum of π-mesons and the subsequent sea level spectrum of μ-mesons, Wolfendale (1963).

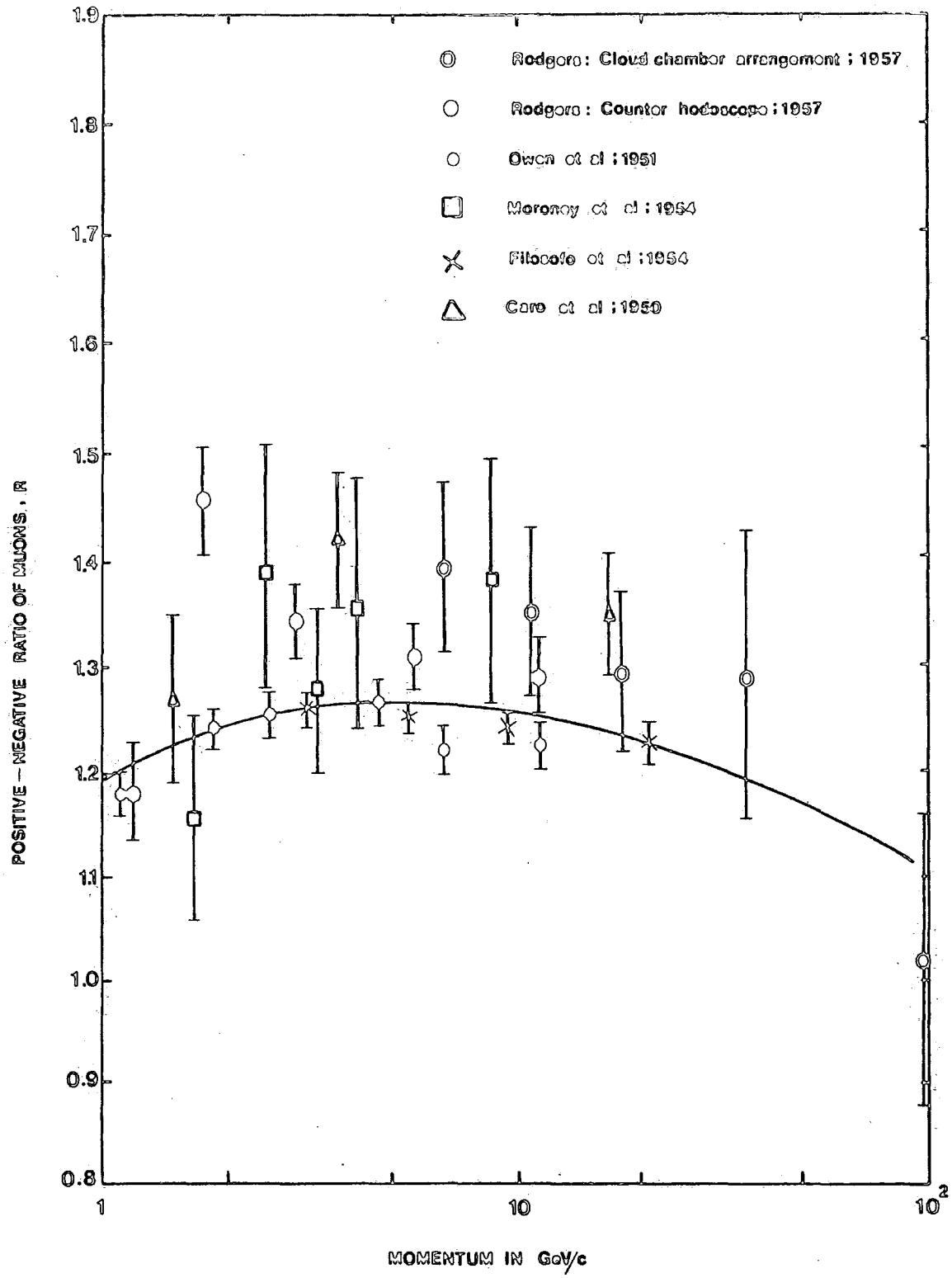

Figure 1.11 Variation of the positive-negative ratio of μ-mesons at sea level. The curve represents an attempt to draw the best smooth curve through the experimental points, Fowler et al. (1961).

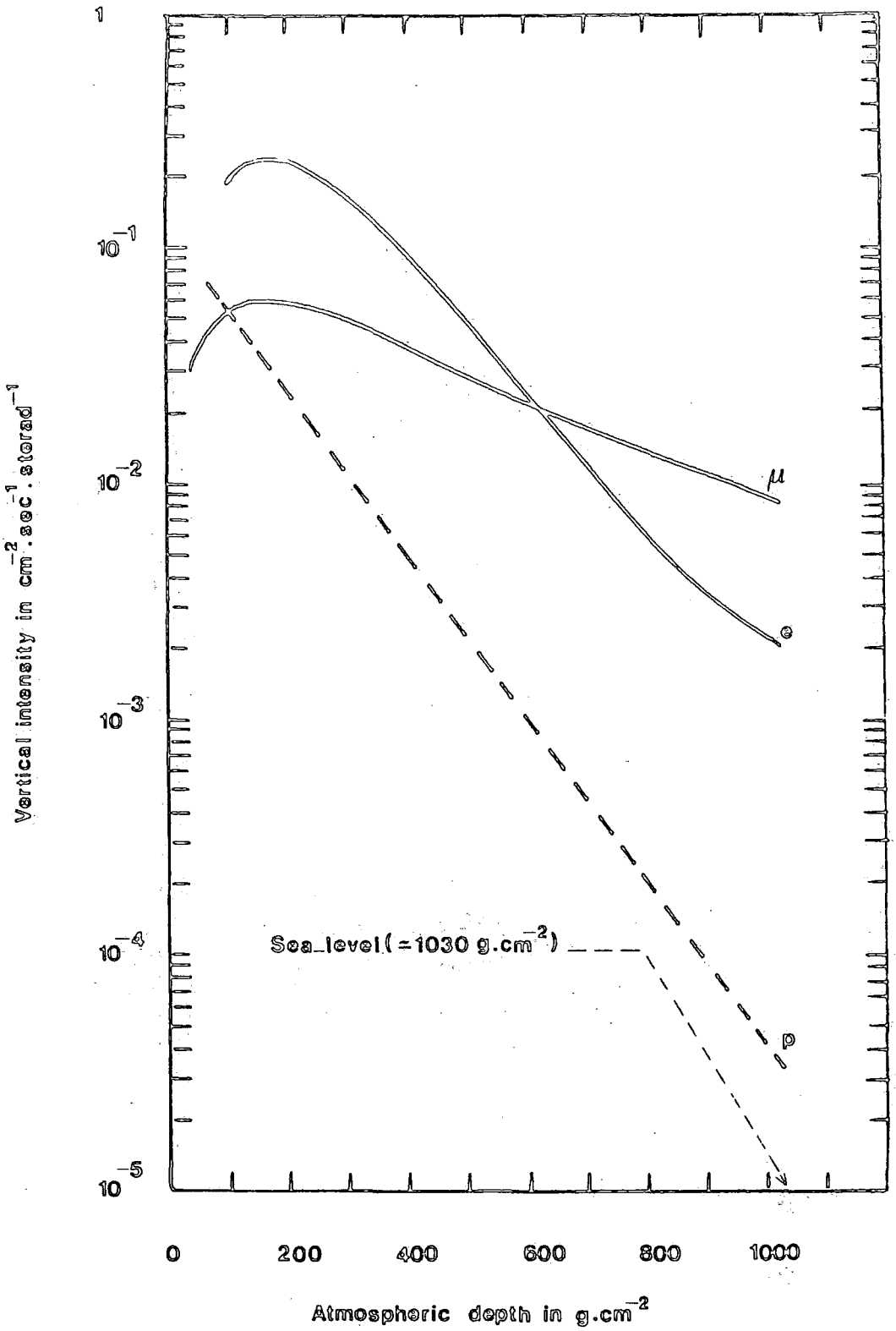

Figure 1.12 Vertical intensities of various Cosmic Ray components at 50^{o} geomagnetic latitude as functions of atmospheric depth, Rossi (1952).

occurring in our own or distant galaxies. In this case, they would be detected in the present work if they generated a shower of size $>10^4$ electrons at sea level as well as they themselves surviving to sea level.

CHAPTER TWO

THEORY OF TACHYONS

2.1) INTRODUCTION

The theory of relativity can be regarded as a continuation and completion of the ideas that have been the basis of our description of nature since the times of Galileo and Newton. Thus, the validity of relativity principle for the phenomena of mechanics is a magnificent consequence of the Newtonian laws of mechanics which prevents a unique determination of the absolute system of reference from studies of mechanical phenomena alone. According to the tenor of the special theory of relativity (i.e; relative motion between non-accelerated frames of reference), all physical phenomena should have the same course of development in all systems of interia and observers installed in different systems of interia should, as a result of their experiments , arrive at the establishment of the same laws of nature. Since the formulation of the special theory objections to superluminal particles have been based on the fact that superluminal particles can never be accelerated to velocities greater than the velocity of light in a vacuum , $c=3.10^{8}$ $m.sec^{-1}$. Bilaniuk , Deshpande and Surdarshan (1962) , Terletskii (1960) and Feldman (1974) proposed that although the relativity theory precluded acceleration of subluminal to superluminal velocities , nevertheless there was nothing in the theory which hindered the production of particles with always superluminal velocities. In other words;

the velocity of light does not represent a barrier but a limit approachable from below and above. Particles of these groups can only exist in their respective velocity domains and in any discussion, acceptability of them in the framework of relativity theory, should be debated.

2.2) SPECIAL RELATIVITY PRINCIPLES

Basically, the laws of nature rest on two postulates. Firstly, the principle of relativity and secondly, the principle of the constancy of the velocity of light. These two postulates can be expressed as follows:

(a) The laws by which the states of physical systems undergo change are not affected, whether these changes of state be referred to the one or the other of two systems of co-ordinates in uniform translatory motion. In other words; the laws of nature are the same for all frames of reference in uniform motion relative to each other.

(b) Any ray of light moves in the stationary system of co-ordinates with the determined velocity c, whether the ray be emitted by a stationary or by a moving body. In other words; the velocity of light is the same in all such frames (i.e; c is independent of the velocity of the source).

This theory contains several important consequences. First, the length of an object at rest in one frame of reference will appear to be contracted in another frame of reference. It implies that the spatial extent in the direction in which a moving reference frame is moving is always smaller in the moving reference frame than in a stationary reference frame. This

phenomenon is known as Lorentz-Fitzgerald contraction. The second consequence is the mass increase with increasing particle velocity. This leads directly to the equation $E=m.c^2$, where E is total energy associated with a mass m. Hence, mass is shown to be a form of energy and when it is demolished (e.g; in nuclear reactions) energy is evolved. Time dilation is another consequence of special relativity which means that if two observers are moving at constant velocity relative to each other, it will appear to each that the other's clocks have been slowed down. In fact, it indicates that the time intervals in a moving reference frame are always smaller than a stationary reference frame. However, the annexation of these consequences imply that no reference frame can be travelling at the speed of light and that temporal and spatial separations have the same sense in all reference frames moving at velocities less than the velocity of light. Relations between energy, momemtum and velocity of particles show that an infinite source of energy would be needed to speed up a particle to the velocity of light from any lower speed. However, no such infinite energy source is available. Besides, to accelerate a particle from a speed less than c to one greater than c, their total energy and momentum would have to be imaginary which has no physical meaning. Therefore, the velocity of light is a limit which may not be crossed. But this does not mean that particles that always travel faster than light could not exist because particles, already travelling faster than light, avoid the need for accelerating them through the light barriers with the attendant expenditure of infinite energy. For instance; photons

and neutrinos which may be created in atomic or nuclear processes, travel with a velocity always equal to the speed of light without ever being accelerated from a slower speed. In fact, there can be no frame of reference in which such particles are at rest. Thus, there are no slow photons or neutrinos.

2.3) BASIC PROPERTIES OF TACHYONS

2.3.1) ENERGY AND MOMENTUM OF TACHYONS

The relativistic expressions for the total energy and momentum of a particle of rest mass m_o and velocity $v<c$ are given as follows:

$$E = T + m_o c^2 = \gamma m_o c^2 \tag{2.1}$$

$$|p| = mv = \gamma m_o v \tag{2.2}$$

$$E^2 - p^2 c^2 = m_o^2 c^4 \tag{2.3}$$

$$\gamma = \frac{1}{(1 - v^2/c^2)^{\frac{1}{2}}} \tag{2.4}$$

where T is the kinetic energy of the particle. The total energy and momentum must be real equations. This is true for velocity less than c as the Lorentz factor (γ) is real and positive. It also holds for velocity equal to c provided that the rest mass of particles (e.g; photons , neutrinos) is set to zero. The above equations indicate that the rest mass of predicted particles travelling with a velocity more than c (known as tachyons) must be an imaginary quantity in order to allow the measurable quantities E and |p| to remain real. In this case, it is

conspicuous that the Lorentz factor is also imaginary. Thus;

$$m_o = i\mu_o \qquad \mu_o \text{ real} \tag{2.5}$$

where μ_o is known as the meta mass of the tachyon. Since tachyons cannot be brought to rest, therefore their rest mass being imaginary would not necessarily create a problem and any objection is invalid. But what is the meaning of an imaginary proper mass? The same can be said of the zero mass of a luxon (a particle that always moves with velocity of c). In both cases, it is impossible for us to travel in the same rest frame as the particle and measure its mass. Also, the proper time and proper length relating to a superluminal particle (i.e; particles moving with velocities greater than c), are imaginary. In the case of tachyons, as results of the above equations, one can write the following equations:

$$c^2p^2 - E^2 = \mu_o^2 c^4 \tag{2.6}$$

$$|p.c| > E \tag{2.7}$$

$$\frac{v}{c^2} = \frac{|p|}{E} > 1 \tag{2.8}$$

where the range of the total energy and momentum are given by:

$$0 \leqslant E \leqslant \infty \quad \text{and} \qquad \mu_o c \leqslant |p| \leqslant \infty \tag{2.9}$$

Hence, both the total energy and momentum (i.e; E and p) are monotonic decreasing functions of the velocity so that tachyons would accelerate as they lose energy. At infinite velocity (called the transcendental or liberty state), a tachyon carries no total energy E=0 but has a finite momentum $|p|=\mu_o c$. In fact, the

terms "at rest" (when p=0 , $E_o=m_oc^2$, v=0), "rest mass" and "rest energy" applied to ordinary particles are replaced by the suggestive analogous terms "at liberty" (when p= $\mu_o c$, E=0 , v=∞), "liberty mass" and "liberty momentum", respectively for tachyons. A plot of the total energy and momentum as a function of β (v/c) as shown in figures 2.1a and 2.1b can be a fascinating subtlety. Bradyons (i.e; ordinary particles moving with velocities less than c) are seen to exist only within the bounds of $-1<\beta<+1$ irrespective of the amount of energy supplied. The minimum energy occurs when the particle is at rest, $E_o=m_oc^2$. Therefore, for a subluminal particle (i.e; particles moving with velocities less than c), with non-zero mass the total energy can never vanish and as their speed increases, their energy also increases. For tachyons, conversely both energy and momentum are monotonic decreasing functions of the velocity, an increase in speed resulting in a decrease in energy. Thus, a tachyon that was losing energy by interaction with matter or by radiating light would speed up, whereas a tachyon that was gaining energy from some outside sources would slow down and its speed will approach c (but never reach this velocity), from above rather than below. So we expect most tachyons to be travelling at very high velocities if they have travelled through regions containing matter with which they could interact. It implies more likely that on production tachyons are travelling with very high velocities, since the production of fast tachyons requires less energy than the production of slow tachyons. The light barrier is a lower limit rather than the upper limit that it is for ordinary

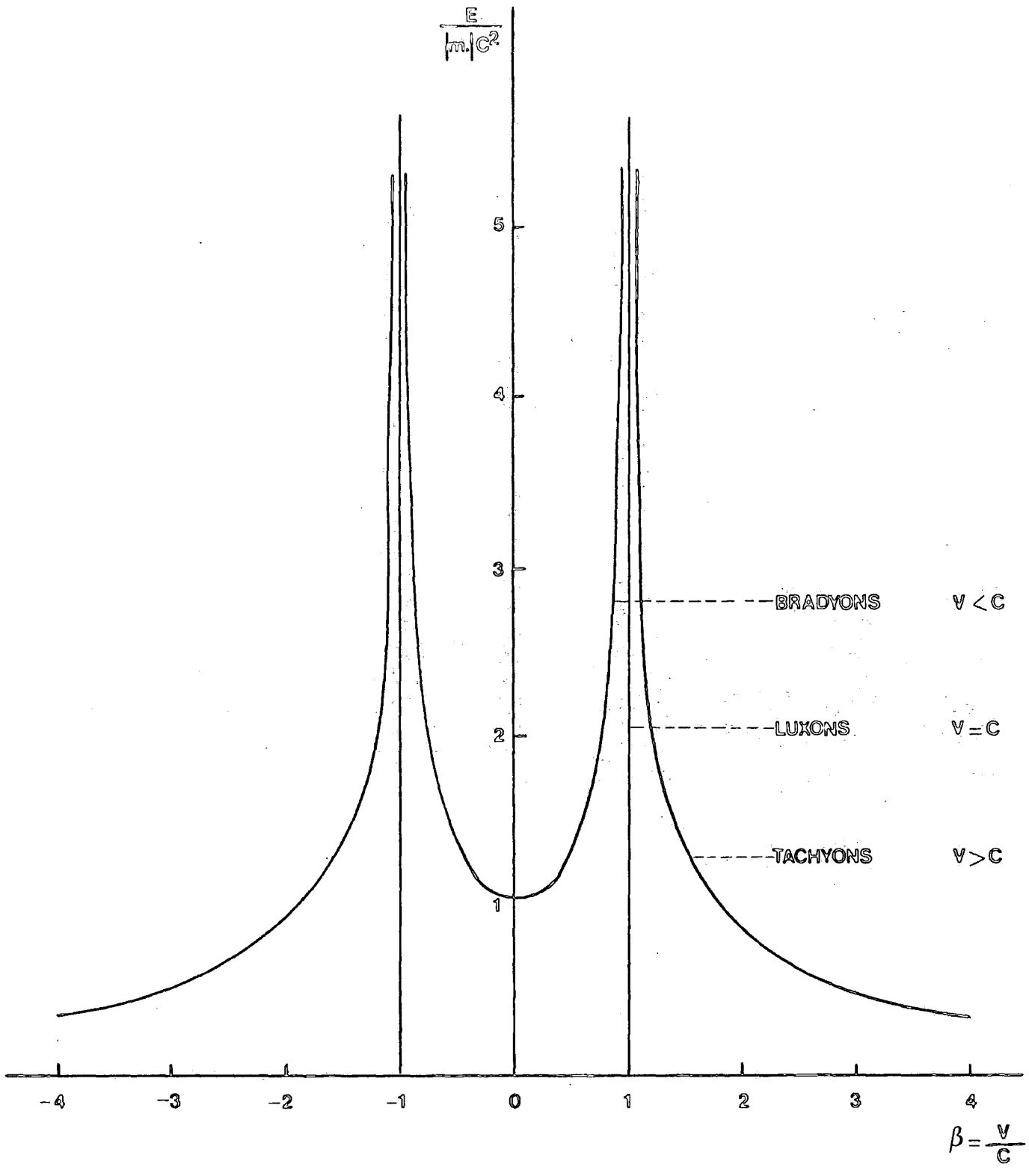

Figure 2.1a Relativistic Energy versus Velocity.

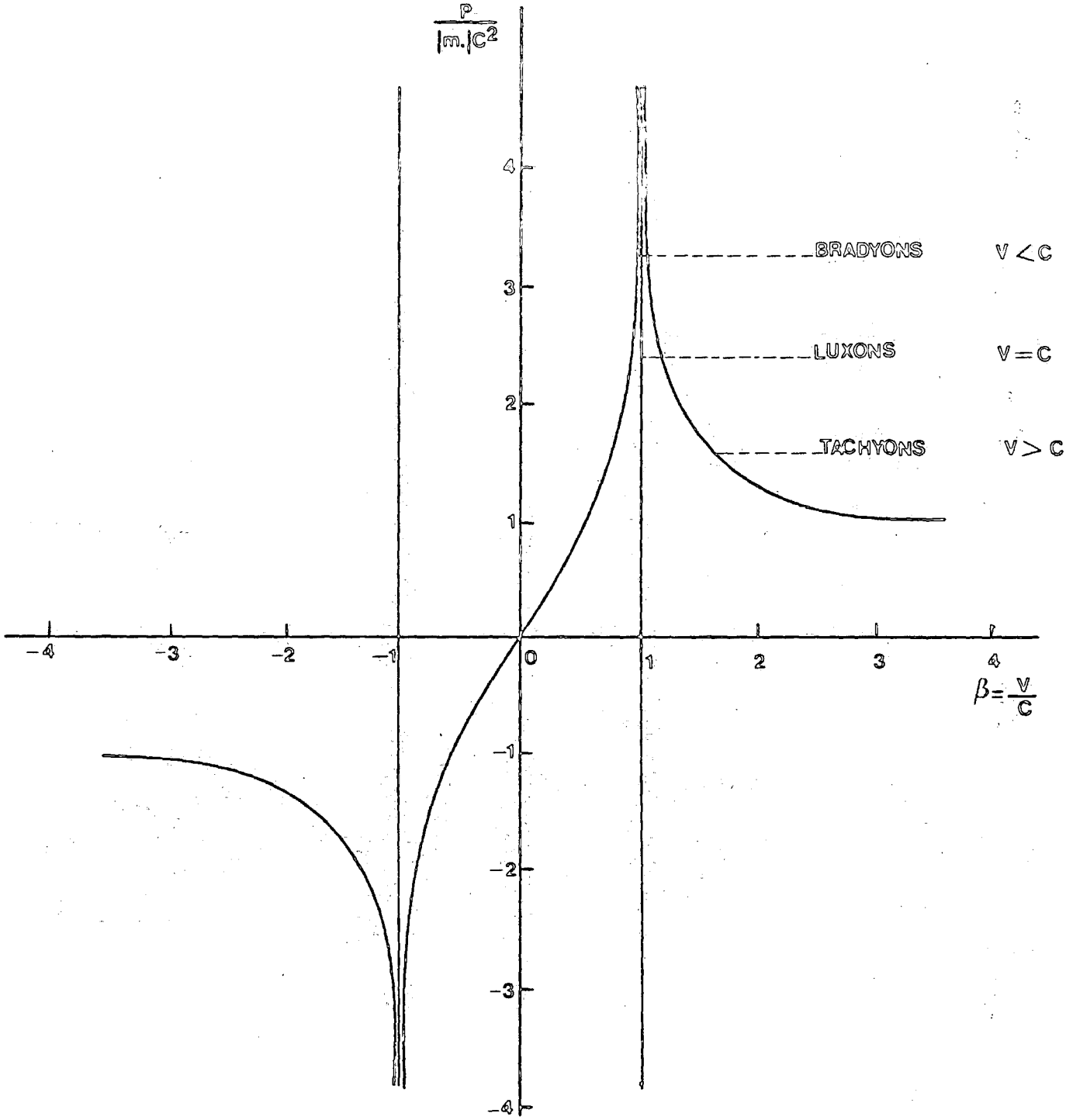

Figure 2.1b Relativistic Momentum versus Velocity.

particles. The minimum total energy for a tachyon will be zero when its velocity is infinite. As is illustrated in the above equations, the momentum of a transcendental tachyon is finite and equal to $\mu_o c$, compared to zero momentum for a bradyon. Spontaneous loss of energy by electrically charged tachyons, through radiation, gives rise to transcendental tachyons. Equation (2.7) shows that the total energy of tachyons is always less than its momentum multiplied by c which does not apply to ordinary particles. However, it is suggested that tachyons and bradyons are essentially different kinds of particle. Figure 2.1c shows the dependence of energy-momentum as a function of velocity β for the three classes of particle, bradyons, luxons and tachyons.

2.3.2) PAIR-PRODUCTION OF TACHYONS

It is strongly believed that faster than light particles are most probably created in pairs, Feinberg (1972). Since tachyons can exist with zero total energy and finite momentum, independent of rest mass m_o, it is not necessary for the available energy in a reaction to exceed twice the rest-mass energy E_o, as in the case for ordinary particles. Hence, they may be created spontaneously (i.e; with zero energy input) with any mass, but this process seems probably to be limited because the particles are supposed to obey Fermi-Dirac (fermions) statistics. In fact, one of the main objections to the possibility of particles travelling faster than light has been the fact that since the energy of a particle of non - zero mass approaches infinity as its velocity approaches the velocity of

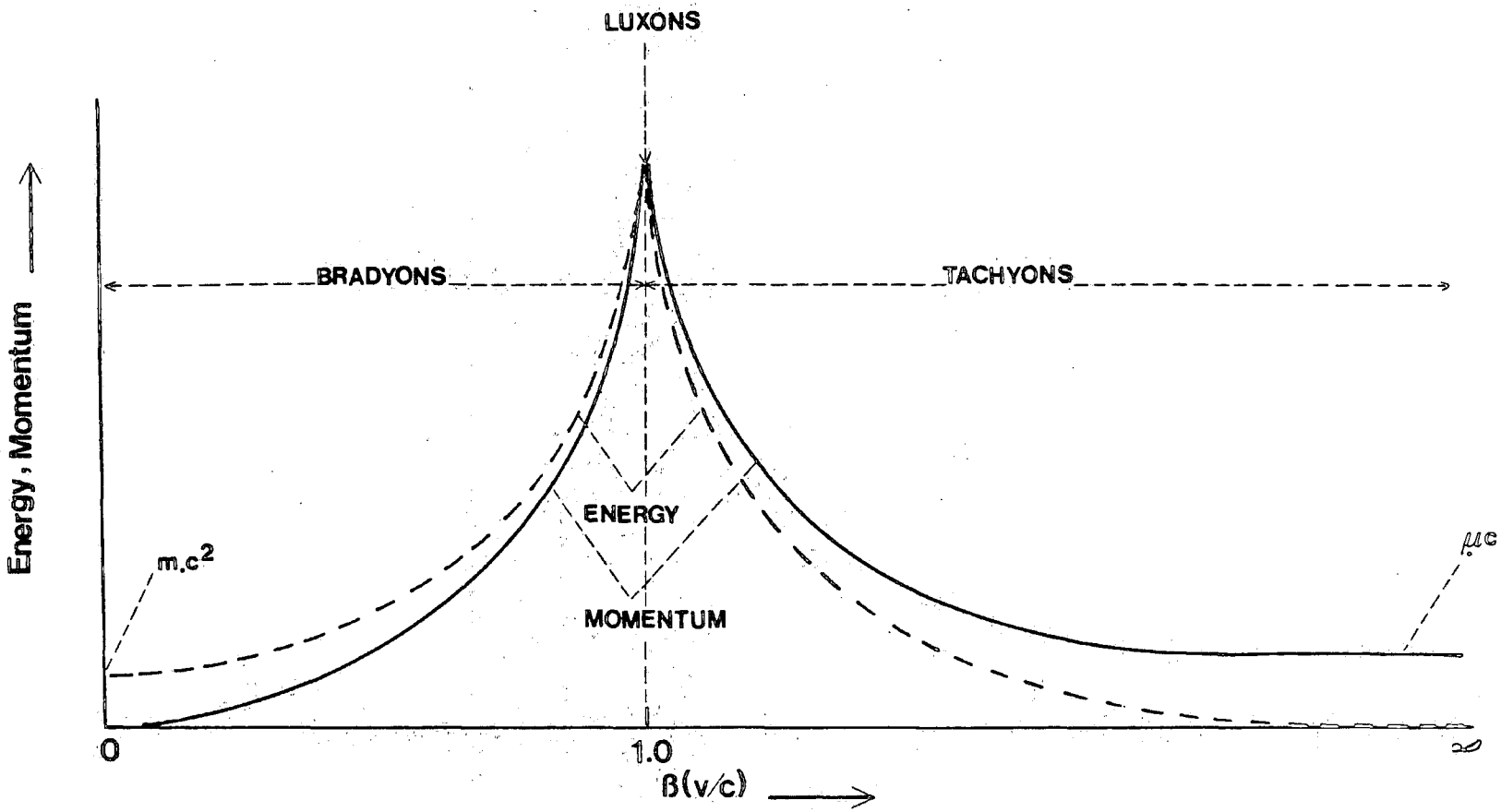

Figure 2.1c Energy momentum dependence as a function of velocity $\beta(v,c)$ for three classes of particles, where v is the velocity of the particle and c is the velocity of light ($c = 3 \times 10^8 m\ sec^{-1}$).

light, it would require an infinite energy source to accelerate such a particle through the light barrier. However, Feinberg (1967,1978) contemplated the possibility of describing, within the special theory of relativity, particles with velocities greater than that of light in vacuum and concluded that the usual objections to the existence of faster than light particles need not be valid in a relativistic quantum theory. He directs his attention to the description of tachyons by the formalism of relativistic quantum field theory, at least for the case of spinless, non - interacting particles. As a first step in finding a wave function to describe a tachyon, it is proposed the Klein-Gordon equation (K.G) with imaginary mass (i.e; $m=i\mu$) as the field equation of a free tachyon. The solutions to the Klein-Gordon equation with an imaginary mass have to be found:

$$(\Box^2 + \mu^2)\Phi(x,t) \equiv (\nabla^2 - \frac{\partial^2}{\partial t^2} + \mu^2)\Phi(x,t) = 0 \qquad (2.10)$$

The set of elementary solutions in one space dimension are:

$$\Phi_{+,k} = \frac{1}{(2\pi)^{3/2}} e^{i(kx - wt)} \qquad (2.11a)$$

$$\Phi_{-,k} = \frac{1}{(2\pi)^{3/2}} e^{-i(kx - wt)} \qquad (2.11b)$$

where

$$w \equiv +(k^2 - \mu^2)^{\frac{1}{2}}$$

For particles of momentum k, creation $a^{\dagger}(k)$ and annihilation a(k) operators are defined and are related to the sign of the energy. For the solutions to represent particles with real energy, a restriction which is $|k| < \mu$ must be imposed. It implies that tachyons cannot be localised in space. The classical field theoretical treatment leads to a quantum field theory of spinless tachyons by considering the field $\Phi(x,t)$ to be an operator. i.e; we expand $\Phi(x,t)$ by:

$$\Phi(x,t) = \int \frac{d^3k}{(2w_k)^{1/2}} \times \frac{1}{(2\pi)^{3/2}} e^{i(kx - wt)} a_k + \int \frac{d^3k}{(2w_k)^{1/2}} \times \frac{1}{(2\pi)^{3/2}} e^{-i(kx - wt)} a_k^{\dagger} \qquad (2.12)$$

in one space dimension

The concequences of investigations about the peculiar properties of the particles described by his formalism would not appear to involve any serious fundamental contradiction with accepted physical principles although they are quite different from those of ordinary particles. For Lorentz transformations that would geometrically change the sign of the energy, the creation operator for particles is changed into the annihilation operator for antiparticles and vice-versa. It is consistent with the comment that these transformations should interchange the roles of emission and absorption. However, the

discussion leads to the conclusion that spinless particles cannot be quantized by Bose-Einstein (bosons) statistics. Furthermore, considerations about the production and scattering process of tachyons introduce the following selection rules on the basis of energy and momentum conservation:

(a) Any system of normal particles (i.e; particles with velocities less than c) is not energetically stable against emission of tachyons. Thus, strong restrictions must exist on the interactions of tachyons in order to be consistent with the observed behaviour of ordinary particles.

(b) Tachyons can probably emit massless particles without changing their own mass which sometimes is called elastic decay. Namely;

$$t \longrightarrow t + \gamma \qquad (2.13)$$

where t represents a tachyon with a fixed value μ^2 and any energy. From this expression, it can be concluded that if the mass of tachyons is much smaller in absolute value than of the normal massive particles, elastic decays involving emission of these particles will be possible only for very energetic tachyons. Therefore, it is probably possible to postulate the emission of Cerenkov radiation by tachyons in a vacuum.

(c) Single tachyons can decay into several tachyons with the same value of μ^2 so that if the self-interaction is very weak there will be a rapid degradation of the energy spectrum of tachyons.

2.3.3) ELECTROMAGNETIC CERENKOV RADIATION (E.C.R)

Cerenkov radiation is the blueish light emitted by a beam of high-energy charged particles passing through a transparent medium with refraction index n, at a speed v that is greater than the velocity of light in that medium. The radiation represents the excess energy resulting from the difference in velocity of the charged particle and the velocity of its associated electric and magnetic fields which cannot exceed the velocity of light in the medium. In fact, electromagnetic Čerenkov radiation (E.C.R) is emitted by the electrons of the material medium, and not by the radiating particle itself. Also, it is a function of the velocity (and not of the acceleration, as is the case of usual electromagnetic radiation) of the particle.

It is suggested, Lemke (1975,1976), that a charged tachyon induces electromagnetic Čerenkov radiation in usual media only in frequency regions (e.g ; at ultraviolet and X-ray frequencies) where the velocity of the charged tachyon exceeds the phase velocity of light and the total radiation energy induced per unit path length is in general smaller than that induced by a relativistic, subluminal charged particle of the same charge in the same medium. As a consequence of this matter, it is deduced that charged tachyons induce the most intense electromagnetic Čerenkov radiation in the lowest frequency region possible which is not the same as subluminal charged particles. Moreover, since the relation among the electric field vector $(\vec{E})$, magnetic field vector $(\vec{H})$ and the velocity of the charged tachyon is probably thought to be the same as for a usual charged particle, the radiation may have the

usual polarization properties. Nevertheless, it seems still to be very much an open question as to whether the quantum theories of tachyons allow the radiation, either in a medium or in a vacuum. Some difficulties are:

(a) If a component of the particle's electric field is produced in a narrow cone along the direction of motion, then a very high density medium is required which then provides high absorption for any radiation produced.

(b) If the radiation is produced by the relaxation of a medium which has been polarised by the transverse component of the particle's electric field, then, in order to produce the radiation in a vacuum, the vacuum should be polarised. This requires a vacuum structure which does not correspond to a physical, real vacuum. Then, it might be deduced that tachyons do not emit Cerenkov radiation in any situation.

(c) On the basis of extended special relativity, Mignani et al (1973 , 1974) derived the formulae for the electromagnetic Cerenkov radiation from charged tachyons passing through a medium. The differential energy loss per unit path length due to electromagnetic Cerenkov radiation from a charged tachyon ze in a medium with refraction index n is given by following expression:

$$\frac{dE}{dl} = \frac{4\pi^2 z^2 e^2}{c^2} \int (1 - \frac{c^2}{v^2 . n^2}) \omega d\omega \qquad (2.14)$$

where v is velocity of charged tachyon and ω is the frequency of the emitted electromagnetic Cerenkov radiation. By using the

above equation , it can be inferred that tachyons lose most of their energy in a fraction of a centimeter from their point of production which makes it very difficult to detect them directly unless the rest mass or charge is very small.

2.3.4) CAPTURE OF TACHYONS

Although it is not clear on theoretical grounds whether capture of a charged tachyon by a nucleus or by an electron is possible or not it seems plausible that investigation of the above possibility can be profitable. The most suitable case for this purpose may be photoreactions , since such processes are best understood theoretically. In fact, it is of interest to consider what limits can be set on the production cross section of tachyons when one examines how well theory can explain experimentally observed total cross sections without any tachyon production.

2.4) CAUSALITY AND THE REINTERPRETATION PRINCIPLE(R.I.P)

Basically , the causality principle denotes that every effect is a consequence of an antecedent cause or causes. The feeling that the existence of faster than light particles must contravene the causality principle arises from the well-known fact that if such a particle is emitted at A and absorbed at B in the laboratory frame , then there will be a class of Lorentz frames in which the tachyon appears to move backwards in time and also to have negative energy. Therefore, these apparent paradoxes led scientists for over half a century to dismiss the possibility of the existence of tachyons. Some earnest

criticisms to the existence of tachyons are related to the causality problems which would ensue:

2.4.1) CRUX OF NEGATIVE TIME

Consider two inertial systems S and S'. Let the x and x' axes of these two frames coincide, and let S' move with a velocity $u<c$ in direction of the positive x axis. Assume that it is possible to create a tachyon with velocity $v>c$, which can be emitted from a source, $A(x_1, t_1)$, and absorbed at a detector, $B(x_2, t_2)$, on the x axis. For one observer, the particle moves through two points with:

$$\Delta x = |x_2 - x_1|$$

$$\Delta t = t_2 - t_1 > 0$$

$$v = \frac{\Delta x}{\Delta t} = \frac{|x_2 - x_1|}{t_2 - t_1} > c$$

For a corresponding time separation in the other frame S', the Lorentz factor shows that:

$$\Delta t' = \gamma(u)\Delta t\left(1 - \frac{v \cdot u}{c^2}\right) \qquad (2.15)$$

$$\Delta x' = \gamma(u)\cdot(\Delta x - u\Delta t) \qquad (2.16)$$

Thus, by choosing $u.v>c^2$ the time difference in the moving frame S', has the opposite sign to Δt (i.e; $\Delta t'<0$). Therefore, it is possible to change the sense of the propagation in time by a Lorentz factor. This seems to indicate that the observer in S' should see the particle being detected before it was emitted

which is a violation of the causality principle. The demonstration of this circumstance might be made as follows:

When going from one inertial system to another, it is important that the form of physical laws is invariant but not necessarily the interpretation of the particular phenomena observed. Thus, the observer in the frame S', could interpret the particle path, not as starting at $A(x_1, t_1)$ and ending at $B(x_2, t_2)$, but the reverse. However, for particles whose velocity is greater than c, there can be changes in the time ordering of points along its trajectory in another frame.

2.4.2) CRUX OF NEGATIVE ENERGY

It is clear from special relativity that the location of an event is uniquely defined by the four-vector (x,y,z,ct) which can be replaced by the four-vector (p_x, p_y, p_z, E) in momentum-energy space. The sign of the fourth component (i.e; energy), can be changed by a Lorentz factor, when the momentum four-vector is spacelike. Hence, a particle which is seen by one observer to have positive energy will have negative energy to another observer. By the principle of relativity, any state which is possible for one observer must be possible for all observers, and hence faster than light particles can exist in negative energy states for all observers. The result follows from the transformation equations of energy and momentum:

$$E' = \gamma(u)(E - p_x u) \tag{2.17}$$

$$\frac{E'}{E} = \frac{\Delta t'}{\Delta t} = \gamma(u)\left(1 - \frac{u \cdot v}{c^2}\right) \tag{2.18}$$

$$p'_x = \gamma(u)\left(p_x - \frac{u \cdot E}{c^2}\right) \qquad p'_y = p_y \qquad p'_z = p_z \tag{2.19}$$

Since $|pc|>E$, one can always choose u so that for instance $E'=-E$ and also its velocity is in the direction opposite to its momentum. However, the occurrence of negative energy states for particles has always been objected to on the grounds that no other system could be stable against the emission of these negative energy particles. Thus, they provide an inexhaustible fund of energy, an entirely unphysical behaviour. A further example is the following:

Any observer insists on a time ordering of events consistent with primitive ideas of causality such that emission occurs before absorption. For one observer, a process may be interpreted as emission of a positive energy tachyon at one space time point A and absorption of the tachyon at a later space time point B. The different observer, Lorentz transformed, will interpret the process as the emission of a positive energy tachyon at point B' and its absorption at the later point A'. Then, for this observer, the second point may be earlier in time than the first, and the energy of the tachyon may be transformed to a negative value by the Lorentz transformation. However, the consequence of the Lorentz transformation is to relate the rates of emission rather than to require the introduction of negative energy states. Using these ideas, a principle which allowed a consistent theory of tachyons to be developed was established. It is known as the reinterpretation principle (also known as the switching principle), and states that a negative energy particle which is observed first and later emitted is equivalent to a positive energy particle which is observed after emission, figure 2.2.

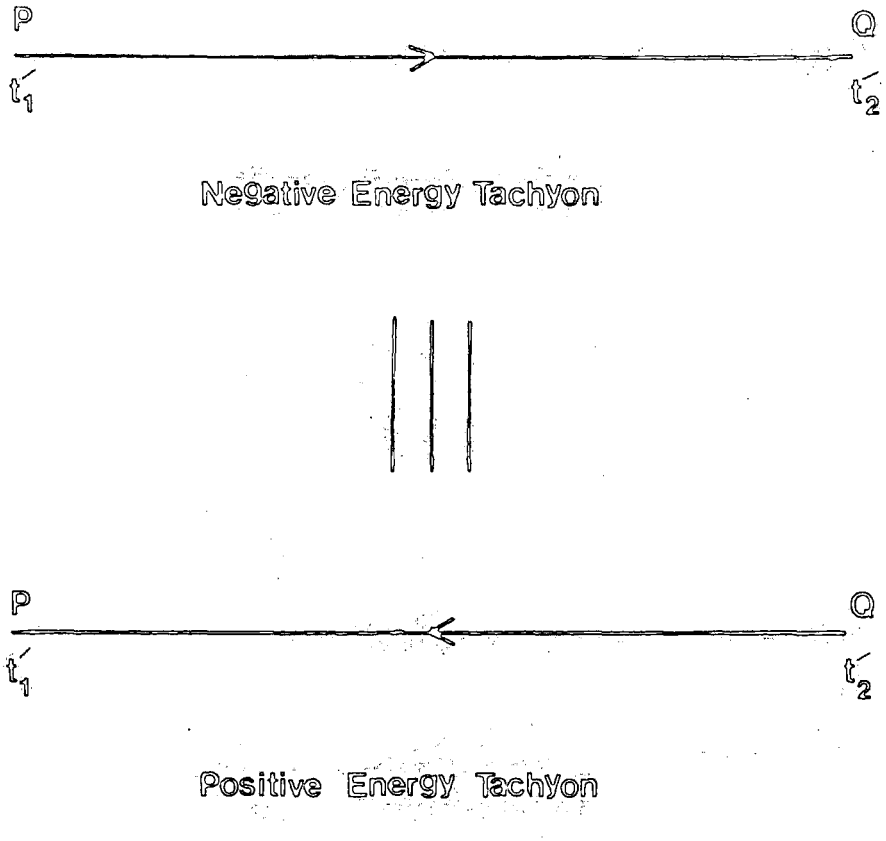

Figure 2.2 The reinterpretation principle for tachyons at work; the negative energy tachyon emitted from P at a time after it is absorbed at Q is reinterpreted as a positive energy tachyon absorbed by P after it had been emitted from Q.

Although two observers will not agree about the direction of travel, the laws of physics remain still the same. Therefore, the reinterpretation principle implies that negative energy tachyons travelling backward in time are to be reinterpreted as positive energy tachyons moving forward in time with the opposite momentum. Essentially, the idea of the reinterpretation principle is similar to the idea of anti-particles, and the Feynman interpretation of positrons as negative energy electrons running backward in time (Feynman 1949). Then, if tachyons carry charge or baryon number ($B = \pm 1$), the reinterpreted particles will be anti-tachyons. However, Csonka (1970) reanalized the various concepts of causality such as "cause" and "effect" and concluded that the reinterpretation principle in itself may be not enough to resolve all the kinds of causal difficulties. As an example, this principle leaves ambiguous the sign of the momentum which an observer in a subluminal frame at rest will attribute to the tachyon, since the energy in the subluminal frame at rest vanishes. Newton (1967,1970) contradicted the possibility of tachyon existence. The controversy is based on the fact that if a signal can travel faster than the speed of light, it might in one frame appear as though the effect preceded the cause. Then, it was concluded that if tachyons did exist either the relativity principle or the fundamental rules of quantum mechanics would be incorrect.

2.5) GEOMETRICAL SYMMETRY AND MINKOWSKI SPACE-TIME

In order to get some idea about negative energy states

and the causality principle, it is necessary to consider the energy-momentum relation in more detail. Figure 2.3 shows a plot of the energy-momentum relationship. Above the x-axis is attributed to particles with positive energy states. As can be seen the velocity of bradyons can never reach to the velocity of light even if it is transformed to a frame where the energy is very large. By choosing $\mu_0=0$, a plot of the energy - momentum vector becomes straight lines which are related to luxons. Everywhere on this straight line, the velocity is c irrespective of the Lorentz - transformation. For tachyons, as can be seen, their velocity is always more than c and their existence would complete the symmetry of the solutions. Branches below the x-axis describe all three types of particles which have negative energy and these can be associated with anti-particles.

Now consider the path of the motion of an object (P), along the x-axis, in a Minkowski space-time diagram in which two space dimensions are ignored, figure 2.4. If the speed of the moving object is uniform (i.e; non-accelerated), its world line is a straight line. Thus, the world line for a stationary object is either parallel or coincident with the ct-axis. It is clear that the x-axis constitutes the locus of all points simultaneous with the origin. If the object moves exactly with the speed of light (i.e; luxon), its world line bisects the angle between both axes (x and ct) and thus its gradient is equal to one. If its speed, v , exceeds the velocity of light (i.e; superluminal particle), its world line makes a smaller angle with the x-axis than with the ct-axis. Thus its gradient

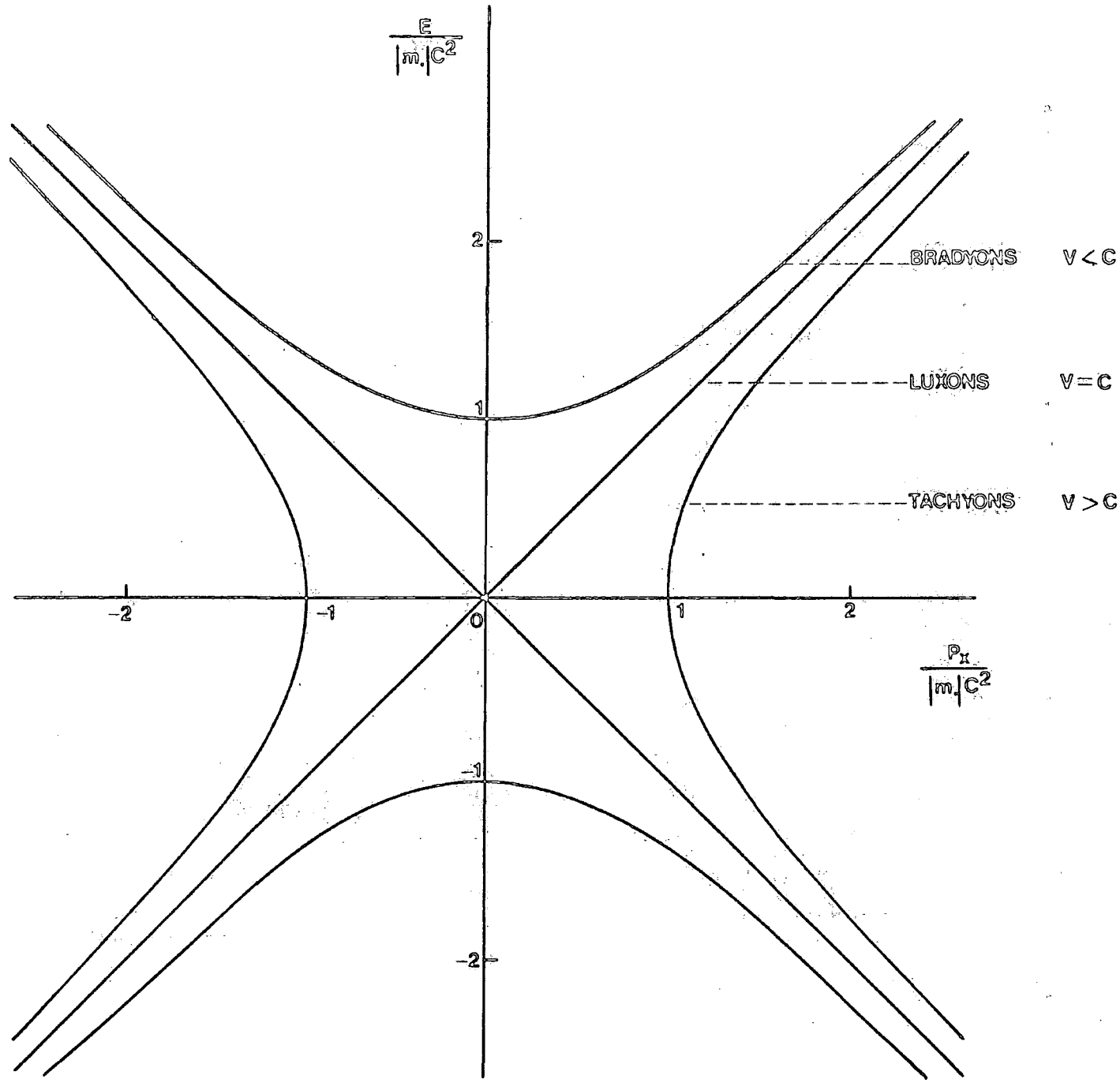

Figure 2.3 Plot of the energy momentum vector invariant, showing the solutions for particles in each of the three velocity domains.

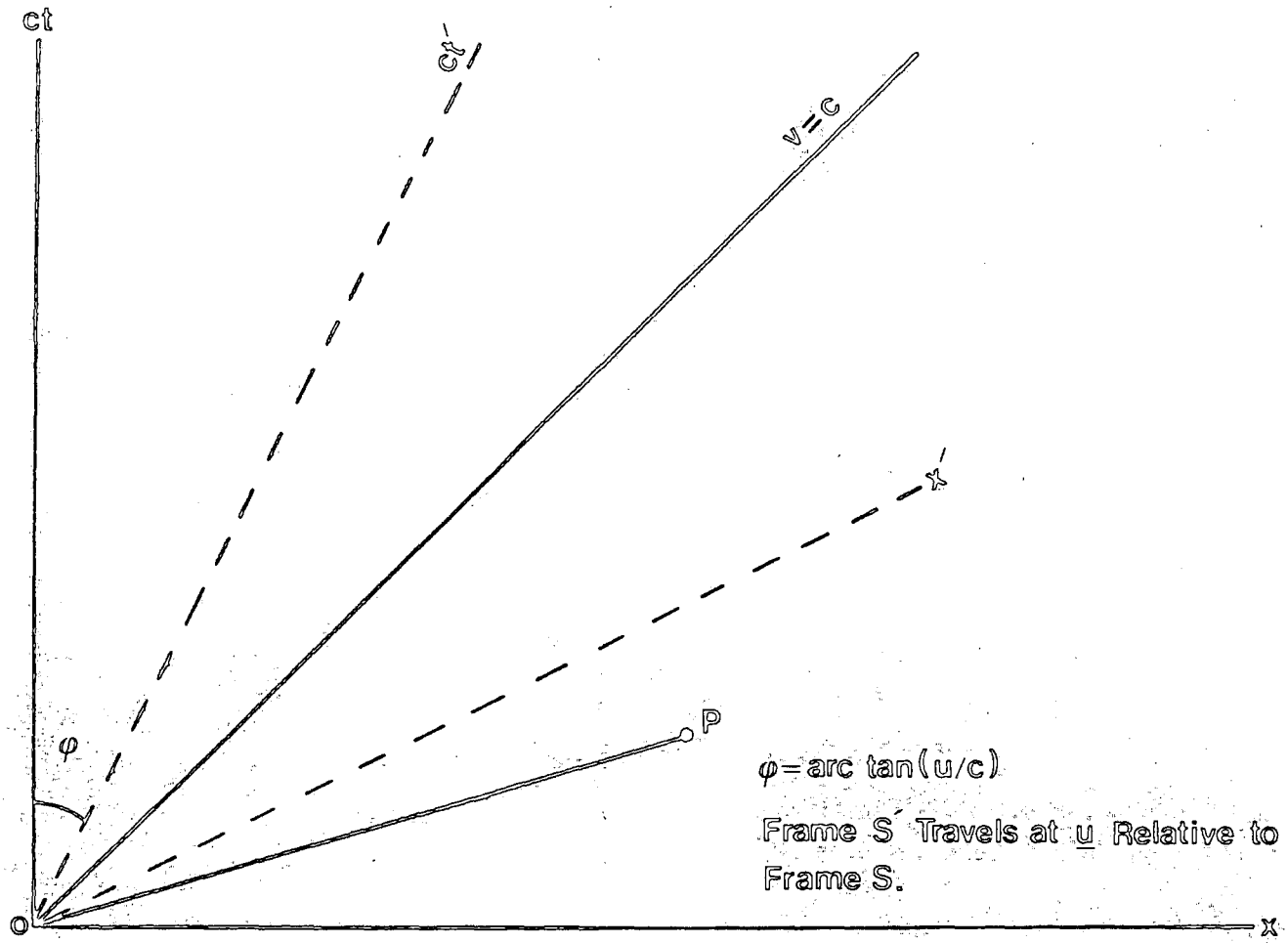

Figure 2.4 Minkowski time-space diagram.

is always less than one and, obviously, the gradient of a subluminal particle must be more than one. Also shown in this figure are the axes (x' and ct') of another uniformly moving reference frame, S', with velocity u<c relative to the unprimed reference frame, S, and making the same angle, φ, with the respective unprimed axes which can be derived from $\varphi=\tan^{-1}(u/c)$. Inevitably, for maintenance of the condition u<c, this angle must be less than 45°.

Suppose that a tachyon P moves from the point O, x=0 and ct=0, to A with coordinates x and ct in the unprimed reference frame, S. As can be seen in figure 2.5 the world line of the tachyon which passes from point O makes an angle, α, with the x-axis. Since the tachyon always moves with velocity greater than the velocity of light, α must be also less than 45°. However, P leaves point O at the time t=0 and arrives at point A at a positive time thus it moves from point O to point A as seen in reference frame, S.

Now if $\varphi < \alpha < 45^\circ$ then nothing out of the ordinary is observed. But if $0 < \alpha < \varphi$, in frame S', the ct' coordinates of points O and A are zero and a negative number. Thus, for an observer in S', the point A occurs before O. In other words; for any motion that is seen in one reference frame as having a speed greater than c, there exist other physical reference frames in which the motion is seen to occur backward as compared with the motion observed in the first. Therefore, when the condition $v.u > c^2$ is satisfied, this paradox will occur.

2.6) EXTENDED RELATIVITY THEORY

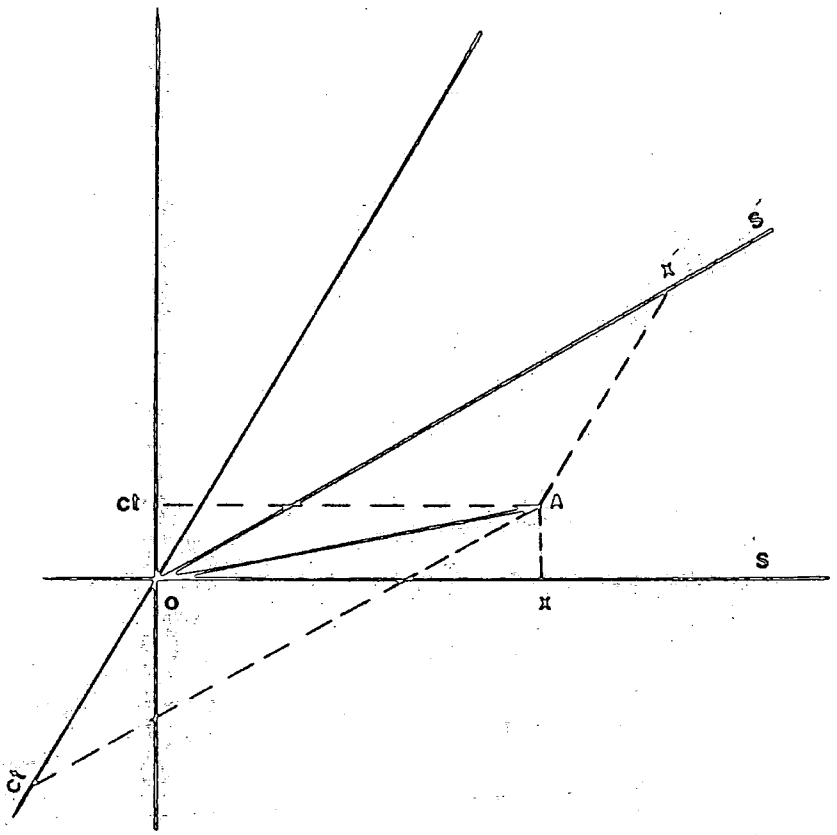

Figure 2.5 OA is the world line of a point, P, moving faster than light. The event O occurs at $x = t = x' = t' = 0$, whereas A occurs at (x,ct) in S and at (x', ct') in S'.

After the appearance of special relativity physicists rejected for a long time the possibility that faster than light particles could exist within the context of that theory. But, the development of special relativity (SR) has given rise to the so-called extended relativity theory (ER) which comprises superluminal particles. In this theory, besides the dominance of the two principles of special relativity, one extra postulate is required which states negative energy objects or particles, travelling forward in time do not exist and physical signals are carried only by objects that appear to carry positive energy. In fact, in extended relativity, both subluminal and superluminal frames are considered.

The introduction of the extended principle of relativity is due to symmetry or duality between subluminal and superluminal frames. It states that the totality of the laws of physics has the same form relative to the superluminal frames as it does relative to the subluminal frames. In general, the laws governing tachyons and subluminal particles (i.e; bradyons) will be interchanged in a transformation between a subluminal and a superluminal frame, but the total structure of the laws will have the same form. Consequently, the laws governing superluminal particles relative to superluminal frames (in which those particles appear like ordinary particles) are the same as the laws governing subluminal particles relative to subluminal frames. Thereby, if the laws of conservation of energy and momentum hold in subluminal frames, then those laws are valid in superluminal frames. In extended relativity theory, a tachyon may be defined as a particle which moves at

velocity less than c relative to a superluminal frame provided that the superluminal frame moves relative to the subluminal frame with velocity u>c. Thus, a tachyon in a subluminal frame is equivalent to a bradyon in a superluminal frame and vice-versa. Luxons have the same properties in both kinds of frames. The existence of anti-particles can be inferred from the third postulate of extended relativity which, indeed, is equivalent to the reinterpretation principle.

Parker (1969) presented a one-dimensional theory of tachyons in terms of a generalisation of the Lorentz-transformation to superluminal inertial frames. It expends the validity of two postulates of special relativity to inertial co-ordinate systems having relative velocities greater than that of light. Principally, his model of the one-dimensional theory of tachyons is based on the following assumptions:

(a) A luxon travelling in vacuum has a velocity of the same magnitude relative to all inertial co-ordinate systems.

(b) the transformation between frames must be recognized to be linear.

He concluded that firstly, a charged tachyon may be similar to a magnetic monopole relative to the reference system in which it has infinite velocity. Secondly, both subluminal and superluminal particles will interact electromagnetically with photons, and thus indirectly with each other. Also, it is expected that a weaker interaction of tachyons with neutrinos exists. In addition, because of the existing complete mathematical symmetry between the two sets of reference systems, some further consequences can be obtained, Mignani et

al (1973a). Light speed invariance allows an exhaustive partition of all inertial frames (i.e; $u \gtrless c$), in the two sets. A subluminal Lorentz — transformation (LT) maps separately subluminal frames and superluminal frames into themselves. This is known, Mignani et al (1972,1973b), as the duality principle (DP) which states that the terms bradyon (B), tachyon (t), subluminal frame and superluminal frame are to be attributed only a relative meaning, but not an absolute one. Roughly speaking, a Lorentz-transformation (LT) does not change the tetravector type, on the contrary, a superluminal Lorentz-transformation (SLT) transforms a time-like vector into a space-like vector and vice-versa. The convention described above essentially requires that each component of the four vector be multiplied by a factor i. This implies that what an observer in a subluminal frame measures for a spatial co-ordinate in the direction in which the observer's superluminal frame is travelling, the observer in superluminal frame will interpret as a temporal co-ordinate and vice-versa. In other words; the reinterpretation principle (R.I.P) follows the Lorentz — transformation to a frame of reference where t and x are reversed as well as energy and momentum. However, tachyons are introduced as bradyons in superluminal inertial co-ordinate systems, and their properties are obtained from those of bradyons by using the extended Lorentz-transformation.

2.7) EXTENDED LORENTZ-TRANSFORMATION

Pavlopoulus (1967) suggested that Lorentz invariance is only approximate and valid in regions of space accessible to

experiment. Such regions can be characterised by a universal length of the order of the diameter of the proton which is approximately equal to the range of strong interactions or the classical radius of electrons. However, it leads to the conclusion that for very short wave lengths the group velocity of an electromagnetic (E.M) wave can exceed the velocity of light. Finally, he concluded that the range of distances over which tachyons may exist is $<10^{-15}$m away from a bradyon, and thus they only take part in strong interactions between bradyons confined to such regions (e.g; quark-quark interactions). Therefore, the special principle of relativity may be violated on a micro-scale.

The transformation from one subluminal frame to the superluminal frame moving at relative velocity $|u|>c$ is called a superluminal transformation. According to Parker's theory of tachyons, it can change the sign of the energy of subluminal and superluminal particles which is contrary to the Lorentz-transformation. Hence, equation (2.6) leads to a parameterization of Lorentz – transformations that is different from the ordinary transformation. While the superluminal transformatios alone do not form a group, a combination of the Lorentz-transformation (LT) together with the superluminal transformation (SLT) do form a group which is called the generalised (extended) Lorentz- transformation (GLT). In two inertial co-ordinate systems (S , S') with the relative velocity of $u \neq c$, Mariwalla (1969) showed that the general form of the transformations which hold equation (2.6) to be unchanged are as follows:

$$E = \acute{E}\cosh\theta + c\acute{P}\sinh\theta \qquad (2.20)$$

$$cP = c\acute{P}\cosh\theta + \acute{E}\sinh\theta \qquad (2.21)$$

In the case of tachyons u>c, these equations reduce to:

$$E = m_o c^2 \sinh\theta = \frac{u}{|u|} \times \frac{m_o c^2}{\left(\frac{u^2}{c^2} - 1\right)^{1/2}} \tag{2.22}$$

$$P = m_o c \cosh\theta = \frac{m_o |u|}{\left(\frac{u^2}{c^2} - 1\right)^{1/2}} \tag{2.23}$$

giving

$$\tanh\theta = \frac{E}{Pc} = \frac{c}{u} \tag{2.24}$$

where in one - dimensional motion, θ is related to the relative velocity of the two reference frames which can be obtained by the following equation:

$$B(u) = \left[\frac{u-c}{u+c}\right]^{1/2} = e^{-\theta} \tag{2.25}$$

Equations (2.22) and (2.23) show that positive-energy bradyons ($m_o > 0$) lead to positive-momentum tachyons and the existence of negative - momentum tachyons would necessarily imply the existence of negative- energy bradyons ($m_o < 0$). Also, it can be concluded that a tachyon reverses the sign of its energy by reversing the sign of its velocity. An application of equations (2.18) and (2.19) is to find the law of addition of velocities for tachyons. Antippa et al (1971). Let $v > c$ be the tachyon velocity in a frame S and $v' > c$ its velocity in a frame S' moving relative to S with a velocity $u < c$. Using equation (2.22)

and the law of tangents, then

$$v = \frac{v' + u}{1 + \frac{v'.u}{c^2}} \tag{2.26}$$

which happens to be the usual law of addition of velocities. Thus , if the particle is a tachyon in S' , then it is also a tachyon in S. Similarly, if the particle is a bradyon in S' , then it is also a bradyon in S.

$$|v'| \gtrless c \quad \Longrightarrow \quad |v| \gtrless c \tag{2.27}$$

Finally, his calculations show that an imaginary particle which carries the signal from one end of an object to the other with infinite velocity as seen in its rest-frame S , has got the velocity of c^2/u in the frame of S' moving relative to the rest frame with velocity of u. In fact, it expresses the result that events which are simultareous in the rest frame are not simultareous in a moving frame.

2.8) PREFERRED DIRECTION THEORIES

This suggests consideration of the question of whether there exists a class of theories (called preferred direction in space or tachyon corridor). which yield predictions for existing experiments in satisfactory agreement with the data . and thus with special relativity, but in which the principle of relativity is only approximately valid. It introduces reference frames whose velocities are along the tachyon corridor and are

identified as preferred frames. The magnitude of their relative velocities can be anything but c. For tachyons in a preferred reference frame the generalised Lorentz tarnsformations (GLT) hold with $\xi = 1/\beta$ substituted for β.

In relation to two inertial co-ordinate systems S snd S', Antippa (1972) and Antippa et al (1973) reconsidered, first one - dimensional and then the three - dimensional, theory of tachyons. In order to overcome the difficulties involved in the interpretation of imaginary quantities and the Lorentz invariance problem, the preservation of causality requires extra postulates to be added which state that the time axis is unidirectional with respect to bradyons but isotropic with respect to tachyons and the space axis is unidirectional with respect to tachyons but isotropic with respect to bradyons. This removes the Lorentz invariance problem as tachyons exist only with one sign of momentum (i.e; negative or positive momentum). According to the above assumption, for the case of bradyons (i.e: $|\beta|<1$), time is unidirectional and thus the sign of the velocity depends on the direction of relative motion of the two systems in space, but space is isotropic. In the case of tachyons (i.e; $|\beta|>1$), space is unidirectional and hence the sign of velocity depends on the direction of relative motion of the two systems in time, but time is isotropic. Therefore, the momentum of a tachyon does not change sign with the velocity. In other words; tachyons reverse their velocity by reversing their direction of motion in time and not their direction of motion in space, while it is found that a bradyon can be thought of as reversing the sign of its velocity by reversing

its direction of motion in space. The summary of these controversies can be illustrated by figure 2.6 in which the world line of luxons divides space-time into four regions. The positive energy bradyons travel forward in time and forward or backward in space. But, the positive momentum tachyons travel forward in space and forward or backward in time. The unidirectionality of motion of tachyons in space diminishes the sensational aspects of backward motion in time. Since it also prevents the formation of causal loops , thus the above model can be fully causal.

In comparison with the Parker tachyon theory, although the derivation of extended transformation equations such as energy and momentum is different, nevertheless , in the both theories , the equations themselves are the same and lead to real mass, space and time in all inertial co-ordinate systems.

2.9) QUANTUM FIELD THEORY AND ELECTROMAGNETIC PROPERTIES

2.9.1) INTRODUCTION

Diverse approaches have been developed to carry out the field theory of tachyons. probably because the fundamental properties of these particles are not yet very well known. Essentially , in the classical theory of tachyons , two main approaches have been followed by different authors. In the first one (e.g; Recami et al), despite preserving the invariance of the speed of light , the components of a four vector in the directions perpendicular to the relative motion become imaginary ($y=iy'$, $z=iz'$) on passing from the subluminal to superluminal realm. In this case, a spherical light wave in

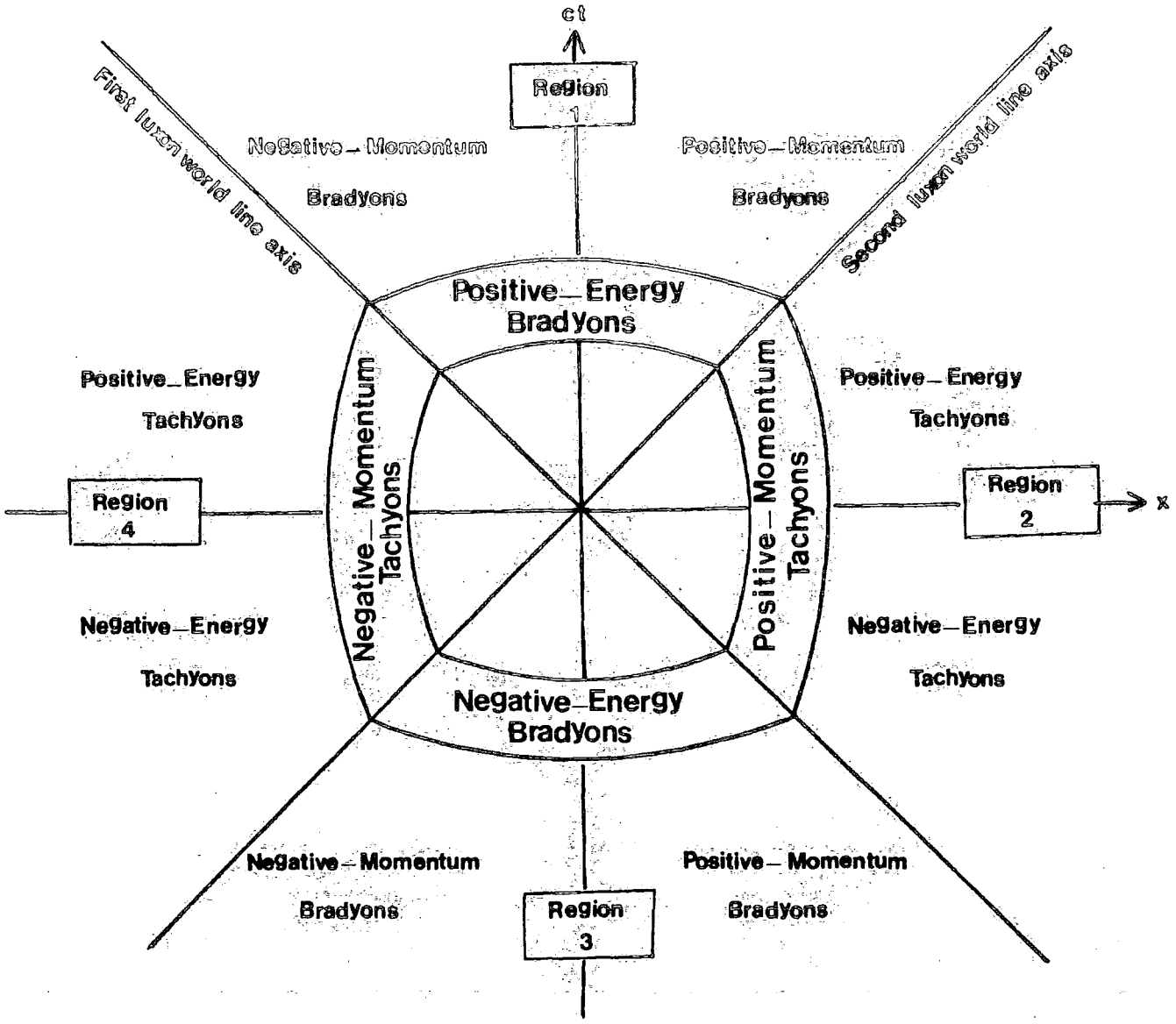

Figure 2.6 The light cone is bounded by the two causal lines and separates two-dimensional space-time into four independent regions. Antippa et al. (1971).

a superluminal frame appears spherical to an observer on earth. In fact, since the four vector in momentum space has the form (cE , ip_x , ip_y , ip_z), the proper expression for the mass of an object of rest mass m_o (real) travelling with velocity β should be $m = \frac{m_o}{(1-\beta^2)^{1/2}}$. While in the second approach (e.g; Antippa et al) one can preserve the invariance of the transvere co-ordinates ($y'=y, z'=z$) at the expense of losing the invariance of the speed of light. A spherical wave in a superluminal reference frame becomes hyperbolic when viewed from a subluminal reference frame and the real superluminal Lorentz transformations are used. However, the possible existence of a class of particles with a space like four-momentum, which presumably travel faster than light in a vacuum, has led to considerable discussion about superluminal entities. Since there seems to be no argument strictly forbidding tachyons, these particles are probably allowed by relativistic quantum mechanics.

2.9.2) QUANTUM FIELD THEORY

Some papers have been published to place tachyons in the framework of a quantum field theory The results obtained by various workers will now be described.

2.9.2.1) S.TANAKA (1960)

Apparently, the quantum field theory of faster than light particles was first given by Tanaka. In order to establish a convenient quantum field theory, under the formalism of the canonical quantization and the requirement of

the Lorentz invariance, he concluded that the quantized super light velocity field (i.e; S - field), cannot have any familiar particle aspect. In fact, it implies that the concept of energy or momentum of the S - field by itself has no objectivity. In other words; it is likely impossible to understand the S-field in the same way as the usual elementary particle field theory.

2.9.2.2) O.M.P.BILANIUK et al (1962)

They postulate two criteria which a consistent relativistic theory should satisfy viz:

(a) In any frame of reference the energy of a particle must be positive.

(b) The laws of particle dynamics must be independent of the frame of reference.

Criterion (a) defines a criterion by which we can test whether a physical state has real significance. i.e; it is a definition of existence in the physical universe. Criterion (b) is identical to postulate 1 of Einstein's original theory. In other words; the constancy of the velocity of light is considered to be a physical law, and hence independent of the frame of reference. As an example, take the transmission of energy from a source to a sink. To an observer stationary with respect to both source and sink the time ordering of event is that first the observer sees the source suffer a decrease in positive energy followed by the sink suffering an increase in positive energy. Now, consider a second observer travelling with a velocity greater than light such that the time ordering of events is reversed. First he sees the sink suffer an

increase of negative energy and followed by the source suffering a decrease in negative energy. Thus, the second observer sees first the sink as source suffering a decrease in positive energy, followed by the source which he calls the sink, suffering an increase in positive energy. In fact, it is the reinterpretation principle in another form.

2.9.2.3) M.E.AARONS et al (1968), J.DHAR et al (1968)

Feinberg's scaler-free field theory (i.e ; $\Phi(x, t)$) and quantization scheme, because of its lack of relativistic invariance, was strongly criticized. An alternative form of quantization is discussed in which annihilation operators are used. . A corollary of this is that Feinberg's restriction to Fermi statistics is no longer relevant. In fact, faster than light particles have either Fermi or Bose statistics. Since the negative energy states can be created by the creation operators, so that a physical postulate is required. It states that the only physically relevant quantities are the transition amplitudes. Any transition amplitude is to be interpreted as the amplitude for transition between positive-energy particles where all negative energy particles (of momentum +p) in the initial state are interpreted as outgoing positive energy particles (of momentum -p). Similarly, for negative energy particles in the final state. Again it can be understood, as another scheme of the reinterpretation principle.

2.9.2.4) B.SCHROER (1971), L.ROBINETT (1978)

Investigations of solutions of the Klein-Gordon equation with any complex value of the mass in general (imaginary mass in particular), have probably demonstrated that the imaginary mass Klein-Gordon field propagates no faster than the speed of light and the quantization of an $m^2<0$ field equation leads to causal fields. Therefore, the usual interpretation of the imaginary mass Klein - Gordon equation as the field equation of a free tachyon is incorrect. Also, they concluded that if tachyons exist, no Lorentz-invariant relation of cause and effect can be constructed for pairs of events in space-time. Conversely, when a Lorentz-invariant causal order relation can be constructed, there can be no tachyons.

2.9.2.5) C.SCHWARTZ (1982)

The earlier tachyon quantum theory of Feinberg which is on the basis of the conservation of four - momentum, is subtly revised. He contemplates the stress - energy - momentum tensor which is a differentially conserved quantity. However, it leads to a different quantization of the field theory. It is found that there is no problem of negative - energy states and no need for the reinterpretation principle used by others.

2.9.3) ELECTROMAGNETIC PROPERTIES

This is an important area for investigation because of its implication for the detection of tachyons.

2.9.3.1) H.LEMKE (1976a,1976b)

Electrodynamic properties of process involving charged

tachyons which is based on the real superluminal Lorentz-transformations are considered. As mentioned earlier, a charged tachyon produces infinite radiation energy and hence must immediately lose all its energy (see 2.3.3). Therefore, one of the main aims of this article can be to underline that this problem does not appear in an electrodynamics based on the real superluminal Lorentz - transformations. He assumes the law of light speed invariance is not valid in its most general form and space is isotropic. Thus, he does not imply the existence of a tachyon corridor but he uses a preferred direction along the instantaneous direction of motion of the tachyon. In other words; one should interpret the x-axis not as a definite preferred direction in space, but as any direction along which the observed tachyon moves. Subsequently, this interpretation was strongly criticized. The field of a uniformaly moving tachyon is deduced and concluded in favour of the possibility of Cerenkov radiation induced by charged tachyons only in usual media. At last, it follows that faster than light electric charges do not behave as magnetic monopoles.

2.9.3.2) L.MARCHILDON et al (1979)

Assuming superluminal reference frames and the hypothesis that tachyons are bradyons as seen by a superluminal observer (i.e; tachyon - bradyon reciprocity) the electromagnetic interactions of tachyons are derived. They assume that the equations governing the superluminal electromagnetic field as seen in a subluminal frame obey differential relations which differ from the ordinary, subluminal, Maxwell's equations and

are not invariant under generalized proper Lorentz-transformations, and hence it can coupled only very weakly to bradyons. Of course, such differences do not contradict the principle of relativity. They claim that Lemke's preferred direction argument is inconsistent. According to them, the transformation equations are used only to relate frames moving along the corridor, which is a definite preferred direction in space. However, their formulation produces the same results but disagree with his interpretation of the meaning of the superluminal transformations since he fails to take into account that the superluminal field does not satisfy Maxwell's equations, so that it cannot be identified with the ordinary field. They also suggest that in subluminal frames, tachyons are acted on by both the subluminal and superluminal fields through an electromagnetic force which is different from the usual Lorentz force. The foregoing conclusion leads to the striking point that Cerenkov radiation should not be emitted unless there is an effective coupling of tachyons to the subluminal electromagnetic field. From the point of view of subluminal reference frames, this reflects the fact that the emission of massless photons by tachyons seem to be always kinematically allowed. But since in their theory, one should expect a very small coupling of the tachyon to the electromagnetic field (i.e; a very small charge for the tachyon), the rate of emission of Cerenkov radiation by charged tachyons would be much less than expected for a charged particle having the usual unit of charge (e) and velocity greater than c, as assumed in searches for tachyons (e.g;

2.12.4.1). It means that the charged tachyons, at least in the theory, may emit Cerenkov radiation through their coupling to the subluminal, but not the superluminal field. The inference is that their electromagnetic behaviour is not exactly analogous to that of an electric charge or magnetic monopoles. However, their behaviour seems to be somewhat closer to that expected of charge rather than magnetic poles.

2.10) MAGNETIC MONOPOLES AND TACHYON MONOPOLES (TM)

The interest of the theory of magnetic poles, Dirac (1931 , 1948), is that it forms a natural generalization of the usual electrodynamics and it leads to the quantization of electric charge. In fact, the existence of one magnetic pole of strength g would require all electric charges to be quantized and, similary, the existence of one electric charge would require all magnetic poles to be quantized. All particles bearing a magnetic charge are probably so massive that monopoles are extremely rare. They are expected to be produced by similar processes that produce electron-positron pairs:

$$\gamma + P \longrightarrow P + g + \bar{g} \qquad (2.28)$$

The main characteristics of monopoles is their very large rate of ionization loss in matter and the ionization density produced along the track of a relativistic monopole is expected to be similar to that produced by a relativistic atomic nucleus with atomic number Z=137. Finally, any monopoles present in the cosmic radiation in the atmosphere could either be produced in high energy cosmic ray interactions or be present in the

primary cosmic radiation itself.

Duality between bradyons and tachyons is essentially the duality between electric and magnetic charges. Mignani et al (1974a , 1975 , 1976) have investigated superluminal (tachyon) magnetic monopoles with the aid of the extended Lorentz transformations. They have asserted that the special theory of relativity does not explicitly predict the existence of subluminal (bradyon) monopoles, but on the contrary predicts the existence of superluminal (tachyon) monopoles with an elementary magnetic charge g(emu) = -e(esu). In other words; extended relativity explicitly predicts one charge (the so-called, electromagnetic charge), that behaves as electric when slower and as magnetic when it moves faster than light. In fact, it may imply that magnetic monopoles are probably expected to exist only as superluminal objects. However, there are some serious objections regarding the foregoing comment.

2.11) OTHER ASPECTS OF TACHYONS

Other physicists who believe in the essence of tachyons, have also investigated the various properties of them.

2.11.1) M.GLÜCK (1970)

The classical motion of a charged tachyon in an electrostatic Coulomb field and its comparison with the behaviour of an ordinary particle is discussed. By utilizing Bohr – Sommerfeld quantization rules (e.g ; energy , angular momentum and so on), it was shown that the only stable orbits are circular ones. This is a different result from that for

ordinary particles where stable precessing ellipses also exist. Concerning the scattering cross-section, it is found that whereas Rutherford's formula (i.e; scattering of a charged particle in the nuclear electric field), holds for ordinary particles almost for all angles. In the tachyon case, it holds only for very small angles, while for almost all other angles, the pertinent formula is a different one.

2.11.2) R.GOLDONI (1972,1973)

This author finds that bradyons and tachyons are able to exchange only internal quantum numbers, e.g strangness. It indicates that they can exchange only those quantum numbers whose conservation appears to be violated in subluminal physical processes. In other words; the four-momentum (e.g; spin) of a subluminal particle is not invariant under a superluminal Lorentz-transformation. This symmetry may allow one to develop a kinematics of tachyons in which the proper mass of a tachyon is interpreted by a real number. It follows that the reinterpretation principle of negative-energy particles appears to be an unnessecary complication.

2.11.3) A.E.EVERETT (1976)

This author discusses the possible theories in which there exists a preferred reference frame (PRF) in nature, so that there is not invariance under proper Lorentz-transformations. In such a theory one can have tachyons without encountering problems with causal loops which usually arise when one endeavours to construct Lorentz invariance tachyon

theories. The paper discusses a class of theories differing from special relativity in the existence of a preferred reference frame and deviations from the Lorentz-transformation or special relativity at large value of $\beta=v/c$. The theories can be made to agree with existing experiments and allow the possibility of accelerating ordinary particles to speeds greater than velocity of light. This indicates that tachyons may be created in states with $v>c$ as a result of the decay of, or collisions between, bradyons if such a process is kinematically allowed. The author concludes that it seems very likely that free tachyons at high energy are unstable, since one can exhibit that their decay into a lower – energy tachyon plus photons (i.e; reaction 2.13) is always kinematically allowed. Thus, it appears unlikely that the highest energy incident cosmic radiation could be tachyons, since they must live long enough to cross galactic distances. Moreover, the dependence of mass and lifetime on velocity is determined.

2.11.4) C.M.EY AND C.A.HURST (1977)

Using the electromagnetic energy – momentum flux, the equation of motion of a charged tachyon within the frame of classical electrodynamics and an unextended special relativity it is found that the Lorentz – Dirac equation in the case of slower than light particles is satisfied. On the basis of classical electrodynamics and the lack of radiation reaction terms in the relevant equation it implies that a charged tachyon undergoing an arbitrary accelerated motion would not radiate under any circumstances. In particular, certainly,

vacuum Čerenkov radiation (although not necessarily Čerenkov radiation in a medium) is excluded. Probably, this can be accounted as a confirmation of previous comments since tachyons appear as bradyons to superluminal frames. In order to get the physical laws for tachyons (as seen in a subluminal frame) it is sufficient to apply a superluminal Lorentz-transformation to the corresponding usual laws for bradyons. Also as an ordinary charged particle at rest never radiates, Mignani et al (1973) concluded that tachyons are not expected to emit electromagnetic Čerenkov radiation in vacuum. In fact, in the usual context, the very expression of Čerenkov radiation in vacuum appears meaningless.

2.11.5) J.V.NARLIKAR et al (1976)

It is speculated that tachyons were produced at or just after the epoch of the big-bang event along with many other particles. A primordial tachyon, produced in this way, would need a very large energy to survive. They conclude that the trajectory on a space-time diagram reaches a limit at some co-ordinate depending on the mass and initial energy of the tachyon. In an indefinitely expanding universe, the trajectory will turn back in time and a mass limit can then be set on the tachyon on the basis of its survival. Also, they suggest that photons and neutrinos are tachyonic.

2.11.6) V.VYSIN (1978), G.DATTOLI et al (1978)

On the basis of Dirac's opinion concerning theoretical mutuality between electricity and magnetism, it is attempted to

show that very similar relations can be obtained by introducing the superluminal Lorentz-transformation and the aid of the manner in which space and time play a symmetrical role. This goal is achieved by assuming that time is considered as a vector in six dimensional space-time with components: t_x , t_y , t_z. In fact, the introduction of two extra time-coordinates may help to interpret the imaginary quantities entering the superluminal Lorentz-transformation. Explicitly, in such a framework, an event P, can be represented as follows:

$$P \equiv (x\ ,\ y\ ,\ z\ ,\ it_x\ ,\ it_y\ ,\ it_z) \qquad (2.29)$$

Three components of the time vector are coupled together giving $|t| = (t_x^2 + t_y^2 + t_z^2)^{\frac{1}{2}}$ as measurable. In other words; the components of this imaginary vector part lose their individual physical meaning. It is inferred that a tachyon moving with infinite velocity behaves as a purely magnetic charge at rest. Furthermore, it is asserted that an electrically charged tachyon behaves like a magnetic monopole with elementary charge g(emu)=-e(esu) which agrees with the previous suggestions (e.g; see 2.10). Although the magnitude of the magnetic charge differs from the magnitude evaluated by Dirac, the derived behaviour of a magnetic monopole in the electromagnetic field seems very similar to Dirac's equations.

2.11.7) O.P.S.NEGI AND B.S.RAJPUT (1982)

The behaviour of Maxwell's equations under imaginary and real superluminal Lorentz—transformations and the expression

for the Lorentz force acting on an electric charge interacting with superluminal electromagnetic fields are reexamined. It is found that the electric and magnetic equations for the superluminal fields seem to be neither similar to those of fields produced by an electric charge source nor to those produced by a magnetic charge source. Hence, it may be concluded that an electrically charged tachyon interacting with superluminal electromagnetic fields observed in a subluminal frame does not behave exactly as expected of either an electric charge or a magnetic monopole. This can be in contradiction with those consequences which state an infinite - speed tachyon behaves as a purely magnetic charge at rest.

A similar conclusion can be drawn by transforming the usual expression for the Lorentz force. In fact, it is similar neither to the Lorentz force acting on an electrically charged particle nor to the corresponding force acting on a magnetic monopole. It may imply that a subluminal electric charge interacting with superluminal electromagnetic fields or an electrically charged tachyon interacting with a subluminal electromagnetic field behaves neither as a purely electric charge nor as a pure magnetic monopole.

2.11.8) ST.MROWCZYNKI (1983)

Although the existence or non — existence of tachyons is still a contentious topic, a study of their properties can be useful since it makes our understanding of the theory of bradyons deeper. The properties of an ideal gas (e.g; temperture; T, pressure; P, entropy; S, energy; U) of classical

tachyons are considered. Since zero point energy tachyons can carry momenta proportional to their masses ($\mu_o c$), it is expected that the value of the pressure at zero temperture would be finite. In general, it is concluded that almost all the properties of a classical gas of tachyons and a classical gas of bradyons are probably similar which implies that the equation of state is the same for both.

2.11.9) S.K.SRIVASTAVA (1983,1984)

In the background of Robertson Walker cosmology and using the Klein-Gordon equation for the space like scalar field, various physical parameters such as: energy, probability density (i.e; $\Psi.\overset{*}{\Psi}$), dissipation of energy and survival of spin-1/2 and spinless primordial tachyons are mathematically investigated. It is shown that the dissipation of energy of a primordial tachyon is large in the early stages of the big-bang but it slows down later on in every phase of the universe. With the help of the uncertainty principle of Heisenberg it is shown that if tachyons survive up to the present epoch and into the future, primordial tachyons moving with high speeds should be much lighter than those moving with low speeds. It is pointed out that the meta — mass (μ_o) of a spinless primordial tachyon ($< 2.447\times10^{-93}$g) surviving up to the present epoch would be much less than that of spin - 1/2 primordial tachyon ($< 8.77\times10^{-54}$g). Hence, it can be inferred that the possibility of survival of spin - 1/2 primordial tachyons is more than the spinless ones. Also if a spinless primordial tachyon survived up to the present epoch as well as the future, its meta — mass would be

very much less than the rest mass of an electron which elegantly conforms to Nalikar's results.

2.12) SEARCHES FOR TACHYONS

2.12.1) INTRODUCTION

Theoretical controversies regarding the existence of tachyons rest on experimental questions. Although there is no consensus on the properties of tachyons which can be amenable to the experimentalist, several experiments designed to detect tachyons and based on their assumed properties have been carried out. Apparently, the most reliable method is to measure time of flight as this is fundamental to the particle's definition. Two further methods have been used. These are the search for the production of Cerenkov radiation by tachyons in a vacuum and the search for tachyon production in bubble chambers. Searches for tachyons associated with cosmic ray air showers have also been carried out and such an experiment is described by the author in chapter six.

2.12.2) INDIRECT METHODS

In the early stages of an expanding universe, distant regions of the universe are receding from each other at the velocity of light. Ordinary matter with $\beta \leq 1$ is bound by short particle horizons which prevents large scale communication in the early stages of a big — bang universe. Hence, there is a problem in understanding why the universe has been so homogenous and isotropic right from the very early stages.

2.12.2.1) M.H.COHEN et al (1977)

Making use of cosmological data obtained using very long baseline interferometry systems containing two to five radio telescopes, the brightness distributions from four extra-galactic sources (i.e; three quasars:3C345 , 3C273 , 3C279 and one galaxy 3C120) are investigated. They have shown that nearly half of strong compact extra-galactic radio sources represent a superluminal effect which appear to be expanding along a preferred direction with velocities in the range 4c to 10c. Various endeavours at explaining these phenomena without invoking the possibility of faster than light objects have been proposed (Blandford et al 1977). However, difficulties are encountered by all models since these sources seem to be primarily two components receding from each other along some preferred direction, rather than spherically symmetric expansions. More comprehensive measurements are required before the more popular explanations can be dismissed.

2.12.2.2) YU.M.ANDREYEV et al (1979)

A scintillation telescope was used for time of flight measurements and the time resolution determined. Particles with anomalous velocities were found and it was concluded that an upper limit on the intensity of penetrating particles with anomalous velocity $\beta>2$ was less than 8×10^{-12} $cm^{-2}.sec^{-1}.sr^{-1}$ at the 90% confidence level.

2.12.3) BUBBLE CHAMBER SEARCHES

As mentioned earlier (see 2.3.3) charged tachyons may

lose most of their energy in a fraction of a centimeter from the point of production (i.e; $\leqslant 10^{-2}$ cm). It may be practically impossible to utilize standard detection techniques to observe them directly. Therefore, one can employ some kind of missing-mass method in which the square of invariant effective mass of the tachyon (sometimes called missing mass squared) is measured. In this case, no direct observation of the tachyons is necessary. In fact, the tachyons should appear as particles with $m^2 \leqslant 0$.

2.12.3.1) C.BALTAY et al (1970)

Since the invariant mass squared of a single tachyon is always negative and similarly for a pair of tachyons, Baltay et al performed a search for uncharged tachyons produced singly or in pairs by the interactions of stopped negative kaons (K^-) and anti-protons ($\bar{P}$) with protons in a bubble chamber. Any events for which $m^2 \leqslant 0$ must contain at least one tachyon. The following reactions were investigated:

$$K^- + P \longrightarrow \Lambda^\circ + t^\circ \longrightarrow P + \pi^- + t^\circ \qquad (2.30)$$

$$K^- + P \longrightarrow \Lambda^\circ + t^\circ + \bar{t}^\circ \longrightarrow P + \pi^- + t^\circ + \bar{t}^\circ \qquad (2.31)$$

$$\bar{P} + P \longrightarrow \pi^+ + \pi^- + t^\circ \qquad (2.32)$$

$$\bar{P} + P \longrightarrow \pi^+ + \pi^- + t^\circ + \bar{t}^\circ \qquad (2.33)$$

Selection of reactions initiated by K^- or $\bar{P}$ at rest is based on two reasons:

(a) The energy and momentum of the initial state is

precisely known.

(b) The outgoing particles have relatively low energy and hence their momenta can be measured more accurately than at higher energies.

Both the K^- and $\bar{P}$ were captured at rest in hydrogen. The incoming energy and momentum (zero) were known , the energy and momentum of the resultant ordinary particles (Λ° and $\pi^\pm$ pairs) were measured. Then the energy and momentum of the remaining neutrals can be calculated, using energy and momentum conservation. If these neutrals are made up of ordinary particles then $E^2-p^2>0$, the presence of a tachyon or tachyon pair would be indicated by $E^2-p^2\equiv m^2<0$. The main experimental problem is a background of events in which the missing neutral is one or more π°'s. However, there is no evidence for tachyon production and the resulting production rates are given as:

$$\frac{K^- + P \longrightarrow \Lambda^\circ + t^\circ}{K^- + P \longrightarrow \Lambda^\circ + \pi^\circ} \leqslant 2\times10^{-3} \qquad \frac{\bar{P} + P \longrightarrow \pi^+ + \pi^- + t^\circ}{\bar{P} + P \longrightarrow 3\pi^\circ} \leqslant 2\times10^{-3}$$

$$\frac{K^- + P \longrightarrow \Lambda^\circ + t^\circ + \bar{t}^\circ}{K^- + P \longrightarrow \Lambda^\circ + \pi^\circ} \leqslant 2.5\times10^{-3} \qquad \frac{\bar{P} + P \longrightarrow \pi^+ + \pi^- + t^\circ + \bar{t}^\circ}{\bar{P} + P \longrightarrow 4\pi^\circ} \leqslant 1\times10^{-3}$$

It is seen that the rate for tachyon production is less than 10^{-3} of the rate for competing strong reactions. Finally, they concluded that if tachyons exist then they must be very weakly interacting with ordinary matter and the coupling constant for tachyon pair production, if non-zero, is also much smaller than any known elementary particle process.

2.12.3.2) J.S.DANBURG et al (1971,1972)

This work studied the interactions of 2.2 GeV/c K^- mesons in a bubble chamber and evidence for tachyon pair-production via the following reaction was searched for:

$$K^- + P \longrightarrow \Lambda^0 + t^+ + t^- \qquad (2.34)$$

In analysing the data it was assumed that:

(a) Charged tachyons of a given momentum follow curved paths in a magnetic field just as singly charged ordinary particles of the same momentum do.

(b) Only those tachyons which move with velocities close to that of light ($v \leq 1.7c$), can produce visible tracks in the bubble chamber (containing a hydrogen-neon mixture).

(c) Cerenkov radiation of the charged tachyons is suppressed so that it is not the dominant energy loss.

The upper limit on the cross-section for the production of charged tachyon pairs with invariant masses between 0.1 GeV and 1 GeV of $\simeq 2.10^{-31}$ cm^2 was determinded and no example of such a reaction was observed. Results of a later experiment were obtained from an examination of 5500 bubble-chamber pictures and a search was made for proton recoils without any incoming particle. In other words; two forms of tachyonic decay were searched for:

$$P \longrightarrow P + t \qquad (2.35)$$

$$P \longrightarrow P + t + \bar{t} \qquad (2.36)$$

where t has negative energy. None were found and the lower limit for the lifetime (τ) of unbound - protons for tachyonic decay via the reaction (2.32) or (2.33) is greater than about 2.10^{21} years. Mignani et al (1973c) asserted that the reinterpretation principle operates in such a way that, in any elementary interaction, a particle appearing in the final (initial) state as travelling backwards in time and with negative energy is equivalent to (and must be reinterpreted as) its anti – particle with positive energy and travelling forwards in time in the initial (final) state. Therefore, reaction (2.35) must be actually reinterpreted as:

$$p + \bar{t}^{+} \longrightarrow p \qquad (2.37)$$

where $\bar{t}^{+}$ is the positive energy anti—tachyon. Then, this experiment seems to look for examples of reaction (2.37) and not of reaction (2.35) or (2.36).

2.12.4) CERENKOV RADIATION SEARCHES

In spite of various objections regarding the production of Cerenkov radiation in vacuum by tachyons, some experiments have been carried out which establish limits for the production cross-section of tachyons.

2.12.4.1) T.ALVAGER et al (1968,1969)

Using the fact that it is kinematically possible for a system with any value of invariant mass squared to decay into a pair of tachyons, each having invariant mass μ, a search was carried out to detect charged tachyons presumed to be produced

by gamma — rays of several hundered KeV incident on a lead target. Following assumptions were made:

(a) Charged tachyons emit Cerenkov radiation which can be calculated analogously to that of ordinary charged particle in matter.

(b) Charged tachyons gain energy in an electrostatic field just as ordinary charged particles.

(c) Tachyons are not very likely to be captured in matter.

A 5 milliCurie cesium — 134 source of γ rays was used to hopefully produce tachyons. The detector consisted of two parallel plates between which an electrostatic field of 3 KeV/cm and a photomultiplier which looked at the region between the two plates. The plates were in a vacuum of approximately 10^{-6} torr. No obvious evidence for the existence of charged tachyons was observed. A limit on their charge was found between about 0.1 and 2 electron charges and the search placed an upper limit on the photoproduction cross section in lead of such particles of less than 3×10^{-30} cm^2 for photon energies of $\simeq$0.8 MeV which is approximately four orders of magnitude lower than the electron-positron pair production cross — section at energies of a few MeV.

A later experiment used a 129 milliCurie cobalt — 60 source producing γ rays of energy $\simeq$ 1.2 MeV. Two detectors were used. Each detector consisted of two parallel plates and a photomultiplier which looked at the region between the plates. The plates were in a vacuum of approximately 5.10^{-5} torr. Again a negative result was found. The cross — section for tachyon

photoproduction in lead by such photons is less than 1.67×10^{-33} cm^2 which holds for tachyons having charge in the range 0.5e to 1.9e. This limit is over eight orders of magnitude smaller than the cross section for the photoproduction of electron–positron pairs at the same energy. Since tachyons may exist with finite momentum and zero total energy, they can be produced with any mass with zero energy input. Hence, these upper limits do not depend strongly on the invariant mass of the particles.

2.12.4.2) D.F.BARTLETT et al (1972)

Since it is speculated that a tachyon might act as a magnetic monopole (see 2.10), Bartlett et al carried out an experiment to search for such objects. Presumably, such tachyons would be produced as a pair of north and south monopoles. Despite strong mutual attraction of the magnetic poles, they assumed that the monopole pair does not recombines immediately after its production and that the magnetic charge is conserved. Thus, an isolated tachyon monopole cannot be lost in a nuclear interaction. It may imply that it seems most likely that once a tachyon is isolated it will readily pass through matter. The same apparatus as the second experiment of Alvager et al was used but with a magnetic field replacing the electric field. From the negative result of the experiment, it was determined that the upper limit for the cross–section of tachyon monopole production by 1 MeV gamma–rays in lead and water were less than 0.6×10^{-36} cm^2 and 2×10^{-33} cm^2 respectively, which holds for tachyon monopoles having a magnetic charge between 1/10g and 4g.

Another investigation based on the possibility that tachyon monopoles strongly interact with nuclear matter rather than electromagnetic radiation was also performed. A 2 Curie plutonium – beryllium source emits fast neutrons. Some of these are thermalized in water and captured in cadmium. The cross section for the production of tachyon monopoles by thermal neutrons bombarding cadmium and water were found to be $\sigma(n - Cd) \leqslant 2\times10^{-26}\ cm^2$ and $\sigma(n - H_2o) \leqslant 3\times10^{-31}\ cm^2$ respectively.

2.12.4.3) D.F.BARTLETT et al (1978)

Assuming that tachyon monopoles will either emit Cerenkov radiation (detectable by eight photomultiplier tubes), or can ionize matter and thus leave etchable tracks in lexan plastic sheets, a search for tachyons in cosmic rays was carried out. They assumed that tachyon monopoles exist in the primary cosmic radiation striking the earth and that locally at Fermilab, they would be influenced by the extensive magnetic field of Fermilab's 15-ft bubble chamber. An upper limit on the tachyon monopole flux of $5\times10^{-12}\ cm^{-2}.sec^{-1}$ was found.

2.12.5) EXTENSIVE AIR SHOWER (E.A.S) SEARCHES

Searches for tachyons associated with extensive air showers make the following assumptions concerning their properties:

(a) They travel always faster than light. i.e; $\beta > 1$

(b) They will lose energy in a scintillator and give rise to photons or will be detectable by the production of secondary particles which can be detected.

(c) They can be produced in the interaction of very high energy cosmic ray primary particles at the top of the atmosphere and can pass through the atmosphere without significant absorption.

In the absence of a comprehensive theory of tachyons these assumptions are considered reasonable.

On average, a primary cosmic ray proton undergoes its first interaction at an atmospheric depth of ≃17.7Km above sea-level (≃80g.cm^{-2} atmospheric depth). If it has sufficiently high energy ($>10^{15}$eV) it will generate an extensive air shower in the atmosphere through hadronic and electromagnetic interactions. In the extensive air showers of the cosmic radiation, the resulting particles travel with velocities near or equal to that of light. The forefront of an extensive air shower forms a well — defined shower front and most of the particles arrive at sea-level with a time spread of only a few nano-seconds, Bassi et al (1953). Heavier particles trailing behind the shower front, which is the basis of some searches for particles with fractional charges (e.g; quarks) in cosmic radiation, arrive at a given location some time later than the electrons. If a tachyon — antitachyon pair is produced in the first interaction of the primary proton via $P+N \longrightarrow N+N+t+\bar{t}+$pions etc then the tachyons will arrive ahead of the shower front at sea level. The magnitude of the earliness depends on such details as the height of the point of production, energy and meta-mass (μ_0) of tachyons. One would expect the most likely tachyon production process to be a tachyon — antitachyon pair created with zero kinetic energy giving an infinite velocity, (see 2.3.2). For

large tachyon kinetic energies the velocity tends to the velocity of light. A tachyon produced in the first interaction of a primary proton with $v \longrightarrow \infty$ would arrive within a period of $\simeq 60\ \mu$sec before the shower front. For showers inclined at 60° (less than 1% of showers have zenith angles greater than 60°) this rises to $\simeq 120\mu$sec. For finite velocity tachyons (i.e; $v \neq \infty$) or for tachyons produced in secondary hadron interactions low in the atmosphere, the delay time would be smaller. The essence of the experiments is thus to record the occurrence of a potential tachyon signal and then look for the arrival of an air shower within a fixed time interval after the detection of the tachyon.

2.12.5.1) F.ASHTON et al (1970)

This experiment determined the velocity of a tachyon by measuring its time of flight over a certain distance and looked for values exceeding the speed of light. Two large scintillation counters (1 m^2) separated by 5.3m and viewed by single photomultiplier tubes were used. No evidence was found for the presence of particles travelling with velocities greater than 1.6c in cosmic rays at sea level. They were able to place an upper limit of less than 2.2×10^{-5} $cm^{-2}.sec^{-1}.str^{-1}$ at 90% confidence level on the flux of tachyons in the incoherent sea level cosmic radiation.

2.12.5.2) P.V.RAMANA MURTHY (1971)

In this experiment, a search for tachyons was made in the 20 μsec time interval between the arrival of a potential

tachyon and the subsequent extensive air shower. Basically, the procedure was to open a 20μsec long gate on the occurrence of a potential tachyon signal and then look for the arrival of an extensive air shower in the following 20 μsec. If the number of events detected in this way is greater than that expected by chance, the excess counts can only be due to tachyons. A potential tachyon signal was selected in two ways:

(a) From a photomultiplier tube looking at a liquid scintillator of dimensions 75cm $\times$ 75cm $\times$ 22cm. Neutral or charged ($t^{\circ}, t^{\pm}$) tachyons interacting with the scintillator medium would produce a potential tachyon signal.

(b) Using a method similar to Alvager et al (1968) where a coincidence was required from a pair of photomultiplier tubes, each 5cm diameter, viewing the air gap between two flat electrodes for the production of Čerenkov radiation caused by the charged tachyons.

The electric field between the aluminium plates was 2.1 Kv/cm. Extensive air showers were detected by a coincidence between the signals from four scintillators situated at the corners of a square of side 10m. The electron density requirement on each of them was $1 m^{-2}$ and the extensive air shower rate (i.e; trigger rate) was 20 min^{-1}. The time of operation was 5079 and 2597 hours for mode (a) and (b) respectively. Null results showed that the observed number of potential tachyons was not more than the expected number of events due to chance and also they were randomly distributed in the region 0-20μsec. It was concluded that the frequency of occurrence of tachyons associated with extensive air showers produced by primary

cosmic rays of energy $\geq 2\times10^{13}$ eV was less than 3×10^{-4} to 10^{-5} relative to that of electrons.

2.12.5.3) R.W.CLAY AND P.C.CROUCH (1974)

This work was similar to the experiment carried out by Ramana Murthy (1971) but the extensive air showers studied were almost two orders of magnitude more energetic. The search was made assuming that tachyons are produced in extensive air shower interactions at heights between 20Km and 40Km above sea level. The extensive air shower trigger was obtained from five plastic scintillators (1m×1m×0.005m) situated in a square array of side 30m, one scintillator being at each corner and one at the centre. Extensive air showers were detected by a coincidence between the central detector and any of three of the outer detectors. This gave a trigger rate of showers 7.2 hr^{-1} corresponding to a minimum cosmic ray shower energy of about 2×10^{15} eV. The output from an additional photomultiplier tube viewing one of the four outer scintillators was recorded by the digital transient recorder which digitised pulse heights to six bit accuracy. The method of analysis was to record the time of arrival of pulses in the 114 μsec time interval preceding the arrival of the shower front. The position of the largest pulse which occurs in this period was noted and then plotted on a histogram. They found the probability that random data (1839 events) and the extensive air shower data (1307 events) are from the same distribution is less than one in 10^4 on the basis of a chi—squared test. In other words; the resulting distribution was found not to be uniform. They then concluded

that non – random events, preceding the arrival of an extensive air shower, had been observed and that this was a result of particles travelling with an apparent velocity greater than that of light.

2.12.5.4) J.R.PRESCOTT (1975)

Prescott repeated Clay and Crouch's original experiments with the original apparatus. The work consisted of comparing the number of pulses in the 0 to 105 μsec time region previous to the shower front with that in the 105 to 210 μsec time region after the shower front with the shower front occurring at a relative time of 105 μsec. No excess of pulses were observed in the former interval and thus the time distribution of events was consistent with a uniform distribution which contradicted the previous results. The discrepancy was traced to the large overshoot generated in the digital transient recorder. In fact, any pulses in the first and second bins would be lowered if a large pulse (the shower front pulse) arrived just prior to them. This led to a deficiency in the number of pulses counted in these bins and hence to an erroneous chi-square.

Also an independent experiment which used a 50cm × 50cm × 10cm plastic scintillator, viewed by a two inch photomultiplier tube, located at 17.5m from the centre of the 'Buckland Park' array, was carried out. The signal to noise ratio was improved by two orders of magnitude, from 0.1 of the mean single particle energy release in the previous experiment to 5×10^{-4}. A total of 4315 showers with energies greater than about

5×10^{15} eV and 5715 randomly triggered events were recorded. In both the shower triggered and randomly triggered events , the time distribution of events was consistent with a uniform distribution. However, when allowance was made for a systematic apparatus effect , the statistical significance of an apparent excess of events preceding the arrival of an extensive air shower was much reduced. In fact, it was found that there is only a 4% chance that the results are consistent with a real tachyon flux. Hence, the experiments of Clay and Crouch and Prescott do not provide positive evidence for the existence of tachyons.

2.12.5.5) D.J.FEGAN et al (1975)

Following Clay and Crouch, Fegan et al carried out a search for tachyons arriving during the 420 μsec time interval prior to an extensive air shower front arriving at sea level. Showers were detected by $500cm^2$ $\times$ 0.5cm circular plastic scintillators placed at the vertices of an equilateral triangle of side 20m. To search for a potential tachyon signal a fourth $2500cm^2$ $\times$ 5cm scintillator viewed by two , five inch, photomltiplier tubes was located at the array centre. The outputs from both photomultiplier tubes were fed into discriminators and standard logic pulses generated. The shower rate was about 1 hr^{-1} which corresponded to a mean shower energy of 2×10^{15} eV. This energy is comparable with the energy of showers detected by Clay and Crouch but presumably with a larger spread of shower size, because of the smaller scintillator area. A 200 bit static shift register was used as

a delay device which contained the profile in time of detected events for the interval 420 μsec before the shower front to 380 μsec after it.

Two modes of operation (A and B) were used. In mode A coincidence events from 2469 showers were recorded and because of its high threshold energy ($\geq$1MeV) has a low event rate, i.e; 900 sec^{-1}. In mode B single events (i.e; an output from only one of the photomultipliers) from 1514 events were recorded. It has a threshold energy approximately equal to 0.5 MeV and hence its event rate was about six times greater than that in mode A. A statistical analysis of the interval 12 μsec and 408 μsec before the shower front based on a chi—squared were performed and represented no significant deviation from random expectation. At a mean energy (i.e; 2×10^{15} eV), the upper limits for the tachyon flux were determined as 2.06×10^{-2} $m^{-2}.sr^{-1}.hr^{-1}$ and 6.58×10^{-2} $m^{-2}.sr^{-1}.hr^{-1}$ for coincidence (A) and single (B) modes respectively.

2.12.5.6) M.W.EMERY et al (1975)

Following the report of a possible observation of tachyons by Clay and Crouch, Emery et al constructed an experiment at Hobart with shielding of 2 $g.cm^{-2}$ wood. In the first experiment, an array of four 1m $\times$ 1m trays, each with 24 Geiger — Muller counters, were set up with three evenly spaced on a circle of radius 21.2 m and one at the centre. The outputs from all Geiger-Muller tubes (96) were connected in parallel to an 18 bit shift register which allowed a time interval of 108 μsec to be recorded preceding the occurrence of the shower

front pulse. Air shower selection was such as to produce a rate of 14.9 per hour corresponding to an energy of about 10^{15} eV. 27449 showers were observed during which 3512 GM pulses preceded the shower front pulse in the 108 μsec time domain. A chi – squared test showed a 0.9 probability that the time distribution was the same as a uniform one.

In a second experiment, because of the possibility that tachyons preceding showers would not trigger Geiger – Muller tubes, but may have the capability of producing pulses in scintillators, they installed a 2.5cm deep, 75cm diameter liquid scintillator viewed by a photomultiplier tube near the centre of the array. In this case, the pulses from the photomultiplier tube were fed into the shift register, instead of the pulses from the Geiger – Muller tube. The system was set to record pulses greater than 0.1 of that produced by a relativistic muon traversing the scintillator. 3766 precursor pulses from the photomultiplier tube were seen in 9521 showers. It was concluded that the frequency distribution of the precursor times in the 108 μsec time preceding the arrival of the extensive air shower fronts showed no evidence for a significant flux of tachyons.

2.12.5.7) W.E.HAZEN et al (1975)

This is a very similar experiment to that of Clay and Crouch and studied the 160 μsec preceding the shower front. The tachyon detectors consisted of plastic scintillators of dimensions 1.2m × 1.2m × 0.38m. The trigger condition was designed to be about the same as that of Clay and Crouch. The

trigger rate of showers was 10 hr^{-1} using three scintillation counters situated at the apices of a 30m triangle. The array covers a little less area than the 30m square used by Clay and Crouch and this implies that the effective minimum shower energy (1.5×10^{15} eV) was somewhat less than theirs. Two runs were considered. The first run consisted partly of using two detectors and partly using one in which the net running time was 104 hrs for 1039 showers. The random trigger was generated by very small showers. The number of largest pulses detected in the interval prior to the shower front was compared with that from a run using a random trigger. Statistical analysis showed that the probability that the two distributions are not samples of the same population is only $\simeq 0.01$. Thus, it gave no evidence for precursors. The second run involved the use of two detectors placed one above the other and the photomultiplier voltages were raised. The net running time was 197 hrs for 2366 showers. The time-frequency distribution of coincident pulses in the 160 μsec prior to the shower front were found. A chi-squared test indicates that the results are satisfactorily represented by a flat distribution. They concluded that the upper limit to the flux of tachyons at sea-level, associated with extensive air shower of size $\simeq 10^5$ is 10^{-8} $cm^{-2}.sec^{-1}.sr^{-1}$. This implies a cross section for the production of tachyons by $P+N \longrightarrow N+N+t+\bar{t}+$pions of less than 60 times the total proton-nucleus cross section.

2.12.5.8) G.R.SMITH et al (1977)

A search for tachyons was made in the 290 μsec time

domain preceding the arrival of an extensive air shower. The experiment was operated inside a steel building with a $\simeq 7$ g.cm^{-2} thick roof situated at an elevation of 236m above sea — level. Air showers were detected by an array of three detectors of dimensions 90 cm $\times$ 90cm $\times$ 1.27cm in which each was viewed by a single five inch photomultiplier tube. The array was sensitive to showers of energy greater than $\simeq 6\times10^{14}$ eV corresponding to a trigger rate of showers of $\simeq 10^{-2}$ sec^{-1}. A potential tachyon signal was defined by a large cosmic ray telescope which contained five plastic scintillators of area 0.7 m^2. Each element could allow the registration of any signal depositing more than one fifth the energy deposited by a singly charged relativistic particle and it detected charged particles at a rate of 27.5 sec^{-1}. The apparatus was run for 223 days during which numerous checks on the stability of the detecting system were carried out. 204702 showers were recorded and a total of 1519 ± 39 tachyon candidate events were observed. When the number of expected coincidences (1473 ± 11) were subtracted an excess of 46 ± 40 events were found. They concluded that this observed excess does not constitute statistically significant evidence for the observation of tachyons and an upper limit of $\simeq 6\times10^{-4}$ can be set on the ratio of tachyons to electrons among air shower particles.

2.12.5.9) F.ASHTON et al (1977)

The 240 μsec time interval before the arrival of a shower front was studied and the search was carried out at sea-level. The extensive air shower trigger was obtained by a four-

fold coincidence of the form $\triangle_c(\geq 3.5)$, $\triangle_{13}(\geq 1.5)$, $\triangle_{33}(\geq 1.5)$, $\triangle_{53}$ (≥ 1.5). The numbers in brackets refer to the minimum electron density requirement from each plastic scintillator. i.e; the threshold densities per m^2. The area and thickness of plastic scintillators 13, 33, 53 and C are $2m^2 \times 2.5cm$ and $0.75m^2 \times 5cm$ respectively. The array was sensitive to showers of energy greater than $\simeq 10^{15}$ eV corresponding to a trigger rate of showers of $(8.53 \pm 0.46)hr^{-1}$. The tachyon detector consisted of a layer of scintillation counters, each of thickness 5cm, with a total sensitive area $2.1m^2$. From top to bottom the equipment comprised a layer of 15cm of lead, 8 layers of neon flash tubes, 15cm of iron, the tachyon detection scintillator and 108 layers of flash tubes. Pulses from the tachyon detection scintillator were added, passed through a 240 μsec delay line and displayed on an oscilloscope which was triggered on the occurrence of an air shower. In this way the ionisation loss of particles traversing the tachyon detection scintillator in the 290 μsec time interval preceding the arrival of an air shower were recorded. In addition, the air shower trigger also applied a high voltage pulse to the neon flash tubes after a time delay of 20 μsec which were photographed. The total running time was 40 hours in which 341 showers were detected. Among them, six precursors were observed with pulse heights greater than three times the height of that due to a relativistic muon. These all occurred in the time interval $0-120$ μsec before the arrival of the air shower front with none in the further $120-240$ μsec. No anomalous tracks in the flash tubes were seen to be associated with these events. The expected number of such pulses was

calculated to be 0.81 which is much less than the observed number. A chi – squared test gave a probability of 4.5×10^{-6} that six events would occur in this region and none in the 120 to 220 μsec region. However, they concluded that the results indicated a possible finite flux of tachyons. Obviously, better statistics were required to established whether the effect is real or not. An explanation of the details of the layout of the Durham E.A.S array can be found in Smith's thesis (1976).

2.12.5.10) P.N.BHAT et al (1979)

They carried out an experiment at 2300m above sea – level to search for tachyons with an experimental arrangement very similar to that described previously. The air shower array used had 20 density detectors (plastic scintillators) and four timing detectors (liquid scintillators). The tachyon detector consisted of two plastic scintillation detectors each 80 cm × 80 cm × 1 cm, located in a stack of 14 $g.cm^{-2}$ iron plates which forms the multi — plate assembly of a large cloud chamber. A 48 $g.cm^{-2}$ layer of lead shielded the chamber from low energy particles. Each of two plastic scintillators was coupled to a photomultiplier tube. The output signal from each of these scintillation detectors was discriminated at the three muon level. The aparatus was run in two modes:

In the first mode, two scintillators were operated in coincidence. The potential tachyon signal in this experiment could be due either to the passage of the tachyon itself interacting in some manner and producing the required signals in both detectors or to a hadron produced by the tachyon in an

interaction in the atmosphere. Following each potential tachyon signal a time interval of 1—401 μsec was scanned for the arrival of an air shower. The rate of air showers was 12 hr^{-1} corresponding to a minimum primary energy of about 6×10^{14} eV. 20988 showers were observed in an effective operating time of 1749 hours and only four events were observed compared to the number of seven chance events expected. Thus, there were no excess of events.

In the second mode, only one detector was operated. The trigger was adjusted and gave a rate of showers of 42 hr^{-1} corresponding to a minimum primary energy of about 3×10^{14} eV. 78624 showers were recorded for an effective running time of 1872 hours and only twenty seven events occurred in comparison with thirty one expected. The observed events were also distributed uniformly over the time interval. Thus, the observations were consistent with the random coincidence expectation. Under the assumption that tachyons produced in high energy interactions have interaction characteristics amenable to detection, they gave upper limits on the flux of tachyons, the production cross-section for tachyons in P—P collisions and the tachyon to hadron ratio, at the 95% confidence level as 2.3×10^{-10} $cm^{-2}.sec^{-1}.sr^{-1}$, 4.2×10^{-26} cm^{-2} and 3.3×10^{-4} respectively.

2.12.5.11) F.ASHTON et al (1979)

Extensive air showers were selected by an array of four plastic scintillators 13,33,53, and C as described previously. The coincidence requirement used was $\Delta_{13}(>4.2\ m^{-2})$, $\Delta_{33}(>4.6\ m^{-2})$,

Δ_{53}($\geq$4.6 m^{-2}) and Δ_{C}($\geq$20.2m^{-2}) which gave a trigger rate of 4.3 hr^{-1} corresponding to a minimum cosmic ray shower energy of about 2.5×10^{15} eV. 1107 showers were recorded. One unshielded plastic scintillator of dimensions $2m^2 \times 0.05m$ was used as the tachyon detector. The electronic system used to display pre-shower pulses of decay time 20 μsec occurring in the tachyon detector consisted of three sections of delay line giving an overall delay of 264 μsec, the output pulse from the delay lines being displayed on an oscilloscope and photographed. The extensive air shower front pulse was preceded by a hump pulse of width 80 μsec and a region of high frequency oscillation which extended for a region of 20 μsec prior to the arrival of the extensive air shower front pulse and both were instrumental in nature. It was found that the hump is not serious in reducing the efficiency of detecting previous particles but the high frequency oscillation which occupies the 20 μsec time domain prior to the extensive air shower pulse can be. Thus, the range 20—260 μsec was investigated. Comparing the number of events observed in the region 20—120 μsec with the number observed in the region 120—220 μsec using a chi—squared test and its probability, there was no evidence for a significant excess of events in the first 100 μsec interval where real tachyons are expected to occur. Also, in a further endeavour to testing the data for anomalous behaviour there was found to be good agreement between the integral rate of pulses of height>V mV produced by the tachyon detector using an amplifier, discriminator and scaler with that obtained from the oscilloscope measurements. Hence again they concluded that the

frequency distribution of events was flat over the related time domain with no evidence for a significant flux of tachyons.

2.12.5.12) D.J.FEGAN et al (1981)

Fegan et al carried out an experiment to search for tachyons in which the following tactics were adopted:

(a) The trigger threshold energy of air showers was increased by more than a factor of ten on previous searches to reduce the dilution effect of many lower energy shower triggers.

(b) The exposure time was made longer (9768 hours) than previous experiments in order to obtain a reasonably large statistical sample at the higher threshold.

The tachyon detection system which was shielded by 25 cm concrete and an additional 15 cm of lead consisted of a $0.5m^2 \times 0.025m$ rectangular sheet of plastic scintillator and the top surface of that was viewed by two photomultiplier tubes each of five inches diameter. The signals from both tubes were linearly summed and fed to a transient recorder. This allowed a period of 480 μsec before the shower to 24 μsec after to be recorded. Extensive air showers were selected by using three circular plastic scintillators each of 0.05 m^2 area located at the vertices of an equilateral triangle of side 20m and the tachyon detector was located at its centre. The minimum shower energy required to trigger the system was 3×10^{16} eV, which corresponds to a shower detection rate of 0.17 hr^{-1}. A total of 1673 shower triggers were recorded. Random triggers were injected throughout the experiment as a system check and also to

generate a comparison data set. Amplitude integrated histograms were produced, both for the real data and the random data. Grouping the data into 12 bin histograms with each time cell corresponding to 40 μsec revealed no significant excess of events. However, on the basis of 960 bins each with width 0.5 μsec, the resulting histogram showed an excess of events in the 48 to 60 μsec region prior to the arrival of the air shower front. The conclusion was that the apparent excess of events in this region is not inconsistent with tachyons but could also be caused by the disintegration of cosmic radiation nuclei in the field of solar photons leading to the production of correlated air showers in the atmosphere, the arrival time of one of the showers at the earth being later in time than the other.

2.13) SUMMARY

The existence of tachyons has been shown to be still very much open to doubt. Various endeavours to form a reasonable, theoretical and comprehensive theory from which their interactions and properties can be formulated are also found to be somewhat confused. The problems are basically:

(a) The mechanism of tachyon production.

(b) The methods that should be used to detect them.

For bubble — chamber searches at accelerators, the only conclusion that one can draw is that tachyons are not easily produced (probably due to a high energy production threshold), or their interactions with matter are so weak that they cannot be detected. Although further searches for tachyons by the technique of Cerenkov radiation could be interesting it is

believed that tachyons do not emit Cerenkov radiation, at least in a vacuum. Cosmic ray searches are summarised in table 2.1 and permit a higher production energy threshold to be studied. From the arguments of Lemke (1975 , 76 , 76a , 76b) , (e.g; see sections 2.3.3 and 2.9.2.1), any electromagnetic interactions between a tachyon and ordinary matter must take place in a narrow angle along the tachyon's trajectory. Hence in order to observe a tachyon directly a dense (i.e; solid) ionization detector is required. If tachyons cannot be detected directly, but only through the secondaries from their interactions with ordinary matter , a dense target is required (e.g; lead or iron), in order that the chance of such an interaction is increased. It seems that the extensive air shower technique is one of the most promising existing methods of search.

Experiment	Altitude of expt. ($g\ cm^{-2}$)	Min. Primary energy (eV)	Area of detector (m^2)	Shielding	Run time (hr)	No. of showers	Min Pulse height detectable (e)
RAMANA-MURTHY (1971) MODE 1	800	$3\ 10^{13}$	0.75	-	5079	$6.1\ 10^{6}$	
MODE 2					2597	$3.1\ 10^{6}$	
CLAY & CROUCH (1974)	SL	$2\ 10^{15}$	1.0	-	181	1307	0.1
PRESCOTT (1975)	SL	$5\ 10^{15}$	0.25	-	~600	4315	$5\ 10^{-4}$
FEGAN (1975) MODE A	SL	$2\ 10^{15}$	2.5	-		2649	0.1
MODE B						1514	0.05
EMERY (1975) EXPT 1	SL	$\sim 10^{15}$	4(GM tubes)	-	1840	27449	0.36
EXPT 2			0.44		640	9521	0.1
HAZEN (1975) RUN 1	SL	10^{15}	2.16	-	104	1039	0.05
RUN 2			1.44		197	2366	0.02
SMITH & STANDIL (1977)	SL	$6\ 10^{14}$	~0.7	$7 gcm^{-2}$ steel	4695	204702	0.2
ASHTON et al (1977)	SL	10^{15}	2.1	$170 gcm^{-2}$ Pb $118 gcm^{-2}$ Fe	40	341	3.0
BHAT (1978) MODE 1	800	$6\ 10^{14}$	1.28	$45 gcm^{-2}$ Pb $112 gcm^{-2}$ Fe	1749	20988	3.0
MODE 2		$3\ 10^{14}$			1872	78624	
ASHTON et al. (1979)	SL	10^{15}	2.0	-	1660	6461	0.35
FEGAN (1981)	SL	10^{16}	0.5	-	9768	1673	<1

Table 2.1 : Summary of EAS searches for tachyons. (e is the pulse height due to a single electron)

CHAPTER THREE

SOME ASPECTS OF SCINTILLATION COUNTERS

3.1) INTRODUCTION

The excitation and ionization of the molecules of a material which is produced by the passage of a fast charged atomic or nuclear particle, is the basis of all the major instruments for the detection and measurement of such particles. The problem of the calculation of the ionization energy loss is usually solved by dividing the collisions into two distinct classes. In the close collisions, the impact parameters are small, with comparison to the atomic dimensions, and hence the electrons taking part in the collisions can be regarded as free. In fact, it may indicate that a close collision between a particle and an atomic electron is not essentially different from a collision between a charged particle and a free electron. In the second case, the distant collisions, the impact parameters are large and the binding of the electrons to the atoms must be taken into account. The various types of detection instrument differ in the material within which the ionization is produced, and in the manner by which it is observed. When the incident particle of energy, E, impinges on certain liquid or solid materials known as phosphors, which possess the property of luminescence, part of the energy dissipated in molecular excitation and ionization is re — emitted as visible or ultra — violet photons. In a non — luminescent material, almost the whole of the expended energy for

ionizing, exciting and dissociating the molecules of the phosphor is ultimately transferred into thermal energy and the molecules return to the normal state by radiationless transitions. The observation and measurement of such light scintillations produced in phosphors is the basis of the scintillation counter instrument. In its original visual form of a thin zinc sulphide screen vived by eye using a microscope, it played a major role in the development of classical nuclear physics. However, this arrangement was insensitive to beta-rays and gamma-rays, because of the weak ionization which they generate in the thin phosphor screen. After the development of photomultiplier tubes which are sensitive to very small light intensities, the scintillations from the phosphor were converted into amplified electrical pulses at the multiplier output. Hence, in addition to the detection and energy measurement of many ionizing particles, it made possible the detection and spectroscopy of gamma-ray and X-ray quanta with relatively high detection efficiency.

Uncharged radiations, X and gamma-ray quanta and neutrons, do not ionize directly but they can transfer some part of their energy to individual charged particles (e.g; electrons) within the phosphor and the ionization produced by these secondary particles give rise to the scintillations. In fact, the energy transformation of such quanta to electrons can be accomplished by three processes:

(a) Photo-electric absorption which can be produced by the interaction of a photon with an atomic electron.

(b) Compton scattering can be produced by the

interaction of a photon with an electron in which the photon transfers part of its energy and momentum to the electron.

(c) Pair-production which arises from the interaction of a photon with the Coulomb field of the nucleus.

The magnitudes of the related absorption coefficients depend on the energy of the incident radiation and the density of the phosphor. Thus, the energies of the secondary electrons produced within the phosphor depend on their production process.

3.2) DYNAMICS AND PROBABILITY OF COLLISION

3.2.1) DYNAMICS OF THE COLLISION

Consider the collision between a particle of mass M and momentum p with an electron, assumed to be initially at rest, of mass m_o. By using the principles of conservation of energy and momentum, the energy of recoil of the electron, E', ejected at an angle θ to the direction of the incident particle is given by:

$$E' = 2m_o c^2 \frac{p^2c^2\cos^2\theta}{[m_o c^2 + (p^2c^2 + M^2c^4)^{1/2}]^2 - p^2c^2\cos^2\theta} \qquad (3.1)$$

The maximum transferable energy corresponds to a "head-on collision" (i.e; $\theta = 0$) and has the value:

$$E'_m = 2m_o c^2 \frac{p^2c^2}{m_o^2c^4 + M^2c^4 + 2m_o c^2 (p^2c^2 + M^2c^4)^{1/2}} \qquad (3.2)$$

For heavy particles with very large momenta (i.e; $p \gg \frac{M^2c}{m_e}$) equation (3.2) can be reduced to:

$$E'_m \simeq p.c \simeq E \tag{3.3}$$

In fact, it implies that a very high energy heavy particle (e.g; meson) might be stopped by a "head-on collision" with an electron. On the other hand, for heavy particles with sufficiently small momenta (i.e; $p \ll \frac{M^2c}{m_e}$) the maximum transferable energy depends only on the velocity and is given by:

$$E'_m \simeq 2m_e c^2 \left(\frac{p}{Mc}\right)^2 \simeq 2m_e c^2 \frac{\beta^2}{1-\beta^2} \tag{3.4}$$

3.2.2) PROBABILITY OF COLLISION

When a particle of charge ze passes through a medium of atomic number Z and atomic weight A, it will pass the atoms at a wide variety of impact parameters and the probability of collision will increase with the thickness of the medium traversed and with its density. When the energy transfer E' is small compared with E'_m , an approximate relation for the differential probability of a particle transferring an energy E' to an electron is expressed by the Rutherford formula:

$$\Phi(E, E')\, dE' = \frac{2Cm_e c^2 z^2}{\beta^2} \times \frac{dE'}{E'^2} \tag{3.5}$$

where $C=0.150Z/A$ $cm^2 . g^{-1}$ which represents the total area covered

by the electrons contained in one gram, each considered as a sphere of radius $r_o \simeq \frac{e^2}{m_o c^2}$.

When the energy of the "knock-on" electron is high (i.e; $E \gg m_o c^2$), the spin of the incident particle is important at the small impact parameters involved. Differential collision probabilities for different kinds of incident particle have been calculated as follows:

For electron-electron collisions; Moller (1932)

$$\Phi(E,E')dE' = 2C\frac{m_o c^2 E^2 dE'}{(E-E')^2 E'^2}\left[1-\frac{E'}{E}+\left(\frac{E'}{E}\right)^2\right]^2 \qquad (3.6)$$

For positron-electron collisions; Bhabha (1936)

$$\Phi(E,E')dE' = 2C\frac{m_o c^2 E^2 dE'}{(E-E')^2 E'^2}\left[1-\frac{E'}{E}+\left(\frac{E'}{E}\right)^2\right]^2 \times \left[1-2\frac{E'}{E}+2\left(\frac{E'}{E}\right)^2\right] \qquad (3.7)$$

The additional factor, $[1 - 2E'/E + 2(E'/E)^2]$ arises from the fact that exchange phenomena have different effects in an electron-electron and in a positron-electron collision.

For a particle of mass M and spin=0 , Bhabha (1938)

$$\Phi(E,E')dE' = \frac{2Cm_o z^2 c^2}{\beta^2} \times \frac{dE'}{E'^2}\left(1-\beta^2\frac{E'}{E'_m}\right) \qquad (3.8)$$

For a particle of mass M and spin=1/2 , Corben et al (1939)

$$\Phi(E,E')dE' = \frac{2Cm_o z^2 c^2}{\beta^2} \times \frac{dE'}{E'^2}\left[1-\beta^2\frac{E'}{E'_m}+\frac{1}{2}\left(\frac{E'}{E+Mc^2}\right)^2\right] \qquad (3.9)$$

For a particle of mass M and spin=1 , Oppenheimer et al (1940)

$$\Phi(E,E')dE' = \frac{2\pi m_e z^2 c^2}{\beta^2} \times \frac{dE'}{E'^2} \left[\left(1-\beta^2 \frac{E'}{E'_m}\right)\left(1+\frac{1}{3}\times\frac{m_e E'}{M^2c^2}\right) + \right.$$

$$\left. \frac{1}{3}\left(\frac{E'}{E+Mc^2}\right)^2 \times \left(1+\frac{1}{2}\times\frac{m_e E'}{M^2c^2}\right)\right] \qquad (3.10)$$

As long as $E' \leq E$, equations (3.9) and (3.10) reduce to (3.8) which means that the collision probability of a heavy particle is independent of the spin. When E' is comparable with E, the collision probability is an increasing function of spin. However, the influence of the spin on the collision probability manifests itself only for very close collisions.

3.3) IONIZATION ENERGY LOSS AND THE DENSITY EFFECT

3.3.1) IONIZATION ENERGY LOSS

As a charged particle moves through matter, some part of its energy is deposited in the form of ionization and excitation of the medium. The average rate of ionization energy loss (i.e: stopping power) of electrons of kinetic energy T (MeV) and other heavy particles can be calculated, in MeV/g.cm^{-2}, by the well-known Sternheimer formula (1952,1953) respectively as:

$$\bar{E}_e = -\frac{1}{\rho}\times\frac{dE}{dx} = \frac{A_e}{\beta^2}\left[B + 0.43 + 2\mathrm{Ln}\frac{p}{m_e c} + \mathrm{Ln}\, T_{Mev} - \beta^2 - \delta(\beta) - U\right] \qquad (3.11)$$

and

$$\bar{E} = -\frac{1}{\rho}\times\frac{dE}{dx} = \frac{A_e}{\beta^2}\left[B + 0.693 + 2\mathrm{Ln}\frac{p}{Mc} + \mathrm{Ln}E'_m - 2\beta^2 - \delta(\beta) - U\right] \qquad (3.12)$$

where

$$A_0 = \frac{2\pi e^4 z^2 n}{m_0 c^2 \rho} = 0.1536 \frac{Z.z^2}{A} \text{ in } \frac{MeV}{g.cm^{-2}} \quad \text{and} \quad B = Ln\left[\frac{m_0 c^2 (10^6 eV)}{I^2(Z)}\right]$$

In the above equations, n is the number of electron per cm^3 (i.e; electron density), ρ is the density of the substance in $g.cm^{-3}$, I(Z) is the average ionization potential of the medium, $\delta(\beta)$ is the density effect term. U is the shell correction term which arises because electrons in different shells of the stopping atoms do not contribute equally to the stopping power and is a small quantity for particles passing through a medium composed of relatively low atomic number, Walske (1952,1956). The other symbols have the same meaning as before. The difference between the average loss of energy for electrons and heavy particles is due to the close collisions. In transparent materials, part of the energy dissipated by high energy particles in their interactions with atomic electron goes into Cerenkov radiation in which the intensity of Cerenkov radiation increases with increasing velocity. The previous equations include the energy loss due to Cerenkov radiation. It has been shown, Sternheimer (1953), that Cerenkov loss will decrease with increasing atomic number and thus it can be very small in comparison with the relativistic rise of the ionization loss for condensed materials. Using data calculated by other physicists, Sternheimer (1956,1966) has represented the expression regarding the average ionization potential of media of $Z \gg 13$ by:

$$\frac{I}{Z} = 9.76 + 58.8\, Z^{-1.19} \quad eV \qquad (3.13)$$

For the case of compounds , the value of the average ionization potential is given by the logarithmic average of the I values of the constituent atoms:

$$\ln I = \sum_i f_i \ln I_i \qquad (3.14)$$

where f_i (oscillator strength) is the fractional number of electrons of the ith atomic species with excitation potential I_i . Figure 3.1 represents schematically the average ionization energy loss as a function of momentum.

3.3.2) DENSITY EFFECT

The reduction in the ionization loss of charged particles due to the density effect of the medium was first treated by Fermi (1940). As long as a charged particle travels in a gas or in a condensed material, it is possible to consider the atoms as isolated only in the case of close collision, i.e; the close collisions are not affected by the density of packing of the atoms. But, it is not applicable when the impact parameter is larger than the atomic distances. As the impact parameter of the distant collisions is increased , a stage will be reached where the atoms between the interacting atom and the particle will exert a shielding effect and greater impact parameters will not result in energy being transferred. Hence, one has to take into account the screening of the electric field of the passing particle by the atoms of the medium. In fact , the screening reduces the interaction and then decreases the energy loss of the incident particle. The density correction to be applied to the expression for the average

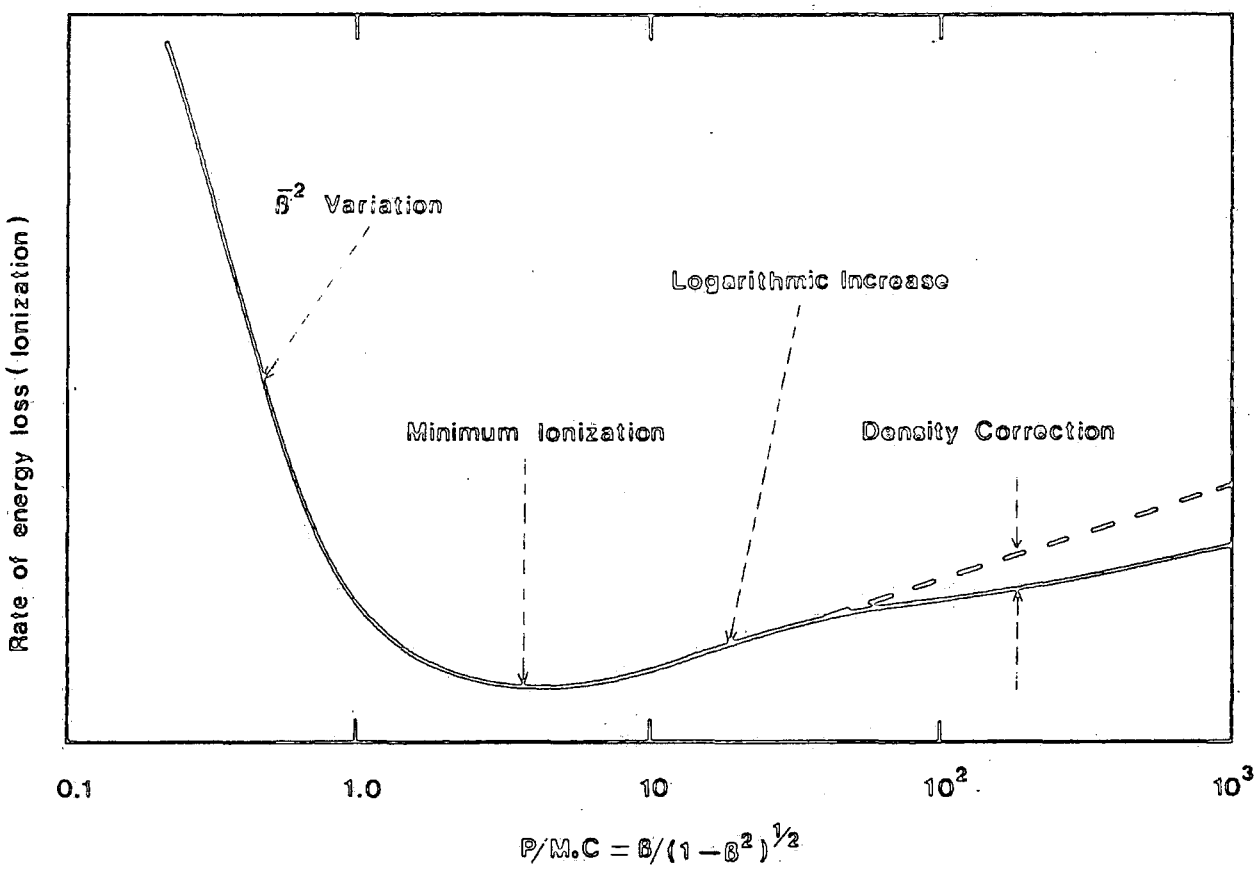

Figure 3.1 The form of the variation of rate of average energy loss with momentum.

energy loss is an increasing function of the velocity. The expression suggested by Sternheimer (1967) which is a relevant approximation of the density effect is given as:

$$\delta = 4.606X + C + \alpha(X_1 - X)^m \quad \text{for} \quad X_0 < X < X_1 \tag{3.15}$$

$$\delta = 4.606X + C \quad \text{for} \quad X > X_1 \tag{3.16}$$

with $X = \text{Log}_{10}\frac{p}{M_0 c} = \text{Log}_{10}\beta.(1-\beta^2)^{-1/2}$

C, α, m, X_0 and X_1 are constants which are characteristic of the substance considered. Indeed, X_0 is the value of X which corresponds to the momentum below which $\delta(\beta)=0$ and X_1 corresponds to the momentum above which the relation between δ and X can be considered to be linear. It may indicate the linearity of δ at large energies. In the above equation, the constant C is given by:

$$C = -2\text{Ln}\left(\frac{I}{h\nu_p}\right) - 1 \tag{3.17}$$

where ν_p is defined as:

$$\nu_p = \left(\frac{ne^2}{\pi m_e}\right)^{1/2} \tag{3.18}$$

Table 3.1 gives the values of these constants for NE102A plastic according to Crispin et al (1964).

3.4) STATISTICAL FLUCTUATIONS AND THE MOST PROBABLE ENERGY LOSS

Since the energy lost by a fast heavy charged particle passing through matter is the result of a large number of independent (i.e; discrete and random) events, the process is a statistical phenomenon. Particles of a given kind and of a

Constant Coefficients	Values		
Constituent elements	$_{1}H^{1}$	0.525×10^{23}	Atoms.cm^{-3}
	$_{6}C^{12}$	0.475×10^{23}	Atoms.cm^{-3}
	$_{7}N^{14}$	0.180×10^{19}	Atoms .cm^{-3}
	$_{8}O^{16}$	0.180×10^{19}	Atoms .cm^{-3}
Density ; ρ	1.032	g.cm^{-3}	
A_o	0.833	MeV/g.cm^{-2}	For muons
Stopping number ; B	18.69		
I	62.60	eV	
C	-3.13		
α	0.514		
m	2.595		
X_o	0.044		
X_1	2		

Table 3.1 Chemical composition and values of useful constants for the plastic scintillator NE 102A according to Crispin et al. (1964).

given energy do not all lose exactly the same amount of energy in traversing a given thickness of material and no unique value for energy loss is obtained. The probability of energy loss, E', in a single collision with an electron is proportional to E'^{-2} (e.g; see equation 3.8). Thus, collisions resulting in a large energy transfer to an electron are relatively infrequent in comparison with small energy transfer collisions. Although they are relatively infrequent, the large energy transfer collisions account for a significant proportion of the total energy loss and contribute a tail to the energy loss distribution.

The shape of the distribution is a characteristic of two parameters E'_m and ξ. The parameter ξ is chosen so that on the average just one collision transferring more energy than ξ occurs in the pathlength considered.

$$\xi = \frac{A_0 t}{\beta^2} \tag{3.19}$$

where t is the thickness of the absorber in $g.cm^{-2}$. The actual shape of the distribution depends on the ratio of these two parameters, K, as:

$$K = \frac{\xi}{E'_m} \tag{3.20}$$

K may be thought of as an estimate of the number of large energy loss collisions suffered by the particle in traversing an absorber. The quantity E'_m is the maximum possible energy transfer which is given approximately in heavy patricle-electron collision by equation (3.4). When $K>1$, the number of collisions in each collision energy interval is large and the

effect of fluctuations negligible. Bohr (1915) showed that the energy loss probability distribution is approximately Gaussian with a variance given by:

$$\sigma = 4\pi z^2 n x \qquad 3.21$$

When K<0.01 , the number of collisions in the highest collision interval is small. i.e; very few collisions take place in the absorber and on average only one in which an energy greater than ξ is transferred. In this case, the distribution of total energy losses is highly asymmetric , Landau 1944 , with a broad peak around the most probable energy loss (E_p) and a long tail corresponding to higher energy losses. The most probable energy loss , which corresponds to the peak of the measured experimental distribution , is significantly less than the average energy loss ($\bar{E}$) and is given by:

$$E_p = \frac{A_o t}{\beta^2}\left[B + 0.891 + \ln\frac{p}{Mc} + \ln\frac{A_o t}{\beta^2} - \beta - \delta(\beta) - U\right] \qquad 3.22$$

The difference between mean and probable energy loss is related to the close collisions , for which no density effect (δ) is involved. Two further conditions for the validity of the Landau theory have been given by Maccabee (1968). First, if ϵ_o is approximately the mean binding energy of the atomic electrons then $\xi \gg \epsilon_o$, hence the theory breaks down in the limit of a very thin absorber. Second, the collision spectrum must be directly proportional to E'^{-2}. Both E_p and $\bar{E}$ have been evaluated , figure 3.2, for NE102A plastic scintillator ($t=5.16 g.cm^{-2}$) as a function of the velocity of incident muons where the constants in

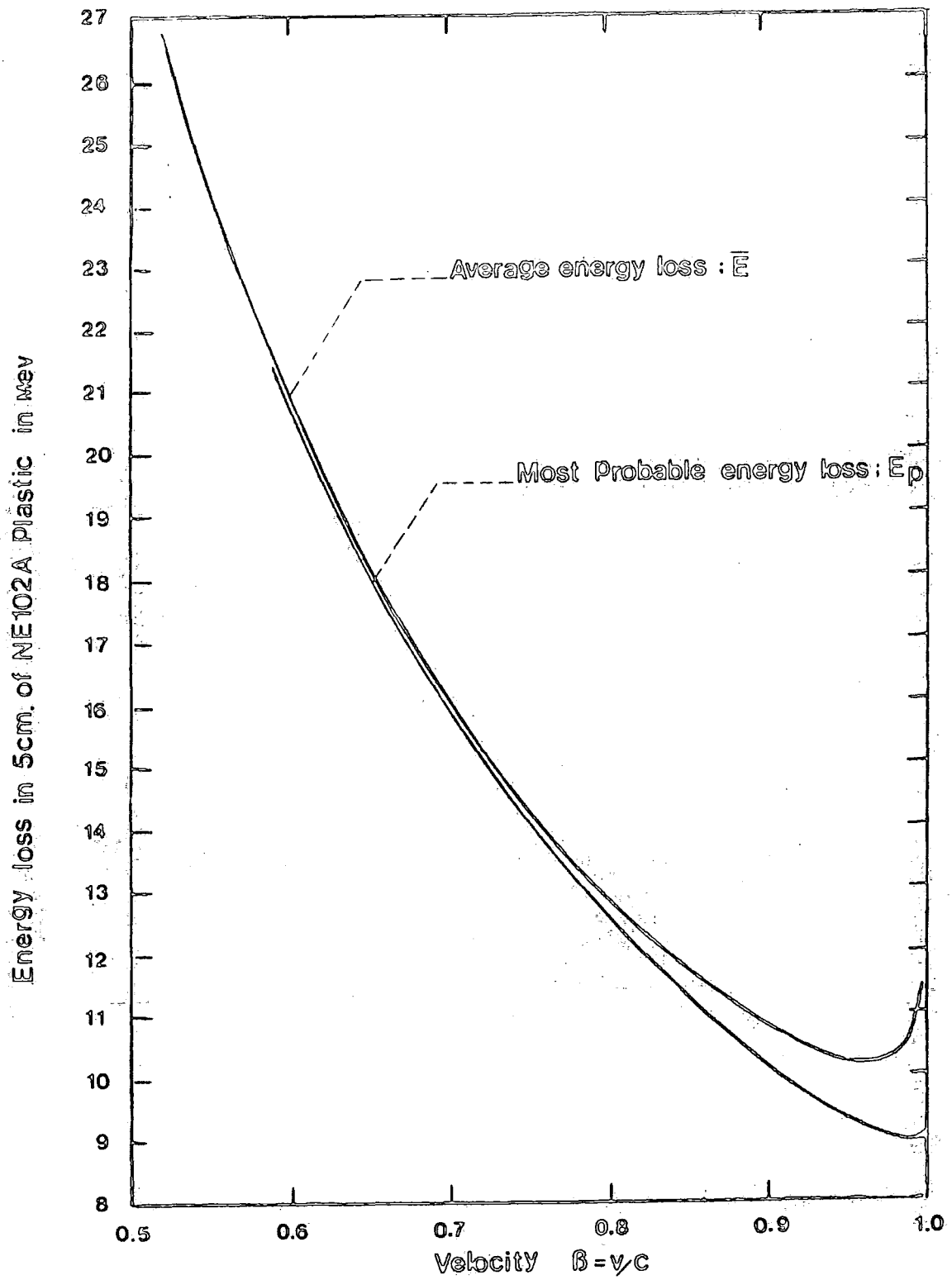

Figure 3.2 The average (upper curve) and most probable (lower curve) energy loss in 5 cm of NE 102A as a function of the velocity of the incident particle.

equations (3.12) and (3.22) are obtained from table (3.1). The intermediate case, $0.01<K<1$, was investigated by Symon (1948) who was able to link approximately the Gaussian and Landau regions for the following conditions:

$$M >> m_e \quad \text{and} \quad Mc^2 \leqslant T \leqslant 10Mc^2$$

where T is the kinetic energy of the incident particle. The complete solution of the energy loss probability distribution function has been given by Vavilov(1957) in which all values of K are considered. Figure 3.3 shows the Vavilov distribution for various values of K. In this figure $\varphi(\lambda)$ is a measure of the probability that a particle will lose an energy between Δ and $\Delta+d\Delta$ in traversing an absorber and λ, the Landau parameter, is given by:

$$\lambda = \frac{\Delta - \bar{E}}{\xi} - 0.423 - \beta^2 - \ln K \qquad 3.23$$

As seen , the Landau distribution approaches the Gaussian limit for large values of K. This means that as the velocity of the incident particle decreases then the Landau distribution of energy loss approaches a Gaussian shape. However, neither the treatment of Landau nor that of Symon applies to extremely thin absorbers since both treatments neglect fluctuations due to distant collisions. i.e; to collisions in which the atomic electrons cannot be treated as free.

3.5) GENERAL OPERATION OF SCINTILLATION COUNTERS

In scintillation counters , the initial energy of a single ionizing particle is transformed into a single voltage

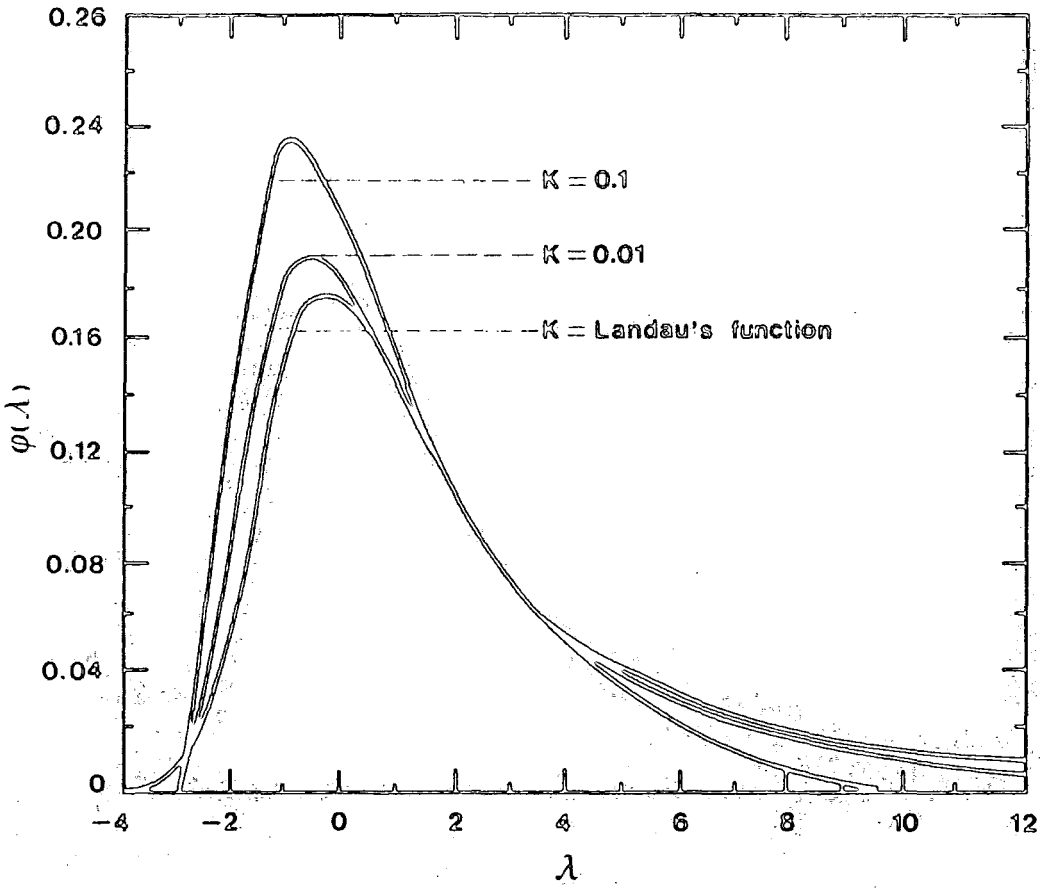

Figure 3.3 The energy loss distribution according to Vavilov (1957). When $K = 0.01$ the exact function is practically the same as Landau's. Thus Landau's approximation is valid for $K \leqslant 0.01$.

pulse which may be used for detection and measurement. The five sequential stages of their operation can be considered as follows:

3.5.1) ENERGY DEPOSITION BY THE INCIDENT PARTICLE

For a heavy charged particle incident normally on a phosphor and travelling through it, energy will be dissipated in the form of excitation and ionization within the phosphor. The particle will emerge with a reduced energy, E_f, and the fraction of the energy dissipated in the scintillator is $A = \frac{E - E_f}{E}$. Uncharged radiation, X and γ – ray quanta and neutrons, do not ionize directly. But, they can transfer some part of their energy to individual charged particles within the phosphor, and the ionization produced by these secondary charged particles gives rise to the scintillations.

3.5.2) PHOTOEMISSION FROM THE PHOSPHOR

Luminescence is the emission of electromagnetic radiation from a substance and is produced when atoms are excited, by ultraviolet light or fast charged particles. If the luminescence ceases rapidly as the source of energy is removed the phenomenon is called fluorescence, but if it persists the phenomenon is called phosphorescence. Phosphorescence corresponds to the emission of longer wavelength light than fluorescence and both of them decay exponentially with specific decay times. The absorbed energy of an incident particle (E_a) is converted by the phosphor with a conversion efficiency (C_p) into N photons of average energy E_p.

$$N = \frac{E_a \cdot C_p}{E_p} \qquad (3.24)$$

where N is the number of photons per scintillation. The photon emission is not instantaneous and the rate of photon emission decays exponentially with a decay period T from its maximum intensity I_o. The intensity after a time t is given by:

$$I = I_o e^{-t/T} \tag{3.25}$$

The number of photons emitted in the time interval t is:

$$N = N_o(1 - e^{-t/T}) \tag{3.26}$$

The decay time of a fluorescence process ($\simeq 10^{-9}$ sec) is much less than that of a phosphorescence process ($\gtrsim 10^{-4}$ sec). Most materials used for scintillation counting produce fluorescence so that fast signal pulses can be generated. Also, in the ideal scintillation material , the conversion of the kinetic energy loss of the incident particles into detectable light should be linear.

3.5.3) TRANSIT TO THE CATHODE OF THE PHOTOMULTIPLIER TUBE

In order to minimise the number of scintillation photons absorbed within the phosphor and to obtain an efficient coupling of the scintillation light to a photomultiplier tube , the medium should be transparent to the wavelength of its own fluorescence and its index of refraction at this wavelength must be near that of glass ($\simeq 1.5$). For a phosphor of optical absorption coefficient μ and a light path of length x:

$$T_p = e^{-\mu x} \tag{3.27}$$

where T_p is the optical transparency of the phosphor. Normally, the fluorescence spectra of organic materials are in the ultraviolet and a wavelength shifter is added to convert the primary fluorescent ultraviolet photons to visible light photons. The light path usually exceeds the thickness of the phosphor because of successive internal reflections before impinging on the photo-cathode. The absorption coefficient varies with wavelength and in most organic phosphors it is small over most of the emission spectrum. Figure 3.4 represents the emission spectrum of NE102A plastic scintillator, Nuclear Enterprises (1980). As can be seen, the wavelength of maximum emission occurs at 4230 Å. However, even for a perfectly transparent phosphor ($\mu=0$) only a small fraction of the number of photons N produced per scintillation fall on the photo-cathode. The number N′ which fall on the photocathode is given by:

$$N' = T_p . G . N \qquad (3.28)$$

G is the fraction of produced photons that would fall on the photocathode in the absence of absorption.

3.5.4) PHOTO-ELECTRON EMISSION FROM CATHODE

Photons are absorbed at the photo-cathode of the photomultiplier tube and converted into photo-electrons with an efficiency $C_p' f(\upsilon_p)$, where C_p' is the photo-electron conversion efficiency of the cathode (i.e; number of electrons per incident photon which is ≤ 1) at its optimum frequency which depends on the photo-electric properties of the cathode

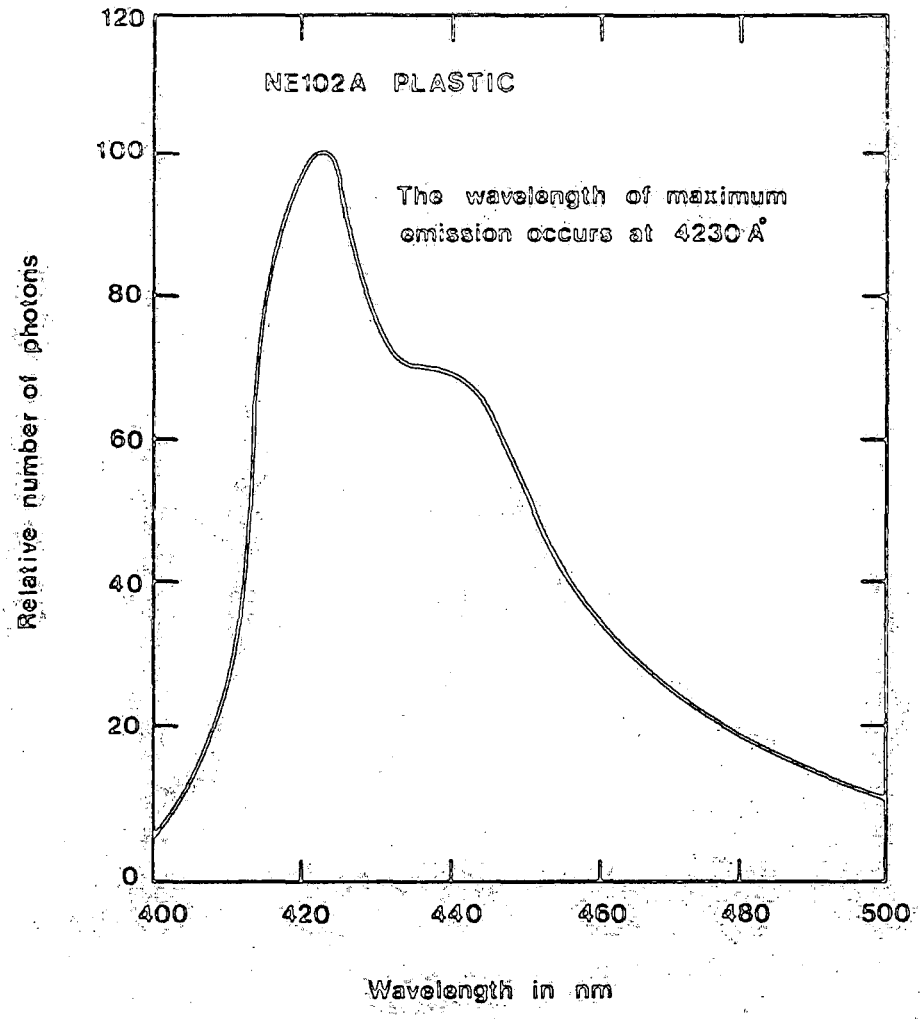

Figure 3.4 Emission spectrum of NE 102A plastic scintillator, Nuclear Enterprises (1980).

material and on its optical absorption for the incident radiation. $f(\upsilon_p)<1$ is the relative response of the photo-cathode at frequency υ_p which depends on the cathode material. The energy that can be transferred from the photon to an electron is given by the quantum energy of the photon. Some of that energy will be lost through electron – electron collision in the migration process inside the photocathode and finally there must be sufficient energy left for the electron to overcome the inherent potential barrier (i.e; work function) which always exists at any interface between material and vacuum. Hence, the finite potential barrier imposes a minimum energy on the incoming light photon for it to produce a photoelectron.

3.5.5) ELECTRON-MULTIPLICATION AND TRANSIT TIME SPREAD

The multiplier portion of a photomultiplier tube is based on the phenomenon of secondary electron emission. For simplicity, the dynode surfaces are usually made of the same material as the photo – cathode, which is chosen for combining high photo-electric and high secondary emission characteristics with low thermionic emission. Because of lack of sufficient energy for overcoming the potential barrier of the dynode surface, only a fraction of the incident electrons ultimately contribute to the secondary electrons which is a sensitive function of incident energy electron. The overall multiplication factor for a single dynode is given by:

$$\delta = \frac{\text{number of secondary electrons emitted}}{\text{number of incident electrons}} \qquad (3.29)$$

This factor which depends on the secondary emission

characteristics of the dynode material and on the electron collection efficiency from the preceding dynode, increases with the energy of the incident electrons, that is with the accelerating voltage. The overall gain of a photomultiplier tube containing X stages is given by:

$$M = \alpha \delta^{x} \tag{3.30}$$

where α is the collection efficiency factor of the photo-electrons by the dynode system and is near unity for well-designed tubes. Thus, the total charge of the signal pulse arriving at the output stage of the multiplier structure (i.e ; anode) produced by n initial photoelectrons is:

$$Q = Me.n \tag{3.31}$$

where e is the electronic charge. The number of electrons produced at the photocathode by an ionising particle is:

$$n = \left(\frac{E_a C_p}{E_p}\right) \tau_p \cdot G \cdot \overline{C_p' f(\upsilon_p)} \tag{3.32}$$

where $\overline{C_p' f(\upsilon_p)}$ is the average quantum efficiency of the photocathode averaged all emission wavelengths of the phosphor.

The focused structures which are used in many photomultiplier tubes, provide a stronge directing field for the secondary electrons and thus constrain them into paths with little spread in position from dynode to dynode. Hence, there is a much smaller spread in electron transit time than with the unfocused structures. Tubes employing focused structures are useful for fast scintillation counting applications. The region between photocathode and first dynode is an important

source of transit time spread. In fact, it determines the time width of the pulse of electrons arriving at the anode of the tube. In order to allow uniform collection over large photocathodes, this distance is kept fairly large compared with interdynode distances. A second source of transit time spread arises from the distribution in initial velocities of photoelectrons leaving the photocathode. This effect may be minimised by using a large voltage difference between photocathode and first dynode.

3.6) BACKGROUND NOISE SOURCES

3.6.1) THERMIONIC ELECTRON EMISSION

Usually, the most significant source of spurious pulses from a photomultiplier tube result from thermionic electrons which limits its sensitivity for the detection of scintillations produced by low energy radiations or weak activities. Normal conduction electrons within the photo-cathode material will always have some thermal kinetic energy. In fact, there is a distribution and those electrons at the extreme upper end of the distribution can occasionally have an energy that exceeds the surface potential barrier. Thus, some of them may escape and give rise to a spontaneous thermally induced signal. The number of such thermionic electrons , n_o, emitted per second by the photo-cathode depends on the thermionic work function φ of the cathode material, and it is proportional to the area, S, of the cathode from which the electrons are collected by the multiplier dynode systems, Birks (1964):

$$n_o = S.A.T^2 \exp\left(-\frac{\varphi.e}{K.T}\right) \qquad (3.33)$$

where T is the absolute temperature , K is Boltzmann's constant (1.38×10^{-16} erg.K^{-1}) and φ and A are characteristic of the cathode material. The rate at which these pulses are observed is proportional to the area of the photo-cathode and hence one can select a tube of the smallest diameter required for a specific application in order to minimise this background. The number of thermionic electrons is also reduced by a reduction in the temperature of the photo-cathode and dry ice or liquid nitrogen are often used for cooling. Problems that can arise in connection with photomultiplier tube cooling include water vapor condensation on exposed cold surfaces and increased photo – cathode electrical resistance at lower temperatures. Large photo – cathode resistance can distort the electrostatic field between the photo-cathode and first dynode (i.e; focusing electrodes) and may lead to a loss in photoelectron collection efficiency. Thermionic emission from the dynodes likewise contributes to the noise background. Since the electrons from the dynodes go through fewer stages of multiplication than those from the cathode, the amplitude of the output pulses from the dynode noise is small in comparison. In metals, because of the relatively high surface potential barrier, the thermal emission rate is low. By using two or more photomultiplier tubes viewing the same phosphor which can be operated in coincidence, noise pulses can in principle be eliminated.

3.6.2) FEEDBACK PROCESSES

Two main types of feedback processes which give rise to spurious pulses following the main pulse, occur between the

anode or dynodes and the cathode, Davison (1952). In fact, these processes have been shown conclusively to originate in the photomultiplier tube and they are not due to delayed photoemission (phosphorescence) of the phosphor. One mechanism that can give rise to after-pulsing is the emission of photons from the later stages of the multiplier structure which finds its way back to the photo – cathode. Such after-pulses will be delayed by a time characteristic of the electron transit time through the tube. Because these pulses often corresponds to a single photon, their amplitude is usually quite small. Another cause of after – pulsing can be an imperfect vacuum within the tube. Traces of residual gas can be ionized by the passage of electrons through the multiplier structure. The positive ions that are formed will drift in the reverse direction and some may find a path back to the photo-cathode. Typical ions will liberate many photoelectrons when they strike the photo-cathode, and the resulting pulse will be of rather large size. The time distribution of the anode pulses caused by these ions will depend on their mobility and the field gradient in the region they traverse. Allen (1953). Since the velocity of the positive ion is relatively low, the time it takes to drift back to the photo – cathode is long. Therefore, the time spacing between the primary pulse and the afterpulse from this mechanism is relatively large. Since the amount of residual gas can vary considerably between tubes of identical design, problems due to after – pulsing may be reduced by simple substitution of another tube but cannot be completely eliminated. Its magnitude depends on the quality of

manufacture, and it is as much a function of the individual tube as of a particular type. However, this effect does occur if the tube is operated at too high a voltage.

3.6.3) EFFECT OF MAGNETIC FIELD

Because of the relatively large spacing between the photocathode and the first dynode, a small magnetic field can cause appreciable deflection of the photo-electrons. In turn, it gives rise to a reduction in the electron collection efficiency of tubes. Even the earth's magnetic field (≈ 0.8 Oersted), may have an appreciable effect for certain alignments of the tube. Increasing the voltage between the photocathode and first dynode reduces the effect.

3.6.6) OTHER SOURCES

Dark pulses can also be produced by other background sources such as:

(a) The natural radioactivity of the constituent materials of the tube itself.

(b) The natural radioactivity of the ancillary equipment, wall of the laboratory, shielding placed in the immediate vicinity of the detector and other far-away structures.

(c) Radiations from the activity of the earth's surface (i.e ; terrestrial radiation) and radioactivity in the air surrounding the detector.

3.7) RESPONSE OF ORGANIC SCINTILLATORS

The intended application has a major influence on

scintillator choice. Where the linearity is important, since the inorganics, especially sodium iodide or caesium iodide crystals, have the best light output and linearity but are relatively slow in their response time, they are the most applicable. The high Z-value of the constituents and high density of them favors their choice for gamma-ray spectroscopy. The organic scintillators are much faster but yield less light and are often preferred for beta spectroscopy and the detection of other fast particles. Some fraction of the kinetic energy lost by a charged particle in an organic scintillator is converted into fluorescent energy, the remainder is dissipated nonradiatively, primarily in the form of heat. The intensity of the scintillations , L , produced in the organic phosphors depends on the energy and on the nature of the incident ionizing particle. The response to different ionizing particles can be compared by considering the variation of the specific fluorescence dL/dx, which is proportional to the number of fluorescent quanta emitted per unit pathlength, with the specific energy loss, dE/dx. A widely used relationship first suggested by Birks (1951) is based on the assumption that a high ionization density along the track of the particle leads to quenching from damaged molecules and a consequent lowering of the scintillation efficiency. i.e; he has ascribed the lack of linear response of the plastic scintillators to the quenching of the primary excitation by the high density of ionized and excited molecules:

$$\frac{dL}{dx} = S \frac{\frac{dE}{dx}}{1 + kB\frac{dE}{dx}} \qquad (3.34)$$

where S is the absolute scintillation efficiency, B is a constant relating the density of ionized and emitted molecules to the dE/dx and k is a quenching parameter. For incident electrons of energy greater than 125KeV (i.e; at small value of dE/dx), the scintillation intensity from an organic scintillator increases linearly with the initial energy, Hopkins (1951). Thus, equation (3.34) reduces as:

$$\left.\frac{dL}{dx}\right]_e = S\,\frac{dE}{dx} \tag{3.35}$$

so that the fluorescent efficiency dL/dE, which is the incremental light output per unit energy loss, is constant:

$$\left.\frac{dE}{dL}\right]_e = S \tag{3.36}$$

For heavier particles (e.g; alpha particle) or for slow electrons of E<125KeV, which produce more intense ionization, a further reduction in the fluorescent efficiency occurs, and the scintillation response is consequently less than that produced by an electron of the same of energy. The specific fluorescence is practically constant and independent of the specific energy loss. Thus, at large values of dE/dx, equation (3.34) becomes:

$$\left.\frac{dL}{dx}\right]_\alpha = \frac{S}{kB} = \text{constant} \tag{3.37}$$

However, by extensive analysis of the response of a number of organic scintillators, Wright (1953) has proposed the following relation in order to fit the experimental data more closely:

$$\frac{dL}{dx} = A\,Ln\left(1 + \alpha'\frac{dE}{dx}\right) \tag{3.38}$$

It reduces to equation (3.34) at low values of dE/dx when the

constants A and α' become S/kB and 2kB respectively. On the basis of $\frac{kE}{L}$ above formula, Gooding et al (1960) calculated the response of NE102A plastic to various incident particles, figure 3.5. To make the response more linear, they also introduced a thin absorber in front of the scintillator. The thickness of absorber to give the best overall linearity depends both on the range of energies over which linearity is required and on the type of particle.

3.8) LIGHT GUIDE

In some scintillation counter applications, it is desirable to locate the phosphor at a distance from the photomultiplier tube. Although a system of mirrors may occasionally be used, more frequently the light is conducted from the scintillation crystal (i.e; phosphor) to the photomultiplier tube window along some sort of light conducting rod known as a light guide. This may arise because the scintillator is located in a strong magnetic field or in a vacuum. in which it is unsuitable or inconvenient to operate the photomultiplier tube close to the phosphor. Magnetic fields influence strongly the sensitivity of photomultiplier performance and can cause a considerable decrease in anode current, Engstrom et al (1952). Alternatively, the size or shape of the scintillator may not conveniently match the circular photocathode area of available tubes. Figure 3.6 shows schematicly a strip light guide which can be used to couple the edge of a large, flat scintillator to a photomultiplier tube. Furthermore, thin scintillators should not be mounted directly

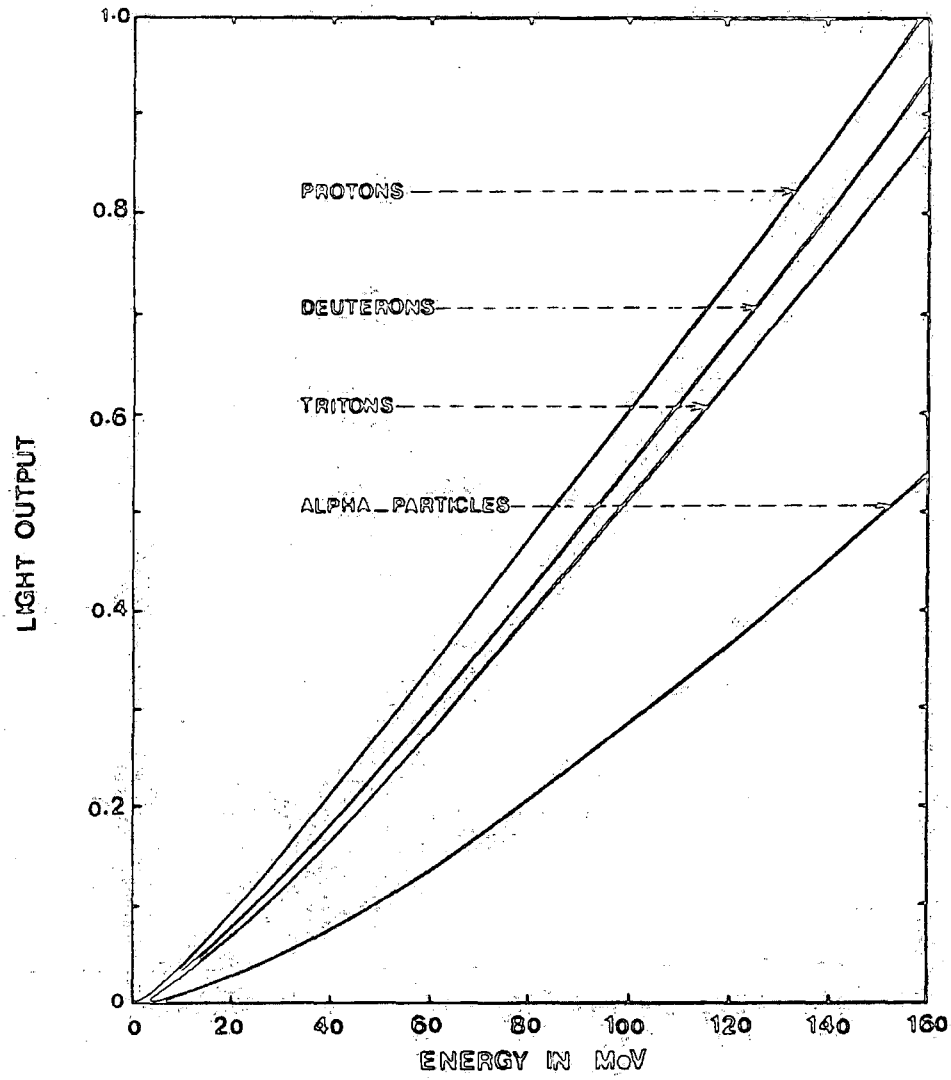

Figure 3.5 The calculated response of NE 102A to Protons, Deuterons, Tritons and alpha-particles, Gooding et al. (1960).

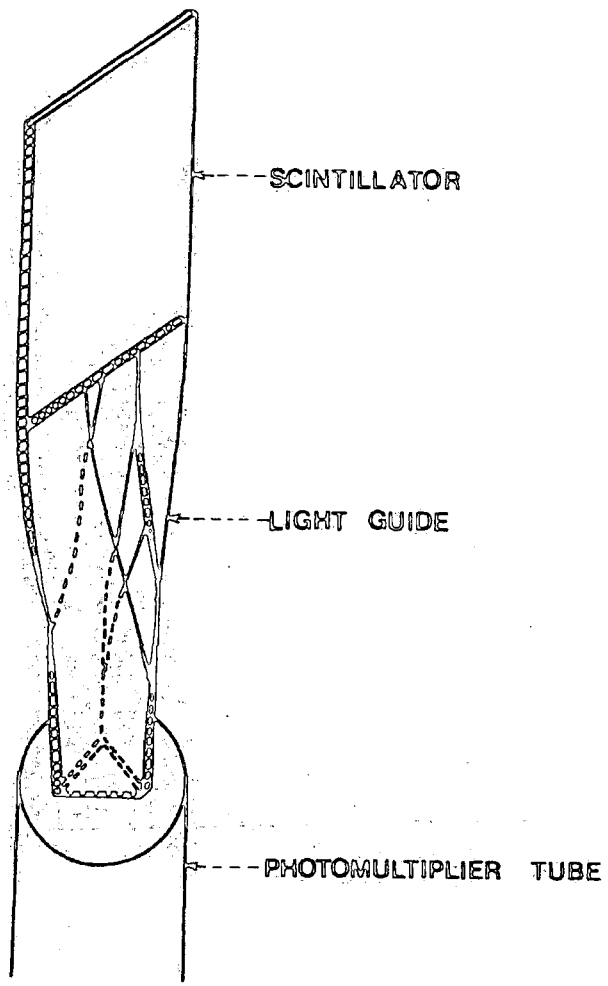

Figure 3.6 A strip light guide can be used to couple the edge of a large, flat scintillator to a photomultiplier tube.

on the photomultiplier tube end window to avoid the pulse height variations which can arise due to photocathode non-uniformities. In fact, an important practical property of photocathodes is the uniformity to which their thickness can be held over the entire area of the photocathode. Variations in thickness give rise to corresponding changes in the sensitivity of the photocathodes, especially those with large diameters, and can be one source of resolution loss in scintillation counters. This problem is further compounded by the difficulties of achieving uniform photoelectron collection to the first dynode from the entire photocathode area. The combination of these two effects can lead to situations in which the anode pulse observed for a given flash of light may vary as the position of the illumination is moved across the photocathode area. A light guide between the thin scintillator and photomultiplier tube will spread the light from each scintillation event over the entire photocathode to average out these nonuniformities and improve the pulse height resolution. They are generally optically transparent solids with a relatively high index of refraction to minimise the critical angle for total internal reflection. The critical angle θ_c is determined by the indices of refraction for the scintillation medium n_0 and the surronding medium n_1 :

$$\theta_c = \sin^{-1} \frac{n_1}{n_0} \tag{3.39}$$

The light guide may probably produce attenuation, so that the photomultiplier signal to noise ratio becomes low, Ettinger (1955). The factors affecting attenuation in a light guide can be

grouped as follows:

(a) Crystal-cement-guide reflection losses.

(b) Attenuation in the volume of the guide.

(c) Absorption losses at the surface of the guide.

(d) Guide-cement-glass reflection losses at the photomultiplier tube envelope.

The major source of light loss is internal reflection at the crystal – cement and at the cement – glass interfaces and can be reduced by selecting cement or other materials of expedient refractive index and by polishing the ends of the guide. Among many materials , fused quartz has the highest transparency , but it is expensive and difficult to fabricate in other shapes. Polymethyl methacrylate (e.g; perspex , lucite , plexiglas) has an adequate transparency for most purposes and is easy to fabricate.

In the present experiment, the relative height of voltage pulses produced by muons traversing an NE102A plastic phosphor (which produces scintillation light) compared to muons traversing the perspex light guide (which produces Čerenkov radiation) can be estimated by calculating the number of primary photons produced by each process which are detected by Philips 53AVP photomultiplier tubes with a typical cesium – antimony (Ce – Sb) photocathode. Assume relativistic single charged particles lose 2 MeV/g.cm^{-2} and that on the average an energy loss of 212 eV is required to produce a scintillation photon, Ashton et al (1965). The number of scintillation photons produced by a particle traversing the phosphor of 5cm thickness at normal incident is $2\times10^{6}\times5/212=4.7\times10^{4}$. For the same

thickness of perspex light guide, the comparable number of Cerenkov photons produced is 1.3×10^3 (Jelley, p279, 1958). Hence, the ratio of the number of resulting scintillation photons to Cerenkov photons is 36/1. Allowing for the absorption of scintillation light in the phosphor (estimated to be a factor of 2.2 at the worst position of particle passage) and assuming that the fraction of produced photons that arrive at a photocathode is the area of the photocathode divided by the cross sectional area of the light guide to which the photomultiplier is attached for both scintillation and Cerenkov light, then the ratio of the number of produced photons that are collected is estimated to be 36/2.2:1=16.36/1. Hence, on the average, pulses produced by Cerenkov radiation in the perspex light guides of the present experiment are estimated to be at least sixteen times smaller than pulses produced by particles traversing the phosphor. Therefore, it is concluded that the resulting noise due to the existence of Cerenkov radiation which is produced in the perspex light guides, is negligible. Full details of the experimental detector will be described in the next chapter.

3.9) CHARACTERISTICS OF ORGANIC PHOSPHORS

In order to specify an ideal scintillation material, many factors (e.g; transparency, decay time of the induced luminescence. linearity of response etc) are involved. In practice, no material simultaneously meets all these criteria, and then the choice of a particular scintillator is always a compromise among these factors. Ultra-short decay time can be

regarded as an important property of the organic phosphor. In comparison with inorganic phosphors, they also have other advantages:

(a) Organic phosphors contain hydrogen as a major constituent , and thus they can be used for the detection of fast neutrons.

(b) The fluorescence conversion efficiency (i.e; C_p) is reasonably high , although lower than some inorganics , such as NaI or ZnS.

(c) The scintillation response for electrons of energy greater than 125 KeV increases linearly with the energy , (see section 3.7).

(d) The emission wavelength of most of the simpler efficient compounds is almost near the peak of the photomultiplier spectral sensitivity curve.

(e) They have a high transparency (i.e;T_p) to their own fluorescence emission.

(f) Only few organic materials exhibit phosphorescence under normal condition.

The main disadvantages of them are:

(a) The reduced scintillation response to heavy particles, and its non-linear variation with incident energy.

(b) The low density and low atomic number of their constituent atoms reduce the photo-electric and pair-production absorption coefficients.

(c) The lower efficiency C_p reduces the pulse-height and energy resolution obtainable.

Table 3.2 taken from the Nuclear Enterprises catalogue (1980) ,

	Scintillator	Type	Density	Refractive Index	Melting Softening or Boiling Point °C	Light Output (% Anthracene)	Decay Constant, Main Component ns	Wavelength of Maximum Emission nm	Content of Loading Element (% by wt.)	H/C No. of H Atoms/ No. of C Atoms	Principal Applications
PLASTIC	NE 102A	Plastic	1·032	1·581	75*	65	2·4	423	···	1·104	γ, α, β, fast n
	NE 104	Plastic	1·032	1·581	75*	68	1·9	406	···	1·100	ultra-fast counting
	NE 104B	Plastic	1·032	1·58	75*	59	3·0	406	···	1·107	with BBQ light guides
	NE 105	Plastic	1·037	1·58	75*	46	··	423	···	1·098	dosimetry
	NE 110	Plastic	1·032	1·58	75*	60	3·3	434	···	1·104	γ, α, β, fast n, etc.
	NE 111A	Plastic	1·032	1·58	75*	55	1·6	370	···	1·103	ultra-fast timing
	NE 114	Plastic	1·032	1·58	75*	50	4·0	434	···	1·109	as for NE 110
	NE 160	Plastic	1·032	1·58	80**	59	2·3	423	···	1·105	use at high temperatures
	Pilot U	Plastic	1·032	1·58	75*	67	1·36	391	···	1·100	ultra fast timing
	Pilot 425	Plastic	1·19	1·49	100*	··	··	425	···	1·6	Cherenkov detector
LIQUID	NE 213	Liquid	0·874	1·508	141*	78	3·7	425	···	1·213	fast n (P.S.D.)
	NE 216	Liquid	0·885	1·523	141*	78	3·5	425	···	1·171	α, β (internal counting)
	NE 220	Liquid	1·036	1·442	104*	65	3·8	425	0·29%	1·669	internal counting, dosimetry
	NE 221	Gel	1·08	1·442	104*	55	4	425	····	1·669	α, β (internal counting)
	NE 224	Liquid	0·877	1·505	169*	80	2·6	425	····	1·330	γ, fast n
	NE 226	Liquid	1·61	1·38	80*	20	3·3	430	···	0	γ, insensitive to n
	NE 228	Liquid	0·71	1·403	99*	45	····	385	····	2·11	n
	NE 230	Deuterated liquid	0·945	1·50	81*	60	3·0	425	D 14·2%	0·984	(D/C) special applications
	NE 232	Deuterated liquid	0·89	1·43	81*	60	4	430	D 24·5%	1·96	(D/C) special applications
	NE 233	Liquid	0·874	1·506	117*	74	3·7	425	····	1·118	α, β (internal counting)
	NE235	Liquid	0·858	1·47	350*	40	4	420	····	2·0	large tanks
	NE 250	Liquid	1·035	1·452	104*	50	4	425	0 32%	1·760	internal counting, dosimetry
LOADED LIQUID	NE 311 & 311A	B loaded liquid	0·91	1·411	85*	65	3·8	425	B 5%	1·701	n, β
	NE 313	Gd loaded liquid	0·88	1·506	136*	62	4·0	425	Gd 0·5%	1·220	n
	NE 316	Sn loaded liquid	0·93	1·496	148·5*	35	4·0	425	Sn 10%	1·411	γ, X-rays
	NE 323	Gd loaded liquid	0·879	1·50	161*	60	3·8	425	Gd 0·5%	1·377	n
NEUTRON (ZnS-type) and GLASS	NE 422 & 426	^{6}Li·ZnS(Ag)	2·36	···	110*	300	200	450	Li 5%	····	slow n
	NE 451	ZnS(Ag)-plastic	1·443	···	110*	300	200	450	····	····	fast n
	NE 901, 902, 903	Glass	2·64	1·58	c. 1200*	28	20 & 60	395	Li 2·3%	····	n, β
	NE 904, 905, 906	Glass	2·5	1·55	c. 1200*	25	20 & 58	395	Li 6·6%	····	n
	NE 907, 908	Glass	2·42	1·566	c. 1200*	20	18 & 62	399	Li 7·5%	····	n
	NE 912, 913	Glass	2·3	1·55	c. 1200*	25	18 & 55	397	Li 7·7%	····	n, β (low background)
CRYSTAL	Anthracene	Crystal	1·25	1·62	217*	100	30	447	····	0·715	γ, α, β, fast n
	Stilbene	Crystal	1·16	1·626	125*	50	4·5	410	····	0·858	fast n (P.S.D.), γ, etc.
	NaI(Tl)	Crystal	3·67	1·775	650*	230	230	413	····	····	γ, X-rays
	NaI(pure)	Crystal	3·67	1·775	651*	440†	60†	303†	····	····	γ, X-rays (fast counting)
	LiI(Eu)	Crystal	4·06	1·955	445*	75	1200	475	····	····	n
	CsI(Tl)	Crystal	4·51	1·788	620*	95	1100	580	····	····	heavy particles, γ (P.S.D.)
	CsI(Na)	Crystal	4·51	1·787	621*	150·190	650	420	····	····	heavy particles, γ (P.S.D.)
	CsI(pure)	Crystal	4·51	1·788	621*	500†	600†	c. 400†	····	····	heavy particles, γ (low energy)
	CaF_2(Eu)	Crystal	3·17	1·443	1418*	110	1000	435	····	····	β, X-rays etc.
	$CaWO_4$	Crystal	6·1	1·92	1535*	36	6000	430	····	····	γ (seldom used)
	ZnS(Ag)	Multi-crystal	4·09	2·356	1850*	300	200	450	····	····	α
	ZnO(Ga)	Multi-crystal	5·61	2·02	1975*	90	1·48	385	····	····	α

*Although NE 160 begins to soften very slightly at approximately 80° C, it retains its shape up to at least 150° C unlike other plastic scintillators such as NE 102A.
†At liquid nitrogen temperature.

Table 3.2 Properties of various scintillation counter phosphors, Nuclear Enterprises Catalogue (1980)

shows some properties of various scintillation phosphors. It can be seen that for the NE102A plastic phosphor, the decay time of fluorescence and its light output are 2.4×10^{-9} sec and 65% of that of an anthracene crystal of the same geometry respectively.

3.10) SUMMARY

At the present time, there are many available scintillation counter phosphors. When linearity is the most important factor, inorganic scintillation phosphors are suitable. Organic phosphors are much faster but yield less light. Also, plastic organic phosphors of large area are readily available (eg; Nuclear Enterprises Type NE102A) and these are the most suitable for cosmic ray work. Photomultiplier tubes are an essential element of scintillation counters and there are two main types. In the first type, known as electrostatically-focused tubes, the short transit time spread ($\simeq 10^{-9}$ sec) makes them suitable for coincidence or fast counting, where a short time resolution is essential. When high light collection efficiency and good pulse height resolution are required, the second type, known as electrostatically-unfocused tubes, are much superior for radiation spectrometry. The very low dark current of them is an advantage for measurements on weak sources or low-energy radiations. Their relatively large transit time spread limits their resolving time to about 10^{-8} sec, compared with that of the first type. An important defect in the behaviour of these photomultiplier tubes has been reported by Raffle et al (1952). It is found

that the output pulse heights are not always proportional to the intensity of light incident on the photo-cathode. The tube ceases to be a linear amplifier when the charge density in the multiplier becomes too great. In other words; the non-linear amplification of them for large pulses limits the advantages to be obtained from their high gain.

CHAPTER FOUR

DESGIN AND PERFORMANCE OF MORE EFFICIENT PLASTIC SCINTILLATORS FOR USE IN THE E.A.S ARRAY

4.1) INTRODUCTIN

Because only relatively few of the scintillation photons produced by the passage of single relativistic charged particles (mainly; muons) were collected by the photomultiplier tubes observing the phosphors, none of the previous scintillation counters used in the Durham extensive air shower array gave a single particle peak due to the passage of the global cosmic radiation flux when their outputs were fed into a pulse height analyser (P.H.A.). The position of the single particle peak was lost in the noise of pulses generated by the thermionic electrons (see section 3.6.1) leaving the photocathodes of the photomultiplier tubes. Accordingly, the average pulse height produced by a single charged particle traversing the phosphors at normal incidence had to be found using a subsidiary cosmic radiation telescope. Furthermore, since the scintillation detectors are located in weatherproof containers situated outside of the physics department building, their calibration obviously was a time consuming and awkward job to carry out. Hence it was decided to construct new scintillation detectors with more light collection efficiency , such that their outputs would show a clearly resolved cosmic radiation peak when displayed on a pulse height analyser. The design of detector investigated is shown in figure 4.1a and

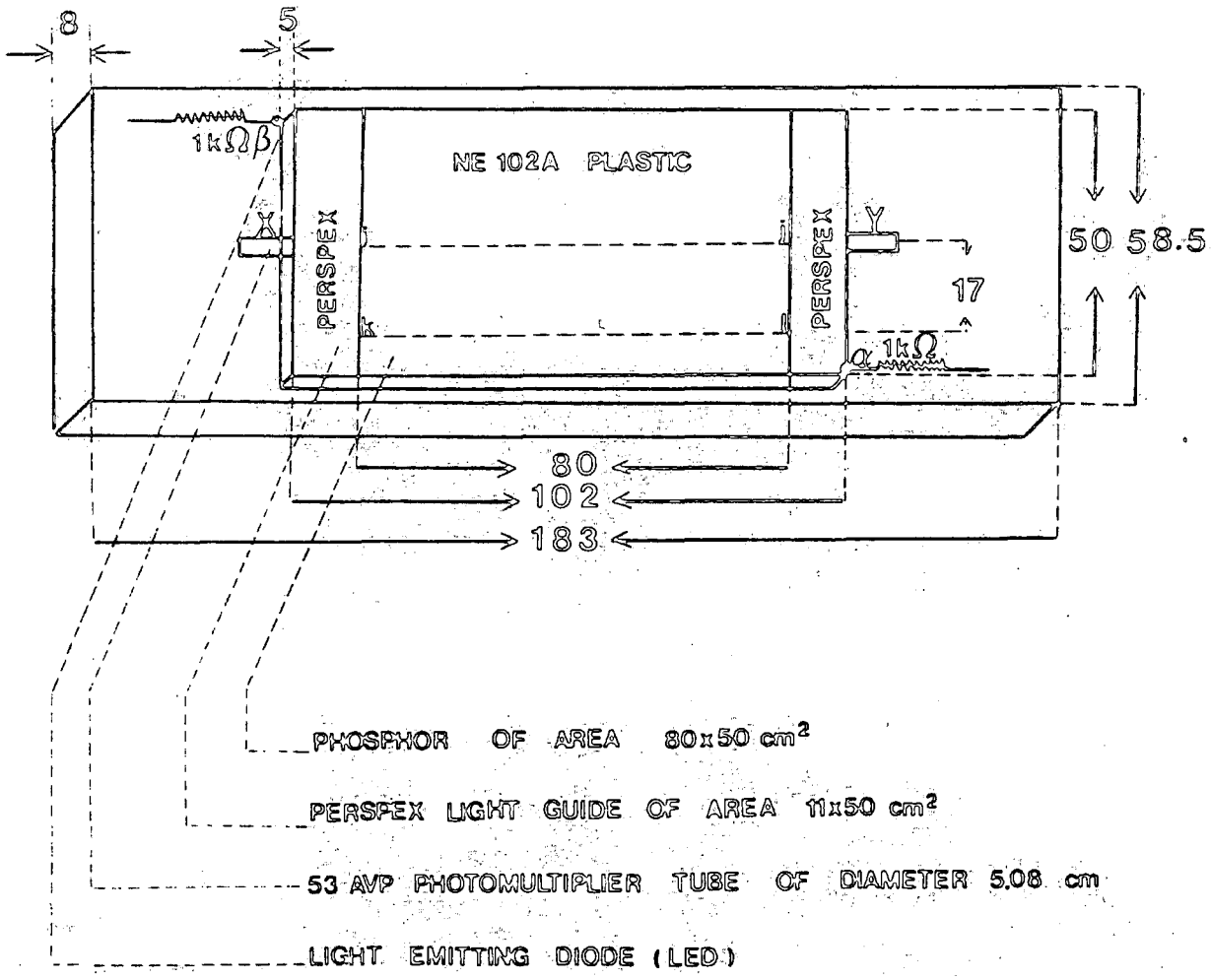

Figure 4.1a Design of plastic scintillation counter. The points α and β indicate the situation of light emitting diodes which were used to match the photomultiplier tubes. All dimensions are in centimetres.

subsequently nine such detectors have been built which will also be useful for investigating other cosmic radiation phenomena.

4.2) PATH LENGTH PROBABILITY DISTRIBUTION OF COSMIC RAY PARTICLES IN TRAVERSING A THIN DETECTOR

When used in an experiment as a proportional detector, it is useful to be able to determine the average pulse height produced by relativistic particles traversing the phosphor at normal incidence from the measured response to the global cosmic radiation flux as it is not always convenient or possible to use a subsidiary narrow angle vertical telescope for calibration purposes. At sea level the cosmic radiation consists predominantly of muons and electrons (see section 1.2), the rate of particles at zenith angle θ, $I(\theta)$ being well represented by:

$$I(\theta) = I(o)\cos^n\theta \qquad (4.1)$$

where I(0) is the rate of particles at normal incidence. For muons $I(0)=0.8\times10^{-2}$ $cm^{-2}.sec^{-1}.st^{-1}$, n=2.1 and for electrons $I(0)=0.3\times10^{-2}$ $cm^{-2}.sec^{-1}.st^{-1}$, n=3.6 (Greisen, 1942; Pathak et al, 1981 ; Aguilar-Benitez et al, 1982). For radiation with the above zenith angle distribution, the track length distribution P(l)dl in traversing a thin phosphor of vertical thickness z can be found by noting that $P(l)dl=P(\theta)d\theta$ where $l=z/\cos\theta$. For a detector of area S with an "on time" t the number of cosmic rays traversing it with zenith angle in the range θ to $\theta+d\theta$ is given by:

$$N(\theta)d\theta = I(o)\cos^n\theta \,.\, S\cos\theta \,.\, 2\pi\sin\theta d\theta \,.\, t \qquad (4.2)$$
$$\propto \cos^{n+1}\theta, \sin\theta\, d\theta$$

Thus, the probability of a particle traversing the phosphor with θ in the range θ to $\theta+d\theta$ is given by:

$$P(\theta)d\theta = B\cos^{n+1}\theta . \sin\theta d\theta = (n+2)\cos^{n+1}\theta . \sin\theta \, d\theta \qquad (4.3)$$

where B is found using:

$$B\int_0^1 \cos^{n+1}\theta \, d(\cos\theta) = 1 \qquad (4.4)$$

Hence, the probability that a cosmic radiation particle has a track length in the phosphor in the range l to l+dl is given by:

$$P(l)dl = -(n+2)\cos^{n+1}\theta \, d(\cos\theta) = -(n+2)\left(\frac{z}{l}\right)^{n+1}\cdot\left(-\frac{z\,dl}{l^2}\right) = (n+2)\frac{z^{n+2}}{l^{n+3}}dl \qquad (4.5)$$

4.3) NON-UNIFORMITY OF SCINTILLATION DETECTORS

Using a subsidiary narrow angle telescope to select near vertical particles traversing the phosphor (figure 4.1a), the average pulse height produced by photomultiplier tube X as the telescope was placed at different positions along the centre line, ij, and along a side line, kl, 17cm from the centre line was measured. The results obtained are shown in figure 4.1b. As it can be seen, there is no significant difference between the response along the centre line and the line 17cm away, and it can be concluded that there is no significant response variation across the 50cm side of the scintillator. Also shown is the response observed when the outputs of both photomultiplier tubes X and Y are added. The total response of the counter is the sum of the curve shown in

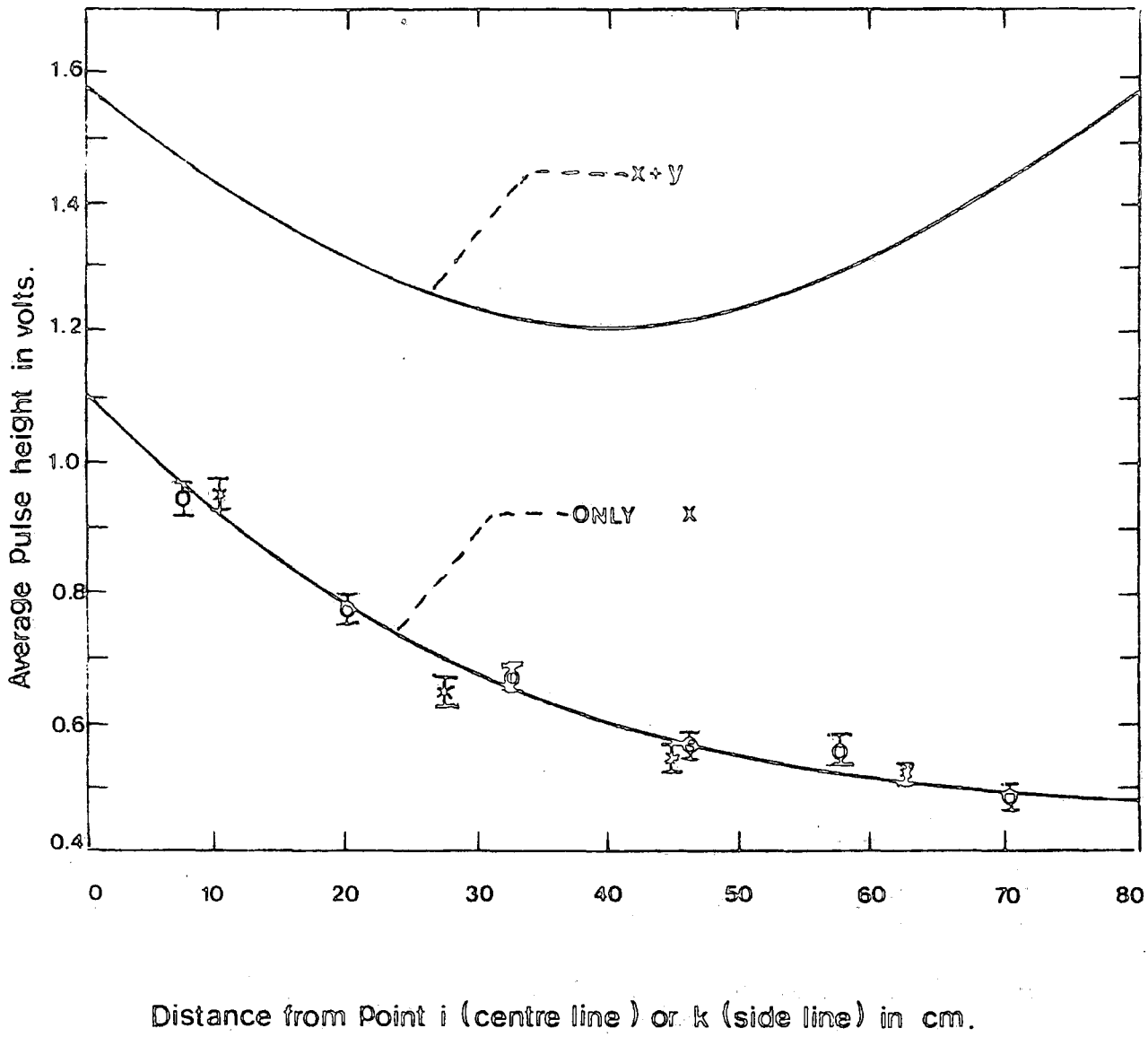

Figure 4.1b Response of the counter to near vertical cosmic ray particles traversing the phosphor at different positions in the phosphor.

Centre Line, ij, side line, kl. Also shown is the output pulse height when the pulses from X and Y tubes are added.

figure 4.1b and its mirror image about the centre point. The maximum non-uniformity , MAX.N.U , of the counter is expressed as:

$$MAX.N.U = \frac{R_o - R_c}{R_c} \times 100\% \qquad (4.6)$$

where R_o is the total response at the end of the phosphor and R_c is the total response at the centre of the phosphor. The value of this parameter was found to be 31%.

4.4) DETERMINATION OF THE RELATIVE SENSITIVITIES OF THE PHOTOMULTIPLIER TUBES

Because of the effect of thermionic electrons, if the output from a single photomultiplier tube shown in figure 4.1a is displayed on a pulse height analyser a clearly resolved peak is not observed. However, the adjustment of two suitable photomultiplier tubes which have the same sensitivity, leads to an observable resolved peak on the screen of the pulse height analyser. Thus, it is necessary to determine the operating voltages of both photomultiplier tubes such that they have the same sensitivity. This was done in an auxiliary experiment using the arrangement shown in figure 4.2. The variation of output pulse height as a function of applied voltage for the eighteen photomultiplier tubes was measured by using standard light pulses from a light emitting diode (L.E.D) and table 4.1 summarises the results obtained for them. The results for tubes numbers 8, 17, 16 and 18 are shown in figures 4.3a, 4.3b, 4.3c and 4.3d respectively. Table 4.2 also depicts the pairs of

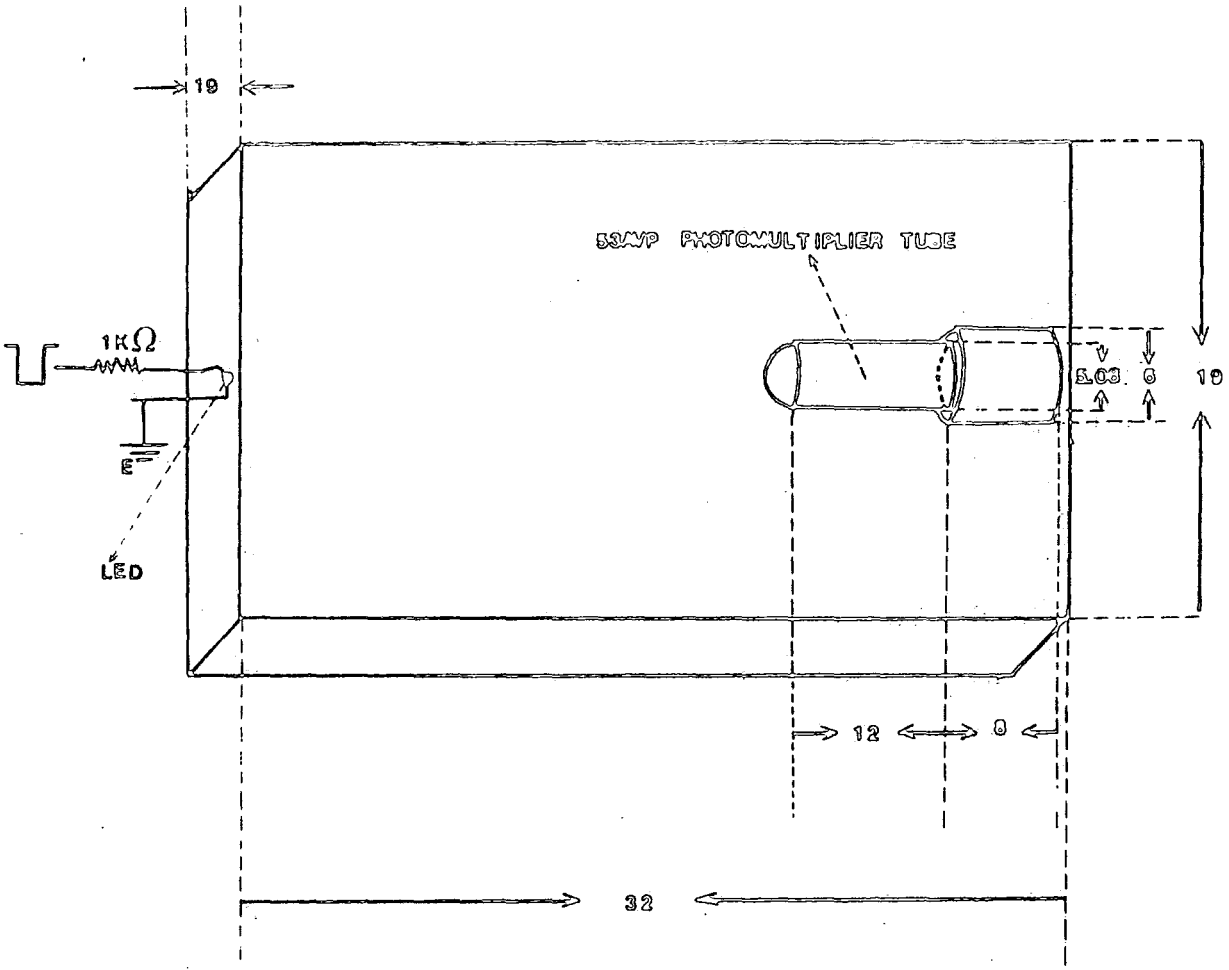

Figure 4.2 Arrangement used for measuring the relative sensitivities of photomultipliers as a function of the voltage applied to the photomultiplier tube. All dimensions are in centimetres. LED is a light emitting diode.

Phototube No.	Equation $v \propto V^n$
1	$v = 3.63 \times 10^{-28} V^{8.49 \pm 0.31}$
2	$v = 2.45 \times 10^{-28} V^{8.30 \pm 0.10}$
3	$v = 9.60 \times 10^{-29} V^{8.37 \pm 0.06}$
4	$v = 5.69 \times 10^{-29} V^{8.40 \pm 0.06}$
5	$v = 1.11 \times 10^{-30} V^{9.07 \pm 0.06}$
6	$v = 5.56 \times 10^{-35} V^{10.34 \pm 0.10}$
7	$v = 2.56 \times 10^{-29} V^{8.87 \pm 0.05}$
8 §	$v = 5.61 \times 10^{-31} V^{9.27 \pm 0.24}$
9	$v = 5.09 \times 10^{-29} V^{8.76 \pm 0.09}$
10	$v = 1.51 \times 10^{-29} V^{8.73 \pm 0.04}$
11	$v = 1.04 \times 10^{-28} V^{8.41 \pm 0.04}$
12	$v = 1.64 \times 10^{-31} V^{9.38 \pm 0.06}$
13	$v = 8.72 \times 10^{-29} V^{8.48 \pm 0.04}$
14	$v = 10^{-27} V^{8.17 \pm 0.06}$
15	$v = 3.08 \times 10^{-28} V^{8.25 \pm 0.12}$
16 †	$v = 2.84 \times 10^{-28} V^{8.22 \pm 0.05}$
17 §	$v = 3.21 \times 10^{-27} V^{8.11 \pm 0.01}$
18 †	$v = 5.59 \times 10^{-30} V^{8.71 \pm 0.06}$

Table 4.1 Variation of output pulse height (v in volts) with the E.H.T voltage (V in volts) applied to a sample of eighteen photomultiplier tubes. The same standard light pulse from a pulsed light emitting diode was applied to all the tubes. The symbols of § and † indicate the photomultiplier tubes used in the present experiment.

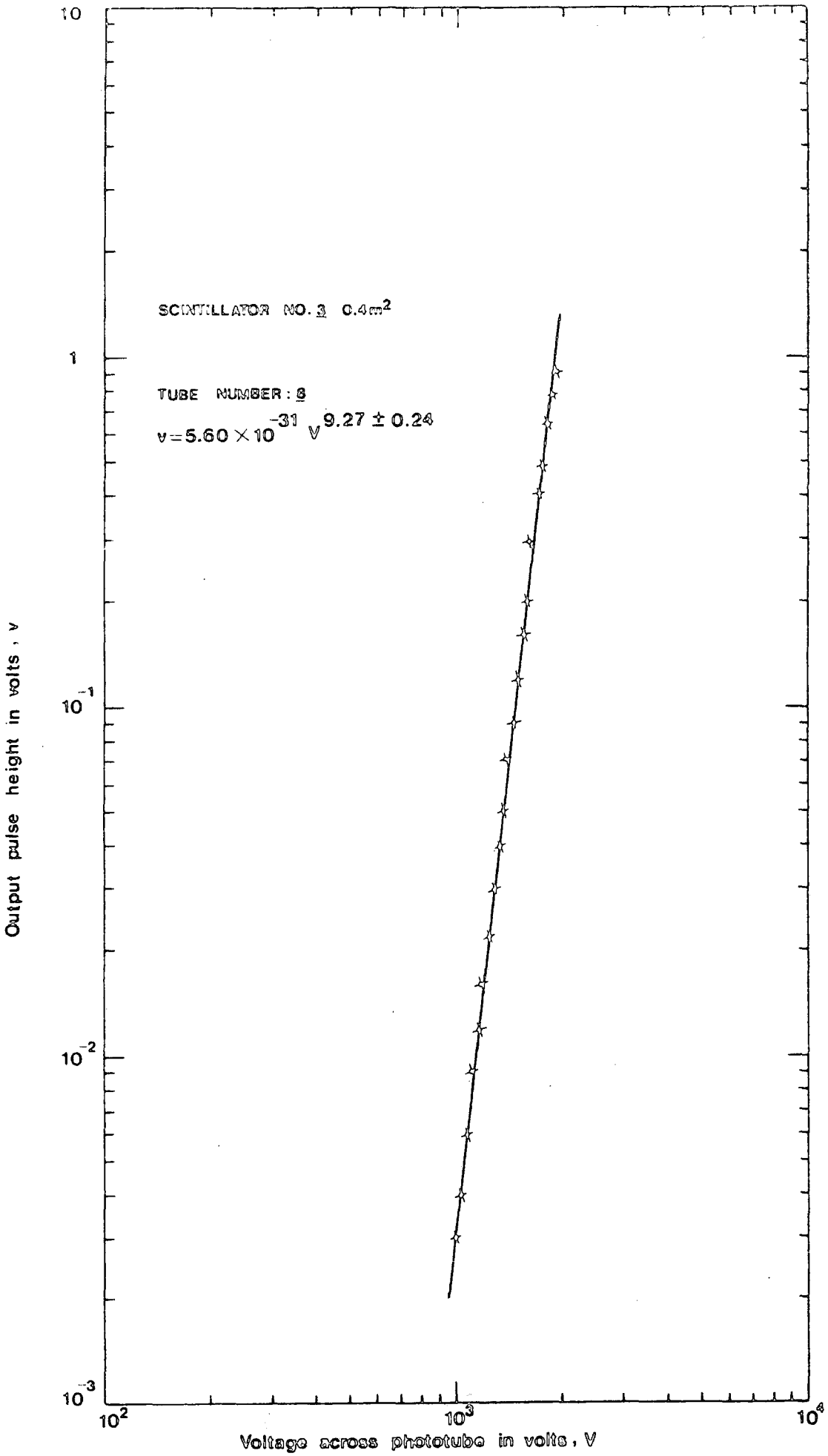

Figure 4.3a Variation of output pulse height, v, with applied E.H.T voltage, V, for photomultiplier tube number 8. Standard light pulses from a light emitting diode were applied to the tube.

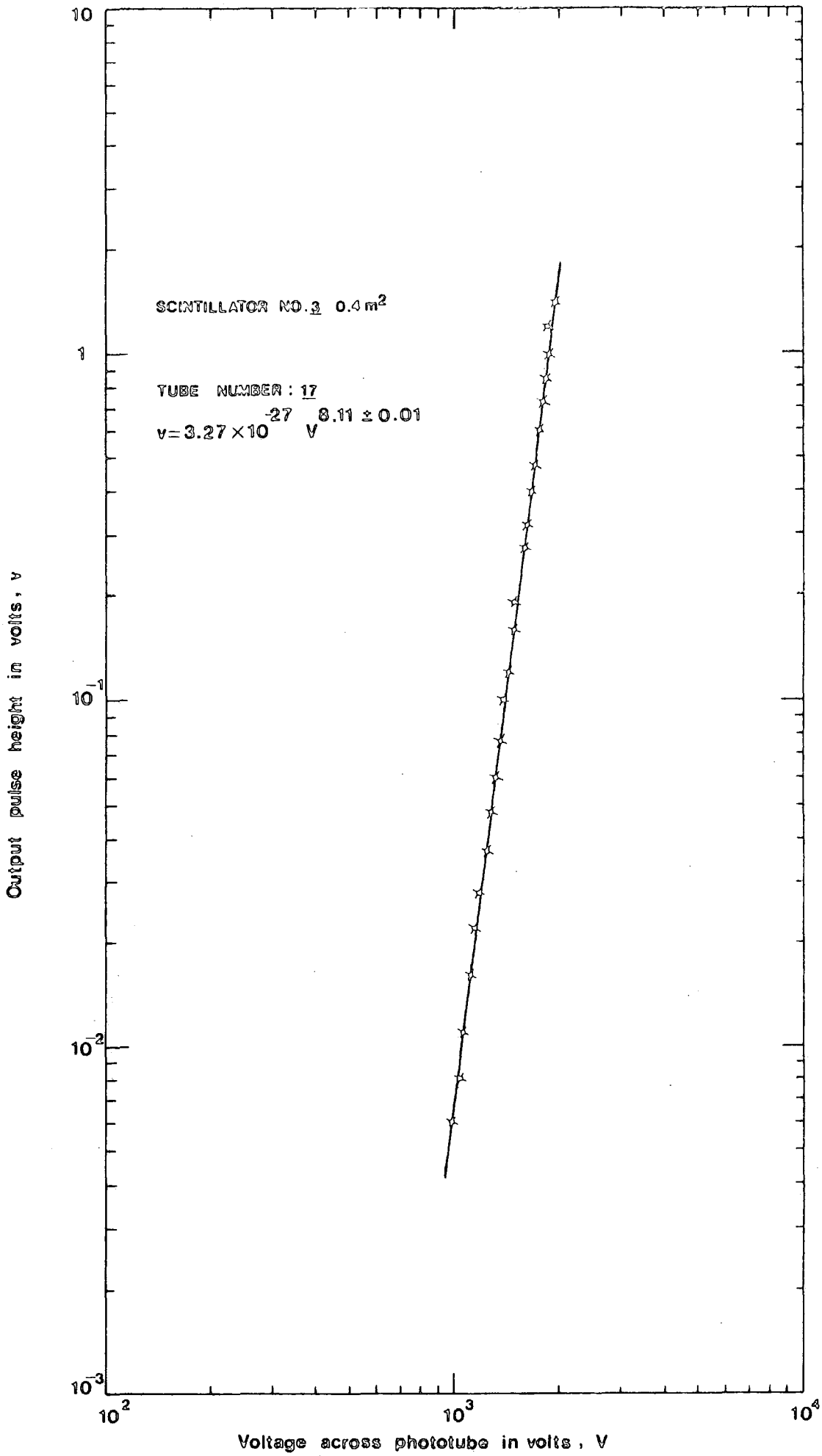

Figure 4.3b Variation of output pulse height, v, with applied E.H.T voltage, V, for photomultiplier tube number 17. Standard light pulses from a light emitting diode were applied to the tube.

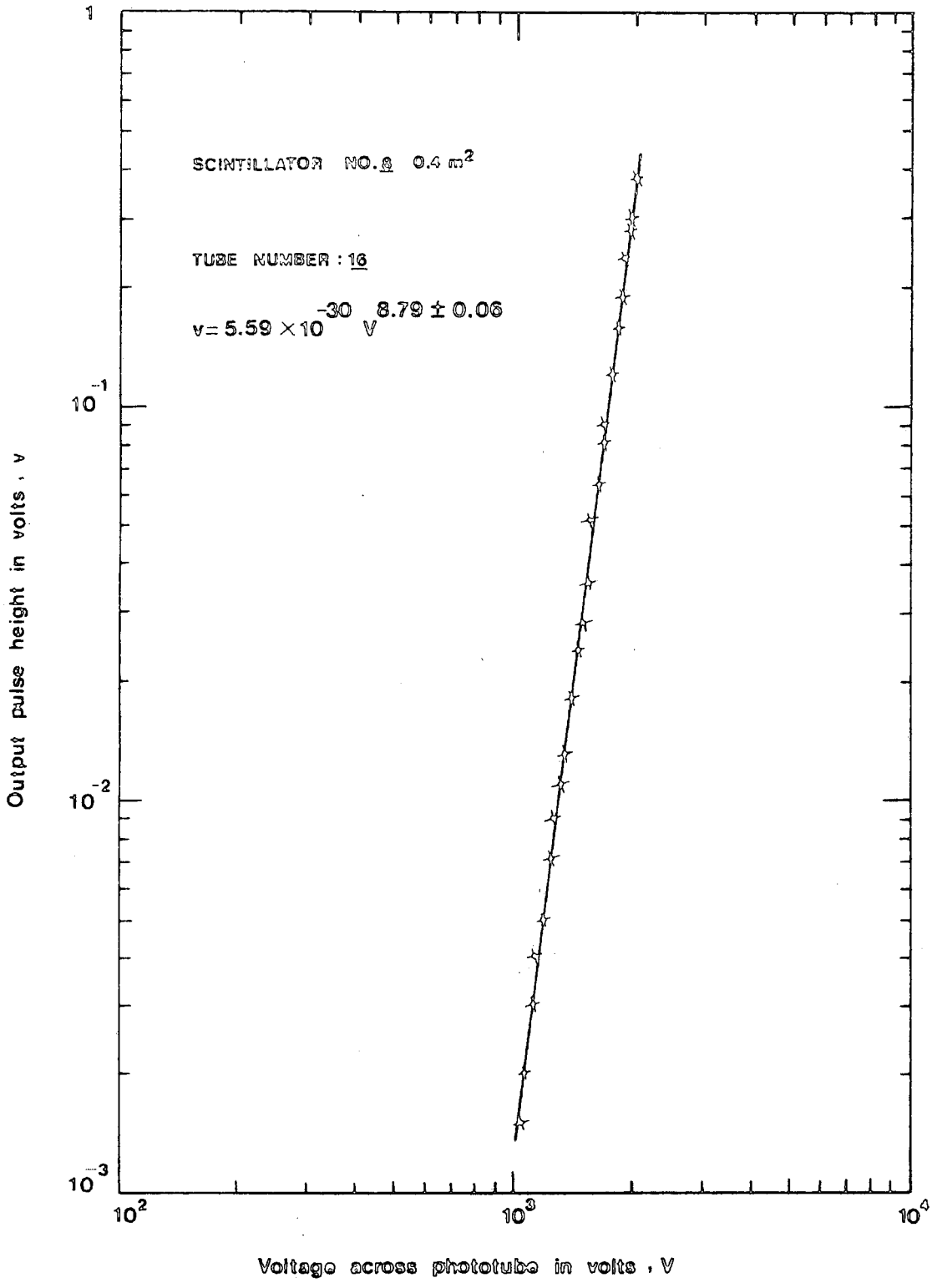

Figure 4.3c Variation of output pulse height, v, with applied E.H.T voltage, V , for photomultiplier tube number 16. Standard light pulses from a light emitting diode were applied to the tube.

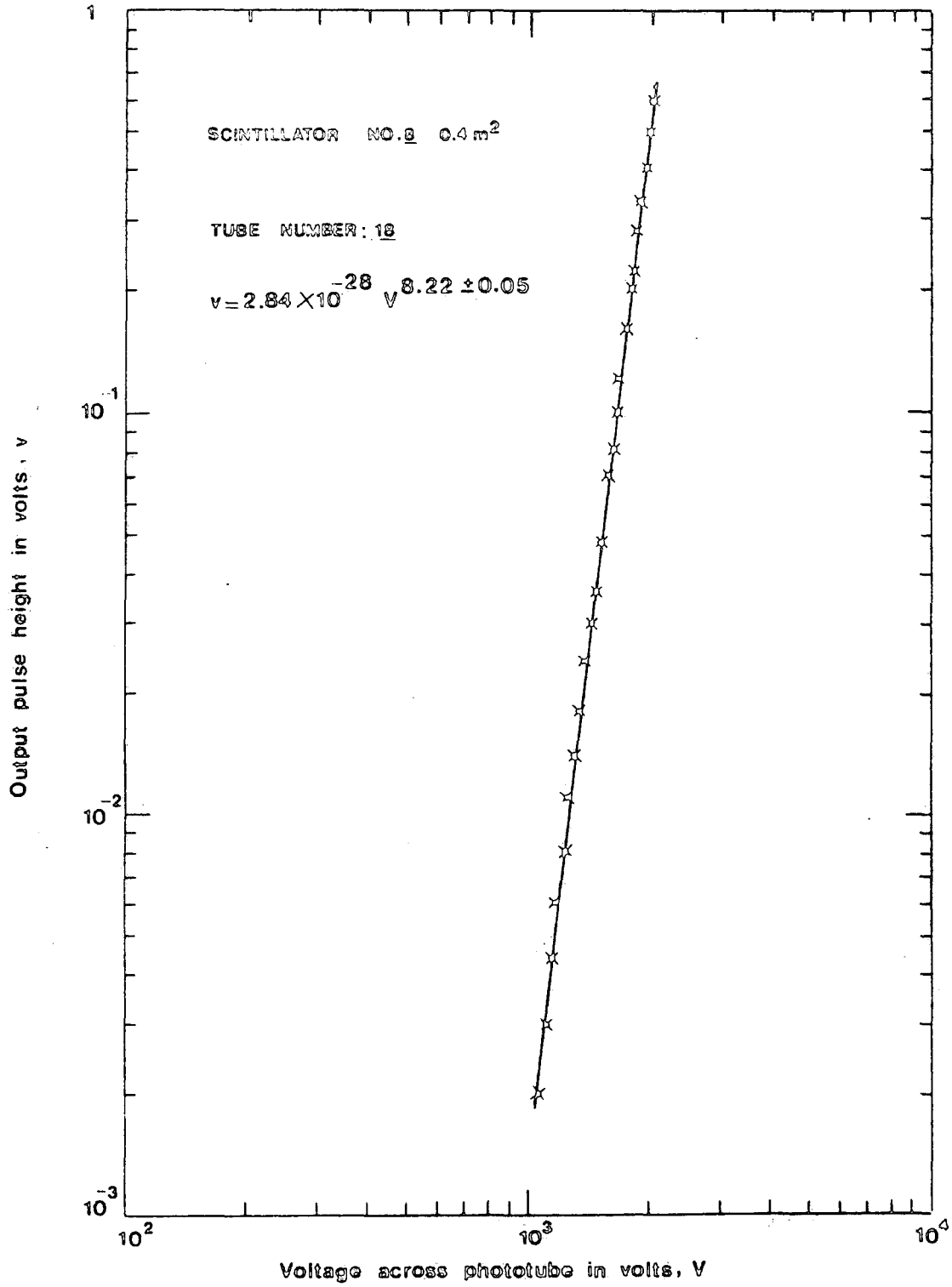

Figure 4.3d Variation of output pulse height, v, with applied E.H.T voltage, V , for photomultiplier tube number 18. Standard light pulses from a light emitting diode were applied to the tube.

NUMBER OF SCINTILLATOR COUNTER	PHOTOTUBE NUMBERS
1	6 and 15
2	9 and 5
3 †	8 and 17
4	13 and 10
5	14 and 3
6	1 and 4
7	11 and 2
8 †	18 and 16
9	7 and 12

Table 4.2 The pairs of phototubes that have been used in the nine scintillation counters that have been constructed. The symbol † indicates the scintillation counters used in the present experiment.

photomultiplier tubes which have been used in the nine scintillation counters. All measurements portrayed in table 4.1 and figures 4.3 used pulses of width 1μsec applied to the light emitting diode.

Some properties of the light emitting diode measured using square voltage pulses from a pulse generator fed through a 1 KΩ series resistor are shown in figures 4.4a and 4.4b. The former figure indicates the dependence of photomultiplier tube output pulse height on the width , in microseconds , of the voltage pulse applied to the light emitting diode. The latter one shows the variation of the photomultiplier tube output pulse height with the voltage applied to the photomultiplier for pulses of width 1μsec, 2μsec and 5μsec applied to the light emitting diode. Figure 4.5 shows the values of the resistors used in the base circuit of the 53AVP photomultiplier tubes used.

4.5) HIGH VOLTAGE SUPPLY OF THE PHOTOMULTIPLIER TUBE AND THE HEAD UNITS

With the main extra high tension (E.H.T) power supply set at -2KV and requiring that the single particle cosmic radiation peak at the output of the head unit is 20mV, The value of the resistance in the distribution box shown in figure 4.6a was suitably adjusted. The correct operating voltage for each photomultiplier tube is obtained by appling Kirchhoff's law in the simple circuit shown in figure 4.6b. The circuit diagram of the head unit used with each scintillation counter which is a simple emitter follower (E.F) is shown in figure 4.7

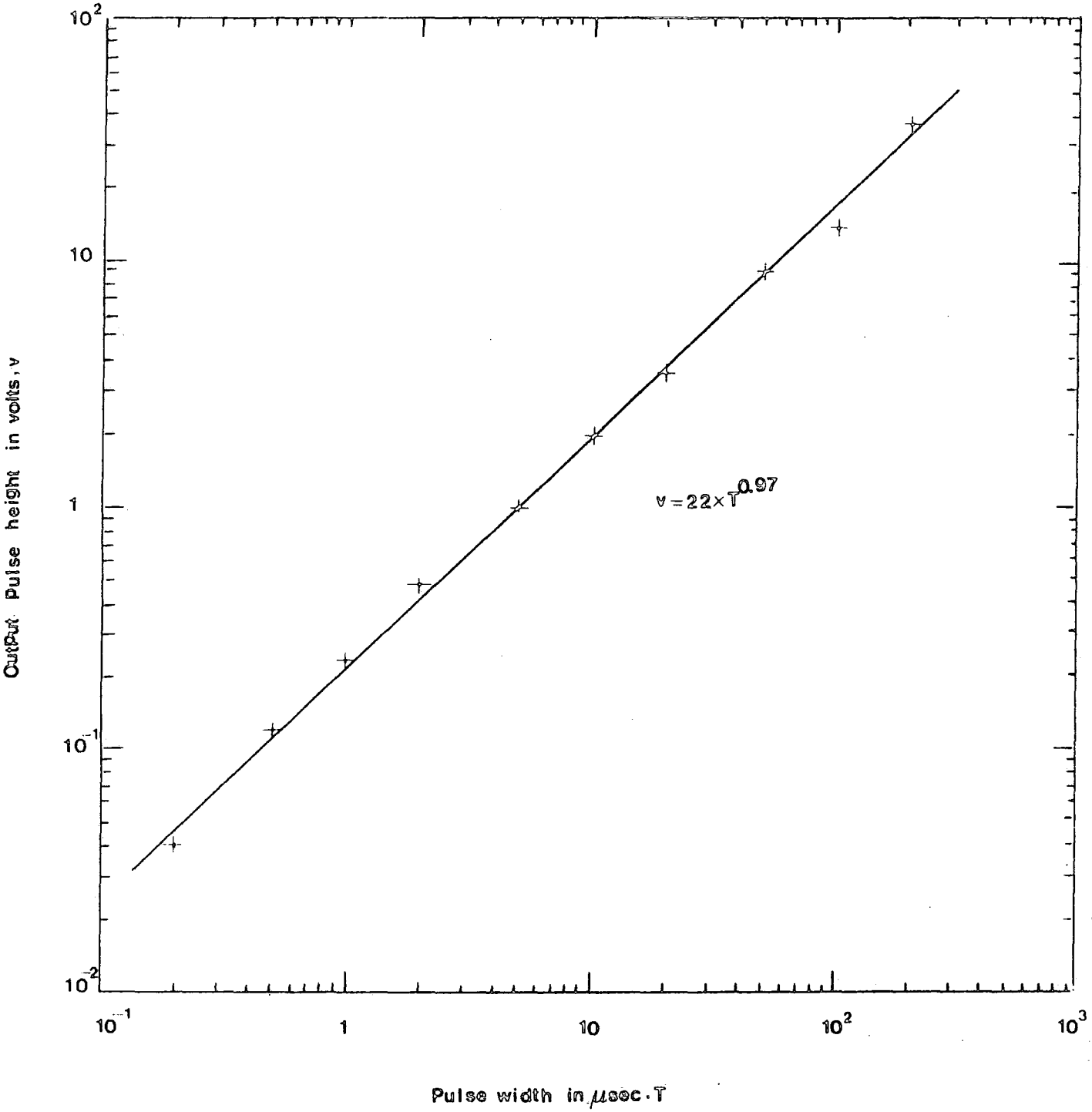

Figure 4.4a Dependence of phototube output pulse height, v, on the width, T, of the voltage pulsed applied to the light emitting diode. The phototube E.H.T was held constant at -1.5 Kv. The measurements are fitted by $v = 22T^{0.97}$ with v in volts and T in microseconds.

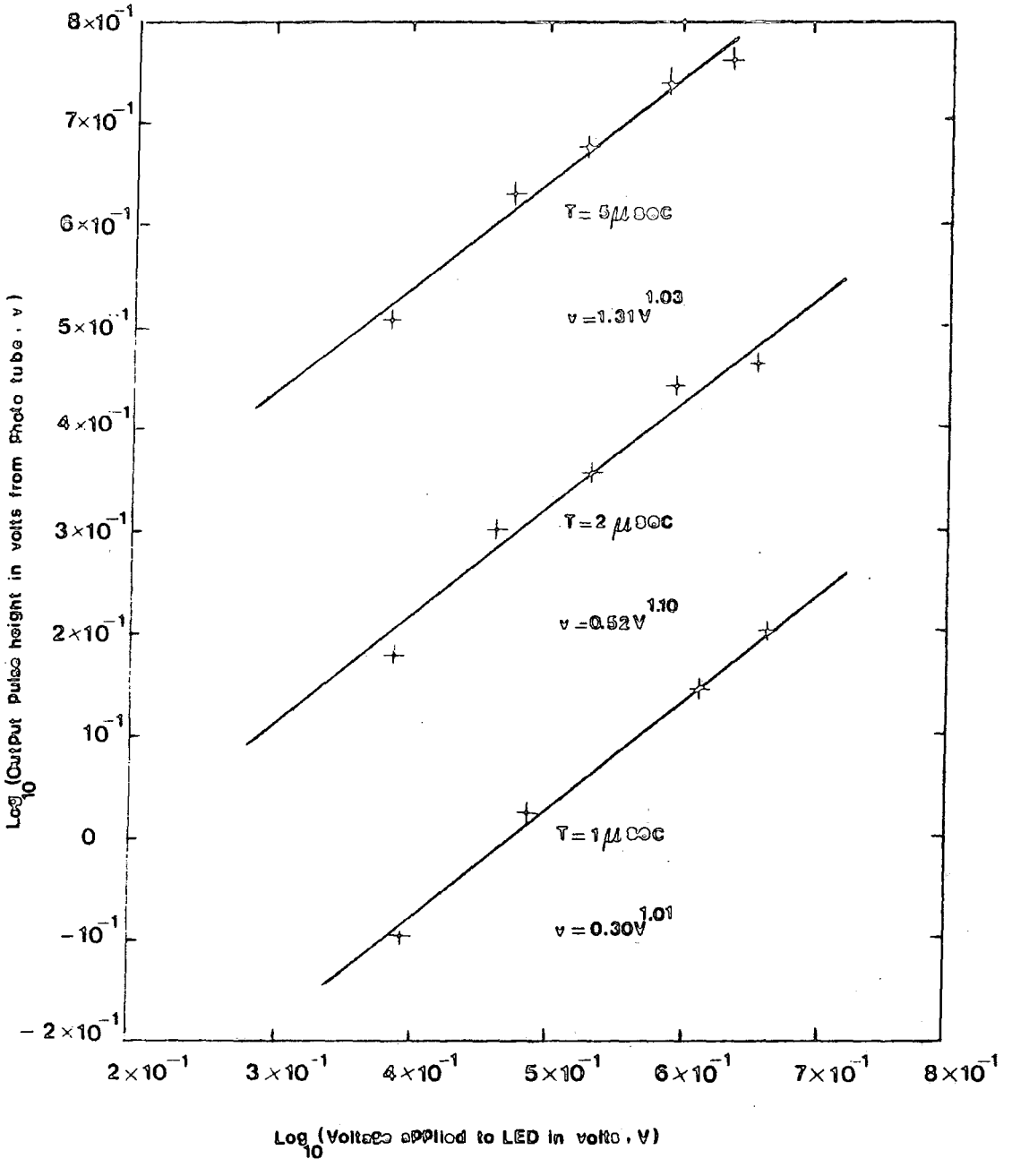

Figure 4.4b Variation of output pulse height, v, from phototube with voltage, V, applied to the light emitting diode for different pulse widths, T. The data is represented by the expressions indicated with both v and V in volts. The phototube E.H.T was fixed at -1.5 Kv.

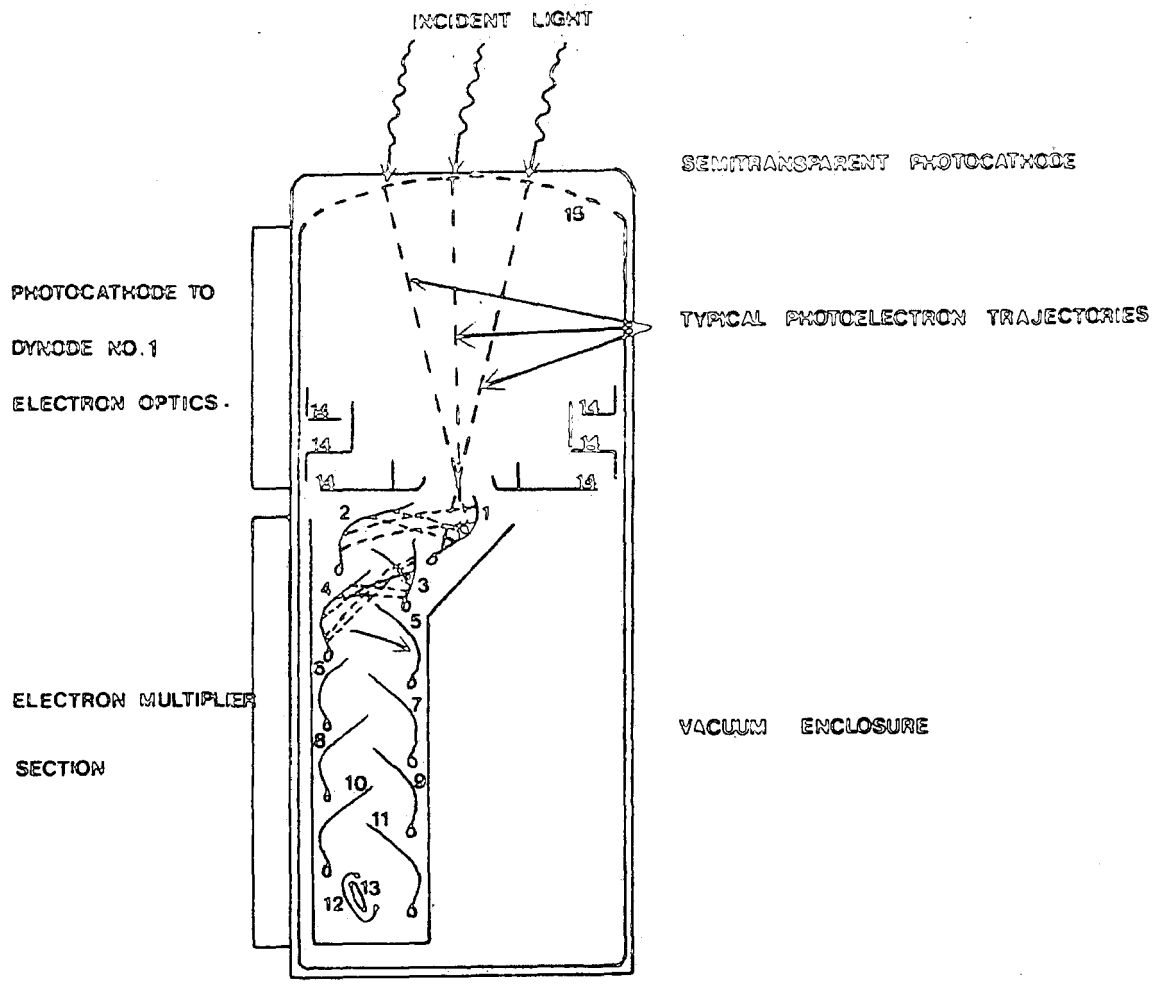

Figure 4.5a Basic Elements of a Photomultiplier Tube

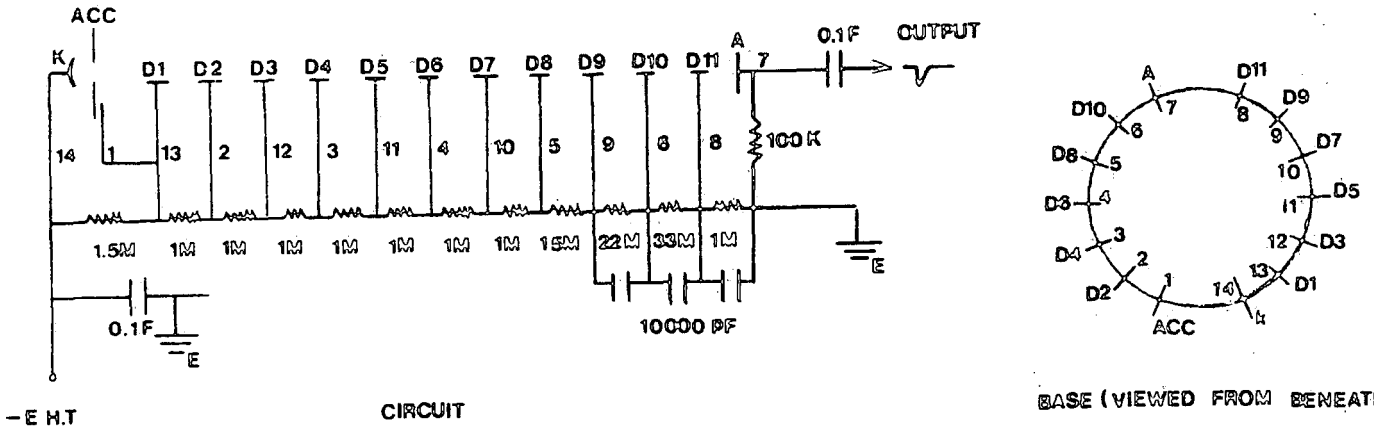

PHILIPS 53AVP

Figure 4.5b Base circuit for Philips 53 AVP photomultiplier tube.

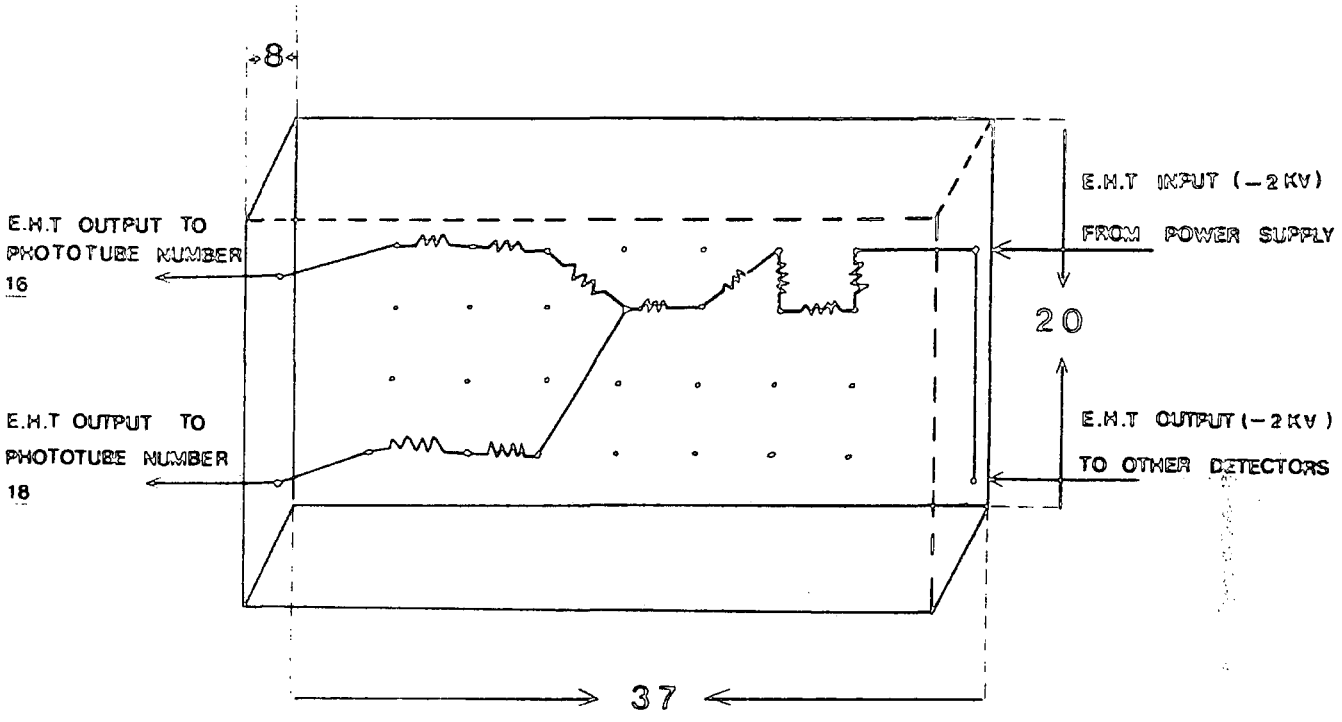

Figure 4.6a The E.H.T distribution box used with each scintillation counter. Dimensions indicated are in centimetres.

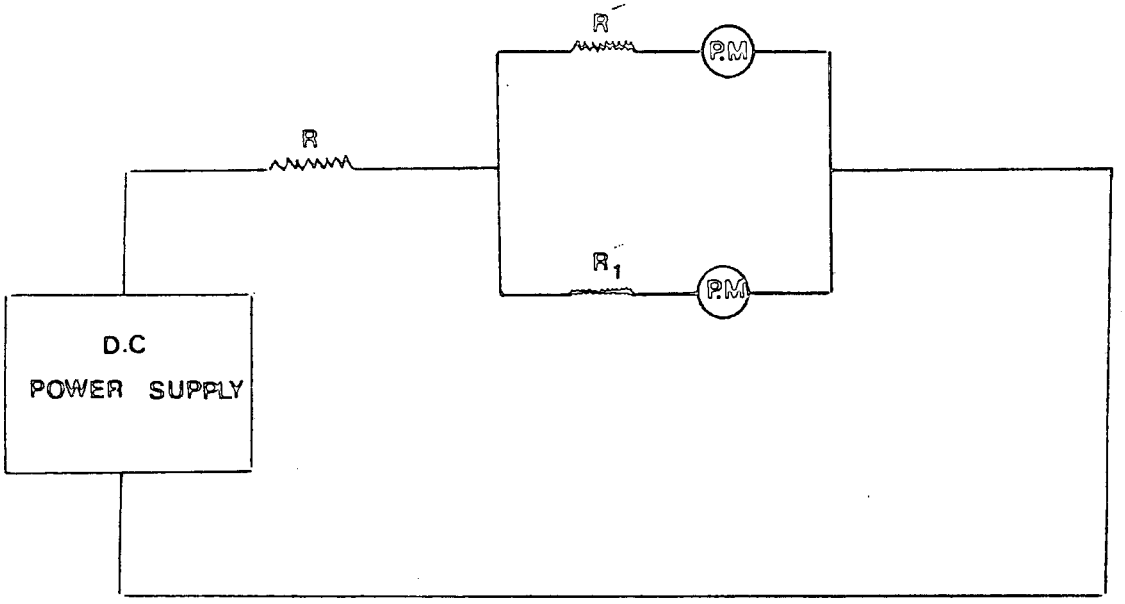

Figure 4.6b Application of Kirchhoff's law in order to match two photomultiplier tubes in each scintillation counter.

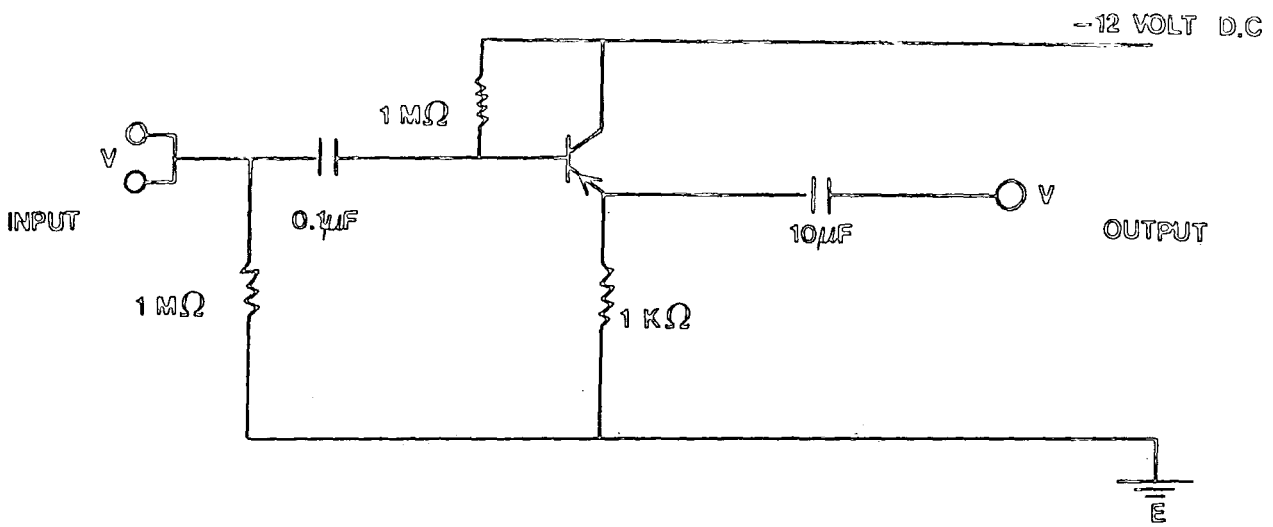

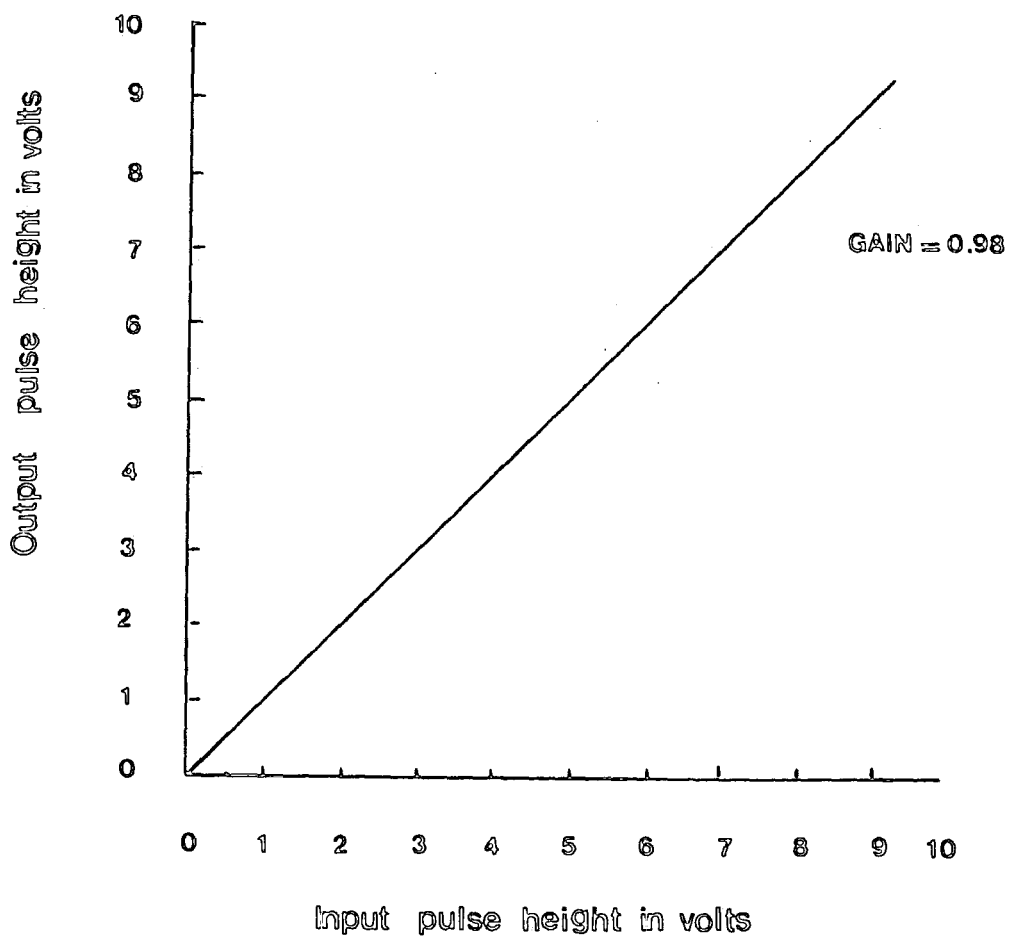

Figure 4.7 Circuit diagram and response of emitter follower.

and it is supplied by -12V direct current from a stabilized voltage supply. Because the outputs from both photomultiplier tubes of each scintillation counter were connected to the same emitter follower input by using short lengths of coaxial cable, the arrangement acts as a charge pulse adder and also as a device with a low output impedance for driving the resulting pulse to the main electronic instruments discussed in the next chapter.

In order to test the performance of the photomultiplier tubes when glued in position on the perspex light guide of a scintillation counter, two matched light emitting diodes were mounted fairly close to one side of the perspex at either end of the counter (see figure 4.1a). Individually, the two photomultiplier tubes in a counter were excited by matched light pulses from the light emitting diode situated on the opposite side of the perspex to them. Figures 4.8a and 4.8b show the variation of photomultiplier tube output pulse height as a function of the extra high tension voltage for detectors numbers 3 and 8 respectively.

4.6) CALIBRATION OF THE PULSE HEIGHT ANALYSER (P.H.A)

A pulse height analyser (P.H.A) is a device which classifies pulses according to their peak amplitudes. Moreover, it records in its memory the relative number of pulses for each class of pulse height which is known as a channel. Each channel has two voltage level limits V and $V+\triangle V$, where $\triangle V$ is constant. Each channel corresponds to an energy level which is proportional to the height of stored pulses. The pulse height

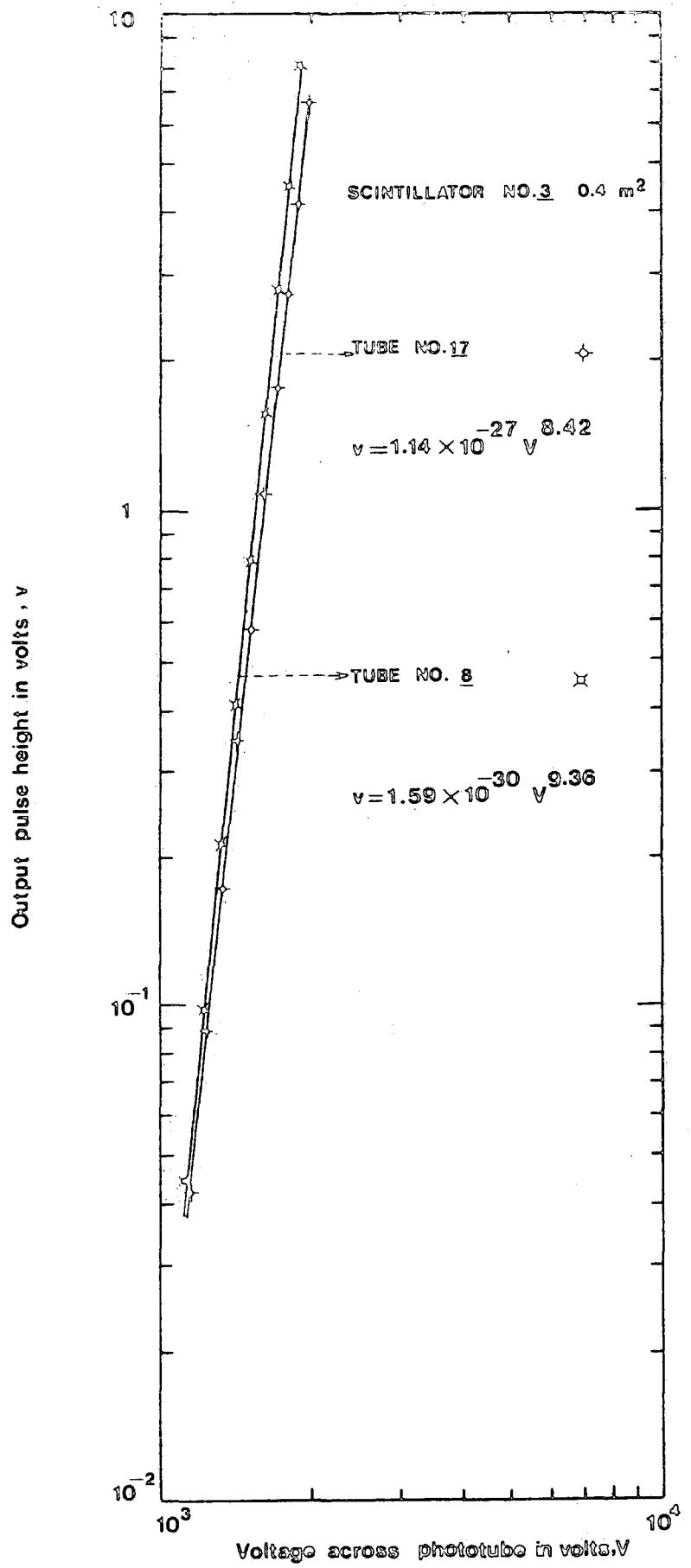

Figure 4.8a Variation of phototube output pulse height with E.H.T when the two photomultiplier tubes in a counter were individually excited with matched L.E.D light pulses from the L.E.D situated on the opposite side of the phosphor to them. The outputs from the tubes are shown by + (tube number 17) and x

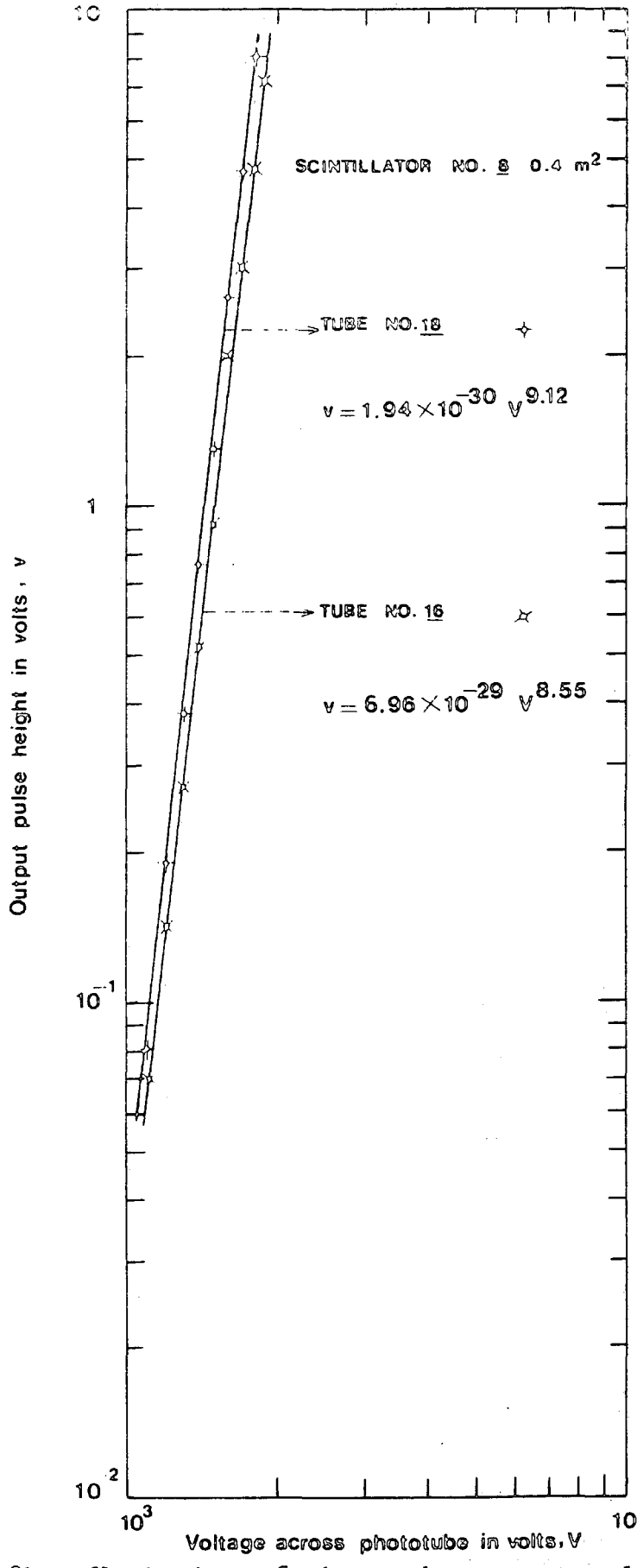

Figure 4.8b Variation of phototube output pulse height with E.H.T when the two photomultiplier tubes in a counter were individually excited with matched L.E.D light pulses from the L.E.D situated on the opposite side of the phosphor to them. The outputs from the tubes are shown by + (tube number 18) and X (tube number 16).

analyser used has one hundered channels and gives detailed information concerning the response of the scintillation counter in the region of pulse heights close to the cosmic radiation peak. The whole 100 channels are open at the same time but only a single pulse can be analysed at a time. In order to calibrate the pulse height analyser, 1μsec wide square pulses from a pulse generator were applied at the input of the analyser and the relation between the input pulse height and the various channel numbers of the pulse height analyser in which the input pulses are recorded, was measured for different values of the gain of the internal pulse height analyser amplifier. The result is shown in figure 4.9. Since all the lines are parallel they can be represented by the following relation: $V=A\times N^{n}$ where V is the pulse height in volts and N is the channel number of the pulse height analyser. Also, the relation between the number of pulses (i.e; number of counts) as a function of the vertical displacement in a channel was measured and the result is shown in figure 4.10.

4.7) DETERMINATION OF THE SCINTILLATION COUNTER RESPONSE

After calibration, the pulse height analyser was employed to investigate the counter response and figures 4.11a and 4.11b show the response of scintillation counters numbers 3 and 8 to the global cosmic radiation flux respectively. A well resolved peak due to the passage of single relativistic cosmic radiation particles through the scintillation counter is observed. With the assistance of the previous data concerning the calibration of the scintillation counter as shown in

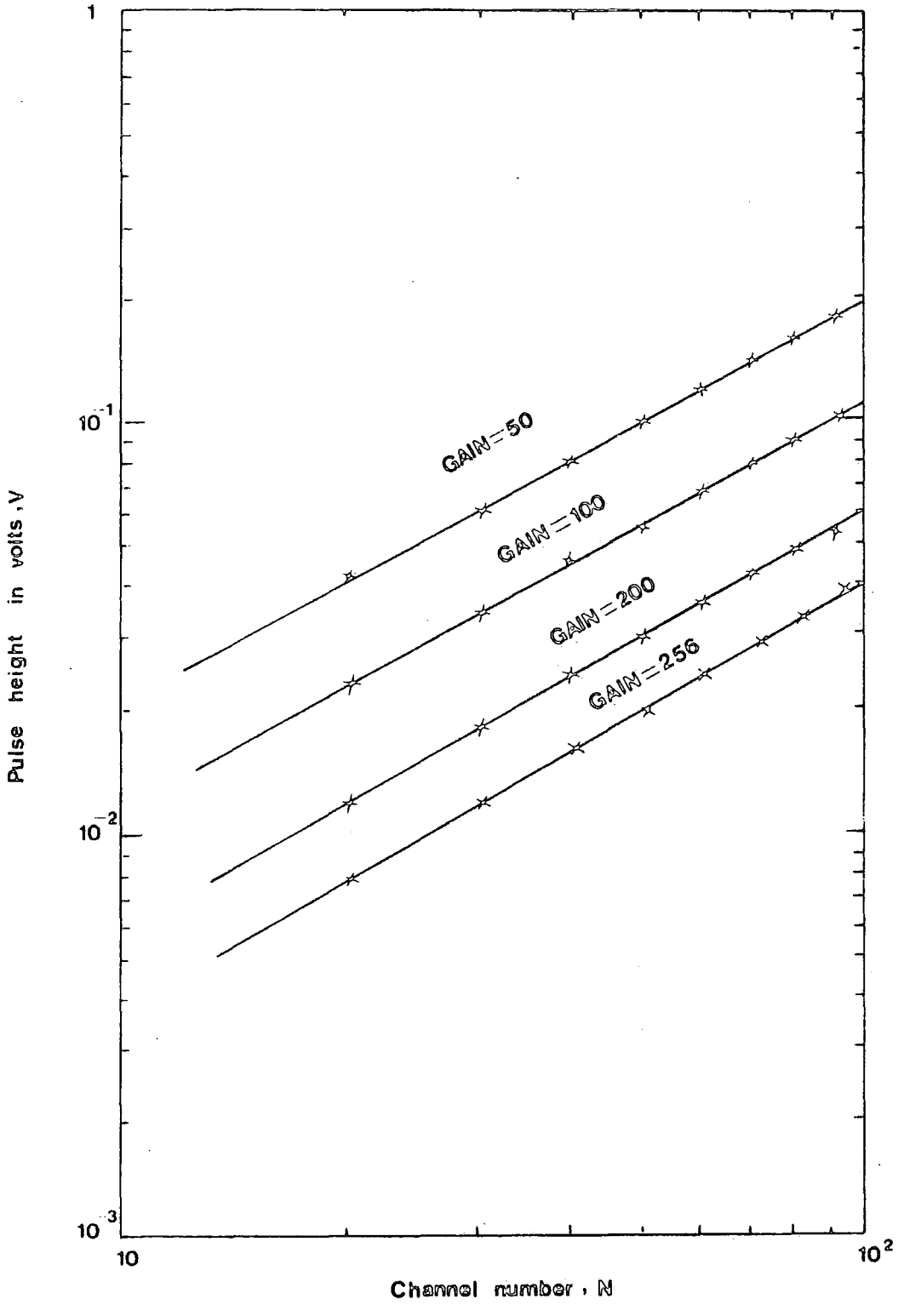

Figure 4.9 Calibration of the pulse height analyser using 1 μsec width input pulses.

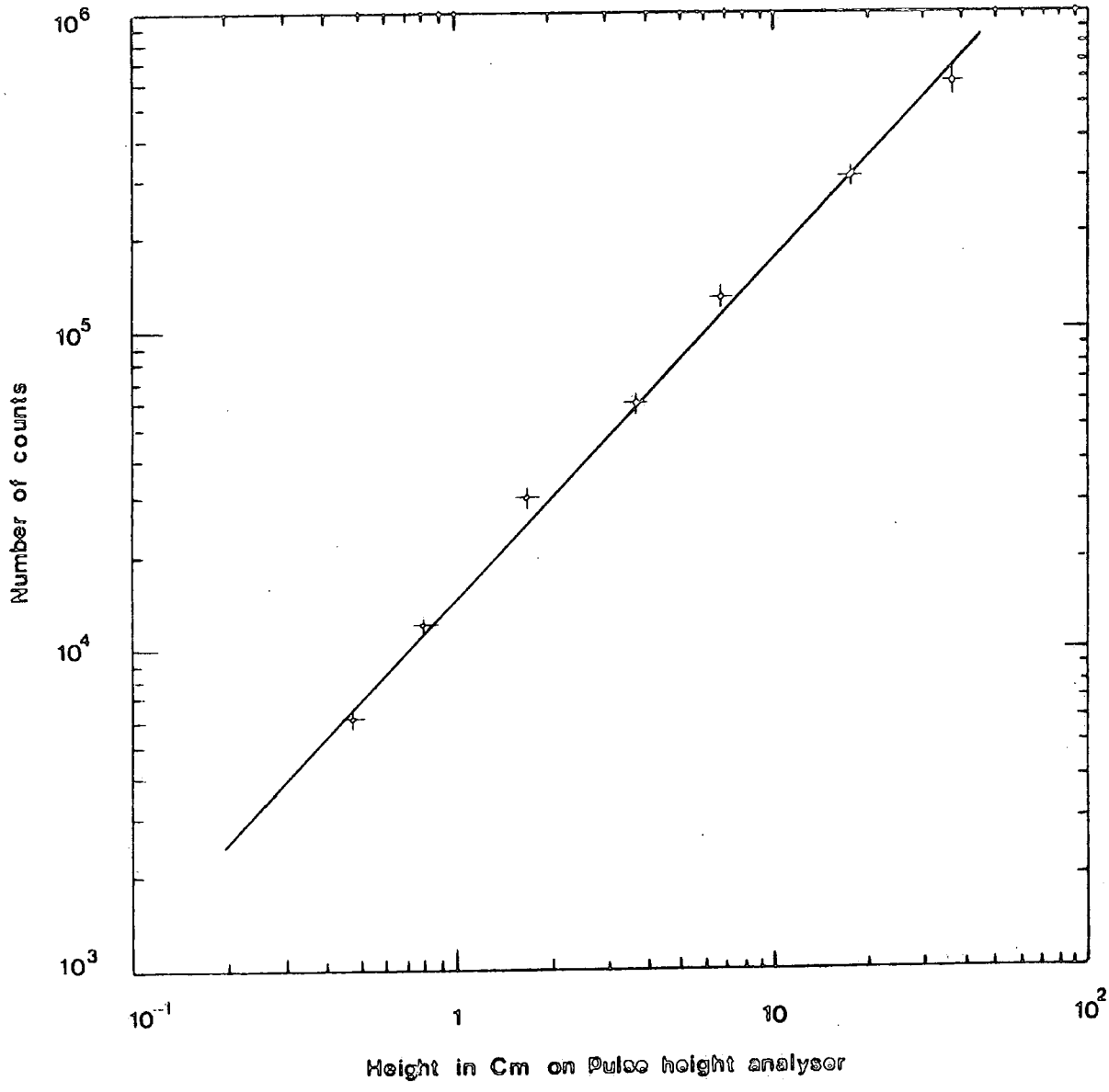

Figure 4.10 Calibration of the pulse height analyser vertical displacement per channel in terms of the number of pulses injected into that channel.

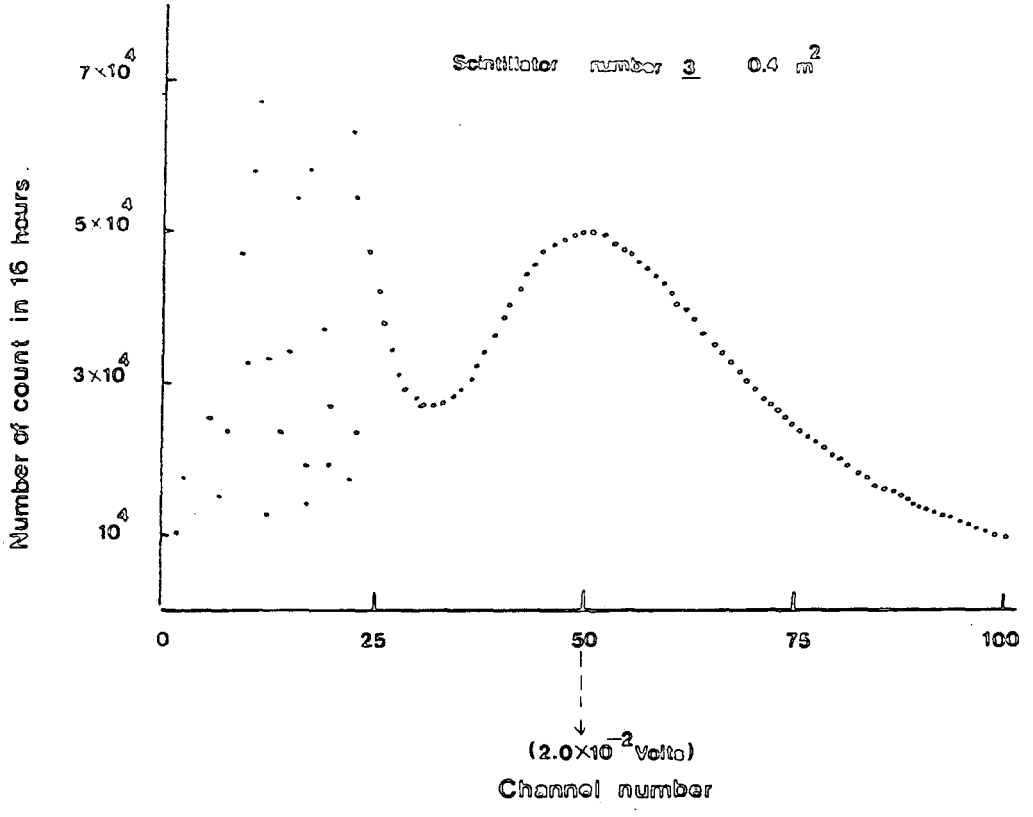

Figure 4.11a Single particle cosmic radiation peak from scintillation counter number 3 as displayed on the pulse height analyser.

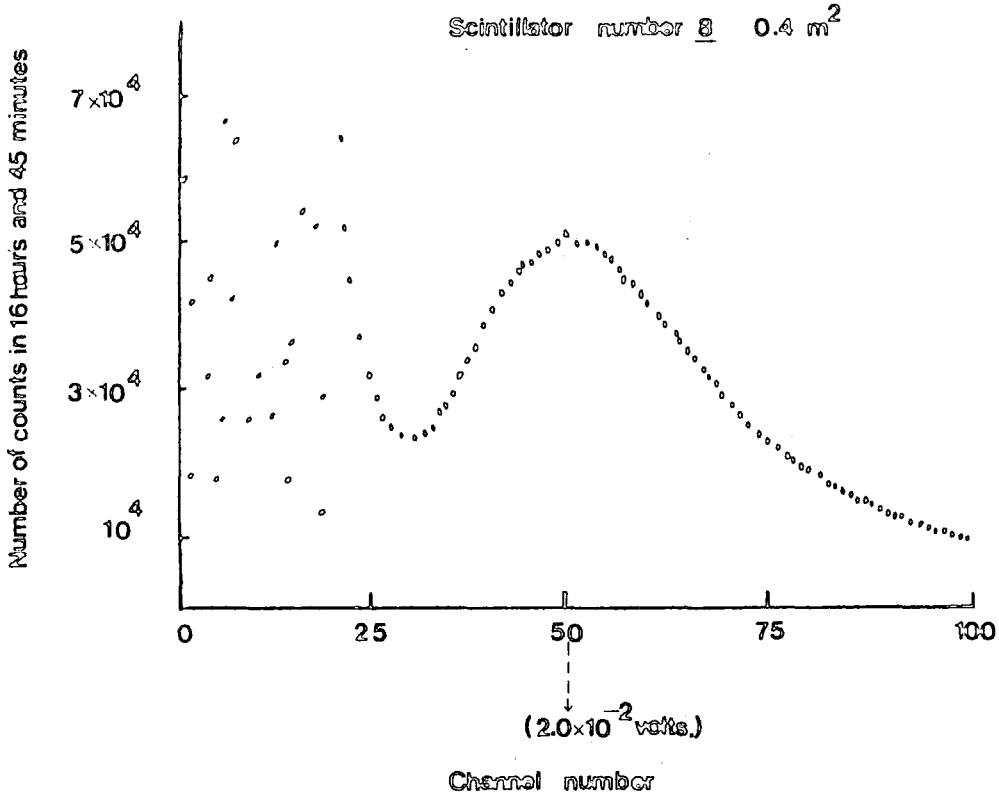

Figure 4.11b Single particle cosmic radiation peak from scintillation counter number 8 as displayed on the pulse height analyser.

figures 4.9 and 4.10, it is possible to calculate the integral rates of pulses as a function of pulse height and the results are shown in figures 4.12a and 4.12b respectively . The variation of the pulse height of the cosmic radiation peak as a function of the extra high tension voltage applied to the photomultiplier tubes is shown in figures 4.13a and 4.13b and is in agreement with the results obtained when individual photomultiplier tubes are excited by the light pulses from a light emitting diode.

For a counter of uniform response over its area and with an output pulse height proportional to particle track length (which implies that sufficient light is produced along the track of the particle that fluctuations in the average number of photoelectrons produced by the photomultiplier tube photocathodes is negligible), the expected output pulse height distribution is $N(v)dv=C/v^{n+3}dv$ for $V>V_0$, where V_0 is the pulse height produced by particles traversing the phosphor of counter at normal incidence. It is seen from figures 4.11 that the response of the present scintillation counter is not precisely of this form even after subtracting off the contribution of thermionic electrons in the channels at the left hand side of the peak. Different processes that convert the expected distribution to the observed one are Landau ionization loss fluctuations that are reflected in the number of scintillation photons which arrive at the photomultiplier tube photocathodes, fluctuations in the number of photoelectrons produced and the non-uniformity of response of the phosphor over its area. For an ideal scintillation counter, the expected most probable

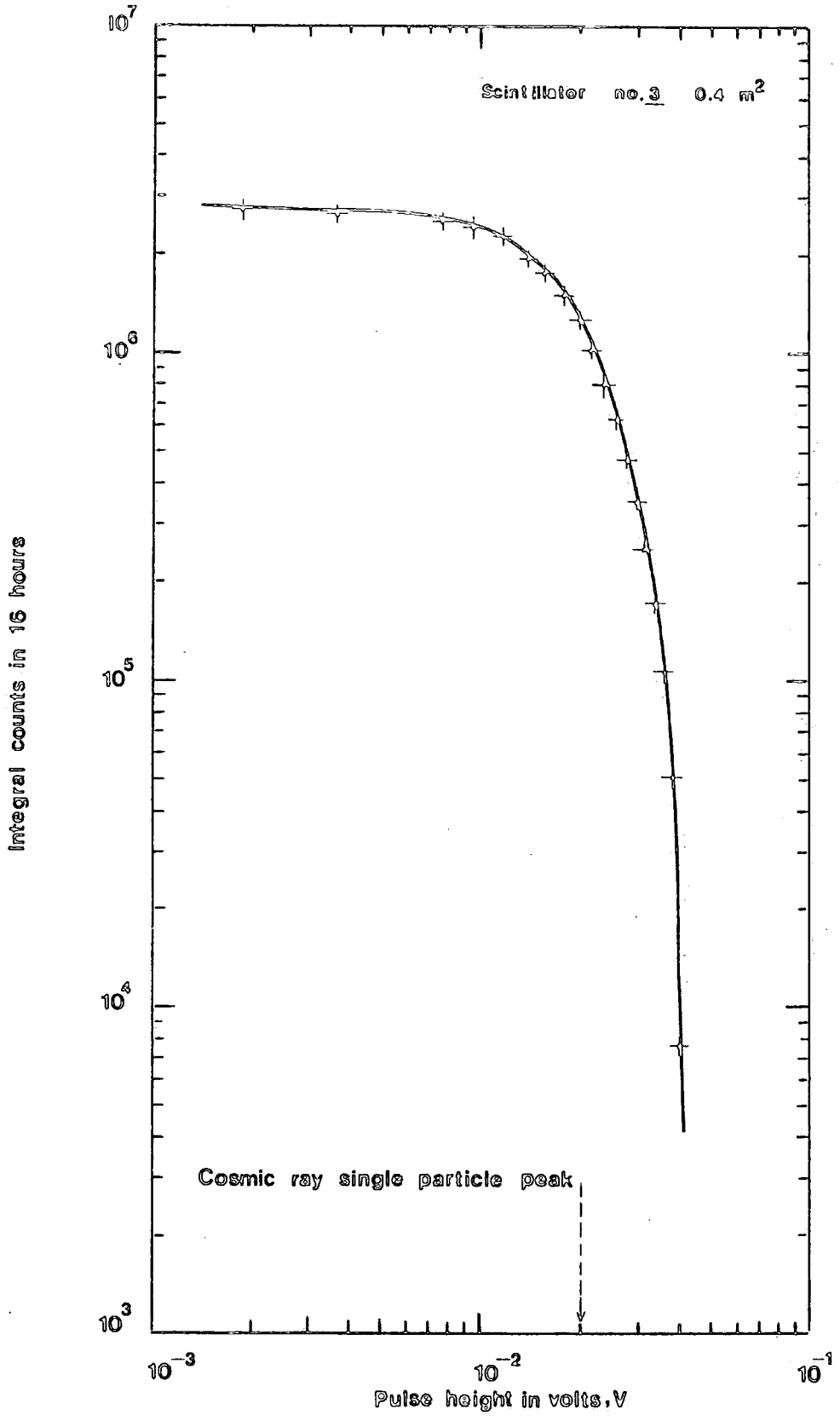

Figure 4.12a Rate of pulses of height >V versus pulse height V as calculated from the pulse height analyser display shown in Figure 4.11a, for scintillation counter number 3. The position of the cosmic ray single particle peak is also shown by the arrow.

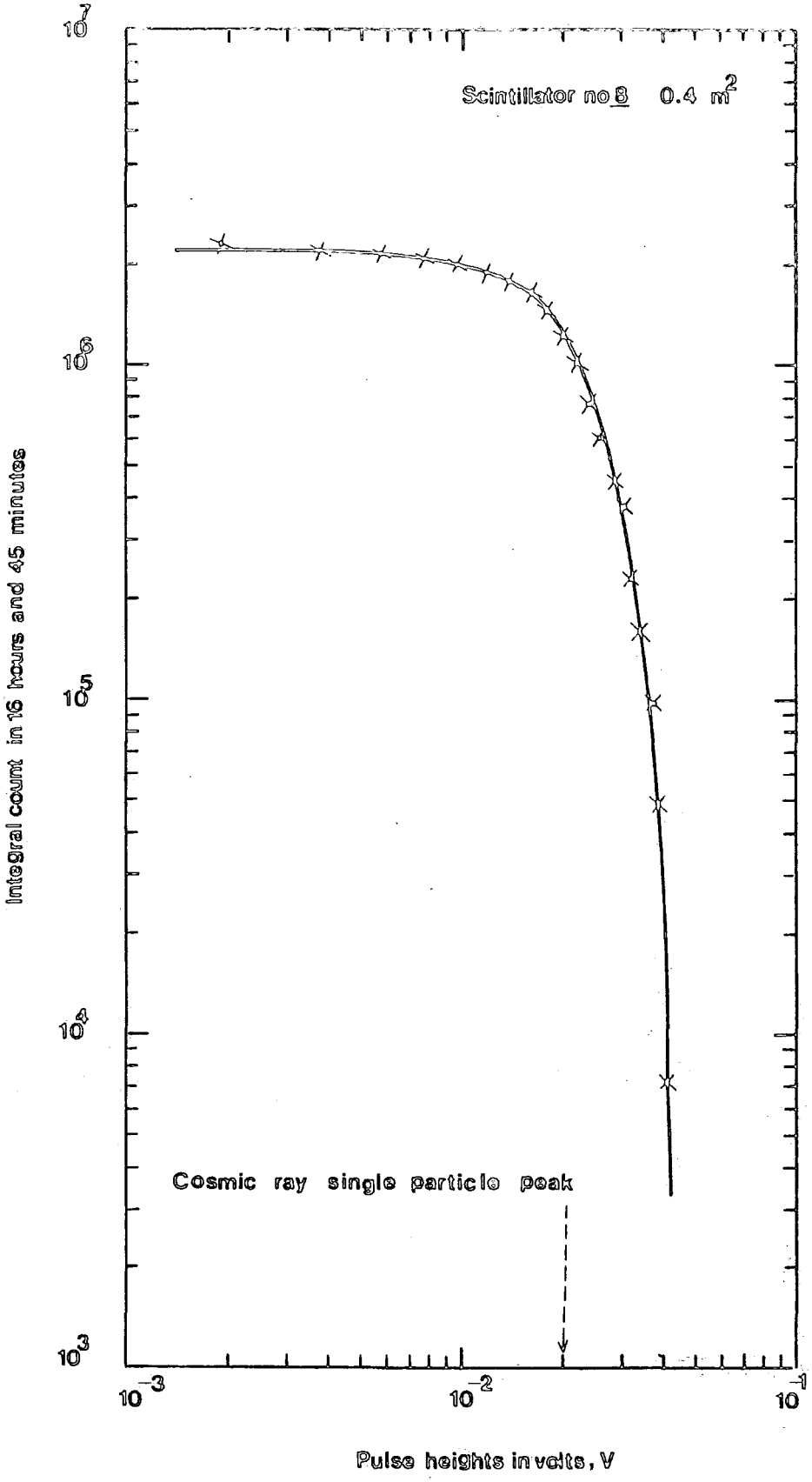

Figure 4.12b Rate of pulses of height >V versus pulse height V as calculated from the pulse height analyser display shown in Figure 4.11b, for scintillation counter number 8. The position of the cosmic ray single particle peak is also shown by the arrow.

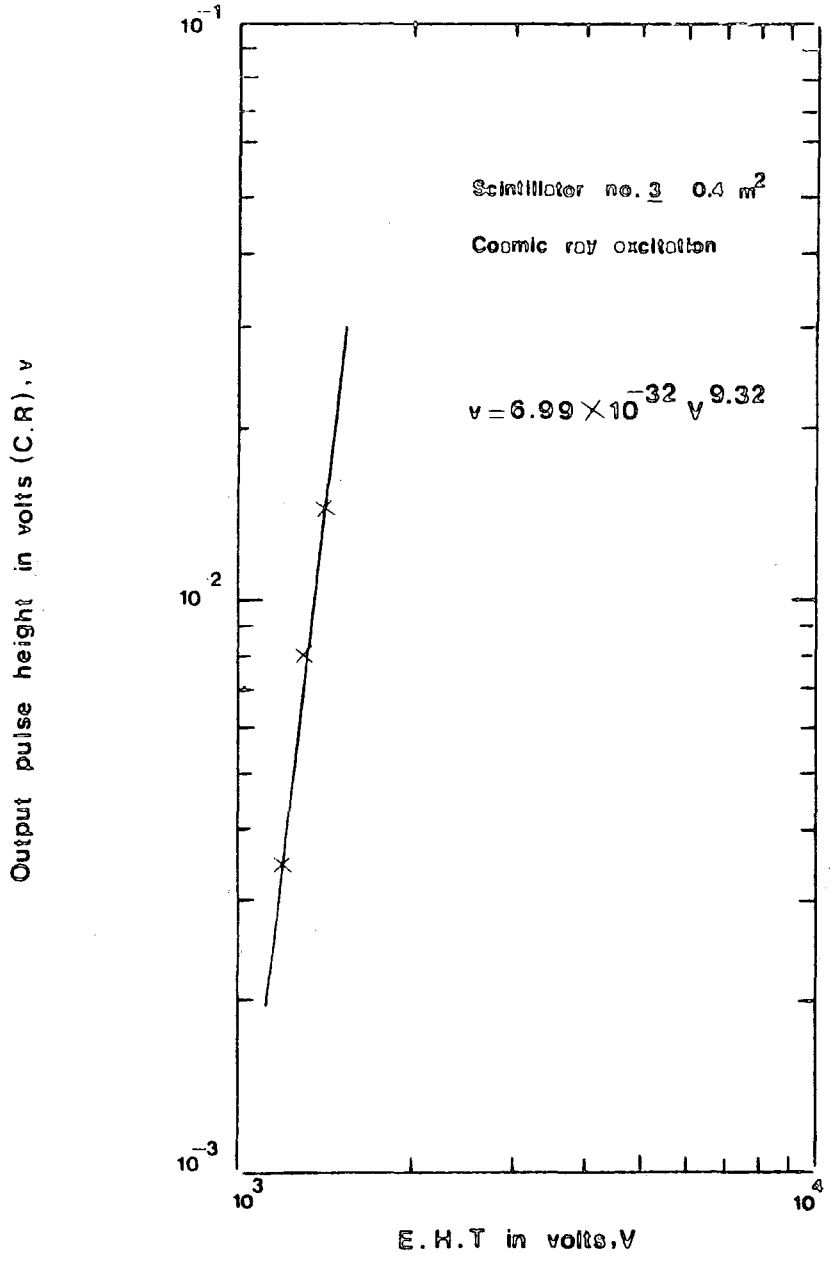

Figure 4.13a Variation of the peak pulse height produced by the global cosmic ray flux traversing the scintillation counter number 3 as a function of the voltage applied to the photo-multiplier tubes. The measurements are fitted by $v = 6.99 \times 10^{-32} V^{9.32}$. This result is consistent with the results obtained when individual phototubes are excited with light pulses from a light emitting diode.

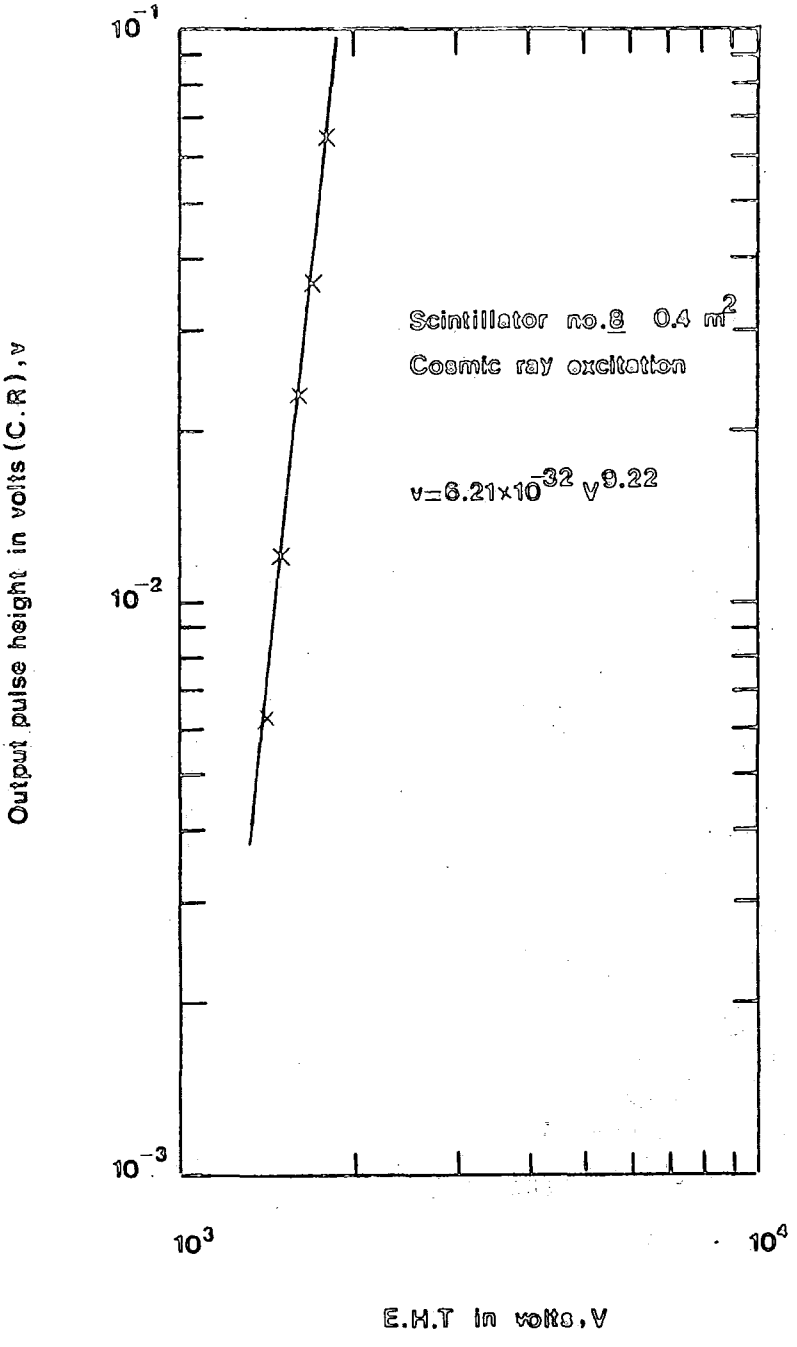

Figure 4.13b Variation of the peak pulse height produced by the global cosmic ray flux traversing the scintillation counter number 8 as a function of the voltage applied to the photomultiplier tubes. The measurements are fitted by $v = 6.21 \times 10^{-32} V^{9.22}$. This result is consistent with the results obtained when individual phototubes are excited with light pulses from a light emitting diode.

value of the observed distribution corresponds to particles traversing the phosphor of the counter at normal incidence. The effect of photon fluctuations is to broaden this distribution but the most probable value of the observed distribution, as shown in figures 4.11a or 4.11b, is expected to correspond closely to the average pulse height produced by cosmic radiation particles traversing the phosphor at normal incidence. Hence, this latter quantity can be determined from the response of the detector to the global cosmic radiation flux without resorting to the use of a narrow angle vertical calibration telescope.

4.8) SUMMARY

Nine plastic scintillation counters, each of area $0.4m^2$ and 5cm thick, have been constructed which are suitable for making electron density measurements in extensive air showers. They are relatively light and can be transported from place to place by two persons. All the counters show a clearly resolved cosmic radiation peak when displayed on a pulse height analyser without the necessity of using a subsidiary cosmic radiation telescope. In the present work, two of them have been used to obtain a local electron density extensive air shower selection trigger and this work is described in the next chapter.

CHAPTER FIVE

EXPERIMENTAL ARRANGEMENT USED FOR THE TACHYON EXPERIMENT

5.1) INTRODUCTION

The lack of tachyon detection at laboratory energies suggests that , if tachyons are produced , then some reasonably high threshold energy for production must exist. Thus the present search was established assuming that if a tachyon penetrates to sea level, afterwards it will interact in some way that provides an output pulse from a scintillator–photomultiplier combination which is sufficiently large to be distinguishable above photomultiplier tube noise, at least in a statistical sense.

5.2) EXTENSIVE AIR SHOWER SELECTION

For measurements of the density spectrum of extensive air showers, one needs a system to identify the arrival of an E.A.S which is known as a trigger system. In the present experiment, a two fold coincidence between scintillators A and B each of area $0.4m^2$ is used. For the tachyon experiment, the threshold electron densities required to be recorded by both scintillators was set at 25 m^{-2}. The design and performance of these scintillators and the head units used have been described in chapter four. The centres of the scintillators were separated by 1.7 metres in the horizontal plane and figure 5.1 shows the experimental arrangement used in the experiment. The

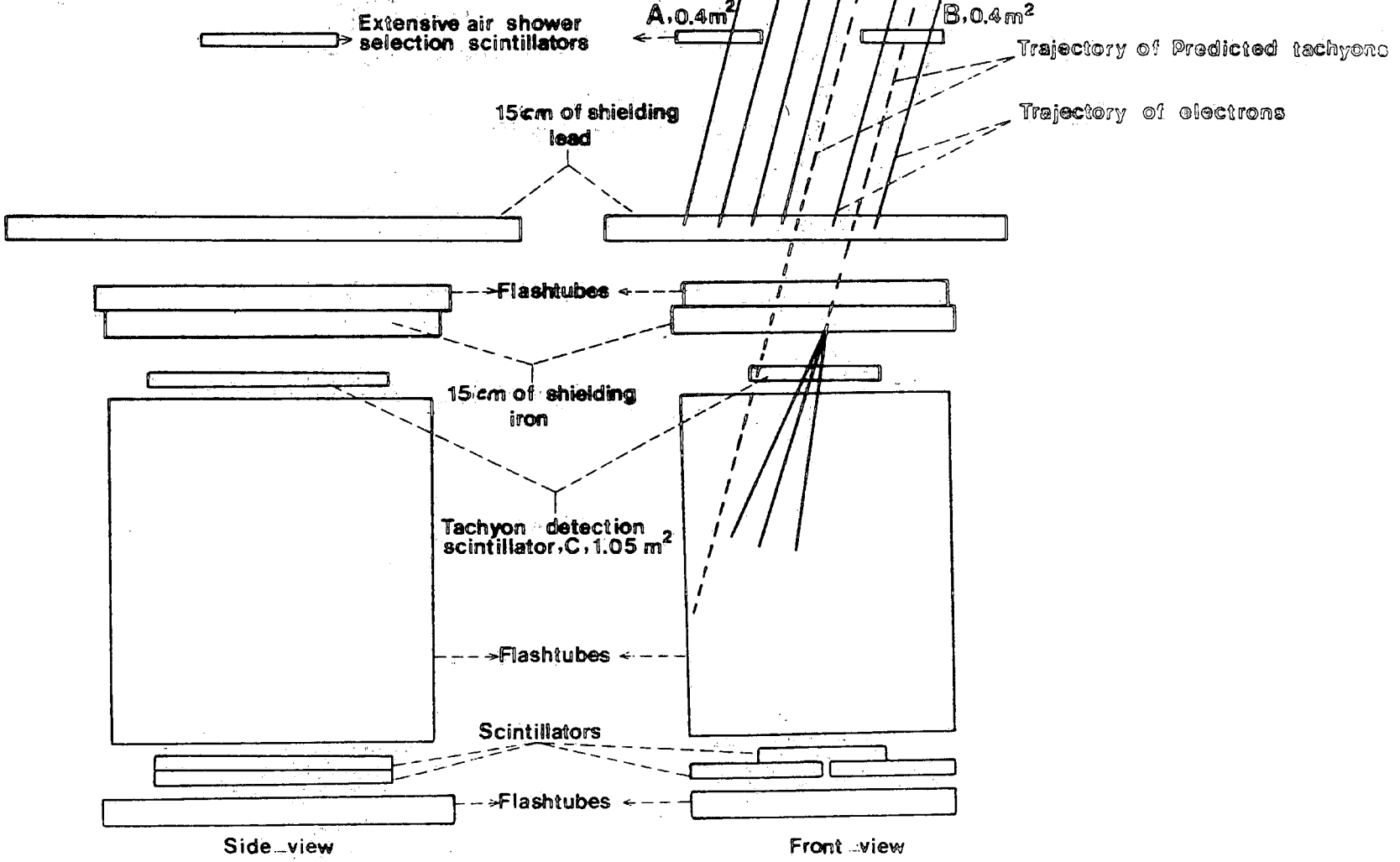

Figure 5.1 Experimental arrangement used in the tachyon experiment. A twofold coincidence between scintillators A and B was used to detect extensive air showers of local electron density $\geq 25\ m^{-2}$. Scintillator C was used as the tachyon detector and could register either penetrating tachyons or the effects of tachyon interactions in the iron or lead absorbers as illustrated. The flash tubes were not operational in the present experiment nor were the three scintillators shown at the bottom of the detector. Phosphor areas of scintillators A,B are 80 x 50 cm^2 (0.4 m^2) and C is 140 x 75 cm^2 (1.05 m^2).

pulses detected by scintillator C which was employed as a tachyon detection scintillator, are recorded in the 265μsec and 235 μsec time domain before and after the arrival of the shower front pulse respectively. In fact, it can register either penetrating tachyons (i.e; by their direct interaction with the phosphor material of scintillator C) or the effects of tachyon interactions in the lead or iron shielding layers situated above it , both of which are 15 cm thick. Finally, the figure shows the modified large flash tube chamber (see appendix C) which is part of the equipment , but it was not operated the present experiment.

5.3) STUDY OF THE RESPONSE OF THE TRIGGERING SCINTILLATORS

To investigate the density spectrum of extensive air showers, one first measures the response of the each scintillator when single relativistic cosmic ray particles pass through it, and it is necessary that the response of each scintillator to the global cosmic radiation flux should yield a distribution whose peak is well resolved from the distribution produced by single thermal electrons. The response of both scintillators A and B to the global cosmic radiation flux was measured using a pulse height analyser as described in the previous chapter. To study the response over a much larger range of pulse heights, it is more convenient to use an amplifier and scaler to obtain the measurements. Both scintillators were adjusted , so that the average pulse height, v, produced by relativistic cosmic ray particles traversing their area at normal incidence produced an average pulse height

of 20mV at the head – unit outputs. If a pulse height , V , is produced by a shower of particles traversing a scintillator of area S at normal incidence , the particle density $\triangle$ is given by $\triangle = V/v.S\ m^{-2}$. Also, the number of particles, N , through the scintillator is given by V/v. Figures 5.2a and 5.2b show the integral response of each scintillator to the global cosmic radiation flux where pulse heights are measured at the output of each scintillator head – unit. In fact, figure 5.2b is the same as 5.2a except that the units of the abscissa have been converted to equivalent electron density (i.e; $\triangle$) and the position of the single particle cosmic radiation peak is also indicated by arrows in the figures. Figures 5.3a and 5.3b demonstrate that the coincidence rate measurements are in reasonable agreement with the summary of such measurements by Greisen (1960).

5.4) BAROMETRIC EFFECT

For extensive air showers the variation in the rate of showers of a given size with change of barometric pressure is of interest because it can provide a measurement of the attenuation of the shower, once past its maximum of development in the atmosphere. An increase in pressure effectively corresponds to the apparatus being situated at a greater depth, and thus the rate of showers of a given total number of particles will diminish. The variation of the rate of any secondary cosmic radiation component with atmospheric pressure at the level of observation can be expressed as follows: $R=R_o \exp(-\beta(P-P_o))\ m^{-2}.sec^{-1}.st^{-1}$ where R is the cosmic radiation rate

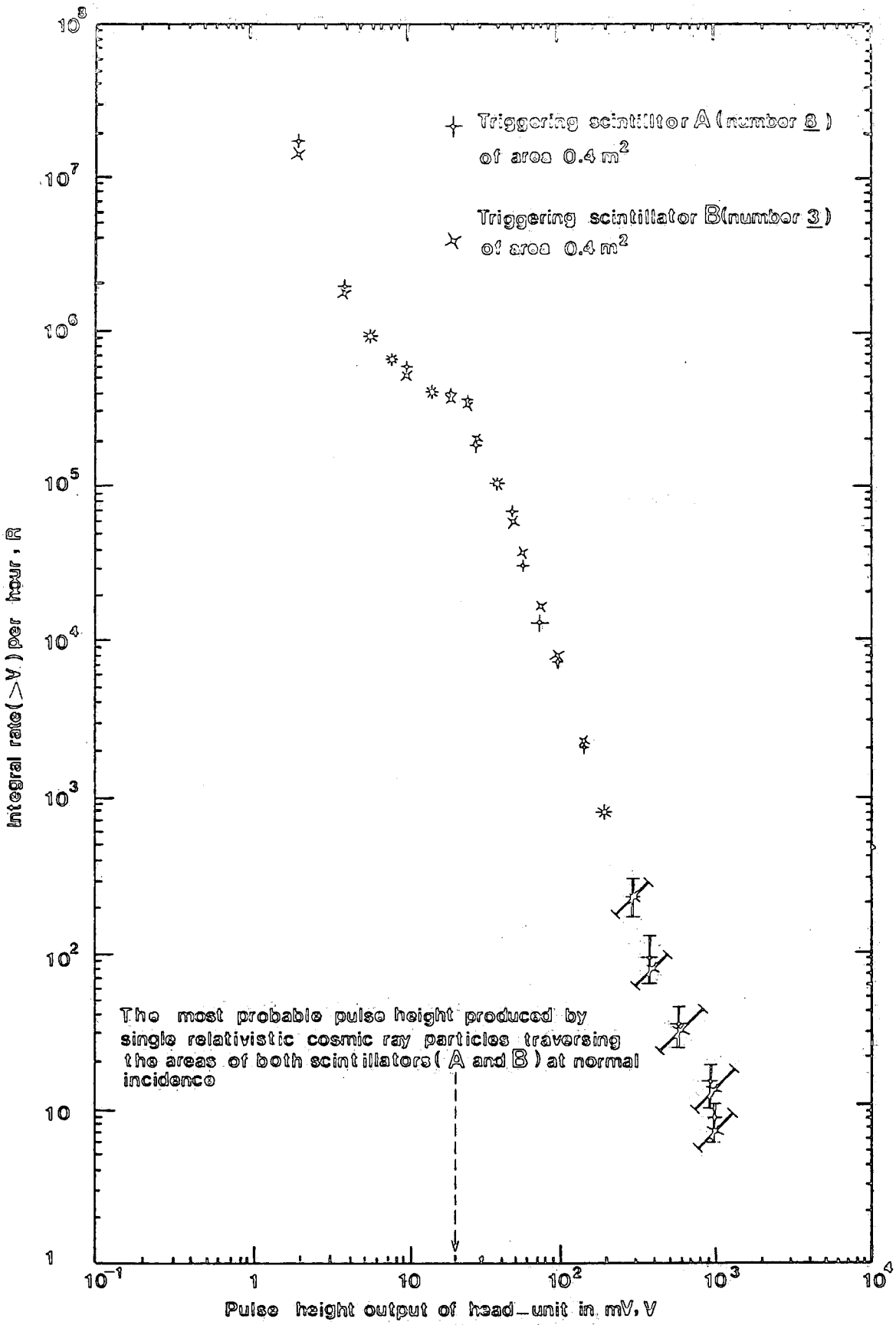

Figure 5.2a Integral rate of pulses of height > V versus pulse height as measured at the output of the head-unit when the counter is exposed to the global cosmic ray flux. The most probable pulse height produced by single relativistic cosmic ray particles traversing the counter at normal incidence is indicated by the arrow.

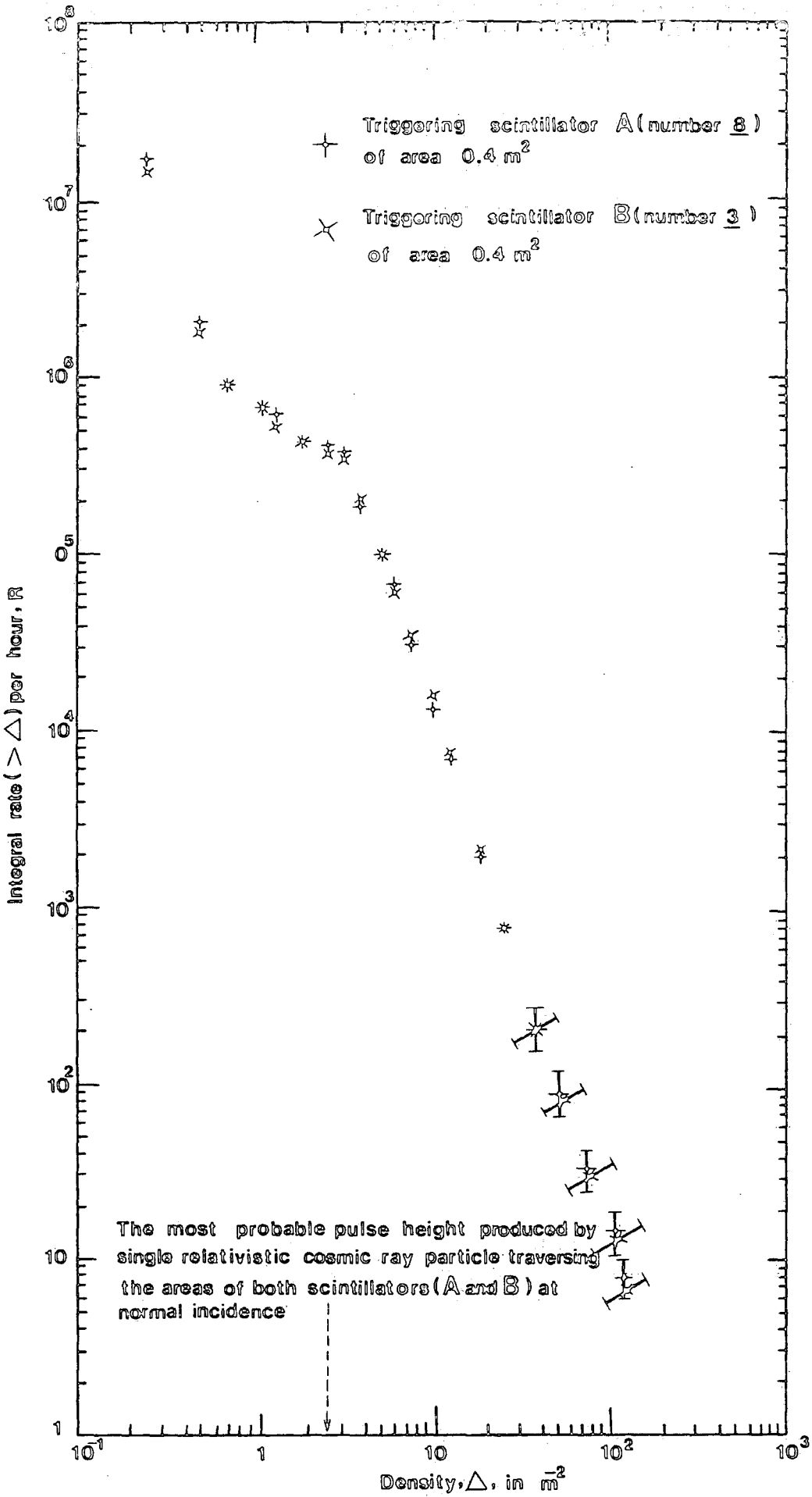

Figure 5.2b Same as figure 5.2a except that the abscissa is plotted in terms of the apparent density of particles traversing the scintillation counter which has area 0.4 m^2. Single relativ-

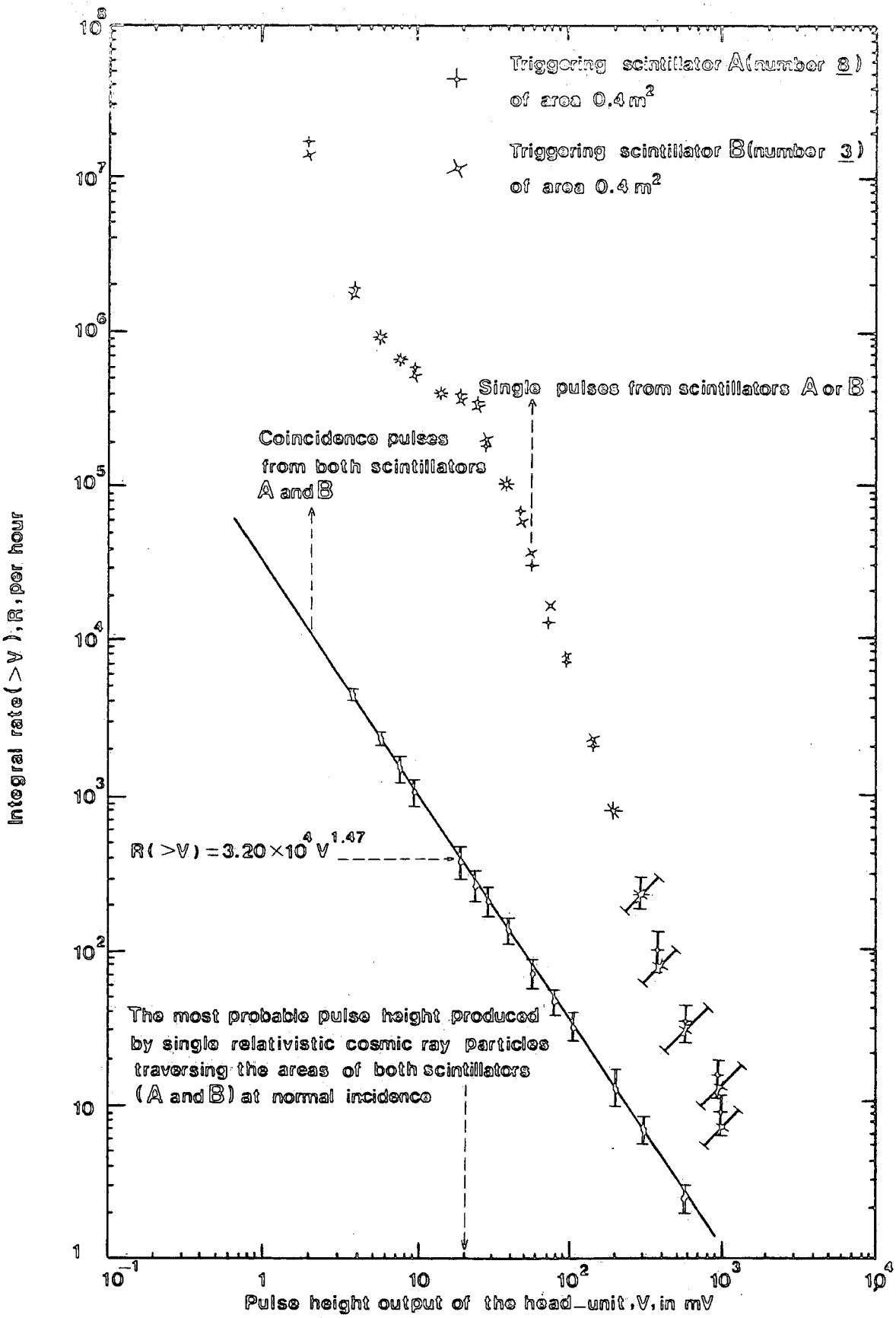

Figure 5.3a Integral rate of pulses of height >V versus pulse height as measured at the output of the head-unit. Also shown is the coincidence rate from both scintillators A (No. 8) and B (No. 3), each of area 0.4 m^2.

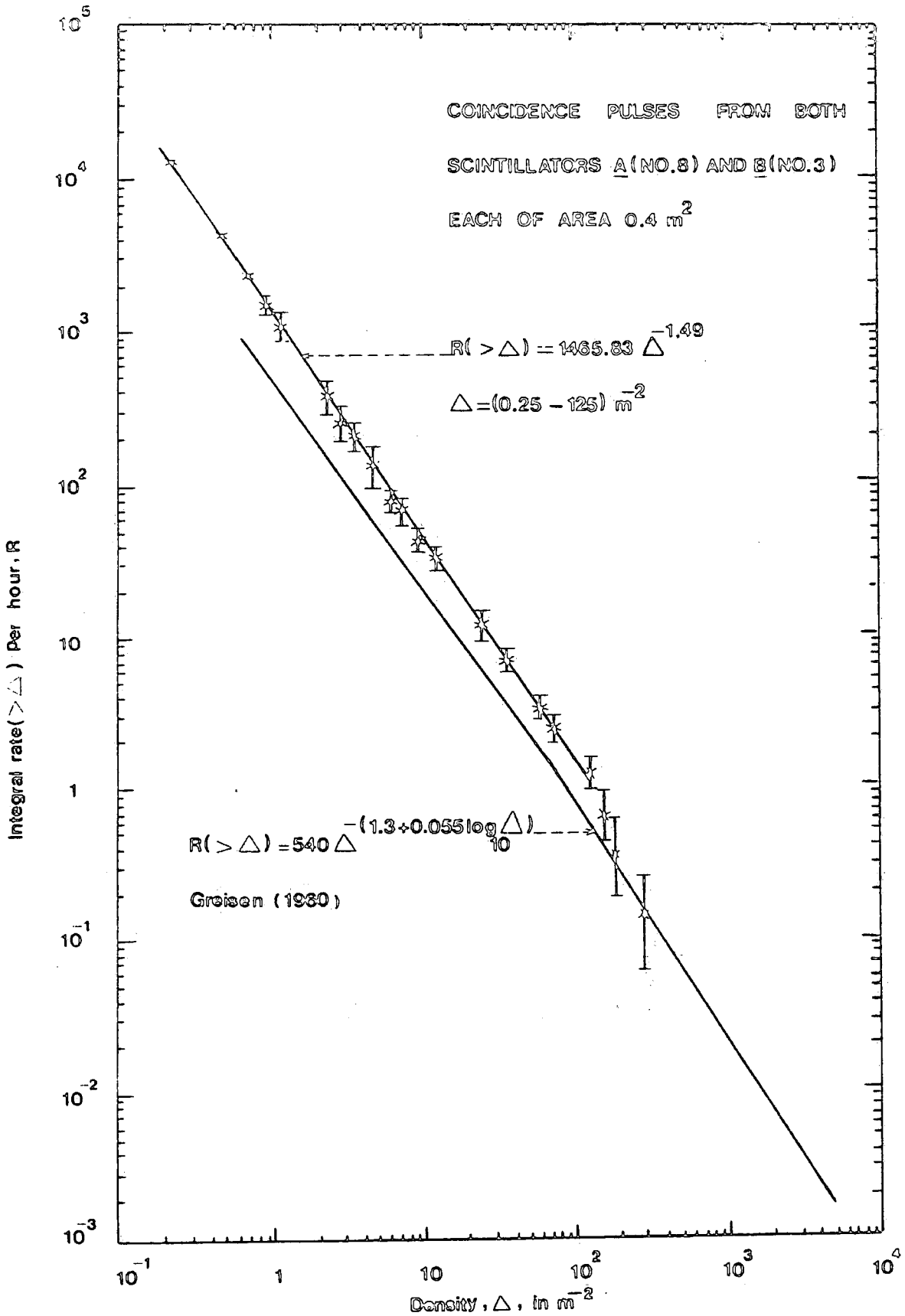

Figure 5.3b The measured integral density spectrum of electrons at sea level compared with the result given by Greisen (1960).

at pressure P , R_o is the rate at the standard atmospheric pressure P_o (76 cm of Hg) and β is the barometric coefficient which is defined as the percentage change in the counting rate with atmospheric pressure calculated from the above formula as follows: $\beta = dR/R.dP$ per cm.Hg. For pure photon—electron cascades, the barometer coefficient is progressively smaller as the energy increases. Some experiments have shown that the barometric coefficient of the extensive showers in the lower atmosphere (below $650 g.cm^{-2}$) is approximately constant and equal to about 10 percent per cm.Hg pressure over quite a wide range of shower sizes. This behaviour seems to be incompatible with the theoretical predictions for a photo—electron cascade , but the accuracy of the measurements does not permit definite conclusions to be made concerning possible variations in the barometer coefficient with shower size. The most recent work suggests that the barometer coefficient of showers is an increasing function of shower size and for showers containing more than 10^7 particles is significantly greater than 10 percent per cm.Hg. Hence, the effect of atmospheric pressure changes on the flux of the low energy muon component is considerably less than on the flux of high energy extensive air showers.

During a running time of 839hr 46min 40sec, a total of 10,142 extensive air shower triggers were recorded. Also, the barometric pressure was recorded and the results are shown in figure 5.4. The mean pressure at which the events were recorded was 75.35cm.Hg and the best fit line shows that the pressure variation of the rate due to pressure changes from the mean value is (7.30±1.15)% per cm.Hg.

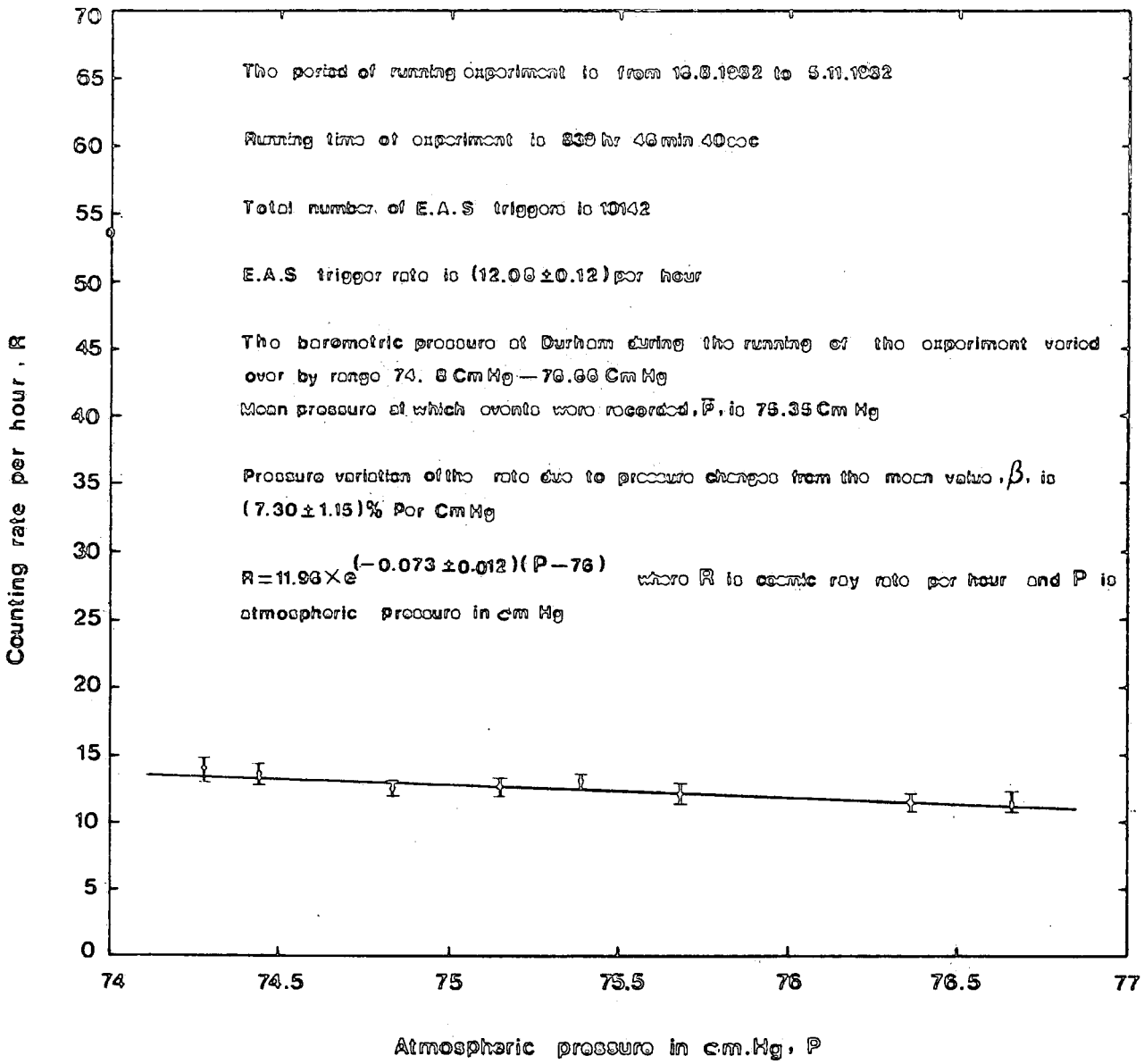

Figure 5.4 The variation of the trigger rate of observed showers with atmospheric pressure.

5.5) DELAY LINE

In order to measure the occurrence of ionizing events occurring in the tachyon scintillator, C, before the arrival of the main air shower front pulse, some method must be used to store the relevant information. In the present experiment , Hackethall HH1600 delay cable which has a delay of approximately 1 μsec per foot , was used. Because of the large attenuation of pulses in the delay cable , it cannot be used as a whole. Thus, it was split into three 80ft lengths. Figure 5.5 shows that the attenuation suffered by 2 μsec square pulses in traversing an 80 μsec length of this cable is a factor of 5. In the actual experimental arrangement , each of them was followed by an amplifier to restore the pulse height to its original value before entering the next section of line. Figure 5.6 shows the relation between the pulse height at the output of the head unit and pulse height recorded on the oscilloscope. To prevent reflection of pulses at the ends of each delay cable, each was terminated by its characteristic impedance of 1.65KΩ . Since the electromagnetic field associated with the pulse travelling down the line, interacts with adjacent sections of the line and produces noise and reflection of pulses, it is impracticable to use the cable in a simple coil arrangement. Each 80 μsec length was wound round a wooden cylinder of 75 cm length and 45 cm diameter , which was found sufficient to space each loop and make the interaction effects negligible. As the figure of 1 μsec per foot for the delay cable is only an approximate value , the total delay was measured accurately and found to be 265 μsec rather than 240 μsec as approximately

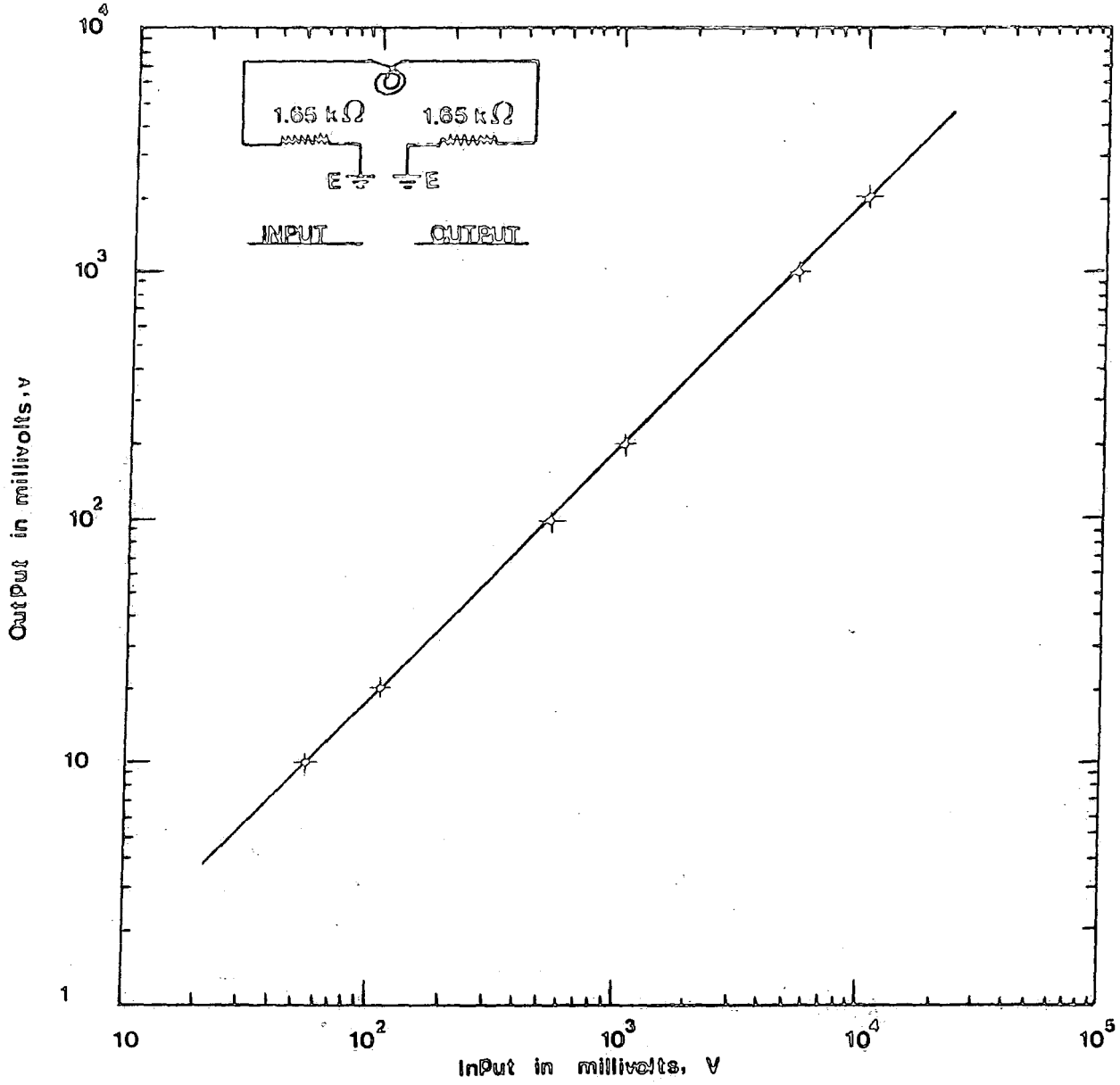

Figure 5.5 The attenuation of a 2 μsec square pulse after transmission down 80 μsec of Hackethall HH 1600 delay line.

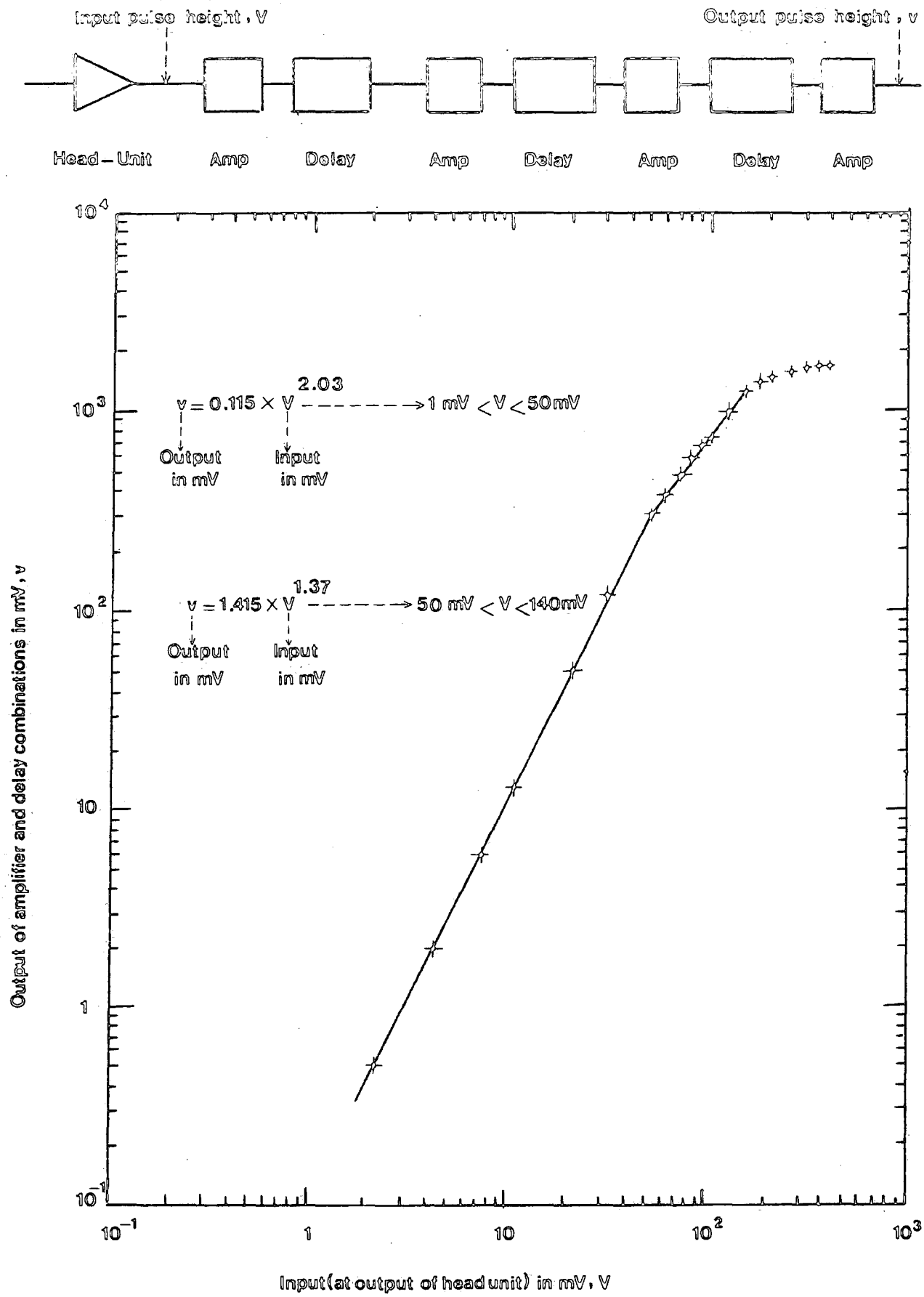

Figure 5.6 Input/output calibration curve used in the tachyon experiment.

expected.

5.6) PRINCIPLES OF THE EXPERIMENTAL ARRANGEMENT

A detailed block diagram of the instruments used in the present experiment is shown in figure 5.7 in which the final output from the delay cables was displayed on a dual beam Tektronix oscilloscope with a total sweep time of 500 μsec so that both the 265 μsec time domain before the arrival of the shower front pulse and the 235 μsec after that could be investigated. To achieve as large a dynamic range as possible for pulse height measurement , one channel of the oscilloscope was operated on a sensitivity of 5mv/cm with a maximum possible deflection of 7cm and the other channel was operated on a sensitivity of 200mv/cm with a maximum possible deflection of 8cm. The oscilloscope was viewed by a standard type of camera with an open shutter and on the occurrence of an extensive air shower event, the time base was triggered and the details could be recorded on 35mm film. Using a digital clock , it was also possible to photograph the time of occurrence of the event on the same film. Figure 5.8 shows the appearance of an ideal event as expected on the screen of the oscilloscope in one of its sensitivity channels.

5.7) THE TACHYON DETECTION SCINTILLATOR, C

The desgin of the tachyon detection scintillator is shown in figure 5.9. It consists of NE102A plastic phosphor of dimensions 140cm $\times$ 75cm $\times$ 5cm. The rectangular perspex light guide of dimensions 75cm $\times$ 30cm $\times$ 5cm is optically connected to

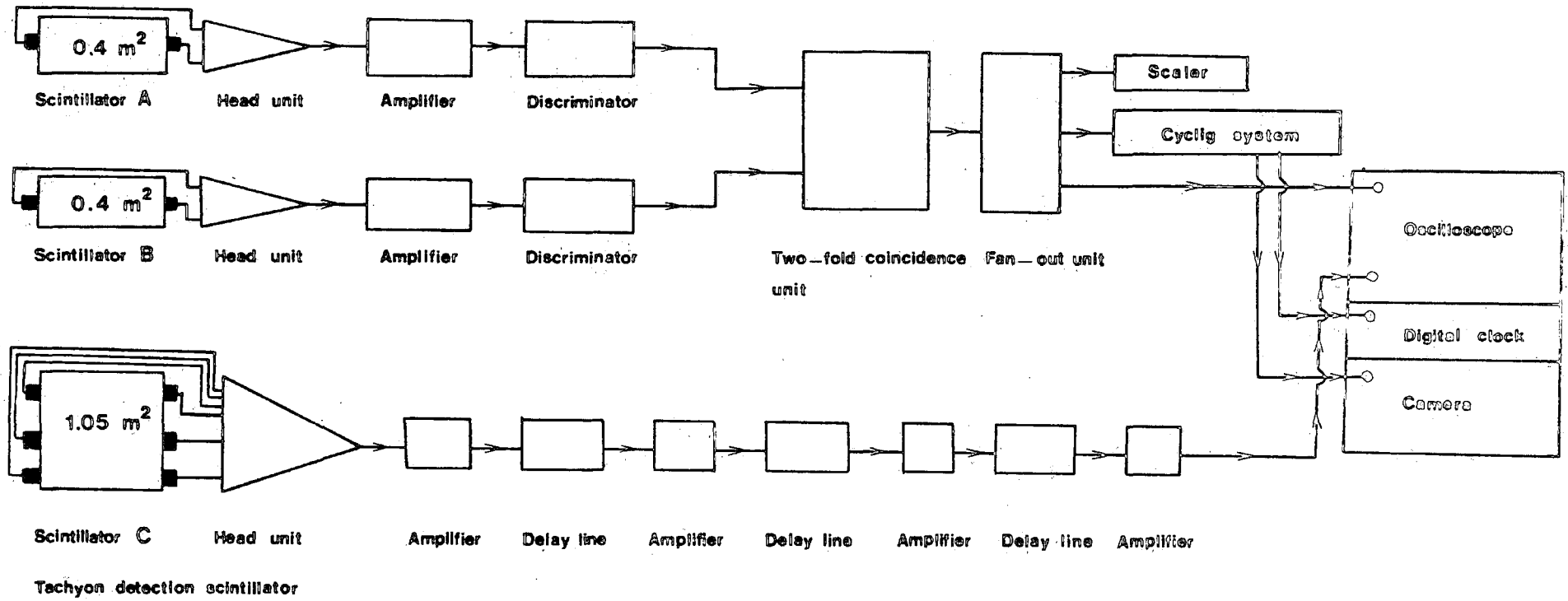

Figure 5.7 Block diagram of the electronics used in the tachyon experiment. Scintillators A and B are used for detecting extensive air showers of local electron density $\geqslant 25\ m^{-2}$. Scintillator C is used as a tachyon detector.

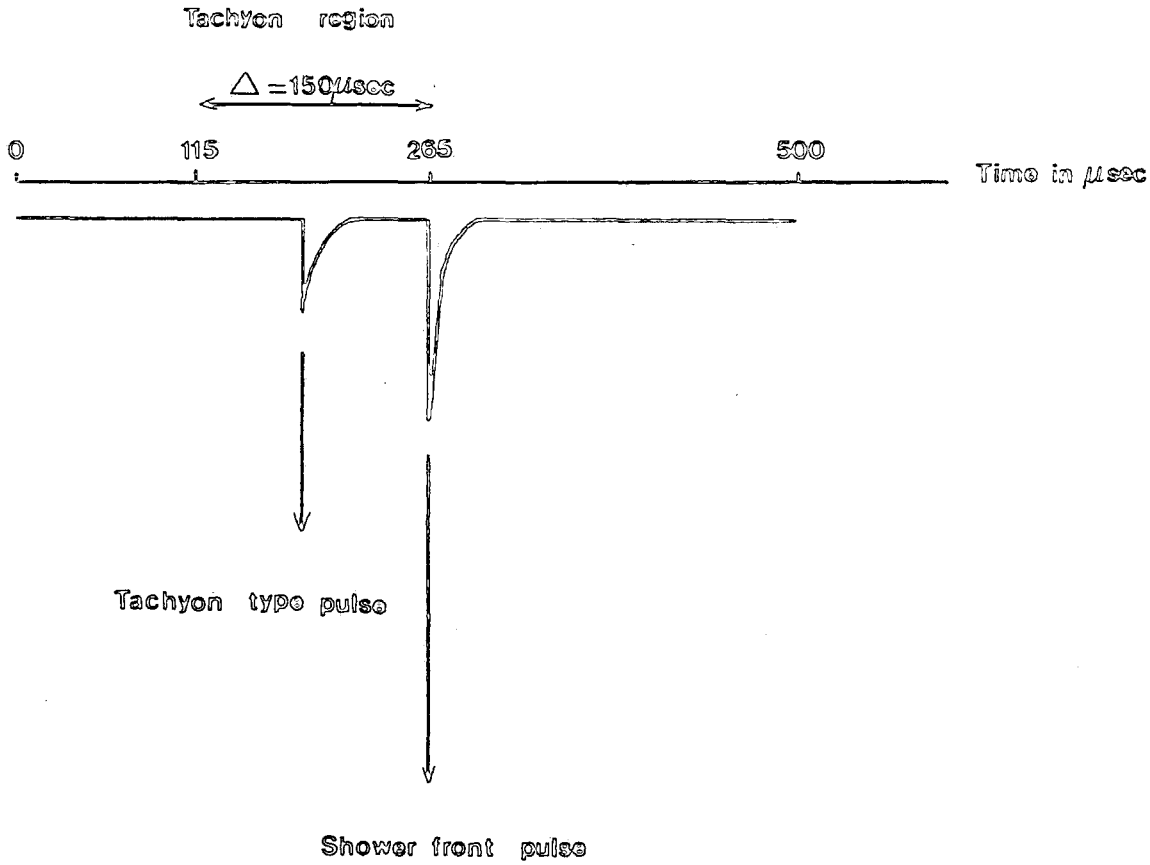

Figure 5.8 The appearance of an idealised event as photographed on the dual beam oscilloscope in one of its sensitivity channels.

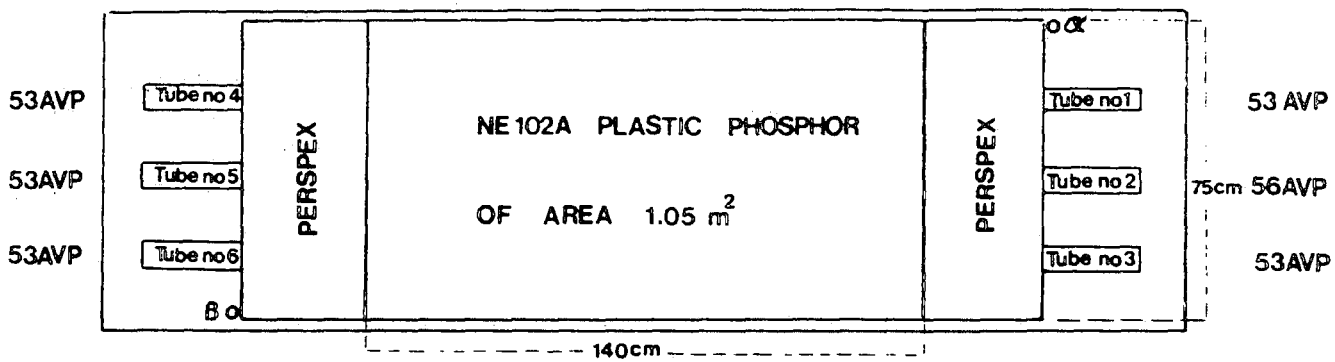

Scale diagram of the top view of the plastic scintillator C used as the tachyon detector with dimensions 140 x 75 x 5 cm^3.

Figure 5.9 Details of the tachyon detector, scintillator C. α and β are the locations of pulsed light emitting diodes which are used to adjust the photomultiplier tubes on the opposite side of the counter to have equal sensitivities.

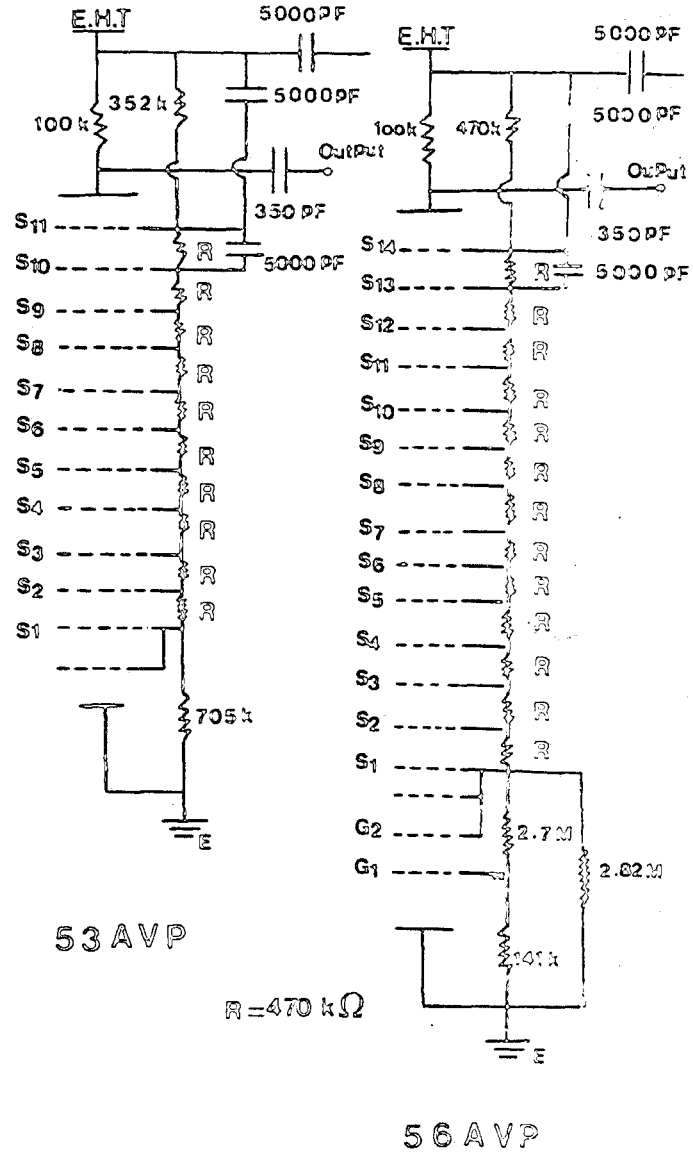

Resistance chains for the two types of photomultiplier tube used in the tachyon scintillator, C.

each 75cm edge of phosphor. In order to attain a large signal to noise ratio, the phosphor was viewed through light guides by a total of six photomultiplier tubes. Of these, five are 53AVP and one is 56AVP and all are of two inches diameter. By using a precision potentiometer, a positive supply voltage was assigned to each tube and then a negative pulse was taken from the anodes. Before proceeding to measure the response of the scintillator , it is necessary to match the six photomultiplier tubes , so that all of them have equal sensitivity. This was accomplished by using a pulsed light emitting diode as a source of light which was mounted successively at the points α and β. Figures 5.10a, 5.10b, 5.10c, 5.10d, 5.10e and 5.10f show the variation of output pulse height as a function of the voltage of the extra high tension power supply for photomultiplier tubes numbers 1 , 2 , 3 , 4 , 5 and 6 respectively. To keep the electronics as simple as possible,the outputs from all six photomultiplier tubes were connected together using short lengths of coaxial cable and the common connection was used as the input to a simple emitter follower of exactly the same type which has already described in the previous chapter. The response of the tachyon scintillator to the global cosmic radiation flux is seen in figure 5.11 and shows that the single particle peak is well resolved from the noise. The integral rates of pulses versus pulses height as calculated from the pulse height analyser is displayed in figure 5.12 in which the position of the cosmic ray single particle peak is shown by the arrow. Figure 5.13 shows the variation of the peak pulse height from each side of the

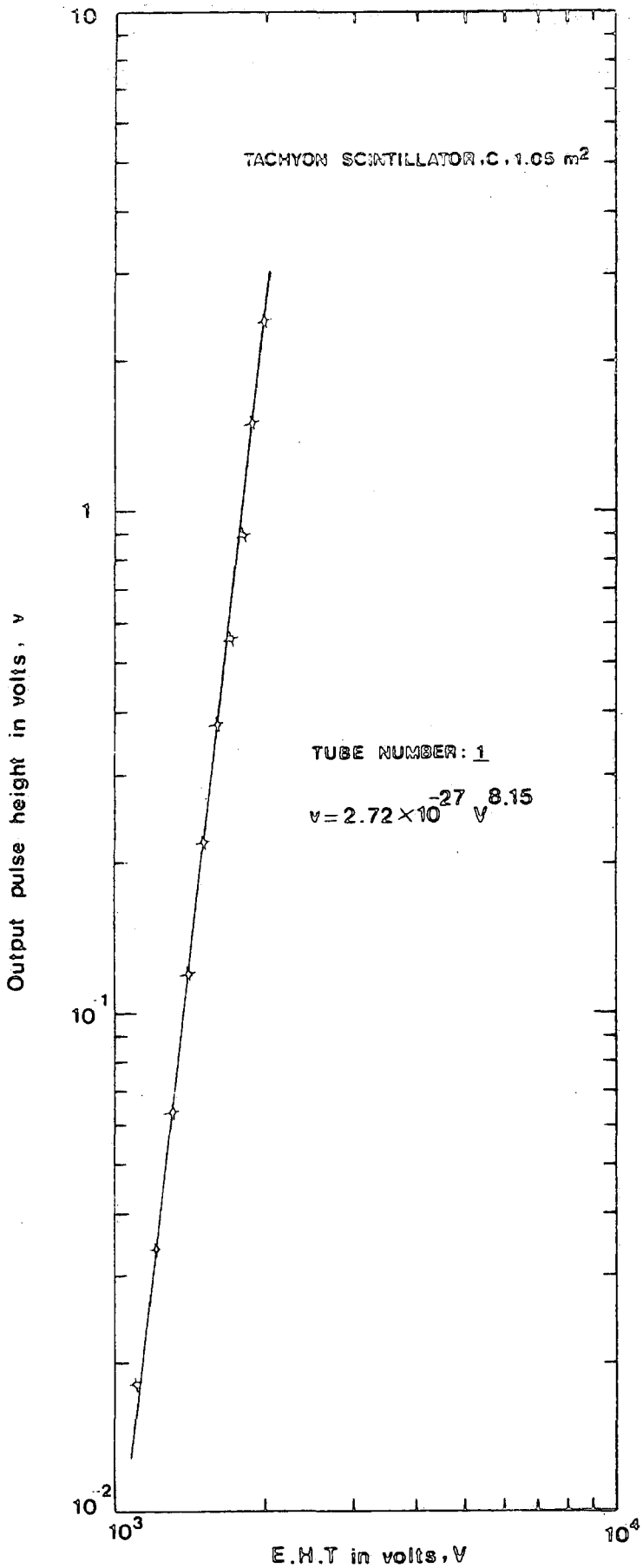

Figure 5.10a Variation of output pulse height in volts with E.H.T for tube No.1. L.E.D excitation.

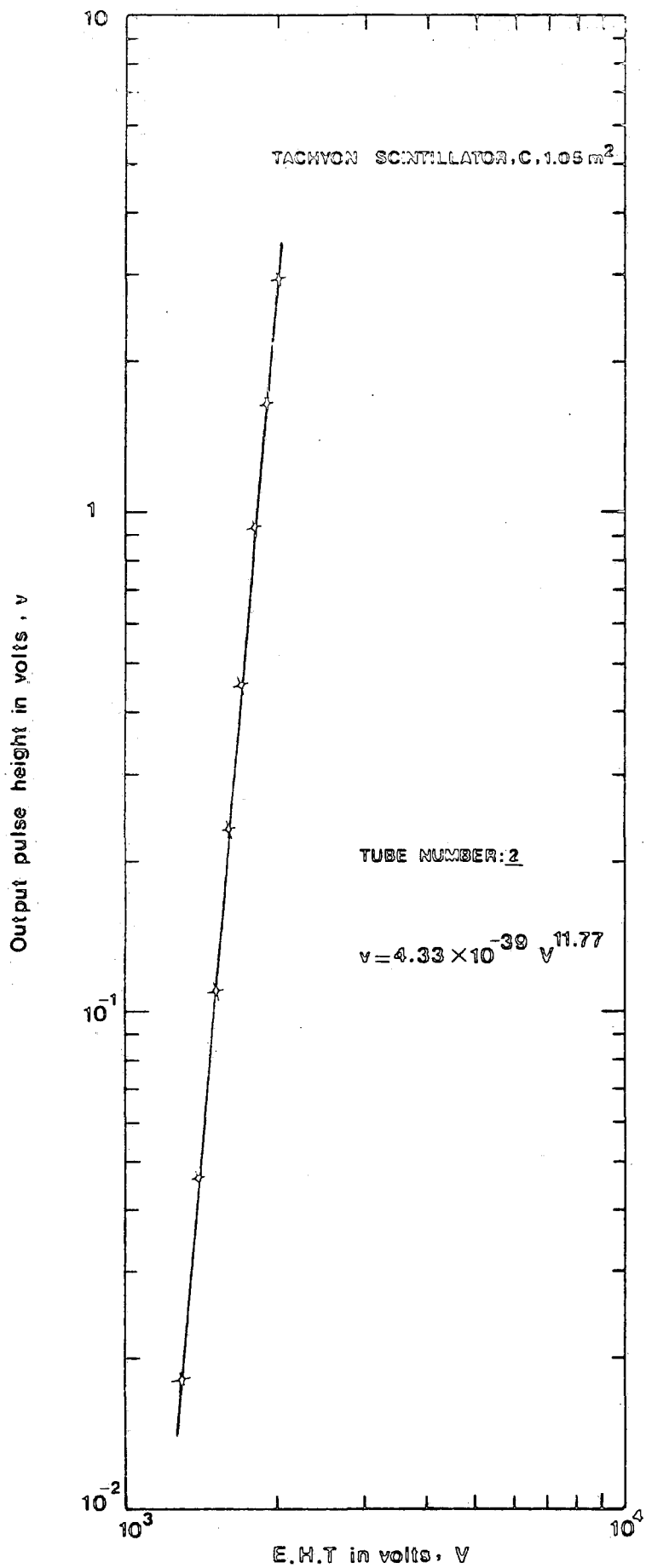

Figure 5.10b Variation of output pulse height in volts with E.H.T for tube No.2. L.E.D excitation.

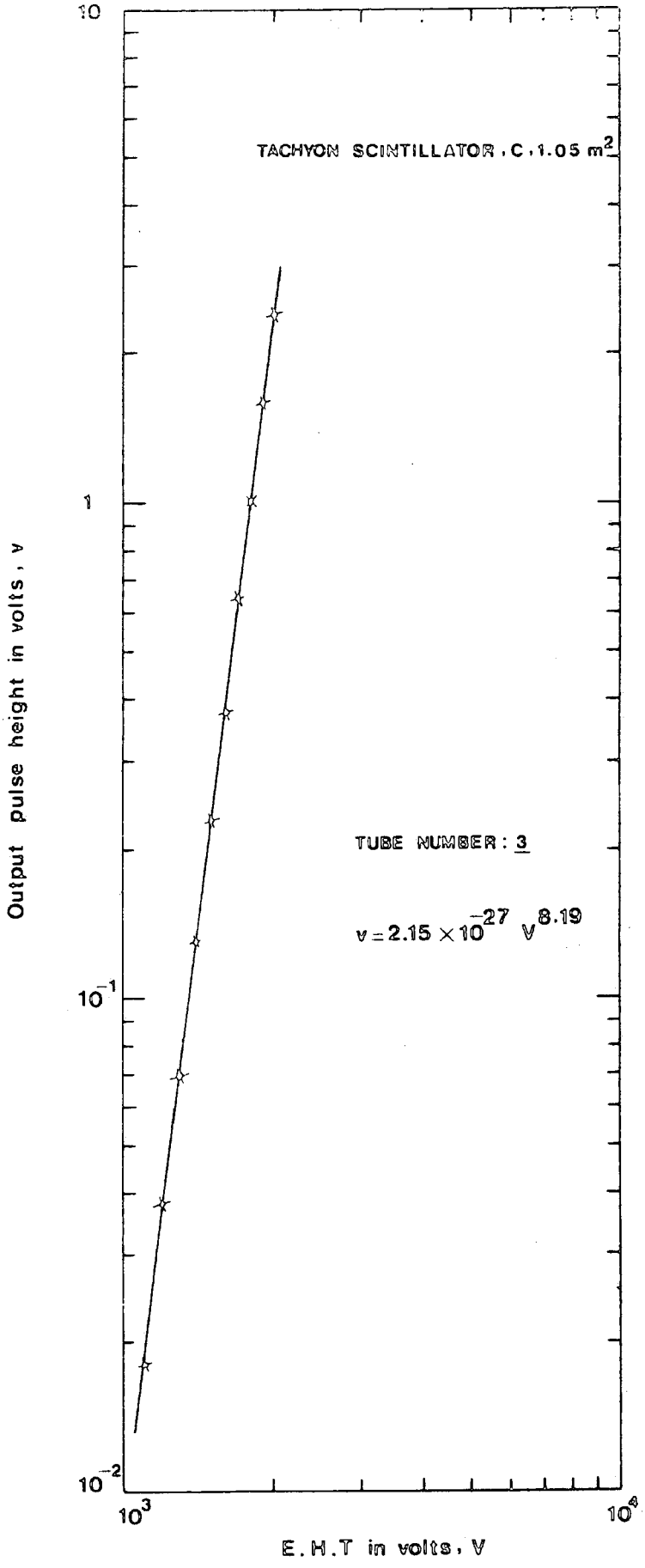

Figure 5.10c Variation of output pulse height in volts with E.H.T from tube No.3. L.E.D excitation.

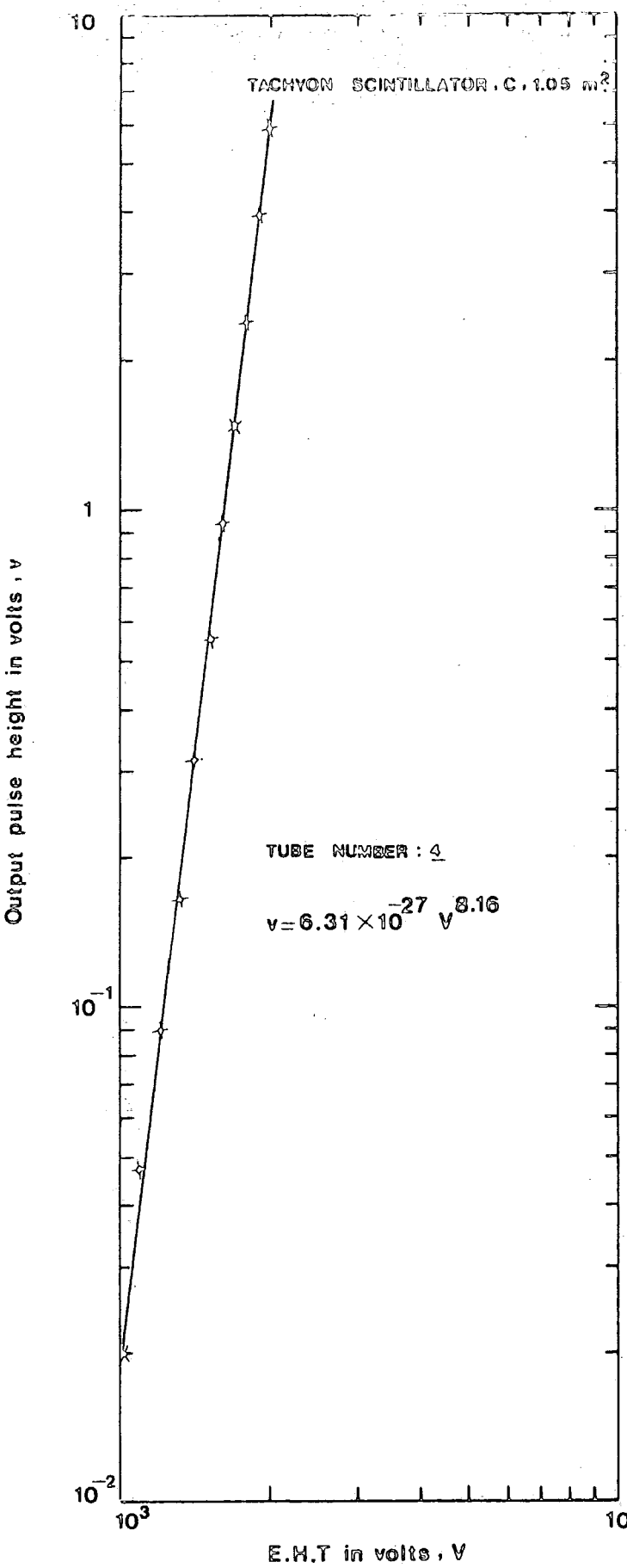

Figure 5.10d Variation of output pulse height in volts with E.H.T from tube No.4. L.E.D excitation

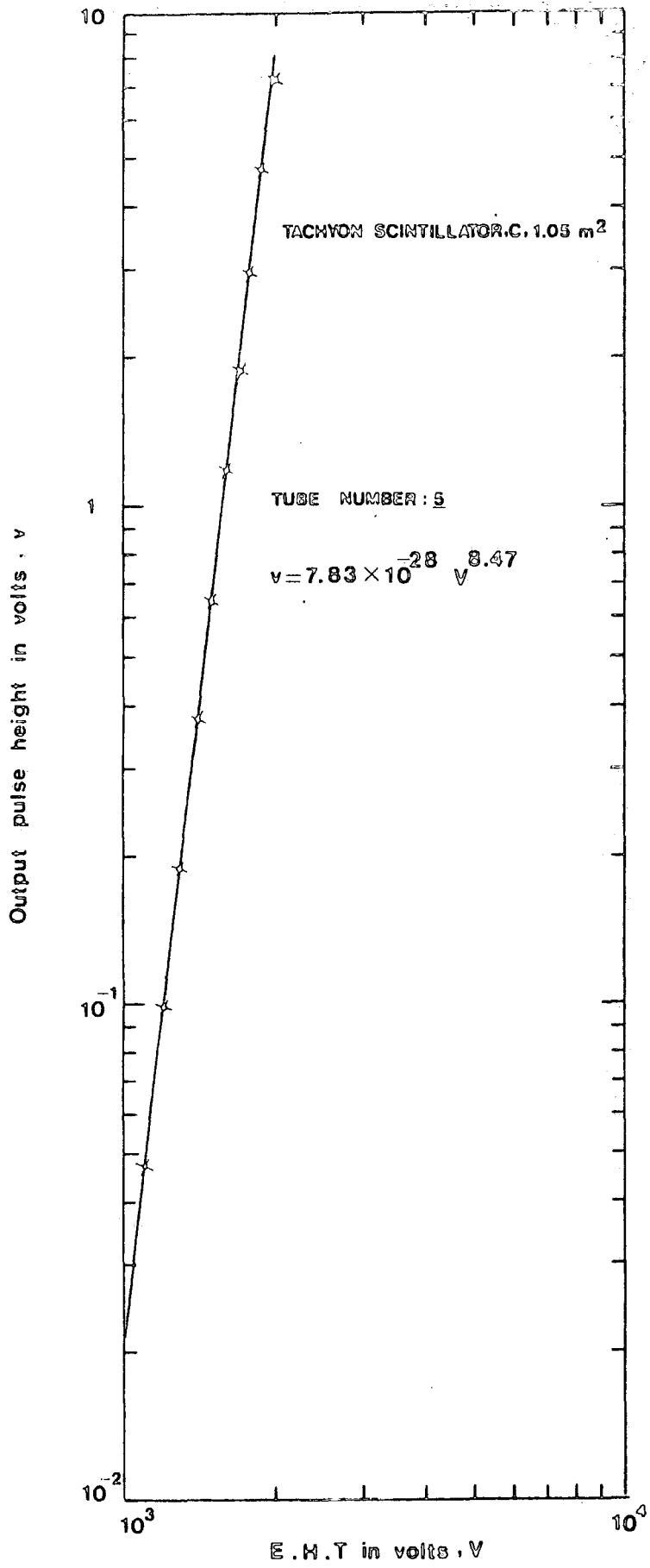

Figure 5.10e Variation of output pulse height in volts with E.H.T from tube No. 5. L.E.D excitation.

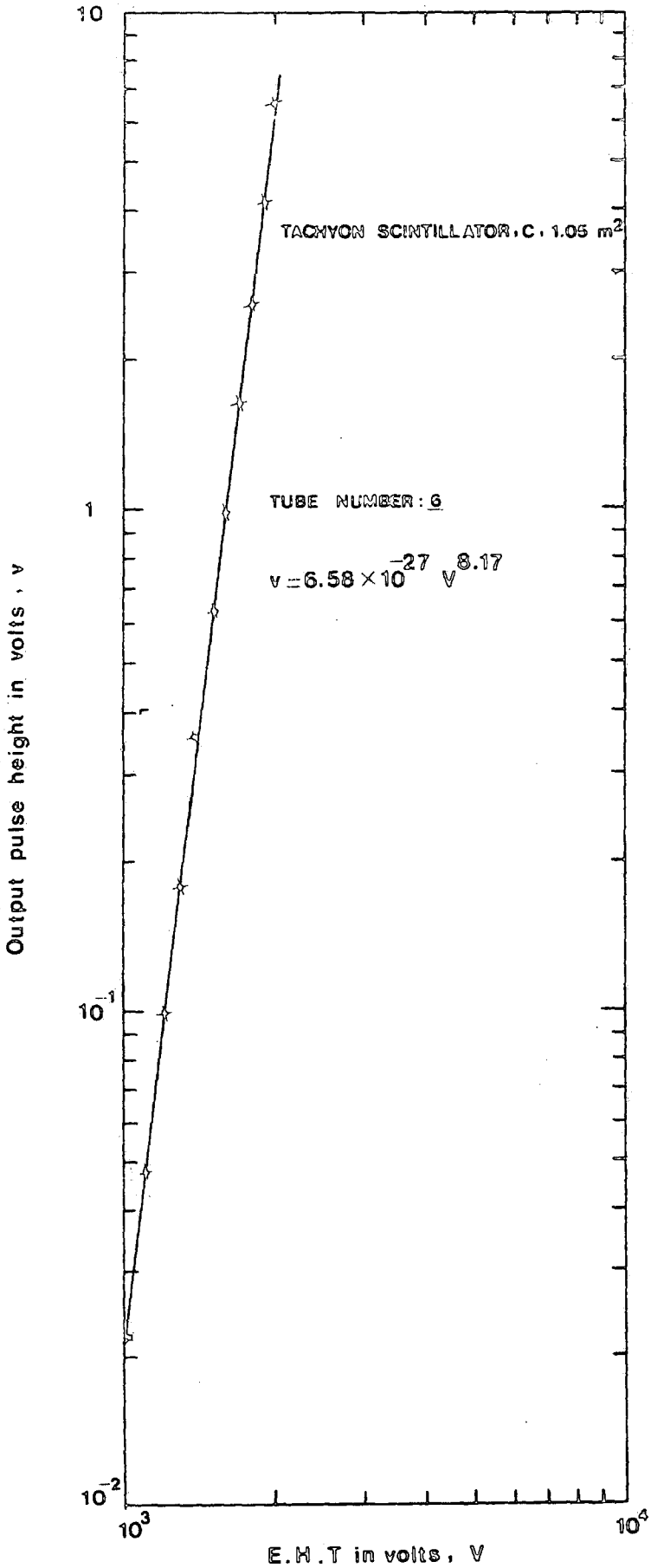

Figure 5.10f Variation of output pulse height in volts with E.H.T from tube No.6, L.E.D excitation

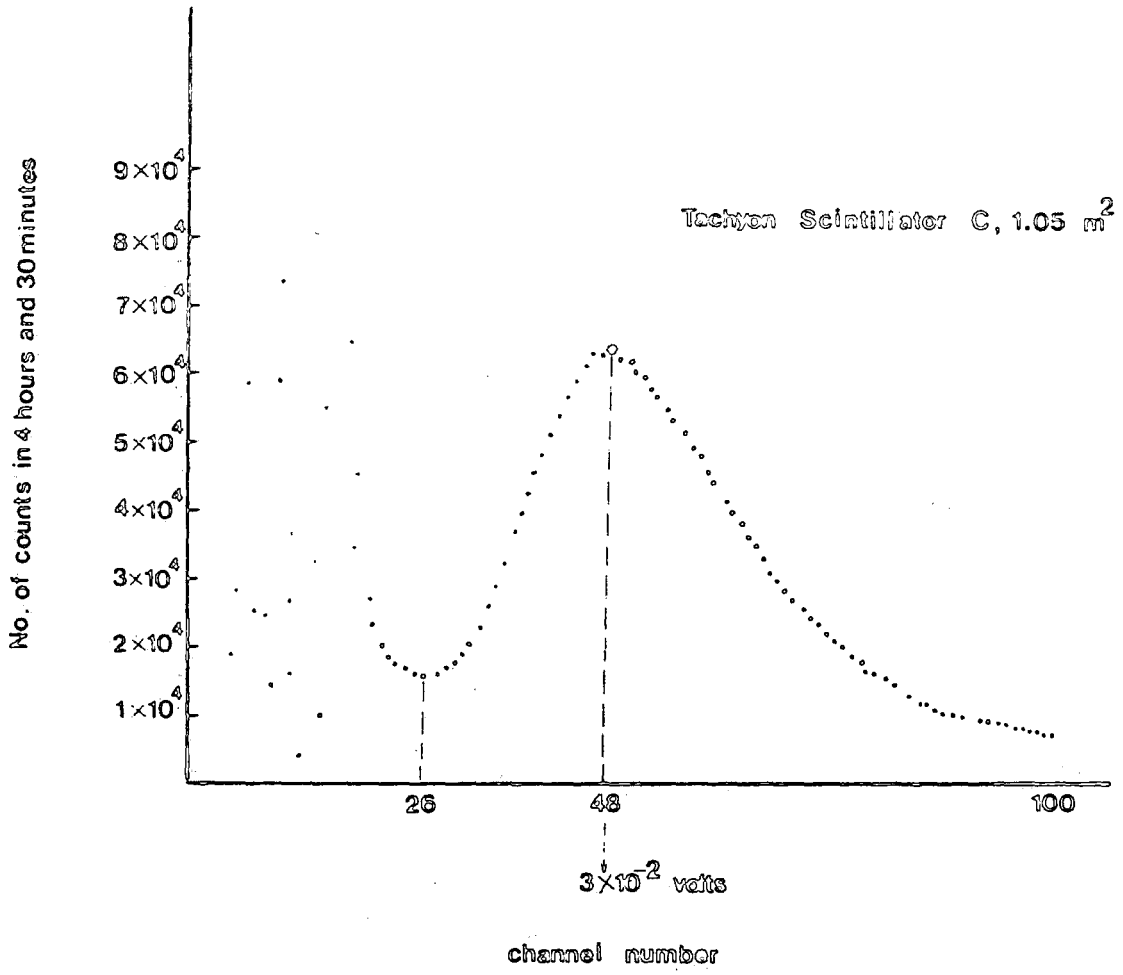

Figure 5.11 Typical single particle cosmic ray peak as displayed on the pulse height analyser for scintillator C of area 1.05 m^2.

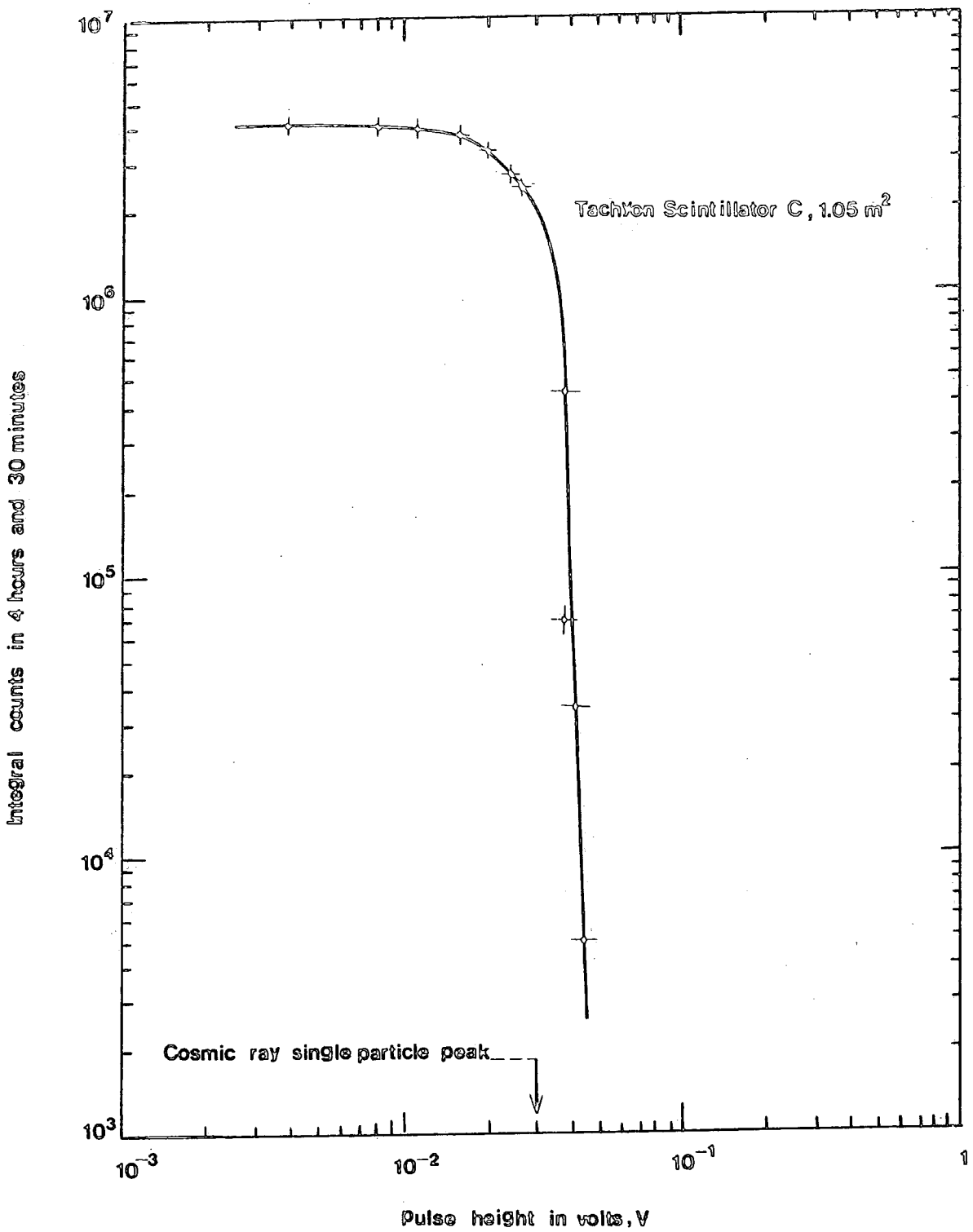

Figure 5.12 Rate of the pulses > V versus pulses height V as calculated from the pulse height analyser display shown in Figure 5.11. The position of the cosmic ray single particle peak is shown by the arrow.

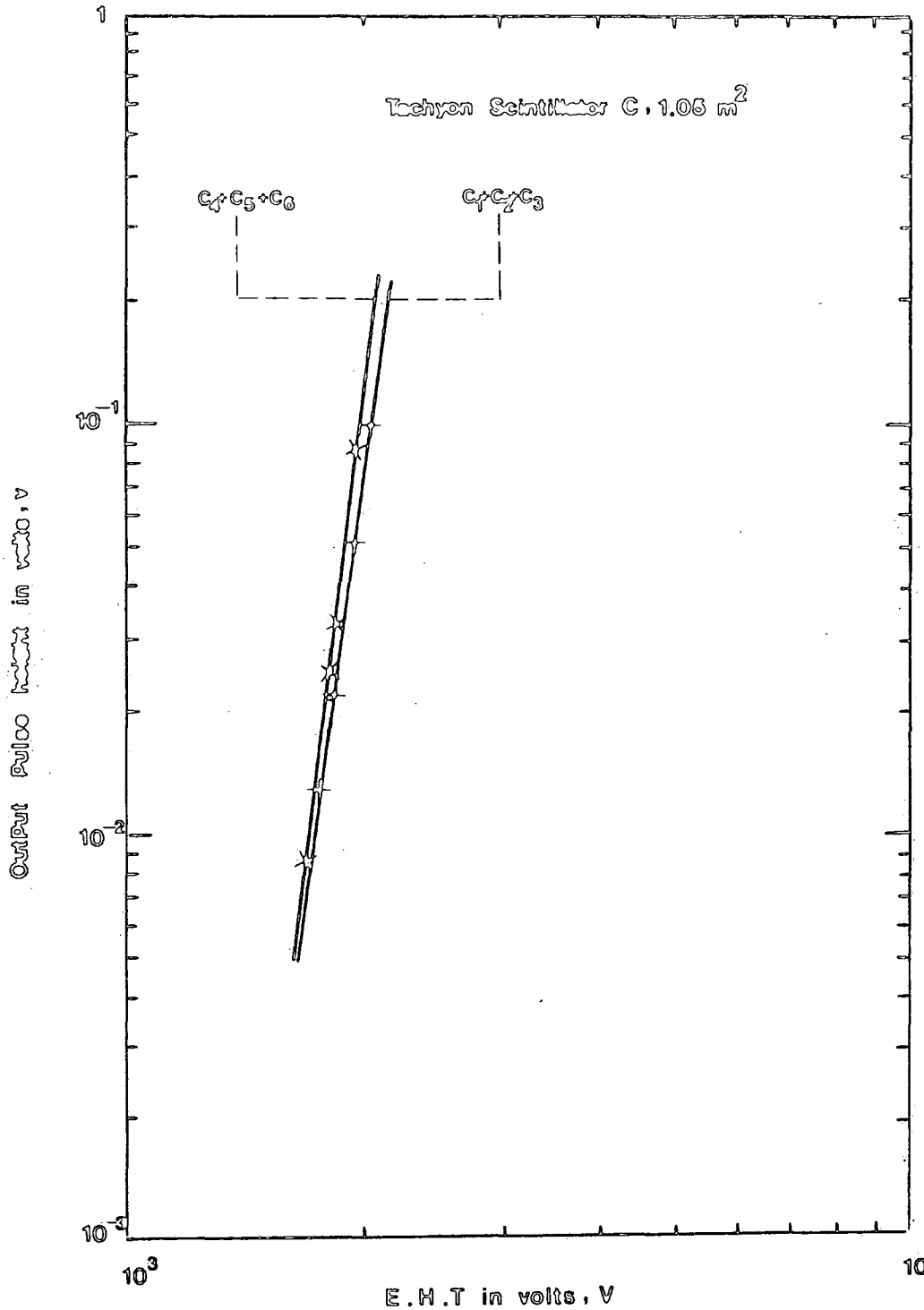

Figure 5.13 Variation of the peak pulse height from each side of tachyon scintillator C (3 matched photomultiplier tubes operational, $C_1 + C_2 + C_3$ and $C_4 + C_5 + C_6$) separately produced by the global cosmic ray flux traversing the scintillator as a function of the voltage applied to the photomultiplier tubes.

tachyon scintillator C separately as produced by the global cosmic radiation flux traversing the scintillator as a function of the voltage applied to the photomultiplier tubes. The variation of the pulse height of the cosmic radiation peak as a function of the extra high tension voltage applied to the matched photomultiplier tubes is shown in figure 5.14 and agrees with the results obtained when individual photomultiplier tubes are excited with light pulses from a light emitting diode. The response of the tachyon scintillator over a much larger range of pulse heights was investigated and figure 5.15a shows the integral pulse height distribution produced by the global cosmic radiation flux which was measured by using an amplifier and discriminator. The corresponding pulse height analyser display (see figure 5.12) shows that the most probable pulse height produced by cosmic ray particles corresponds to a pulse height of 30mV. The integral response of the scintillator in terms of the density of particles traversing the phosphor is also shown in figure 5.15b. Single relativistic charged particles traversing the phosphor at normal incidence correspond to a density of 0.95 per m^2.

5.8) DESCRIPTION OF THE ELECTRONIC INSTRUMENTS

As shown in figure 5.7, various electronic instruments have been used in the present tachyon experiment. Each of them will now be described.

5.8.1) VOLTAGE AMPLIFIER UNIT

By using 1 μsec wide negative input pulses from a pulse

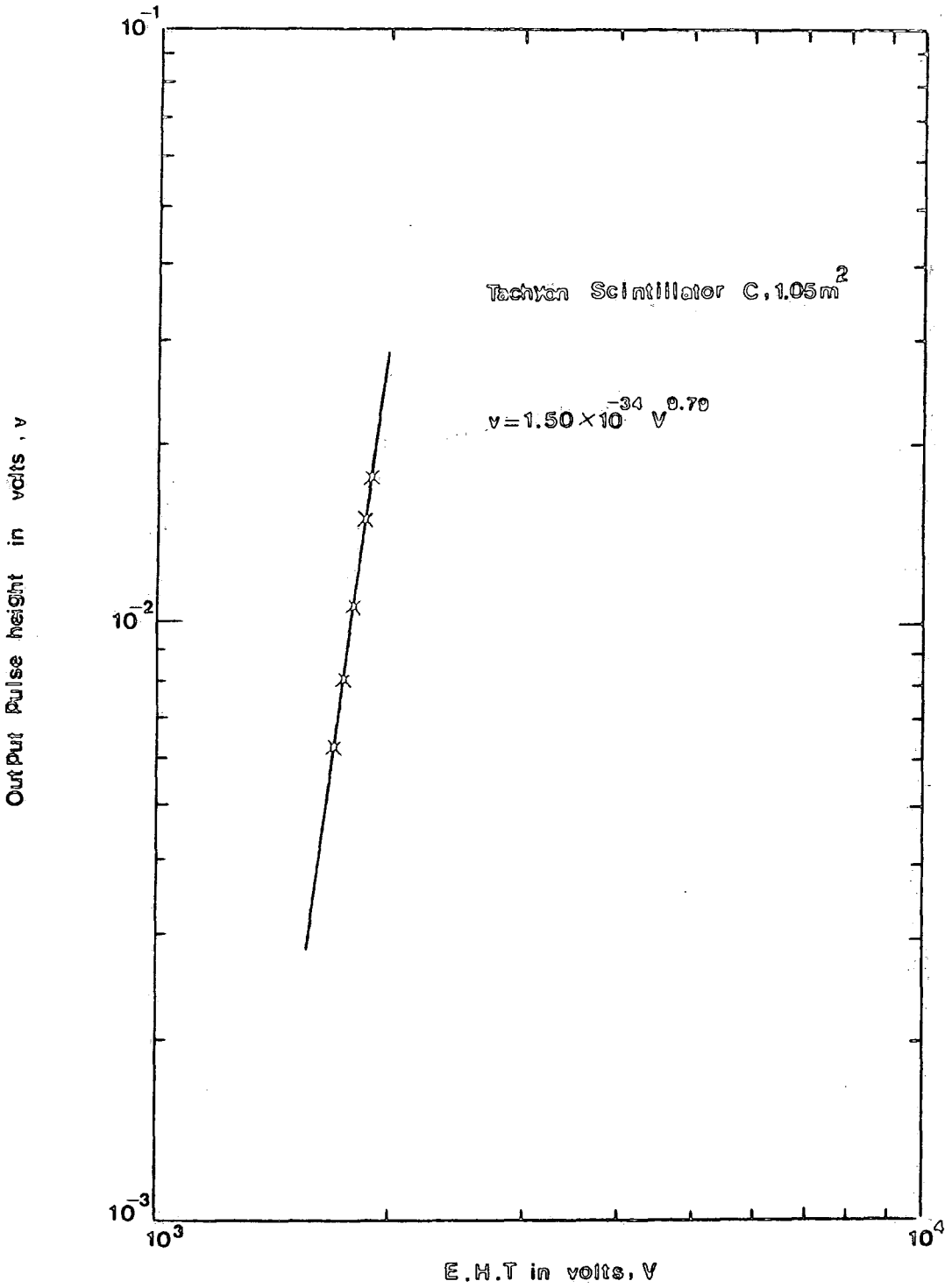

Figure 5.14 Variation of the peak pulse height produced by the global cosmic ray flux traversing the tachyon scintillator C as a function of the voltage applied to all the matched photomultiplier tubes. The measurements are fitted by $v = 1.50 \times 10^{-34} V^{9.79}$. This result is consistent with the result obtained when individual photomultiplier tubes are excited with light pulses from a light emitting diode.

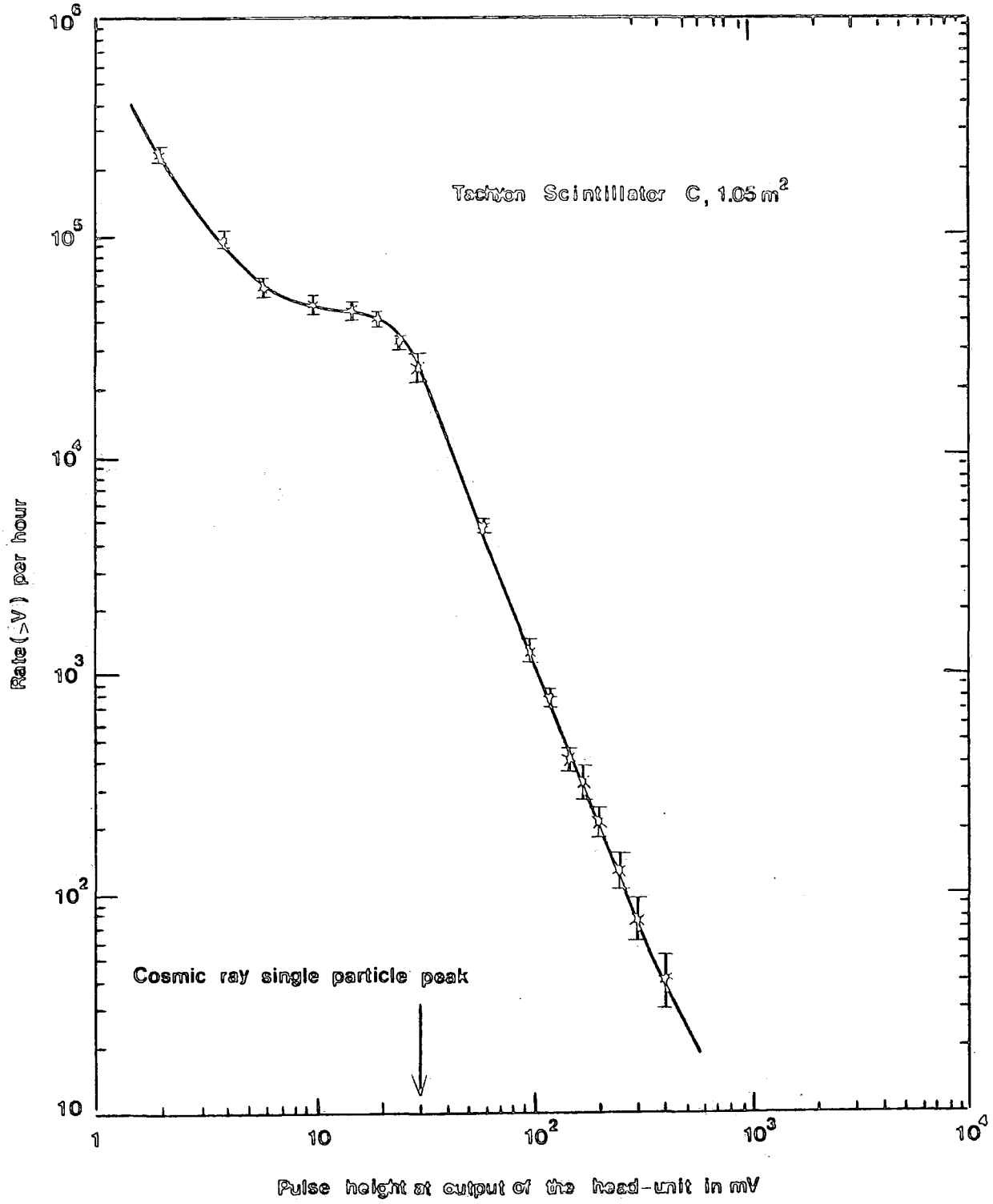

Figure 5.15a The integral pulse height distribution produced by the global cosmic ray flux measured using an amplifier and discriminator for tachyon scintillator C. The corresponding pulse height analyser display shows that the most probably pulse height produced by cosmic ray particles corresponds to a pulse height of 30 mV which is indicated by the arrow.

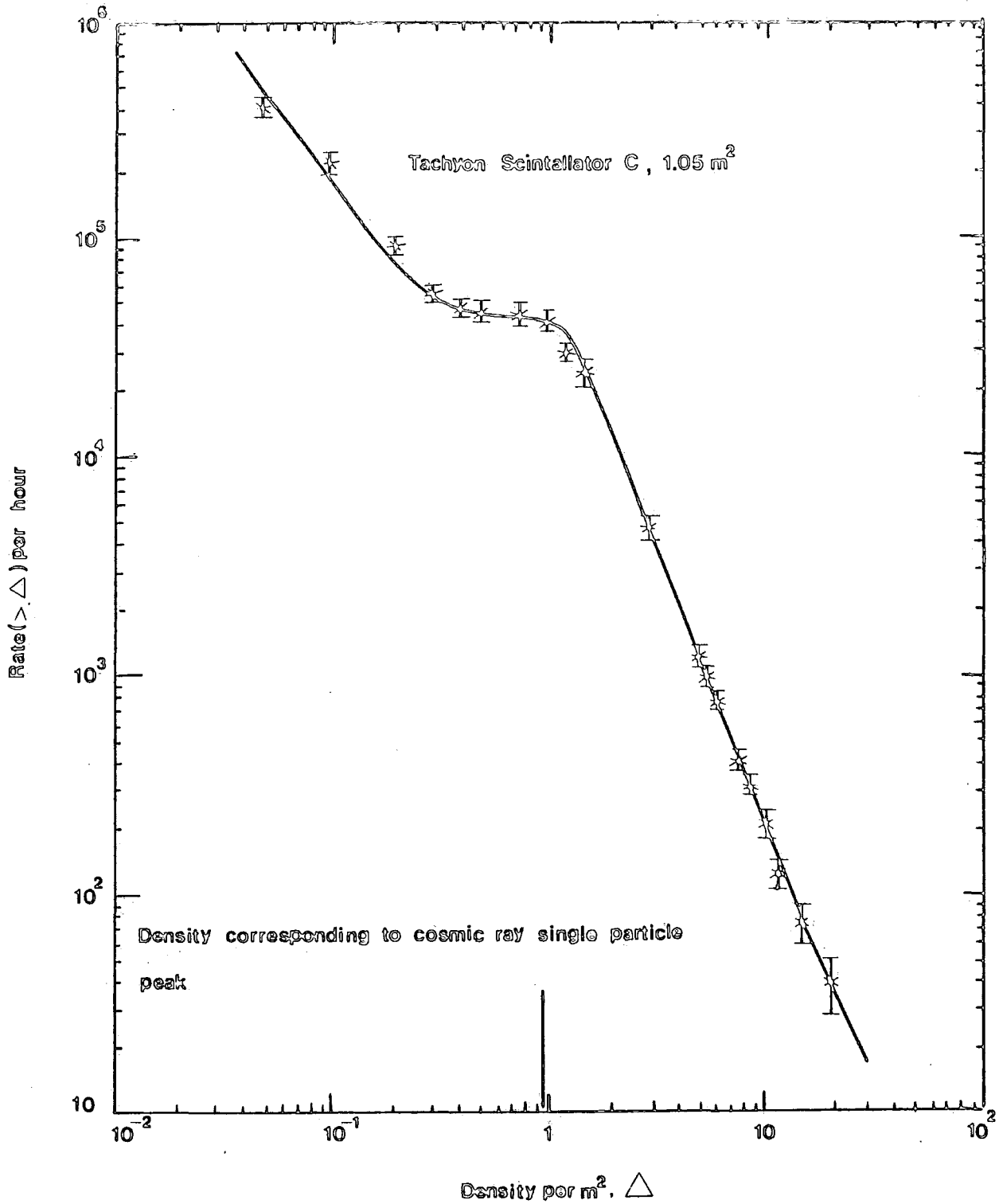

Figure 5.15b The integral response of tachyon scintillator C expressed in terms of the density of particles traversing the phosphor which has area 1.05 m^2. Single relativistic particles traversing the phosphor at normal incidence correspond to a density of 0.95 per m^2 which is shown by arrow.

generator, the gain produced by various values of the feedback resistance, R, was measured. The results obtained along with the circuit diagram of voltage amplifier is shown in figure 5.16.

5.8.2) DISCRIMINATOR UNIT

Figure 5.17 shows the discriminator circuit and the relationship between the d.c level on the base of the first transister and the minimum input pulse height required to trigger the circuit. Also shown is the relationship between the knob setting of the discriminator and the minimum input pulse height to trigger. The measurements were made using 1 μsec wide negative input pulses from a pulse generator. For input pulse heights above threshold , the output pulse height has the constant value of 5.2 volts which is independent of input pulse height.

5.8.3) TWO-FOLD COINCIDENCE UNIT

Two suitable pulses arriving from both plastic scintillators A and B , enter a two-fold coincidence unit and the output pulse is applied to the fan-out unit. Figure 5.18 shows the diagram of the two-fold coincidence unit and the inserted table was produced using 1 μsec wide , -3 volt input pulses from a pulse generator.

5.8.4) FAN-OUT UNIT

The action of the fan-out unit is the division of the input pulse into several similar outputs without changing the amplitude from that of the input pulse amplitude. It is seen

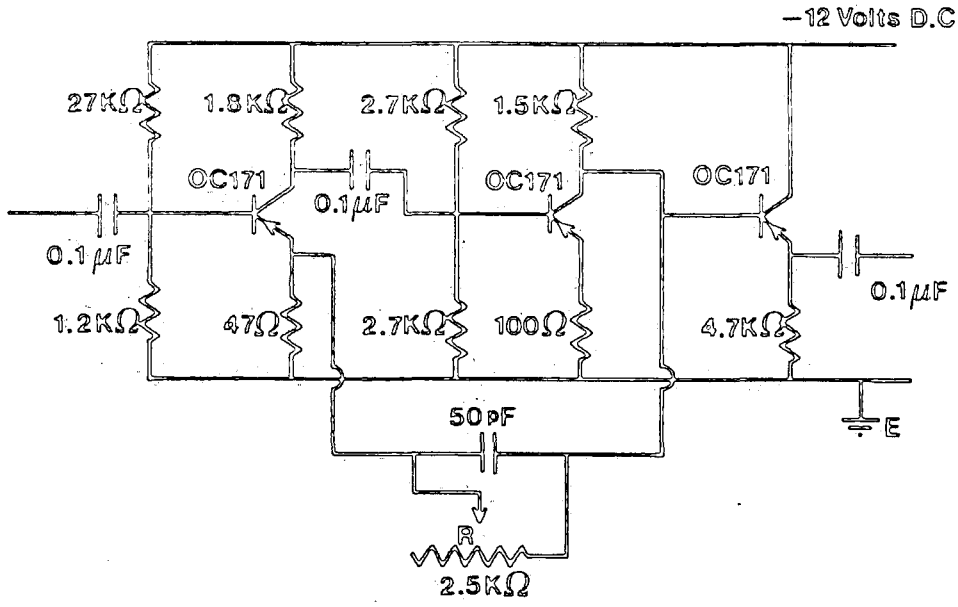

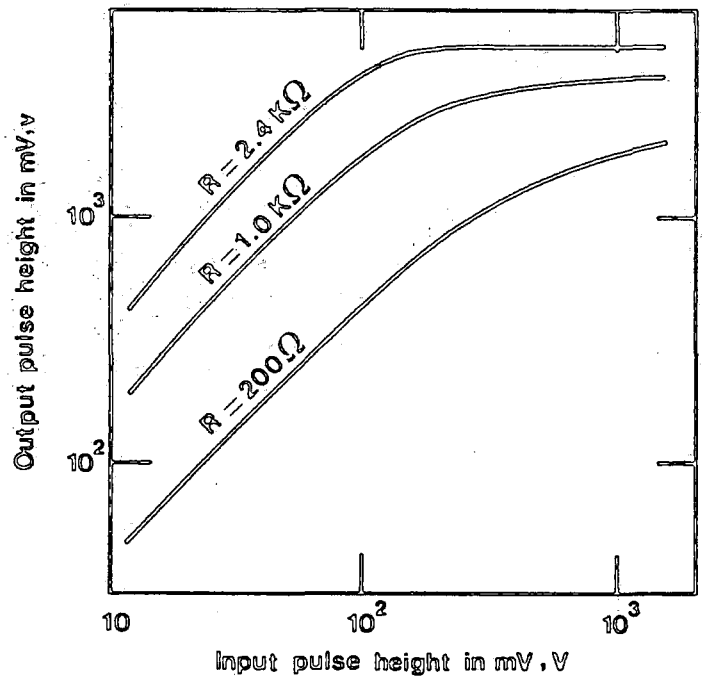

Figure 5.16 The voltage amplifier and its characteristics for various values of feedback resistance, R. Measurements made using 1μsec wide-ve input pulses from a pulse generator.

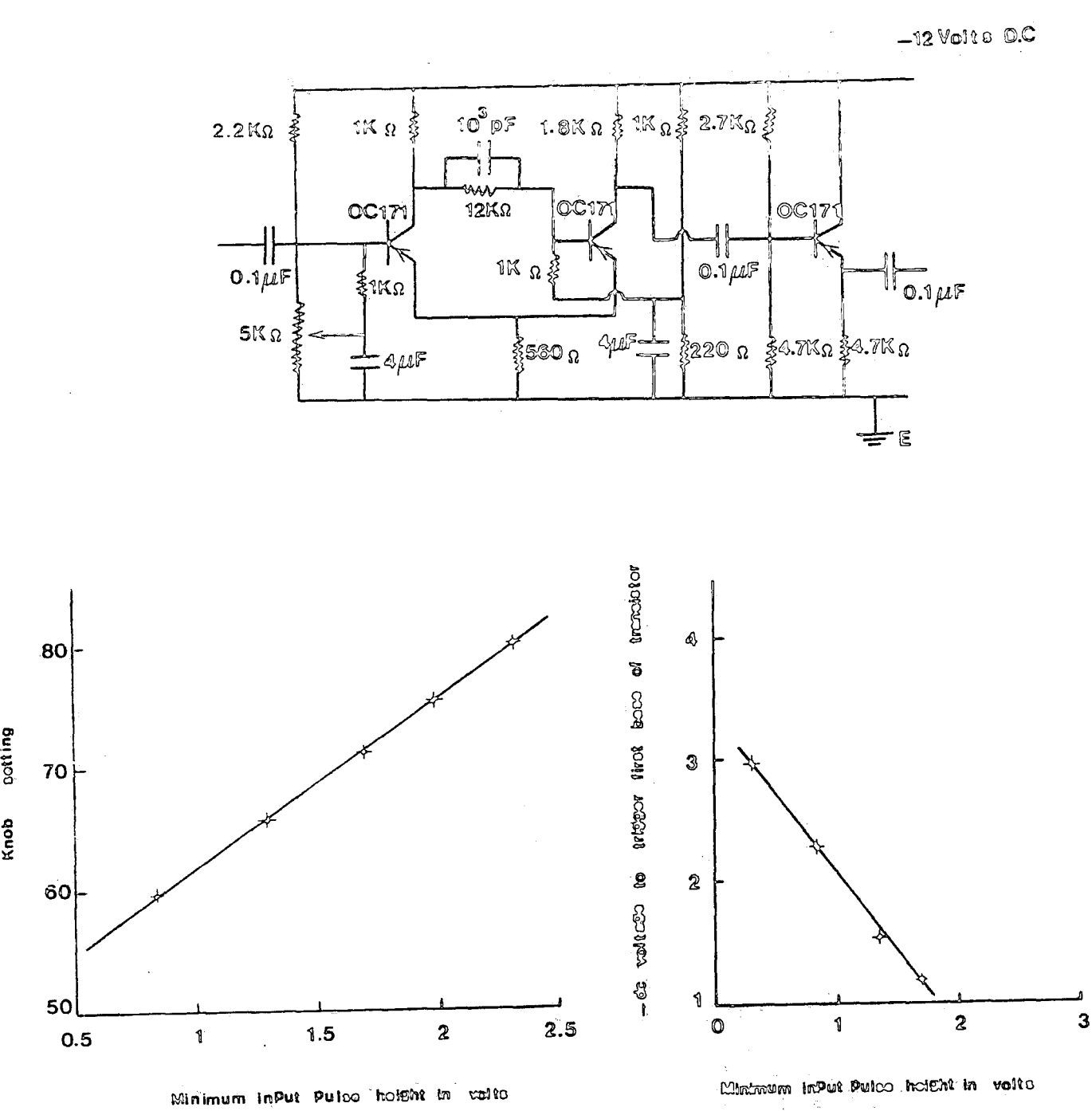

Figure 5.17 The discriminator circuit and the relationship between the d.c. level on the base of the first transister and the minimum input pulse height required to trigger the circuit and also the relationship between knob setting and minimum input pulse height.

Measurements made using 1 μsec wide -ve input pulses from a pulse generator. For input pulse heights above threshold, the output pulse height was the constant value of 5.2 volts independent of input pulse height.

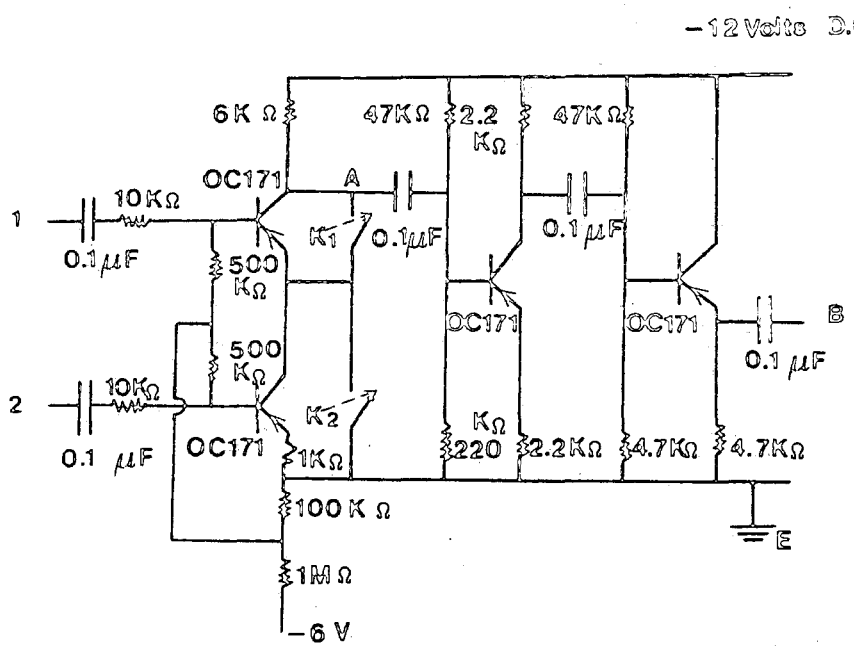

	INPUT FROM PULSE GENERATOR	OUTPUT AT A		OUTPUT AT B		
		1 FOLD	2 FOLD	1 FOLD	2 FOLD	PULSE WIDTH
Channel 1	−3 VOLTS	0.0044 VOLTS	+6 VOLTS	− 0.03 VOLTS	−4 VOLTS	1 μSEC
Channel 2	−3 VOLTS	0.0081 VOLTS		− 0.015 VOLTS		1 μSEC

Figure 5.18 Two-fold coincidence unit.
Table produced by test using 1 μsec wide -3 volt input pulses using the pulse generator.

from the block diagram (Figure 5.7) that the input pulse into the fan-out unit is divided into three channels. Figure 5.19 shows the diagram of the fan-out circuit and the related performance curve was measured using 1 μsec wide negative input pulses from a pulse generator.

5.8.5) CYCLING SYSTEM TRIGGER

Figure 5.20 shows the cycling system trigger circuit. One channel of the output pulses from the fan-out unit leads to the cycling system and its output triggers the digital clock and camera. For test purposes, 1 μsec wide, -3 volt input pulses from a pulse generator were used. A single shot pulse causes x,y to be connected for about one second.

5.9) SUMMARY

The tachyon scintillator can register either penetrating tachyons or the effects of tachyon interactions in the shielding layers. The presence of the shielding layers acts both as a target for tachyon interactions and also as an absorber of background γ-radiation which reduces the noise in the tachyon detector. The use of six matched photomultiplier tubes in the tachyon scintillator produces a single particle peak well resolved thermionic noise. The total sweep time of 500μsec gives an opportunity to investigate time domains both before and after the arrival of the shower front pulse. Also, using both channels of the dual beam oscilloscope with different sensitivity, makes it possible to measure a wide range of pulse heights produced in the tachyon detection

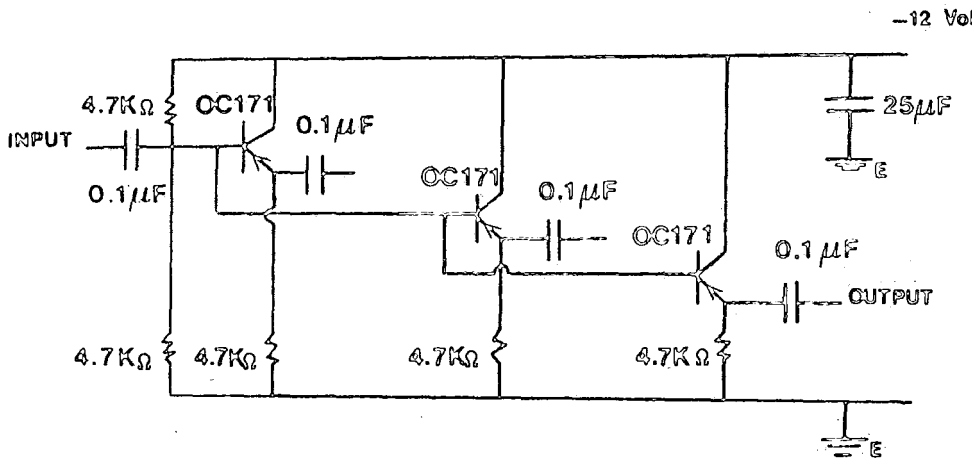

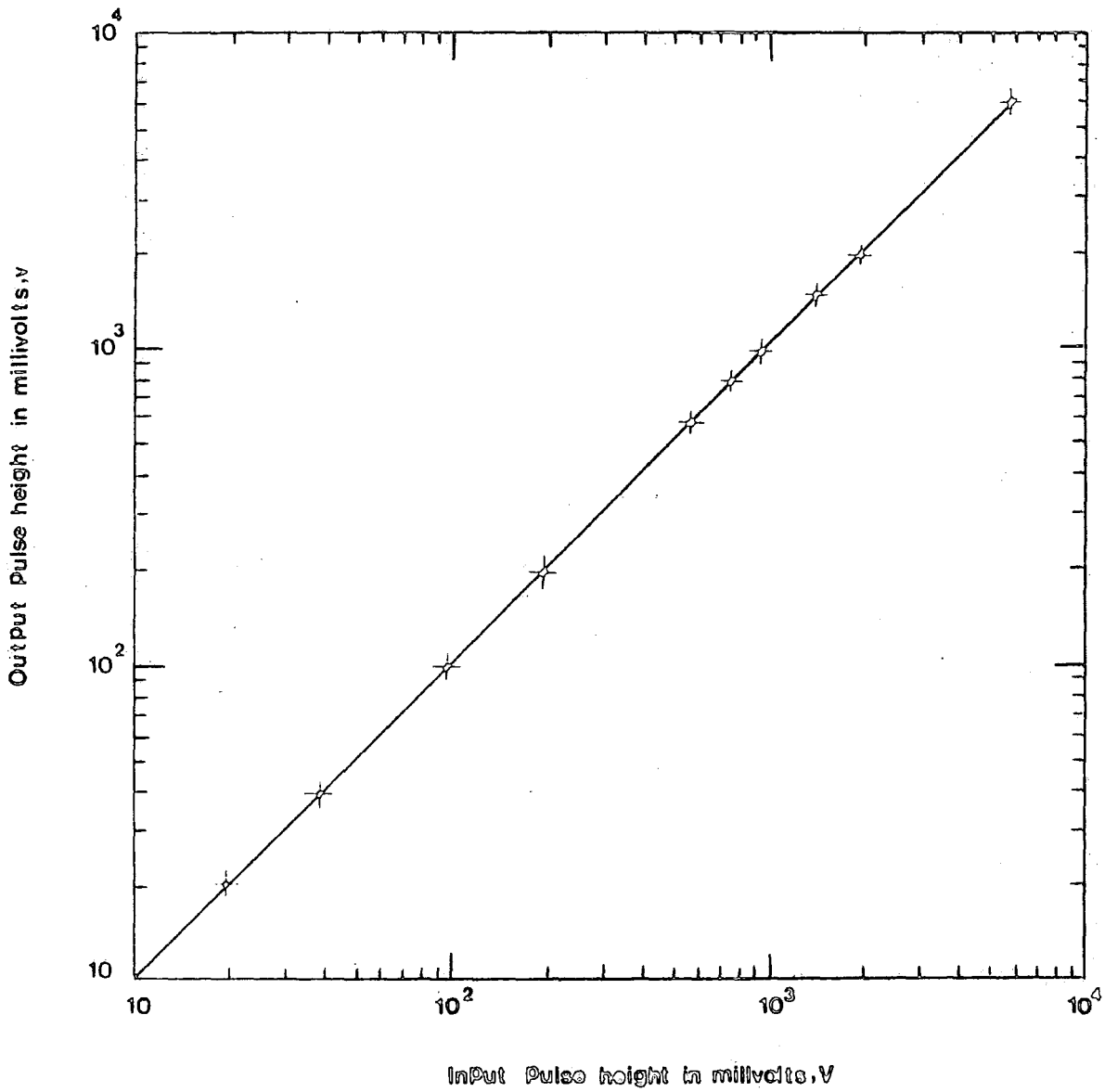

Figure 5.19 The fan out and its input-output characteristics. Test using 1 μsec wide -ve input pulses from a pulse generator.

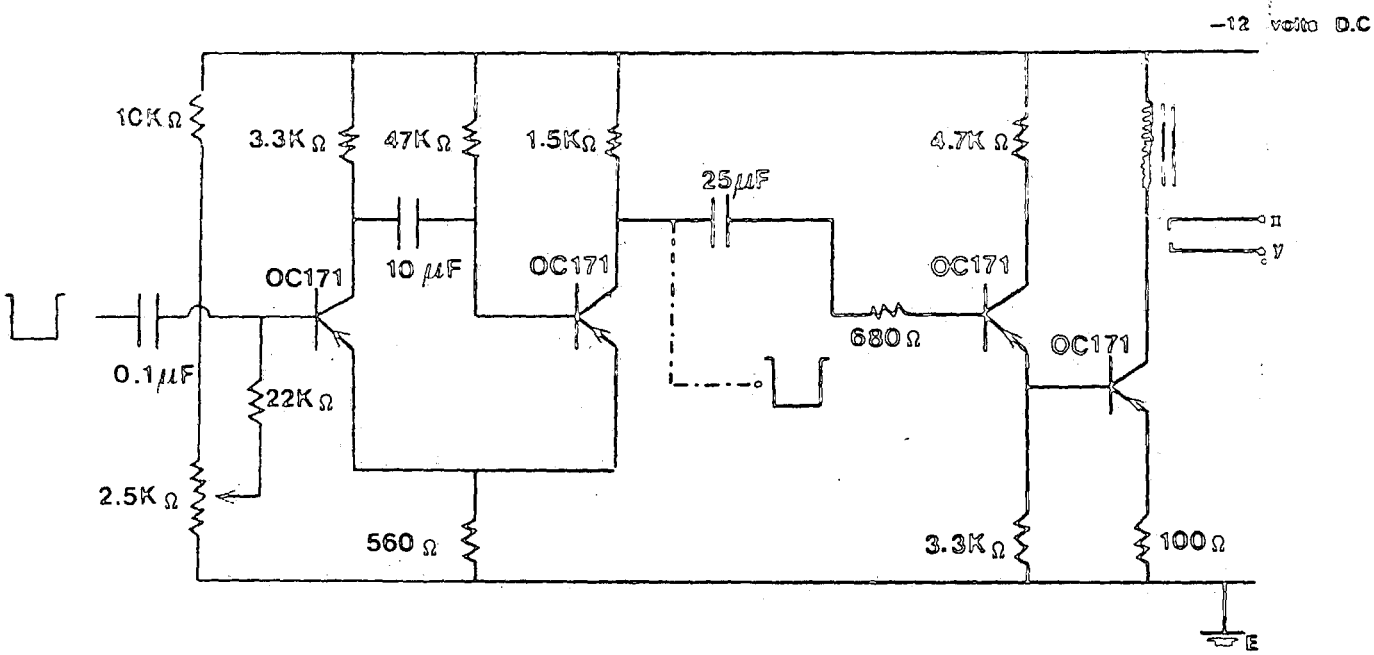

Figure 5.20 The cycling system trigger.
A -5 volt, 1 μsec pulse at the input will close the relay and start the cycling system.
Test using 1 μsec wide -3 volt pulses from a pulse generator.
A single shot pulse causes x,y to be connected for about 1 second.

scintillator.

CHAPTER SIX

RESULTS OF THE TACHYON EXPERIMENT

6.1) INTRODUCTION

It is assumed that tachyons are produced as particle-antiparticle pairs in interactions of the sort that occur when a high energy cosmic ray primary proton collides with a nucleus of air in the upper atmosphere:

$$P + N \longrightarrow N + N + t + \bar{t} + \text{mesons} \qquad (6.1)$$

Of course, if tachyons are produced in cosmic radiation sources and have an interaction length comparable with that of a proton primary, thus initiating an extensive air shower, then they will also be detected by the experimental arrangement used. Also, it is assumed that a tachyon will lose energy in a scintillator and give rise to photons or will be detectable by the production of secondarys which can be detected. In the absence of a comprehensive theory, these assumptions are considered reasonable.

On average, a primary cosmic ray proton undergoes its first interaction at an atmospheric depth of $80 g.cm^{-2}$ of air corresponding to an altitude of 17.7Km above sea-level. If it has sufficiently high energy ($\gtrsim 10^{15}$ eV), then it will produce an extensive air shower with the main electron-photon shower front propagating at a velocity very close to that of light, figure 6.1a. The most likely kinetic energy for a tachyon is zero. In

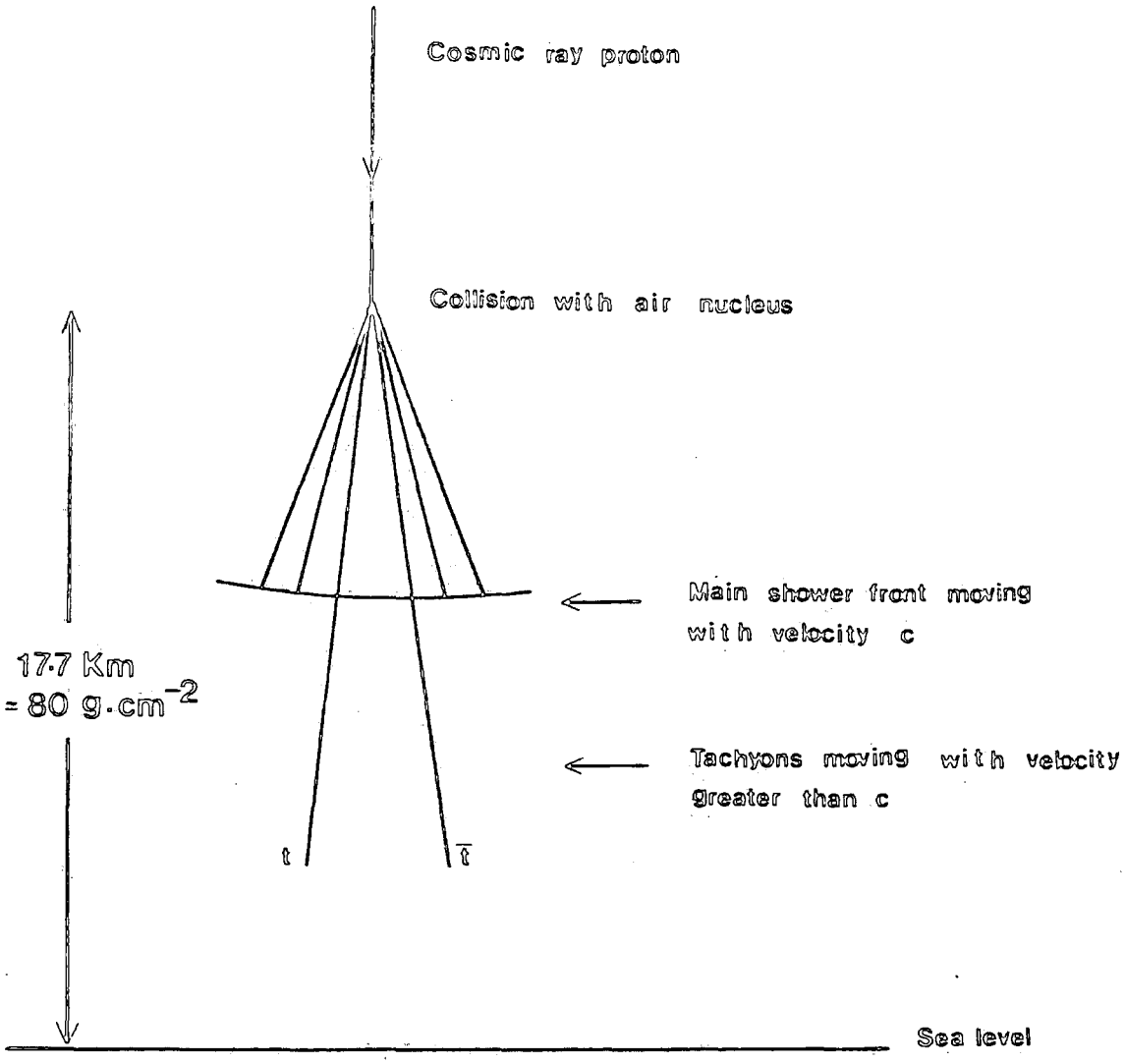

Figure 6.1a Diagram illustrating the possible production of tachyon–antitachyon pairs in the interaction of a primary proton with an air nucleus at an atmospheric depth of 80 g.cm^{-2} (one mean free path) corresponding to an altitude of 17.7 Km above sea level.

other words; it might be created at the production thresholed energy, (see 2.3.2). In this case its velocity will be infinite. Also, if the initial kinetic energy is greater than zero, any interaction with the nuclei of the atmosphere will lower its kinetic energy and its velocity will increase. For the case of infinite velocity, a tachyon would arrive at sea-level at a time of 57μs before the arrival of the shower front. For showers incident at a zenith angle of 60°, the relevant time increases to 115 μs. However, less than 1% of extensive air showers have zenith angles greater than 60°. It is clear that for finite velocity tachyons or for tachyons produced in secondary hadron interactions, low in the atmosphere, the delay time would be smaller. The present tachyon detector is able to record the occurrence of pre-shower front pulses in the 265 μs time domain preceding the shower. Unfortunately, other pulses can also be observed in these time domains due to:

a) Random thermal noise pulses originating from thermionic electron emission from the photomultiplier photocathodes.

b) Background radioactivity (presumably mainly gamma-rays) from the enviroment.

c) The chance passage of cosmic radiation particles through the scintillation detector which are not associated with the detected air shower trigger.

In general, the cases of (a) and (b) are expected to produce very much smaller detected pulse heights than case of (c).

The ideal type of event expected from the present experiment is shown in figure 6.1b. A total of 10,142 extensive

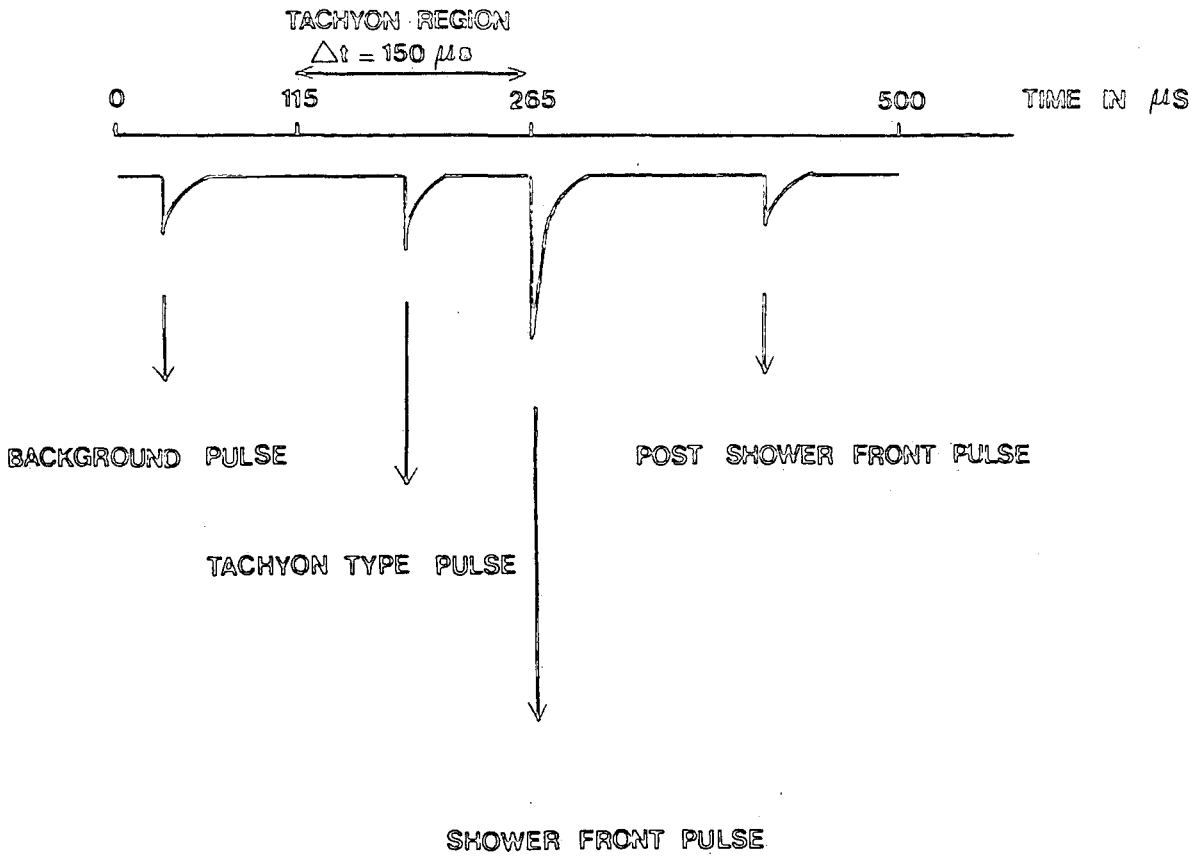

Figure 6.1b Types of pulse expected to be observed in the present experiment.

air shower triggers were recorded and some typical traces as observed on the oscilloscope are shown in figures 6.2a and 6.2b. Analysis of the oscilloscope photographs showed a significant number of background pulses, so a sample of 508 photographs were taken in which the oscilloscope time base was triggered at random (by a pulse generator) rather than by the arrival of an extensive air shower so as to have a sample of data from which the magnitude of the random background could be established.

6.2) TIME DISTRIBUTION OF RECORDED PULSE HEIGHTS SELECTED BY THE E.A.S TRIGGER

During the running of the experiment, a number of calibration checks such as ; the gain of amplifier units , the rates of each of the triggering detectors, camera output and so on were frequently made and then the whole of the photographed events were scanned by eye. A summary of the basic experimental data is presented in table 6.1.

The time distribution of pulses occurring in six different ranges of pulse height which was measured on the oscilloscope from a sample of 10,142 shower triggers are shown in the table 6.2 and figure 6.3. The table and corresponding figure were produced by using the "DATABIN" program (see appendix A) which was run twice with the following program requirements:

Maximum time = 550 μs	Maximum time = 550 μs
Number of time bins = 55	Number of time bins = 55
Maximum pulse height = 31.5 mV	Maximum pulse height = 1455 mV
Number of pulse height bins = 15	Number of pulse height bins = 29

Figure 6.2a

a) Trace showing one pre-shower front pulse occurring at 180 μs after the start of the osilloscope sweep.

b) Trace showing one post-shower front pulse occurring at 415μs after the start of the oscilloscope sweep.

The time between the start of the time base and the arrival of the shower front is 265 μs. The vertical scale is 1cm:5mv

TOTAL NUMBER OF TRIGGERS $\triangle_A(\geq 25 m^{-2})$, $\triangle_B(\geq 25 m^{-2})$	10142
RUNNING TIME	839 hr 46 min 40 sec
EXTESIVE AIR SHOWER TRIGGER RATE	$(12.08 \pm 0.12)\ hr^{-1}$
NUMBER OF RANDOM TRIGGER EVENTS USED TO ASSESS THE BACKGROUND	508

Table 6.1 Summary of basic experimental data.

Time Range on Oscilloscope in μs	NUMBER OF PULSES					
	0.5mv≤v≤2mv	2mv<v≤4mv	4mv<v≤30mv	30mv<v≤120mv	v>120mv	v≥700mv
0-10	61	23	14	3	3	0
10-20	83	38	11	4	7	0
20-30	84	43	13	6	3	0
30-40	96	48	7	3	5	0
40-50	94	33	10	6	2	0
50-60	88	38	15	11	6	0
60-70	80	39	7	5	5	0
70-80	75	39	10	3	1	0
80-90	76	36	11	7	2	0
90-100	81	40	12	5	4	0
100-110	68	28	7	6	4	1
110-120	89	33	10	8	4	0
120-130	87	45	15	8	5	1
130-140	86	39	8	4	4	0
140-150	85	31	3	7	5	1
150-160	97	33	9	11	2	0
160-170	65	45	12	6	4	0
170-180	59	46	10	3	5	1
180-190	89	43	13	5	6	0
190-200	60	20	7	2	5	0
200-210	75	29	7	8	8	0
210-220	65	42	11	10	4	2
220-230	68	52	9	4	2	0
230-240	63	34	6	9	3	0
240-250	57	29	6	7	7	0
250-260	52	17	6	4	5	0
260-270	2045	1100	1795	1293	2929	717
270-280	33	20	13	3	4	0
280-290	57	29	19	3	2	0
290-300	69	40	13	5	2	0
300-310	51	33	19	9	5	1
310-320	71	36	11	8	3	0
320-330	63	51	24	6	3	0
330-340	55	39	20	3	2	0
340-350	53	40	28	8	5	0
350-360	43	34	22	16	5	0
360-370	70	39	37	8	3	0
370-380	68	74	33	14	2	0
380-390	56	52	27	17	2	0
390-400	50	47	29	8	4	0
400-410	66	46	34	17	6	1
410-420	54	52	29	14	5	1
420-430	71	44	38	20	5	0
430-440	65	47	20	15	5	0
440-450	83	46	37	14	8	0
450-460	62	47	26	14	3	1
460-470	85	51	27	19	7	3
470-480	55	48	35	15	10	0
480-490	56	48	28	17	6	0
490-500	85	67	32	17	7	0
	Σ = 3404	Σ= 1973	Σ = 850	Σ = 425	Σ=215	Σ= 13

Table 6.2 Tachyon data. Time distribution of events in different ranges of pulse height (measured on the oscilloscope) from a sample of 10142 shower triggers.

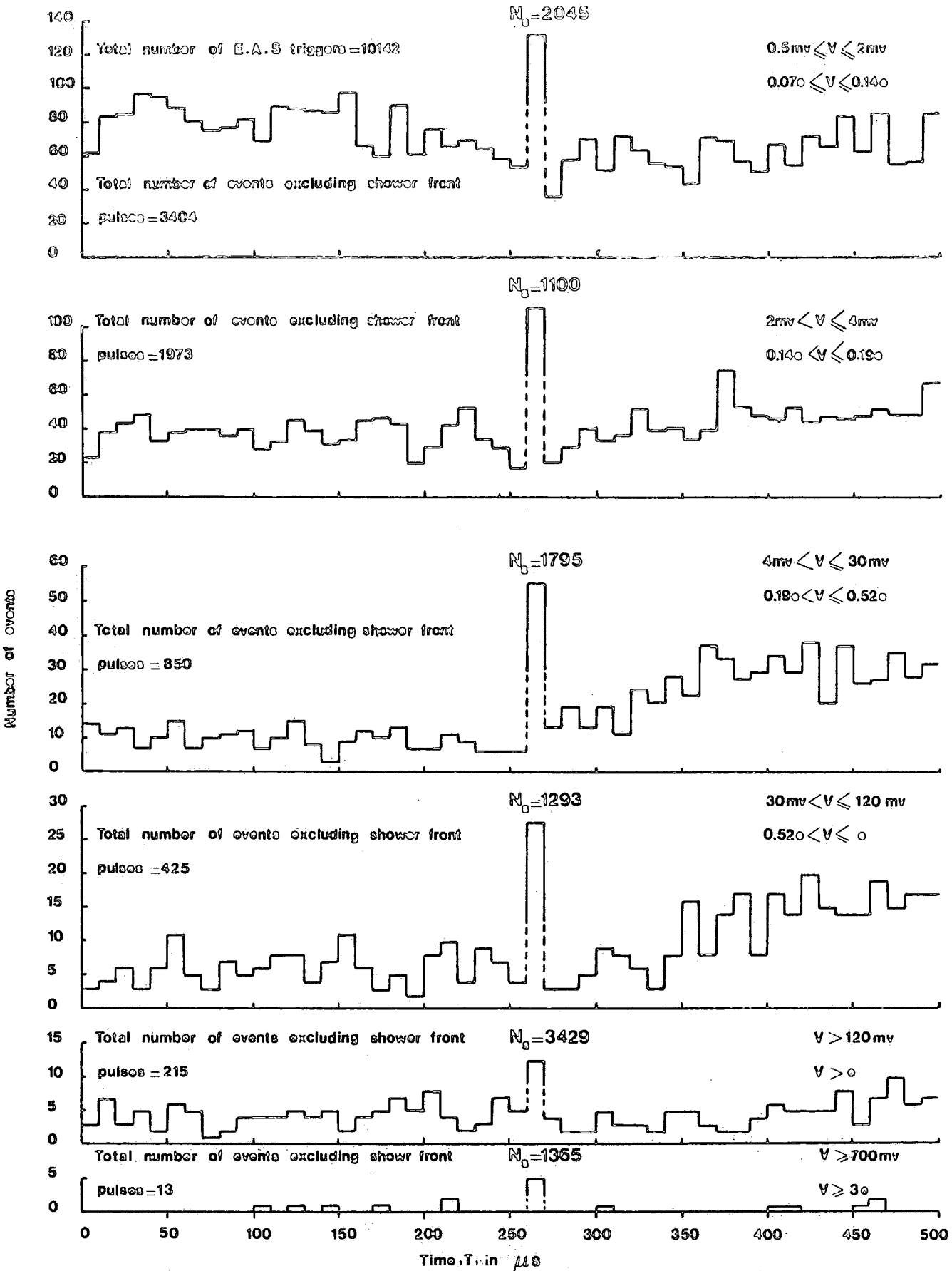

Figure 6.3 Time distribution for pulse heights between two limits of threshold energy loss in the tachyon detection scintillator C. In each range N_s is the total number of shower front pulses.

In each range of energy deposition in the scintillator , N_s corresponds to the total number of shower front pulses. Moreover, the corresponding ranges of energy deposition in the tachyon scintillator of thickness 5cm in terms of 'e' where 'e' is the energy loss (10MeV) produced by a relativistic particle (mainly; muons) traversing the scintillator at normal incidence, are also given. Since the amplifiers used in conjunction with the delay lines have a non-linear response (see figure 5.6), the range of pulse height is not linearly related to the range of energy loss. In order to write the pulse height at the output of the head-unit in terms of 'e' , the average pulse height at the output of the head-unit produced by relativistic particles traversing the phosphor at normal incidence was taken to be 30mv. As can be seen in figure 6.3, for the all ranges of energy deposition in the present tachyon detector, no obvious anomalous effects are observed in the time domain before the arrival of the shower front pulse where tachyons are expected to be observed. The only striking point for almost all ranges, especially in the ranges of $4mv < V < 30mv$ and $30mv < V < 120mv$, is the excess of events found to trail the arrival of the air shower front pulse. This observation will be discussed in more detail in subsequent sections.

6.3) DISTRIBUTION IN HEIGHT OF THE SHOWER FRONT PULSES

The measured distribution in size of shower front pulse heights is shown in table 6.3. To obtain the pulse height distribution of the shower front pulses, the "DATABIN" program

Pulse Height Range on oscilloscope in millivolts	Pulse Height Range at output of Head-unit in millivolts	Frequency (N)
0.5-2	2.06-4.08	2045
2-4	4.08-5.75	1100
4-6	5.75-7.02	518
6-8	7.02-8.08	344
8-10	8.08-9.02	201
10-12	9.02-9.87	122
12-14	9.87-10.65	111
14-16	10.65-11.37	101
16-18	11.37-12.05	83
18-20	12.05-12.69	74
20-22	12.69-13.30	56
22-24	13.30-13.89	40
24-26	13.89-14.45	39
26-28	14.45-14.98	41
28-30	14.98-15.50	65
30-32	15.50-16.00	0
32-34	16.00-16.49	0
34-36	16.49-16.96	0
36-38	16.96-17.42	0
38-40	17.42-17.86	201
40-42	17.86-18.30	0
42-44	18.30-18.72	0
44-46	18.72-19.13	0
46-48	19.13-19.54	0
48-50	19.54-19.94	81
50-100	19.94-28.05	796
100-150	28.05-34.25	462
150-200	34.25-39.47	407
200-300	39.47-48.19	551
300-400	48.19-61.56	328
400-500	61.56-72.45	223
500-600	72.45-82.76	186
600-700	82.76-92.61	137
700-800	92.61-102.09	106
800-900	102.09-111.26	105
900-1000	111.26-120.15	97
1000-1100	120.15-128.81	75
1100-1200	128.81-146.26	73
1200-1400	146.26-170.00	242
> 1400	> 170.00	648
		Σ = 9658

Table 6.3 Tachyon data. The distribution in size of the shower front pulse height measured from a sample of 10142 extensive air shower triggers. The total number of measured pulse heights is also shown at the bottom of the column.

was used and run twice with the following requirements:

Maximum time = 265 μs	Maximum time = 265 μs
Number of time bins = 1	Number of time bins = 1
Maximum pulse height = 31.5 mV	Maximum pulse height = 1455 mV
Number of pulse height bins = 15	Number of pulse height bins = 29

In order to convert the pulse height measured on the oscilloscope to pulse height at the output of the head – unit , the calibration curve (see figure 5.6) which is fitted by the following equations was used:

$$v = 0.115\, V^{2.03} \qquad 1\,mV < V \leq 50\,mV$$

$$v = 1.415\, V^{1.37} \qquad 50\,mV < V < 140\,mV$$

where the pulse height at the output of head-unit , V , and the pulse height on the oscilloscope, v , are measured in mv. Table 6.4 shows the differential and integral spectra of the shower front pulse heights as measured at the output of head – unit. Plots of the differential and integral pulse height distributions of shower front pulses are shown in figures 6.4a and 6.4b respectively. The differential distribution shows a well resolved peak at a pulse height of 30mv and this feature is interpreted as being due to the passage of single muons through the tachyon detector.

6.4) CLASSIFICATION OF DIFFERENT TYPES OF EVENT

In the analysis of the results of the tachyon experiment described in section 6.2 (i.e; table 6.2 and figure 6.3) no

Pulse Height range on Oscilloscope in Millivolts	Pulse Height Range (v_1,v_2) at the output of head-unit in Millivolts	$\Delta v = v_2 - v_1$ in Millivolts	Mean $\bar{v} = \frac{v_2+v_1}{2}$ in Millivolts	No. of events with pulse height in range (v_1,v_2) $N_1(v_1,v_2)$	No. of events with pulse height in range $\frac{N_1(v_1,v_2)}{\Delta v}$ i.e; differential frequency per Millivolt, N	$N(>v_1)$
0.5-4	2.06-5.75	3.69	3.90	3145 ± 56	852 ± 15	9658
4-6	5.75-7.02	1.27	6.39	518 ± 23	408 ± 18	6513
6-8	7.02-8.08	1.06	7.55	344 ± 19	324 ± 17	5995
8-10	8.08-9.02	0.94	8.55	201 ± 14	214 ± 15	5651
10-12	9.02-9.87	0.85	9.45	122 ± 11	143 ± 13	5450
12-30	9.87-15.50	5.63	12.68	610 ± 25	108.3 ± 4.4	5328
30-50	15.50-19.94	4.45	17.72	282 ± 17	63.4 ± 3.8	4718
50-110	19.94-29.40	9.46	24.67	861 ± 29	91.0 ± 3.1	4436
110-120	29.40-30.69	1.29	30.05	148 ± 12	114.7 ± 9.4	3575
120-200	30.69-39.47	8.78	35.08	656 ± 26	74.7 ± 2.9	3427
200-300	39.47-48.19	8.72	43.83	551 ± 23	63.2 ± 2.7	2771
300-500	48.19-72.45	24.26	60.32	551 ± 23	22.71 ± 0.97	2220
500-600	72.45-82.76	10.31	77.61	186 ± 14	18.0 ± 1.3	1669
600-700	82.76-92.61	9.85	87.69	137 ± 12	13.9 ± 1.2	1483
700-900	92.61-111.26	18.65	101.93	211 ± 14	11.31 ± 0.78	1346
900-1100	111.26-128.81	17.55	120.03	172 ± 13	9.80 ± 0.75	1135
1100-1400	128.81-170.00	41.19	149.40	315 ± 18	7.65 ± 0.43	963
> 1400	> 170.00	-	-	-	-	648

Table 6.4 Shower front pulse height data. Basic data obtained from a sample of 10142 extensive air shower triggers and calculation of the differential and integral spectra of the measured pulse heights.

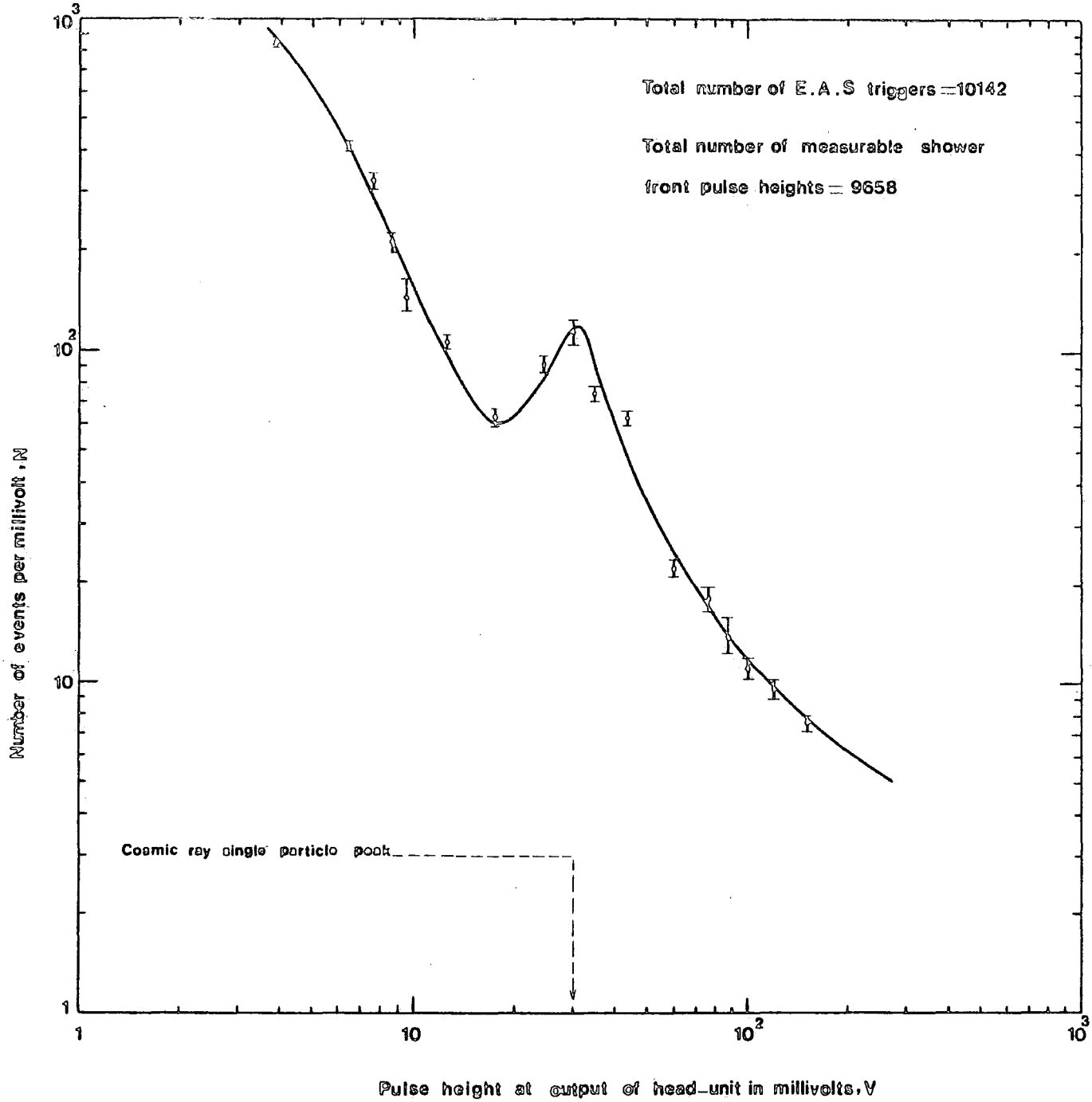

Figure 6.4a Differential distribution of shower front pulse height as measured at the output ofthe head-unit. Position of cosmic ray single particle peak is shown by arrow.

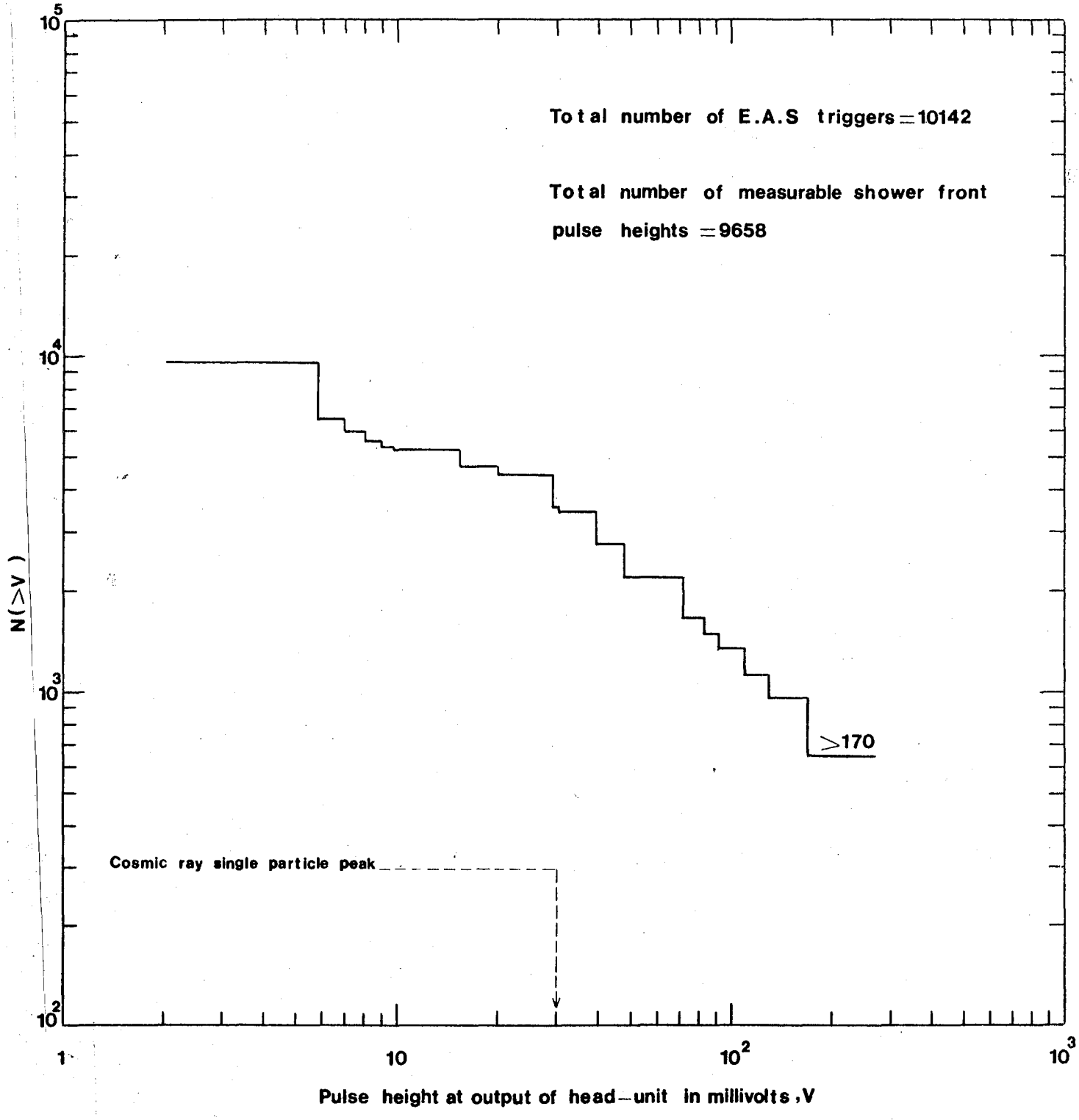

Figure 6.4b Integral distribution of shower front pulse height as measured at the output of head-unit.

account was taken of experimental bias as it was believed to be a small effect. Basically, bias arises because large shower front pulses saturate the recording electronic instruments and time domains occur in which small pulses would not be recorded even if present. As mentioned earilier, the output of the delay line used in the tachyon experiment (see figure 5.7) was connected to both channels of a dual beam oscilloscope of sweep time 500 μs. The lower beam of the oscilloscope was operated at a sensitivity of 5mv/cm with a maximum measurable pulse height of 30mv and the upper beam at a sensitivity of 200mv/cm with a maximum measurable pulse height of 1400mv. The classification of different types of event can be constructed as follows:

a) Figure 6.5a shows a recorded event in which no bias effect is present.

b) Figure 6.5b represents a large shower front pulse which saturates the oscilloscope electronics on the lower time base but it is accurately recorded on the upper time base. The shower front pulse on the lower time base is preceded by an oscillation which occupies the ≃ 90 μs time domain preceding the shower front pulse. It is estimated from scanning the film that input pulses in the smallest size range (i.e; 0.5-2mv) would not be detectable in this type of event in the ≃ 90 μs time domain before the shower front pulse although larger input pulse heights would be.

c) Figure 6.5c shows that small pulse heights can be recorded after the shower front pulse even if the oscilloscope amplifiers overswing.

d) If the overswing goes off scale as displayed in

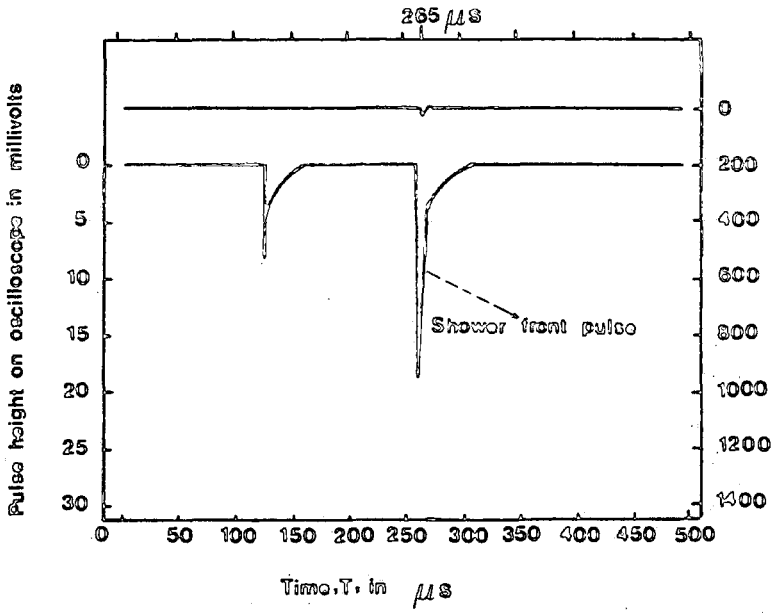

Figure 6.5a Event with no bias.

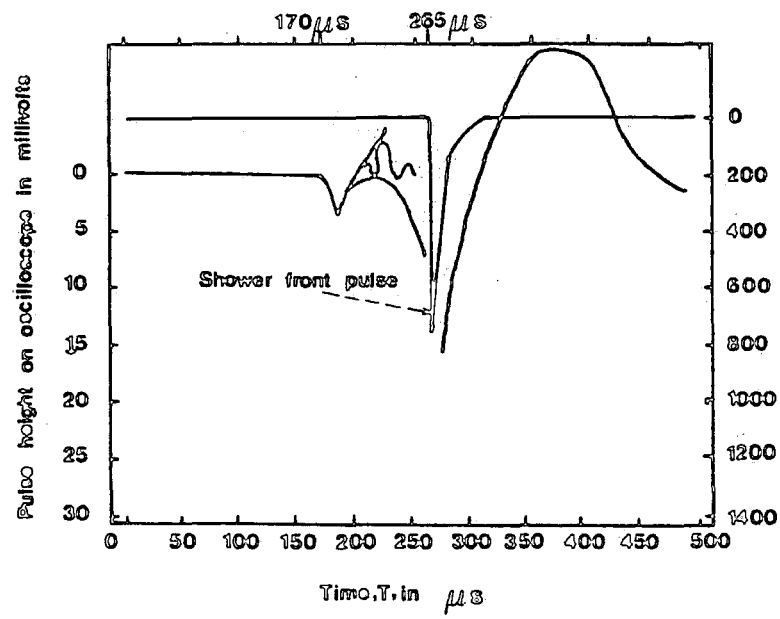

Figure 6.5b Oscillation that produces bias before the shower front pulse on the 5mv/cm recording scale but not on the 200mv/cm recording scale.

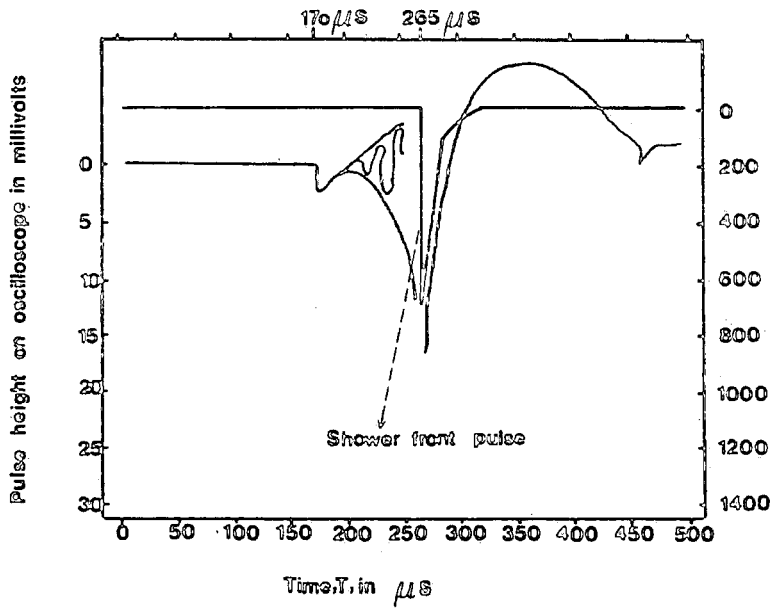

Figure 6.5c Event measurable after large shower front pulse.

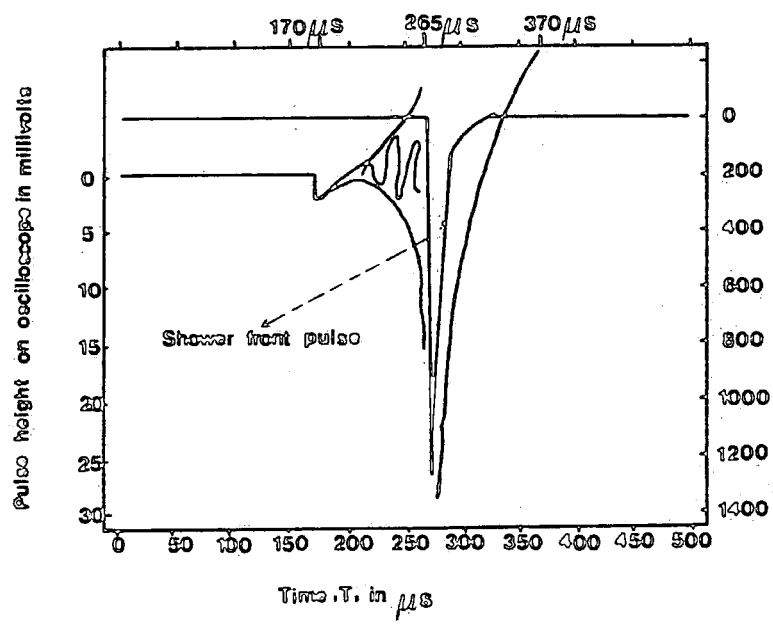

Figure 6.5d No event measurable after shower front pulse in the time domain 370-500 μs.

figure 6.5d, then no input pulses are recorded by the lower time base but they will be measurable on the upper time base if their height is ≥20mv.

6.5) DETERMINATION OF THE CORRECTION FACTOR OF THE TIME DISTRIBUTION OF RECORDED PULSE HEIGHTS FOR EXPERIMENTAL BIAS

In order to calculate the bias effect for the time distribution of recorded pulse heights, a correction factor to apply to the measured number of events in a given size range and a given time range has been found in the following way. Let N be the total number of triggers and X be the number of triggers in which the time range $t_1 \longrightarrow t_2$ is not sensitive, so N-X is the number of triggers in which the time range $t_1 \longrightarrow t_2$ is sensitive. The required correction factor , f , to give the number of events that should have been recorded if the time domain $t_1 \longrightarrow t_2$ was sensitive for all N triggers, is $f = \frac{N}{N-X}$. X has been found from scanning the film and figure 6.6 shows the variation of correction factor with time which is measured from the start of oscilloscope time base. The correction factor shown in figure 6.6 is to be applied to pulse heights in the size range 0.5-2mv recorded before the shower front pulse and to pulses in the size range 0.5-20mv after the occurrence of the shower front pulse. Table 6.5 shows the measured and corrected number of events in different time ranges for different ranges of pulse height. Figure 6.7 shows the corrected number of events presented in histogram form in which the effect of applying the correction for experimental bias is

Time Range in μs	Correction Factor	0.5mV ≤ V ≤ 2mV		2mV < V ≤ 4mV		4mV < V ≤ 30mV	
		No. of events before correction	No. of events after correction	No. of events before correction	No. of events after correction	No. of events before correction	No. of events after correction
0- 10	1.01	61	61.6	23	23	14	14
10- 20	1.00	83	83.0	38	38	11	11
20- 30	1.01	84	84.8	43	43	13	13
30- 40	1.01	96	97.0	48	48	7	7
40- 50	1.01	94	94.9	33	33	10	10
50- 60	1.01	88	88.9	38	38	15	15
60- 70	1.01	80	80.8	39	39	7	7
70- 80	1.01	75	75.7	39	39	10	10
80- 90	1.01	76	76.8	36	36	11	11
90-100	1.01	81	81.8	40	40	12	12
100-110	1.01	68	68.7	28	28	7	7
110-120	1.01	89	89.9	33	33	10	10
120-130	1.01	87	87.9	45	45	15	15
130-140	1.01	86	86.9	39	39	8	8
140-150	1.01	85	85.8	31	31	3	3
150-160	1.01	97	98.0	33	33	9	9
160-170	1.01	65	65.6	45	45	12	12
170-180	1.11	59	65.5	46	46	10	10
180-190	1.15	89	102.3	43	43	13	13
190-200	1.17	60	70.2	20	20	7	7
200-210	1.21	75	90.7	29	29	7	7
210-220	1.28	65	83.2	42	42	11	11
220-230	1.39	68	94.5	52	52	9	9
230-240	1.52	63	95.8	34	34	6	6
240-250	1.63	57	92.9	29	29	6	6
250-260	1.77	52	92.0	17	17	6	6
260-270	-	2045	2045	1100	1100	1795	1795
270-280	1.90	33	62.7	20	38.0	13	24.7
280-290	1.42	57	80.9	29	41.2	19	26.1
290-300	1.42	69	98.0	40	56.8	13	18.0
300-310	1.42	51	72.4	33	46.9	19	27.0
310-320	1.42	71	100.8	36	51.1	11	15.2
320-330	1.41	63	88.8	51	71.9	24	32.6
330-340	1.41	55	77.5	39	55.0	20	28.2
340-350	1.41	53	74.7	40	56.4	28	39.1
350-360	1.37	43	58.9	34	46.6	22	29.8
360-370	1.36	70	95.2	39	53.0	37	48.9
370-380	1.32	68	89.8	74	97.7	33	42.3
380-390	1.30	56	72.8	52	67.6	27	34.8
390-400	1.28	50	64.0	47	60.2	29	36.6
400-410	1.26	66	83.2	46	58.0	34	42.8
410-420	1.25	54	67.5	52	65.0	29	35.5
420-430	1.23	71	87.3	44	54.1	38	46.3
430-440	1.22	65	79.3	47	57.3	20	24.2
440-450	1.19	83	98.8	46	54.7	37	43.6
450-460	1.18	62	73.2	47	55.5	26	30.0
460-470	1.17	85	99.4	51	59.7	27	31.4
470-480	1.16	55	63.8	48	55.7	35	40.1
480-490	1.14	56	63.8	48	54.7	28	31.8
490-500	1.14	85	96.9	67	76.4	32	36.2
		$\sum$ = 3404	$\sum$ = 4044.9	$\sum$ = 1973	$\sum$ = 2276.5	$\sum$ = 850	$\sum$ = 1014.2

Table 6.5 Tachyon data based on a sample of 10142 extensive air shower triggers. Time distribution of events in three different ranges of pulse height (measured on the oscilloscope) before and after correction for experimental bias. Time is measured from the start of the oscilloscope time base and the shower front pulse occurs at 265 μs. The bias correction shown in Figure 6.6 applies only to the pulse height range 0.5-2mV for times < 260μs and for >270μs, it applies to the pulse height range 0.5-20mV. For large pulse heights there is no bias correction.

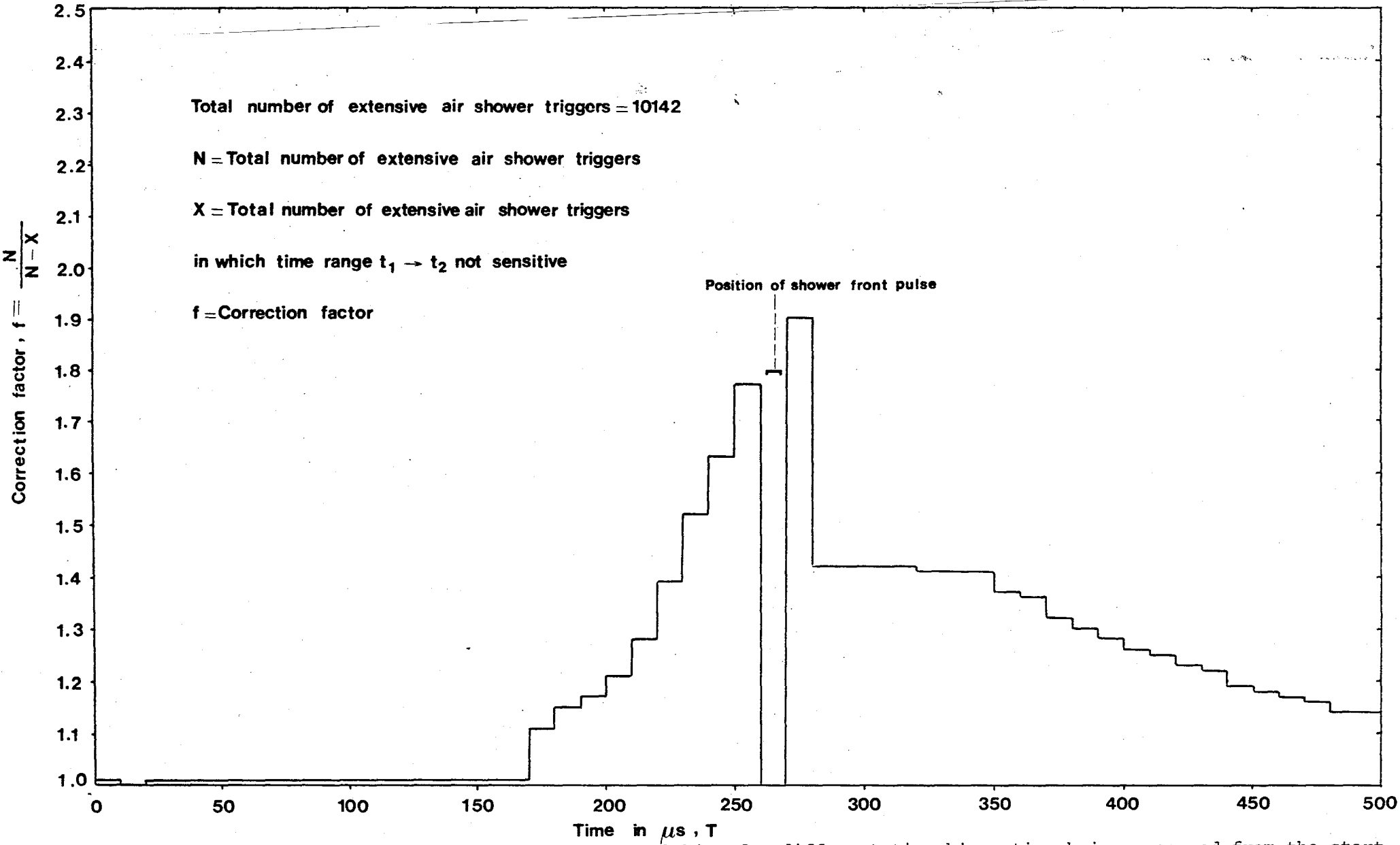

Figure 6.6 The correction factor, f, due to experimental bias for different time bins, time being measured from the start of the oscilloscope time base. The shower front pulse occurs at a time of 265 μs. For times < 260 μs the correction factor applies only to pulse heights in the range 0.5-2 mv. For times > 270 μs the correction factor applies only to pulse heights in the range 0.5-20 mv, there is no bias correction for pulse heights ⩾ 20 mv.

Pulse height range	N(0 - 260 μs)		N(270 - 500 μs)		$\frac{N(0 - 260\ \mu s)}{N(270 - 500\ \mu s)}$	
	Before correction	After correction	Before correction	After correction	Before correction	After correction
0.5mv≤v≤2mv 0.07e≤v≤0.14e	1983	2195.2	1421	1849.7	1.40±0.05	1.19±0.04
2mv<v≤4mv 0.14e<v≤0.19e	943	943	1030	1333.5	0.92±0.04	0.71±0.03
4mv<v≤30mv 0.19e<v≤0.52e	249	249	601	765.2	0.41±0.03	0.32±0.02
30mv<v≤120mv 0.52e<v≤e	155	155	270	270	0.57±0.06	0.57±0.06
v > 120 mv v > e	111	111	104	104	1.07±0.15	1.07±0.15
v ≥ 700 mv v ≥ 3e	6	6	7	7	0.86±0.48	0.86±0.48

Table 6.6a The ratio of the number of events $\frac{N(0\text{-}260\ \mu s)}{N(270\text{-}500\mu s)}$ occurring in the time regions 0-260 μs and 270-500 μs with the time measured from the start of the oscilloscope time base. The shower front pulse occurs at 265 μs from the start of the oscilloscope time base.

Pulse height range	N(120 - 260 μs)		N(270 - 410 μs)		$\frac{N(120 - 260\ \mu s)}{N(270 - 410\ \mu s)}$	
	Before correction	After correction	Before correction	After correction	Before correction	After correction
0.5mv≤v≤2mv 0.07e≤v≤0.14e	1008	1211.3	805	1119.7	1.25±0.06	1.08±0.05
2mv<v≤4mv 0.14e<v≤0.19e	505	505	580	800.4	0.87±0.05	0.63±0.04
4mv<v≤30mv 0.19e<v≤0.52e	122	122	329	446.1	0.37±0.04	0.27±0.03
30mv<v≤120mv 0.52e<v≤e	88	88	125	125	0.70±0.10	0.70±0.10
v > 120 mv v > e	65	65	48	48	1.35±0.26	1.35±0.26
v ≥ 700 mv v ≥ 3e	5	5	2	2	2.5 ±1.7	2.5 ±1.7

Table 6.6b The ratio of the number of events $\frac{N(120\text{-}260\ \mu s)}{N(270\text{-}410\ \mu s)}$ occurring in the time regions 120-260 μs and 270-410 μs with the times measured from the start of the oscilloscope time base. The shower front pulse occurs at 265 μs from the start of the oscilloscope time base.

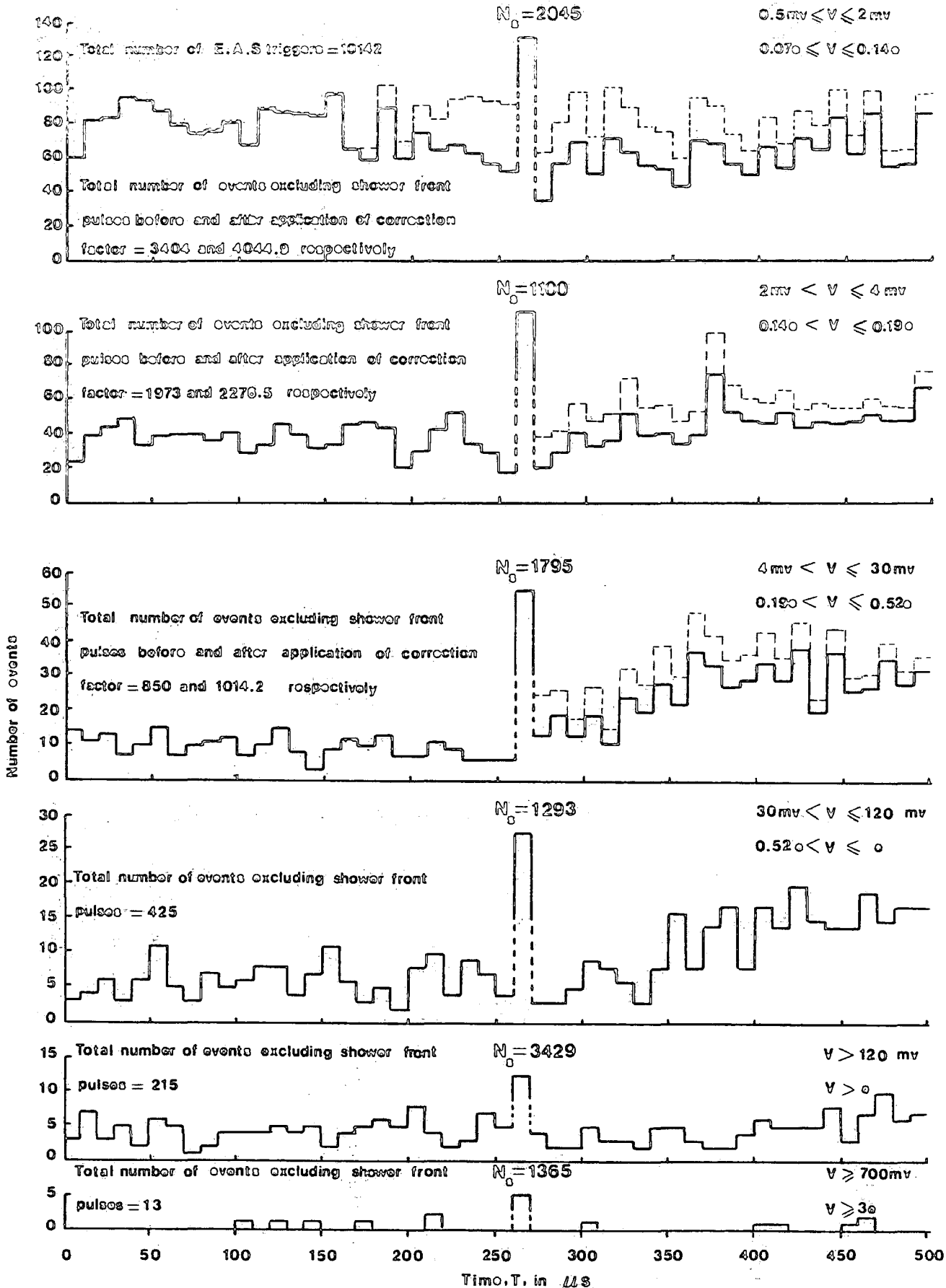

Figure 6.7 Occurrence time distribution of pulse heights between the two stated pulse height limits and energy deposit limits expressed in terms of e where e ($\simeq$ 10 MeV) is the energy deposited in the tachyon detector by a relativistic muon traversing it at normal incidence. Time is measured from the start of the oscilloscope time base and the shower front pulse occurs at 265 μs. The effect of applying the correction factor, f, for experimental bias is represented by the dashed lines in the histograms.

depicted by the dashed lines.

Apart from a search for tachyons associated with extensive air showers, the present data can also be used to assess whether there are a significant number of ionizing events produced in the tachyon detection scintillator, C , that occur after the arrival of the shower front pulse. Tables 6.6a and 6.6b give the values of the ratio $\frac{N(0-260\,\mu s)}{N(270-500\,\mu s)}$ and $\frac{N(120-260\,\mu s)}{N(270-410\,\mu s)}$ as a function of the energy deposited in the tachyon detection scintillator respectively. The times quoted in the above ratios are measured from the start of the oscilloscope time base with the shower front occurring at a time of 265 μs after the start of the oscilloscope time base. Assuming no significant tachyon flux and that no particles arrive at long time delays (i.e; >5 μs) after the arrival of the shower front pulse, the expected values of the above ratios are $\frac{260-0}{500-270} = \frac{260}{230} = 1.13$ and $\frac{260-120}{410-270} = \frac{140}{140} = 1.00$. It is seen from table 6.6a that all the measured ratios are consistently less than the above value (i.e; 1.13) except the one that refers to the smallest range of pulse heights (0.5-2mv) measured. Table 6.6b shows that all the measured ratios are less than the corresponding above value (i.e; 1) except the ones that refer to the three different ranges of pulse heights, namely; 0.5-2mv, ≥120mv and ≥700mv. The smallest measured ratio is for pulse heights measured on the recording oscilloscope of 4 − 30mv corresponding to a range of energy deposition in the tachyon scintillator of 1.9MeV-5.2MeV. Such delayed pulses could be produced by photons in the extensive air shower electromagnetic cascade which have

undergone large angle scattering from the wings of the shower or by low energy evaporation neutrons from air nuclei produced in the extensive air shower hadron cascade which subsequently interact in the detection scintillator.

6.6) DISTRIBUTION IN HEIGHT OF PULSES OCCURRING IN THE 265 μS TIME DOMAIN BEFORE AND THE 235 μS AFTER THE ARRIVAL OF E.A.S SHOWER FRONT

In order to measure the distribution in height of pulses occurring in the 265 μs time period before and the 235 μs time period after the arrival of E.A.S shower front pulse, The "DATABIN" program was run twice with the following requirements:

Maximum time = 530 μs	Maximum time = 530 μs
Number of time bins = 2	Number of time bins = 2
Maximum pulse height = 31.5 mV	Maximum pulse height = 1455 mV
Number of pulse height bins = 15	Number of pulse height bins = 29

The result is shown in table 6.7, where N(<265μs) is the number of pulses observed in the first 265μs of the oscilloscope sweep of 500 μs and N(>265μs) is the number of pulses observed in the final 235 μs. Also, N(0-500μs) is the number of observed pulses in the total sweep time of the oscilloscope. i.e;

$$N(0-500\,\mu s) = N(<265\,\mu s) + N(>265\,\mu s)$$

By using the data in this table, it was possible to determine the differential and integral pulse height distributions for the two time domains (i.e; 265μs and 235μs before and after the

Pulse Height Range $V_1 \rightarrow V_2$ on oscilloscope in millivolts	Pulse Height Range At output of head-unit in millivolts	N(<265μs)	N(>265μs)	N(0-500μs)
0.5- 2	2.06- 4.08	1983	1421	3404
2- 4	4.08- 5.75	943	1030	1973
4- 6	5.75- 7.02	175	280	455
6- 8	7.02- 8.08	45	144	189
8- 10	8.08- 9.02	11	48	59
10- 12	9.02- 9.87	4	36	40
12- 14	9.87- 10.65	3	23	26
14- 16	10.65- 11.37	3	11	14
16- 18	11.37- 12.05	1	12	13
18- 20	12.05- 12.69	0	8	8
20- 22	12.69- 13.30	0	9	9
22- 24	13.30- 13.89	3	6	9
24- 26	13.89- 14.45	1	5	6
26- 28	14.45- 14.98	0	2	2
28- 30	14.98- 15.50	3	17	20
30- 32	15.50- 16.00	0	0	0
32- 34	16.00- 16.49	0	0	0
34- 36	16.49- 16.96	0	0	0
36- 38	16.96- 17.42	0	0	0
38- 40	17.42- 17.86	15	65	80
40- 42	17.86- 18.30	0	0	0
42- 44	18.30- 18.72	0	0	0
44- 46	18.72- 19.13	0	0	0
46- 48	19.13- 19.54	0	0	0
48- 50	19.54- 19.94	3	24	27
50- 100	19.94- 28.05	115	154	269
100- 150	28.05- 34.25	39	49	88
150- 200	34.25- 39.47	35	36	71
200- 300	39.47- 48.19	34	23	57
300- 400	48.19- 61.56	10	10	20
400- 500	61.56- 72.45	4	2	6
500- 600	72.45- 82.76	2	2	4
600- 700	82.76- 92.61	3	3	6
700- 800	92.61-102.09	0	4	4
800- 900	102.09-111.26	1	1	2
900-1000	111.26-120.15	2	0	2
1000-1100	120.15-128.81	0	1	1
1100-1200	128.81-146.26	1	0	1
1200-1400	146.26-170.00	2	0	2
> 1400	> 170.00	0	0	0
		Σ=3441	Σ=3426	Σ=6867

Table 6.7 Tachyon data. Pulse height distribution obtained from a sample of 10142 extensive air shower triggers. N(<265μs) is the number of events observed in the first 265μs of the oscilloscope sweep of 500μs and N(>265μs) is the number observed in the final 235μs. N(0-500μs) = N(<265μs) + N(>265μs).

arrival of shower front pulse respectively) and for both of them lumped togather (i.e; total time of sweep). The results are shown separately in tables 6.8a , 6.8b and 6.8c and are plotted in the figures 6.8a , 6.8b and 6.8c. In each case there is a well resolved peak occurring at a pulse height of 30mv at the output of the head-unit. This is consistent with the events in the peak being produced by cosmic ray muons which are not correlated with the E.A.S trigger traversing the plastic detector in the relevant time periods. If n pulses of size $>v$ at the output of the head-unit are observed to occur in a time $\triangle t$ in a sample of N time base triggers (in the present experiment N=10,142), the absolute rate of pulses from the detector of size $>v$ is given by $R(>v)= \frac{n}{N \cdot \triangle t}$ per second. Using this result, the integral rate of pulses of size $>v$ at the output of the head-unit as a function of v for the two time domains (i.e; 265 μs and 235 μs before and after the arrival of the shower front pulse) and also for both of them lumped together were calculated and the results are separately shown in figures 6.9a, 6.9b and 6.9c. Figures 6.10a and 6.10b compare the differential and integral pulse height distributions for the 265 μs and 235 μs time domains before and after the arrival of the shower front pulse. In principle, the two distributions should agree exactly and the difference between them is attributed to a small finite flux of delayed ionizing events occurring in the 235 μs after the occurrence of the air shower front pulse. The integral distribution can be compared directly with that found using an amplifier , discriminator and scaler. Such a comparison is shown in figure 6.11. It is seen that

Pulse heights range on oscilloscope in millivolts	Pulse heights range, $v_1 \rightarrow v_2$, at output of head-unit in millivolts	$\Delta v = v_2 - v_1$ in millivolts	mean $\bar{v} = \frac{v_2+v_1}{2}$ in millivolts	No.of events with pulse height in range; $v_1 \rightarrow v_2$ $N_1(v_1,v_2)$	No.of events with pulse height in range, $\frac{N_1(v_1,v_2)}{\Delta v}$ i.e. differential frequency per millivolt, N_2	$N(>v_1)$	Integral Rate $>v_1$ per second
0.5- 4	2.06- 5.75	3.69	3.91	2926 ± 54	793 ± 15	3441	1280 ± 22
4- 6	5.75- 7.02	1.27	6.39	175 ± 13	138 ± 10	515	191.6 ± 8.4
6- 8	7.02- 8.08	1.06	7.55	45.0 ± 6.7	42.4 ± 6.3	340	126.5 ± 6.9
8- 10	8.08- 9.02	0.94	8.55	11.0 ± 3.3	11.7 ± 3.5	295	109.8 ± 6.4
10- 12	9.02- 9.87	0.85	9.45	4.0 ± 2.0	4.7 ± 2.3	284	105.7 ± 6.3
12- 18	9.87- 12.05	2.18	10.96	7.0 ± 2.7	3.2 ± 1.2	280	104.2 ± 6.2
18- 24	12.05- 13.89	1.84	12.97	3.0 ± 1.7	1.63 ± 0.94	273	101.6 ± 6.1
24- 28	13.89- 14.98	1.09	14.44	1.0 ± 1.0	0.92 ± 0.92	270	100.5 ± 6.1
28- 38	14.98- 17.42	2.44	16.20	3.0 ± 1.7	1.23 ± 0.71	269	100.1 ± 6.1
38- 90	17.42- 26.63	9.21	22.03	99.0 ± 9.9	10.7 ± 1.1	266	99.0 ± 6.1
90- 100	26.63- 28.05	1.41	27.34	34.0 ± 5.8	23.9 ± 4.1	167	62.1 ± 4.8
100- 200	28.05- 39.47	11.42	33.76	74.0 ± 8.6	6.48 ± 0.75	133	49.5 ± 4.3
200- 300	39.47- 48.19	8.72	43.83	34.0 ± 5.8	3.90 ± 0.67	59	22.0 ± 2.9
300- 400	48.19- 61.56	13.37	54.88	10.0 ± 3.2	0.75 ± 0.24	25	9.3 ± 1.9
400- 600	61.56- 82.76	21.20	72.16	6.0 ± 2.4	0.29 ± 0.12	15	5.6 ± 1.4
600- 900	82.76-111.26	28.50	97.01	4.0 ± 2.0	0.14 ± 0.07	9	3.3 ± 1.1
900-1100	111.26-128.81	17.55	120.04	2.0 ± 1.4	0.11 ± 0.08	5	1.86 ± 0.83
1100-1400	128.81-170.00	41.19	149.41	3.0 ± 1.7	0.07 ± 0.04	3	1.12 ± 0.64
> 1400	> 170.00	-	-	-	-	-	-

Table 6.8a The measured pulse height distribution of pulses observed in the 265 μs period before the arrival of the shower front pulse and determination of their differential size distribution and their integral rate distribution.

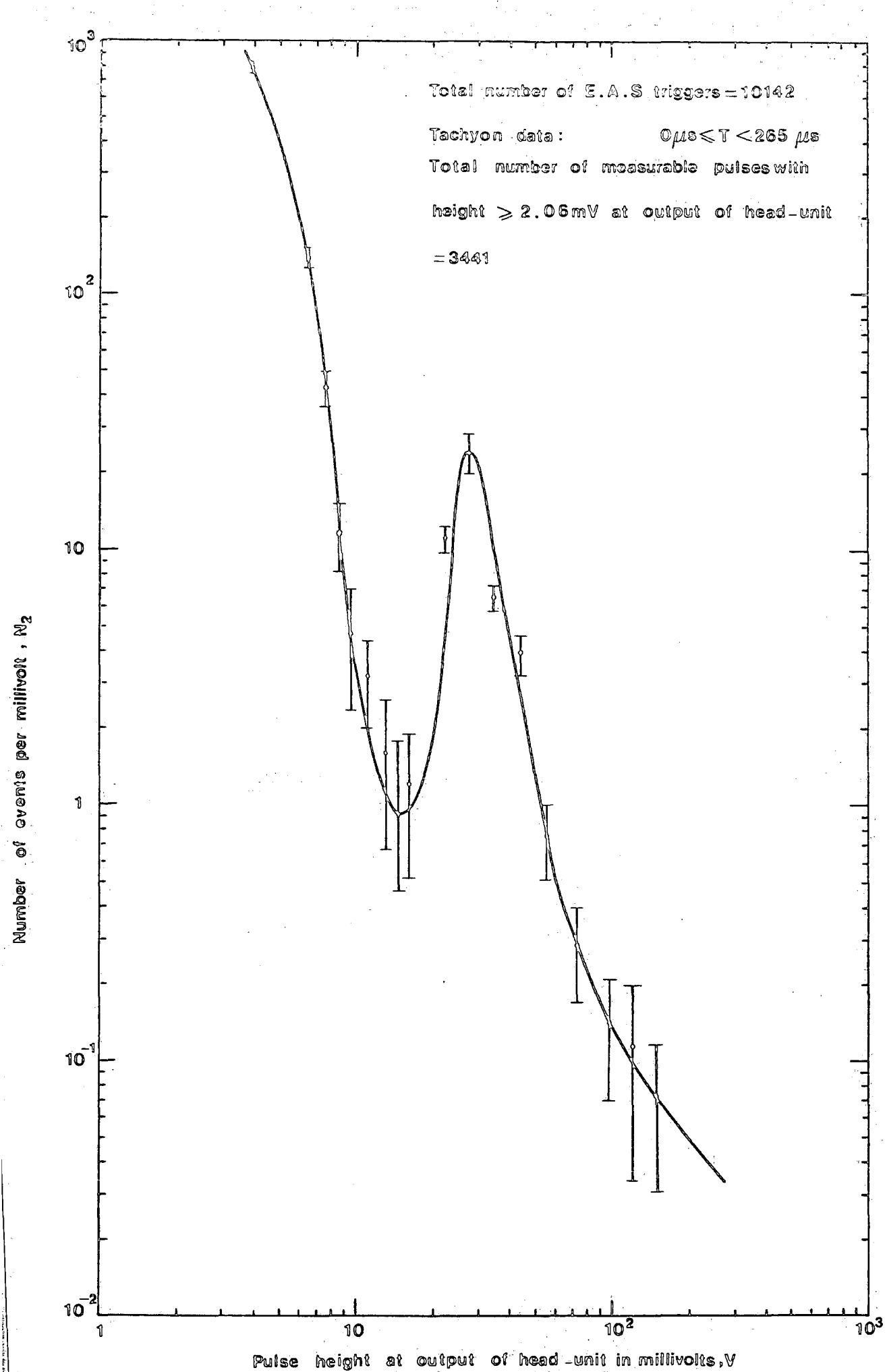

Figure 6.8a The differential distribution of pulse height occurring in the 265 μs period before the arrival of the shower front pulse at the output of head-unit for the sample of 10142 shower triggers.

Pulse heights range on oscilloscope in millivolts	Pulse heights range, $v_1 \rightarrow v_2$ at output of head-unit in millivolts	$\Delta v = v_2 - v_1$ in millivolts	mean $\bar{v} = \frac{v_2 + v_1}{2}$ in millivolts	No. of events with pulse height in range; $v_1 \rightarrow v_2$ $N_1(v_1, v_2)$	No. of events with pulse height in range, $\frac{N_1(v_1, v_2)}{\Delta v}$ i.e. differential frequency per millivolt, N_2	$N(>v_1)$	Integral rate $>v_1$ per second
0.5- 4	2.06- 5.75	3.69	3.91	2451 ± 49	664 ± 13	3426	1437 ± 25
4- 6	5.75- 7.02	1.27	6.39	280 ± 17	220 ± 13	975	409.1 ± 13
6- 8	7.02- 8.08	1.06	7.55	144 ± 12	136 ± 11	695	292 ± 11
8- 10	8.08- 9.02	0.94	8.55	48.0 ± 6.9	51.1 ± 7.4	551	231.2 ± 9.8
10- 12	9.02- 9.87	0.85	9.45	36.0 ± 6.0	42.3 ± 7.1	503	211.0 ± 9.4
12- 20	9.87- 12.69	2.82	11.28	54.0 ± 7.3	19.1 ± 2.6	467	195.9 ± 9.1
20- 24	12.69- 13.89	1.20	13.29	15.0 ± 3.9	12.5 ± 3.2	413	173.3 ± 8.5
24- 28	13.89- 14.98	1.09	14.44	7.0 ± 2.6	6.4 ± 2.4	398	167.0 ± 8.4
28- 38	14.98- 17.42	2.44	16.20	17.0 ± 4.1	7.0 ± 1.7	391	164.0 ± 8.3
38- 90	17.42- 26.63	9.21	22.03	206 ± 14	22.4 ± 1.6	374	156.9 ± 8.1
90- 100	26.63- 28.05	1.42	27.34	37.0 ± 6.1	26.1 ± 4.3	168	70.5 ± 5.4
100- 200	28.05- 39.47	11.42	33.76	85.0 ± 9.2	7.44 ± 0.81	131	55.0 ± 4.8
200- 300	39.47- 48.19	8.72	43.83	23.0 ± 4.8	2.64 ± 0.55	46	19.3 ± 2.8
300- 400	48.19- 61.56	13.37	54.88	10.0 ± 3.2	0.75 ± 0.24	23	9.6 ± 2.0
400- 700	61.56- 92.61	31.05	77.09	7.0 ± 2.6	0.22 ± 0.08	13	5.4 ± 1.5
700-1400	92.61-170.00	77.39	131.31	6.0 ± 2.4	0.08 ± 0.03	6	2.5 ± 1.0
> 1400	> 170.00	-	-	-	-	-	-

Table 6.8b The measured pulse height distribution of pulses observed in the 235 μs period after the arrival of the shower front pulse and determination of their differential size distribution and their integral rate distribution.

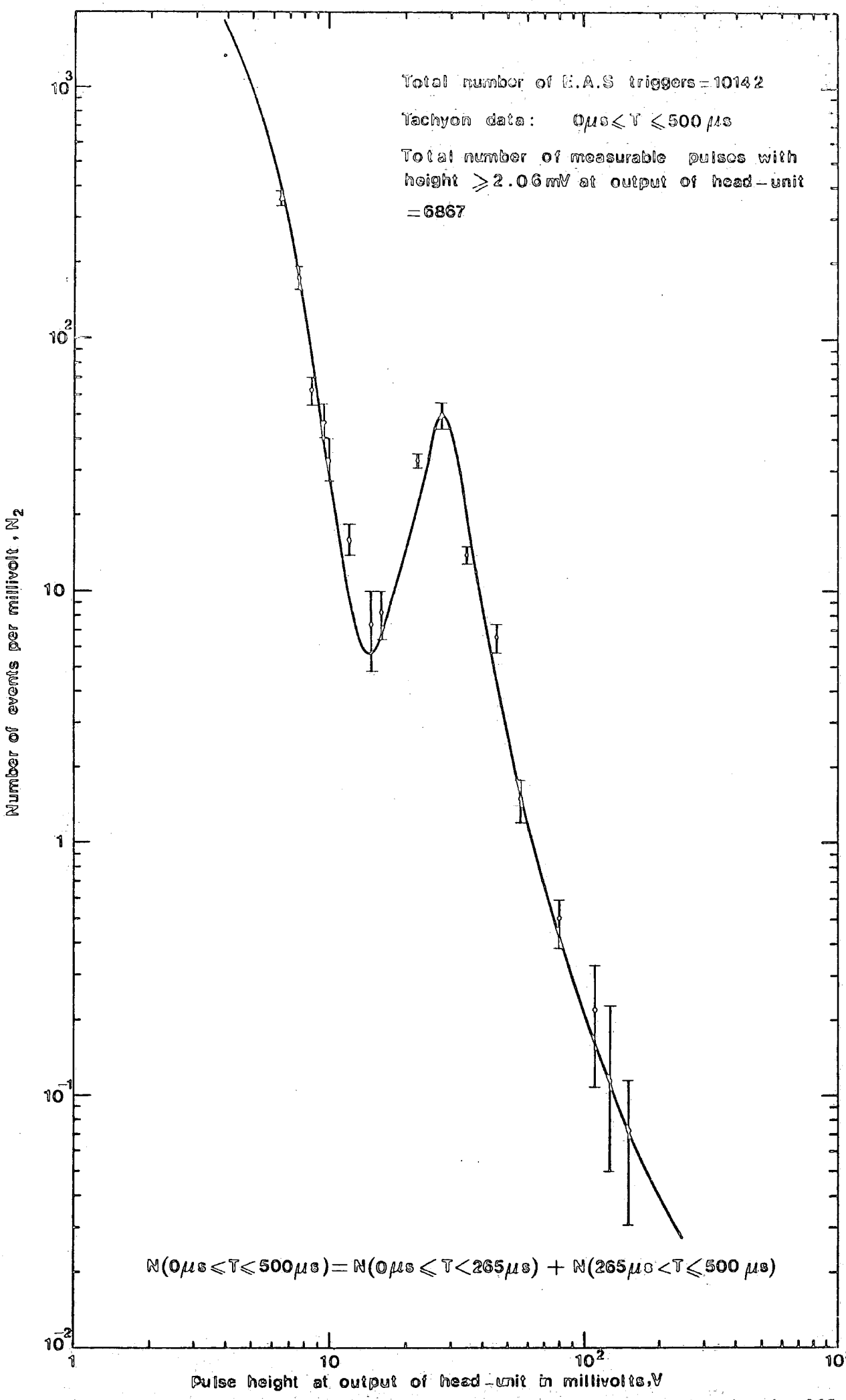

Figure 6.8c The differential distribution of pulse height occurring in the 265 μs period before the shower front and the 235 μs period after the arrival of the shower front pulse at the output of head-unit for a sample of 10142 shower triggers.

Pulse heights range on oscilloscope in millivolts	Pulse heights range, $v_1 \rightarrow v_2$, at output of head-unit in millivolts	$\Delta v = v_2 - v_1$ in millivolts	mean $\bar{v} = \frac{v_2 + v_1}{2}$ in millivolts	No. of events with pulse height in range: $v_1 \rightarrow v_2$ $N_1(v_1, v_2)$	No. of events with pulse height in range, $\frac{N_1(v_1, v_2)}{\Delta v}$ i.e. differential frequency per millivolt, N_2	$N(>v_1)$	Integral rate $>v_1$ per second
0.5- 4	2.06- 5.75	3.69	3.91	5377 ± 73	1457 ± 20	6867	1354 ± 16
4- 6	5.75- 7.02	1.27	6.39	455 ± 21	358 ± 17	1490	293.8 ± 7.6
6- 8	7.02- 8.08	1.06	7.55	189 + 14	178 ± 13	1035	204.1 ± 6.3
8- 10	8.08- 9.02	0.94	8.55	59.0 ± 7.7	62.8 ± 8.2	846	166.8 ± 5.7
10- 12	9.02- 9.87	0.85	9.45	40.0 ± 6.3	47.1 ± 7.4	787	155.2 ± 5.5
12- 14	9.87- 10.65	0.78	10.26	26.0 ± 5.1	33.3 ± 6.5	747	147.3 ± 5.4
14- 24	10.65- 13.89	3.24	12.27	53.0 ± 7.3	16.4 ± 2.2	721	142.2 ± 5.3
24- 28	13.89- 14.98	1.09	14.44	8.0 ± 2.8	7.3 ± 2.6	668	131.7 ± 5.1
28- 38	14.98- 17.42	2.44	16.20	20.0 ± 4.5	8.2 ± 1.8	660	130.1 ± 5.1
38- 90	17.42- 26.63	9.21	22.03	305 ± 17	33.1 ± 1.9	640	126.2 ± 5.0
90- 100	26.63- 28.05	1.42	27.34	71.0 ± 8.4	50.0 ± 5.9	335	66.1 ± 3.6
100- 200	28.05- 39.47	11.42	33.76	159 ± 13	13.9 ± 1.1	264	52.1 ± 3.2
200- 300	39.47- 48.19	8.72	43.83	57.0 ± 7.5	6.54 ± 0.87	105	20.7 ± 2.0
300- 400	48.19- 61.56	13.37	54.88	20.0 ± 4.5	1.50 ± 0.33	48	9.5 ± 1.4
400- 800	61.56-102-09	40.53	81.83	20.0 ± 4.5	0.49 ± 0.11	28	5.5 ± 1.0
800-1000	102.09-120.15	18.06	111.12	4.0 ± 2.0	0.22 ± 0.11	8	1.58 ± 0.56
1000-1100	120.15-128.81	8.66	124.48	1.0 ± 1.0	0.11 ± 0.11	4	0.79 ± 0.39
1100-1400	128.81-170.00	41.19	149.41	3.0 ± 1.7	0.07 ± 0.04	3	0.59 ± 0.34
> 1400	> 170.00	-	-	-	-	-	-

Table 6.8c The measured pulse height distribution of pulses observed in the 265 μs period before and the 235 μs period after the arrival of the shower front pulse and determination of their differential size distribution and their integral rate distribution.

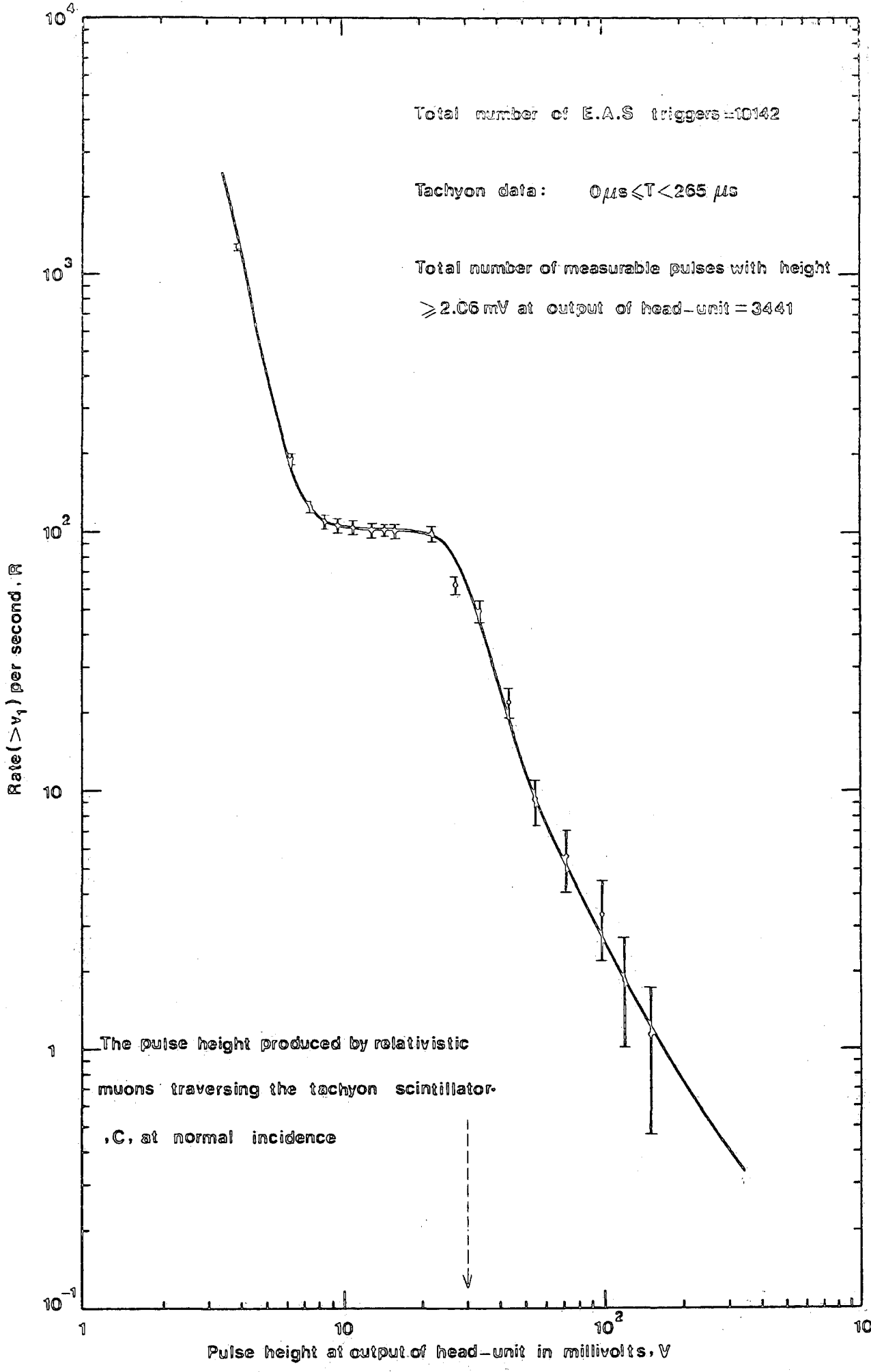

Figure 6.9a The integral rate of pulses of size > V at the output of the head-unit as a function of V determined from pulses observed in the 265 μs period before the arrival of the shower front pulse for a sample of 10142 shower triggers.

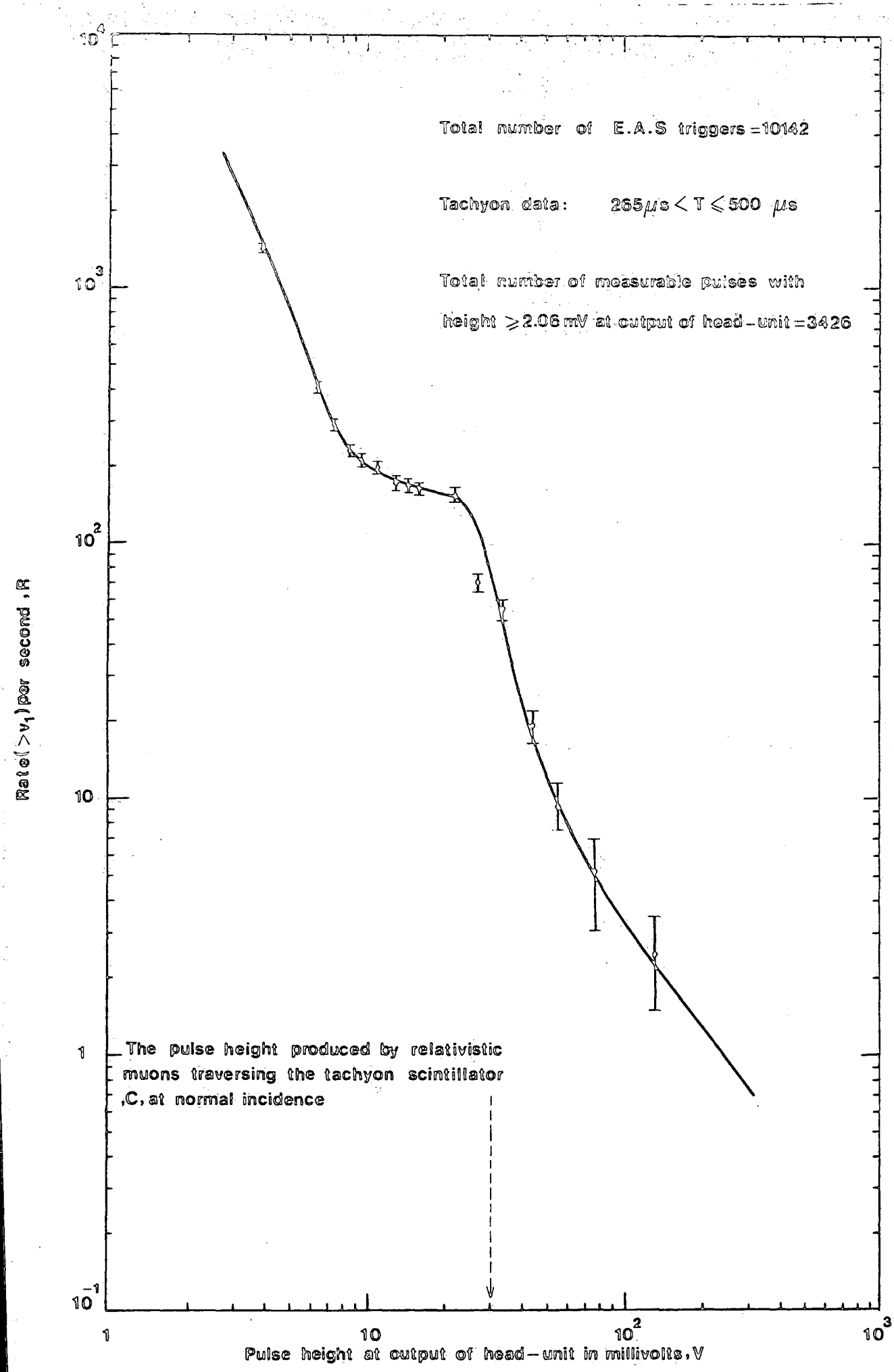

Figure 6.9b The integral rate of pulses of size > V at the output of the head-unit as a function of V determined from pulses observed in the 235μs period after the arrival of the shower front pulse for a sample of 10142 shower triggers.

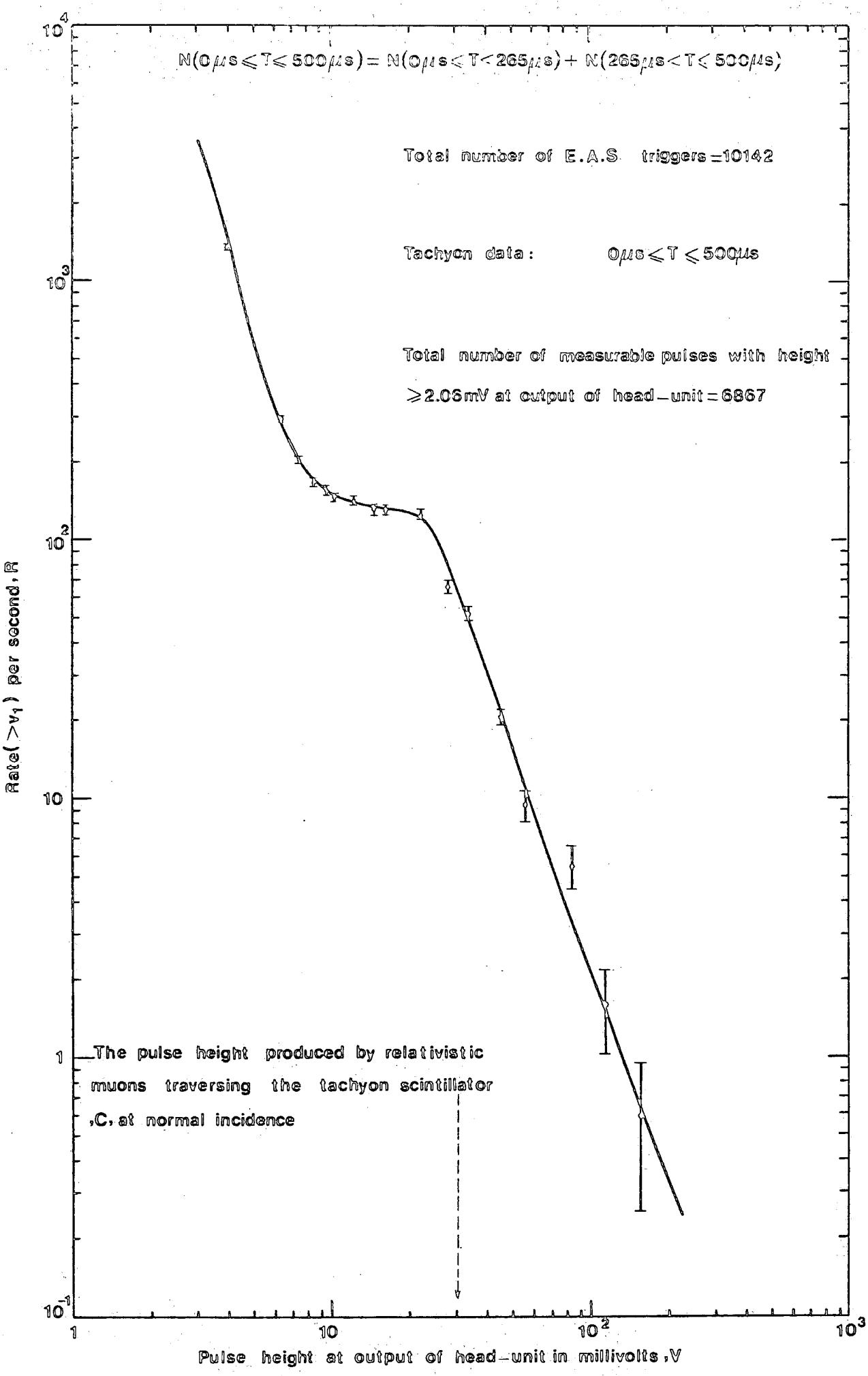

Figure 6.9c The integral rate of pulses of size > V at the output of the head-unit as a function of V determined from pulses observed in the 265μs period before the arrival of shower front and the 235μs period after the arrival of shower front pulse for a sample of 10142 shower triggers.

Pulse heights range on oscilloscope in millivolts	Pulse heights range, $v_1 \rightarrow v_2$, at output of head-unit in millivolts	$\Delta v = v_2 - v_1$ in millivolts	mean $\bar{v} = \frac{v_2+v_1}{2}$ in millivolts	No.of events with pulse height in range; $v_1 \rightarrow v_2$ $N_1(v_1,v_2)$	No.of events with pulse height in range, $\frac{N_1(v_1,v_2)}{\Delta v}$ i.e. differential frequency per millivolt, N_2	$N(>v_1)$	Integral Rate $> v_1$ per second
0.5- 4	2.06- 5.75	3.69	3.91	3138 ± 56	850 ± 15	3653	1359 ± 22
4- 6	5.75- 7.02	1.27	6.39	175 ± 13	138 ± 10	515	191.6 ± 8.4
6- 8	7.02- 8.08	1.06	7.55	45.0 ± 6.7	42.4 ± 6.3	340	126.5 ± 6.9
8- 10	8.08- 9.02	0.94	8.55	11.0 ± 3.3	11.7 ± 3.5	295	109.8 ± 6.4
10- 12	9.02- 9.87	0.85	9.45	4.0 ± 2.0	4.7 ± 2.3	284	105.7 ± 6.3
12- 18	9.87- 12.05	2.18	10.96	7.0 ± 2.6	3.2 ± 1.2	280	104.2 ± 6.2
18- 24	12.05- 13.89	1.84	12.97	3.0 ± 1.7	1.63 ± 0.94	273	101.6 ± 6.1
24- 28	13.89- 14.98	1.09	14.44	1.0 ± 1.0	0.92 ± 0.92	270	100.5 ± 6.1
28- 38	14.98- 17.42	2.44	16.20	3.0 ± 1.7	1.23 ± 0.71	269	100.1 ± 6.1
38- 90	17.42- 26.63	9.21	22.03	99.0 ± 9.9	10.7 ± 1.1	266	99.0 ± 6.1
90- 100	26.63- 28.05	1.41	27.34	34.0 ± 5.8	23.9 ± 4.1	167	62.1 ± 4.8
100- 200	28.05- 39.47	11.42	33.76	74.0 ± 8.6	6.48 ± 0.75	133	49.5 ± 4.3
200- 300	39.47- 48.19	8.72	43.83	34.0 ± 5.8	3.90 ± 0.67	59	21.9 ± 2.9
300- 400	48.19- 61.56	13.37	54.88	10.0 ± 3.2	0.75 ± 0.24	25	9.3 ± 1.9
400- 600	61.56- 82.76	21.20	72.16	6.0 ± 2.4	0.29 ± 0.12	15	5.6 ± 1.4
600- 900	82.76-111.26	28.50	97.01	4.0 ± 2.0	0.14 ± 0.07	9	3.3 ± 1.1
900-1100	111.26-128.81	17.55	120.04	2.0 ± 1.4	0.11 ± 0.08	5	1.86 ± 0.83
1100-1400	128.81-170.00	41.19	149.41	3.0 ± 1.7	0.07 ± 0.04	3	1.12 ± 0.64
> 1400	> 170.00	-	-	-	-	-	-

Table 6.10a The measured pulse height distribution of pulses observed in the 265 μs period before the arrival of the shower front pulse after application of correction factor, f, and determination of their differential size distribution and their integral rate distribution.

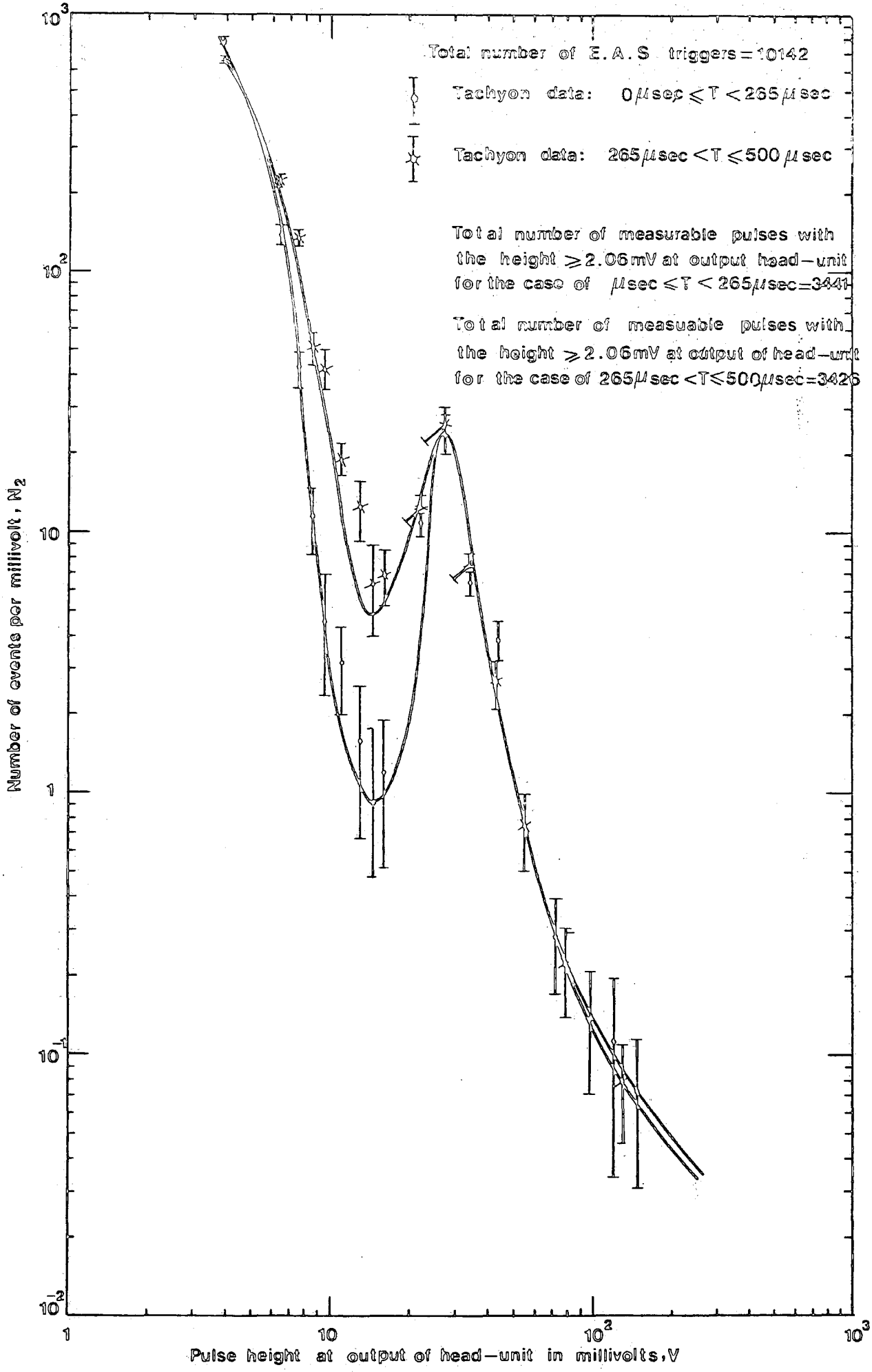

Figure 6.10a The comparison between the differential distributions of pulse occurring in the 265μs period before shower front and 235μs period after the arrival of the shower front pulse at the output of head-unit for a sample of 10142 shower triggers.

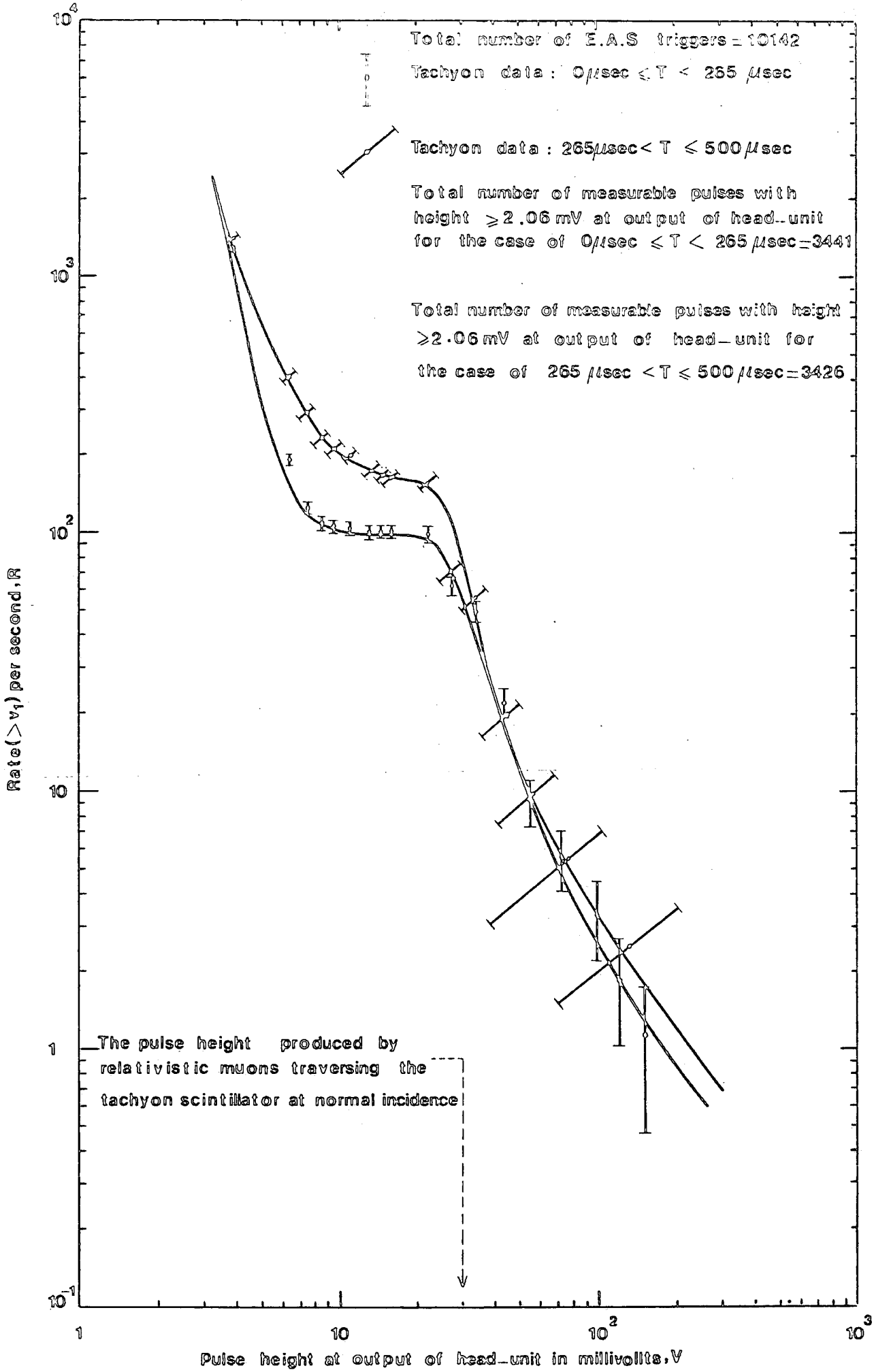

Figure 6.10b The comparison between the integral rate of pulses of size > V at the output of head-unit as a function of V determined from pulses observed in the 265μs period before the arrival of the shower front and in the 235μs period after the arrival of the shower front pulse for a sample of 10142 shower triggers.

Pulse heights range on oscilloscope in millivolts	Pulse heights range, $v_1 \rightarrow v_2$ at output of head-unit in millivolts	$\Delta v = v_2 - v_1$ in millivolts	mean $\bar{v} = \frac{v_2 + v_1}{2}$ in millivolts	No. of events with pulse height in range; $v_1 \rightarrow v_2$ $N_1(v_1, v_2)$	No. of events with pulse height in range, $\frac{N_1(v_1, v_2)}{\Delta v}$ i.e. differential frequency per millivolt, N_2	$N(>v_1)$	Integral rate $>v_1$ per second
0.5- 4	2.06- 5.75	3.69	3.91	3183 ± 56	863 ± 15	4320	1814 ± 28
4- 6	5.75- 7.02	1.27	6.39	363 ± 19	286 ± 15	1137	478 ± 14
6- 8	7.02- 8.08	1.06	7.55	183 ± 13	173 ± 13	774	325 ± 12
8- 10	8.08- 9.02	0.94	8.55	63.0 ± 7.9	67.3 ± 8.5	591	249 ± 10
10- 12	9.02- 9.87	0.85	9.45	46.0 ± 6.8	54.8 ± 8.0	528	222.0 ± 9.6
12- 20	9.87- 12.69	2.82	11.28	69.0 ± 8.3	24.7 ± 3.0	482	202.5 ± 9.2
20- 24	12.69- 13.89	1.20	13.29	15.0 ± 3.9	12.5 ± 3.2	413	173.3 ± 8.5
24- 28	13.89- 14.98	1.09	14.44	7.0 ± 2.6	6.4 ± 2.4	398	167.0 ± 8.4
28- 38	14.98- 17.42	2.44	16.20	17.0 ± 4.1	7.0 ± 1.7	391	164.0 ± 8.3
38- 90	17.42- 26.63	9.21	22.03	206 ± 14	22.4 ± 1.6	374	156.9 ± 8.1
90- 100	26.63- 28.05	1.42	27.34	37.0 ± 6.1	26.1 ± 4.3	168	70.5 ± 5.4
100- 200	28.05- 39.47	11.42	33.76	85.0 ± 9.2	7.44 ± 0.81	131	55.0 ± 4.8
200- 300	39.47- 48.19	8.72	43.83	23.0 ± 4.8	2.64 ± 0.55	46	19.3 ± 2.8
300- 400	48.19- 61.56	13.37	54.88	10.0 ± 3.2	0.75 ± 0.24	23	9.6 ± 2.0
400- 700	61.56- 92.61	31.65	77.09	7.0 ± 2.6	0.22 ± 0.08	13	5.4 ± 1.5
700-1400	92.61-170.00	77.39	131.31	6.0 ± 2.4	0.08 ± 0.03	6	2.5 ± 1.0
> 1400	> 170.00	-	-	-	-	-	-

Table 6.10b The measured pulse height distribution of pulses observed in the 235 μs period after the arrival of the shower front pulse after application of correction factor, f, and determination of their differential size distribution and their integral rate distribution.

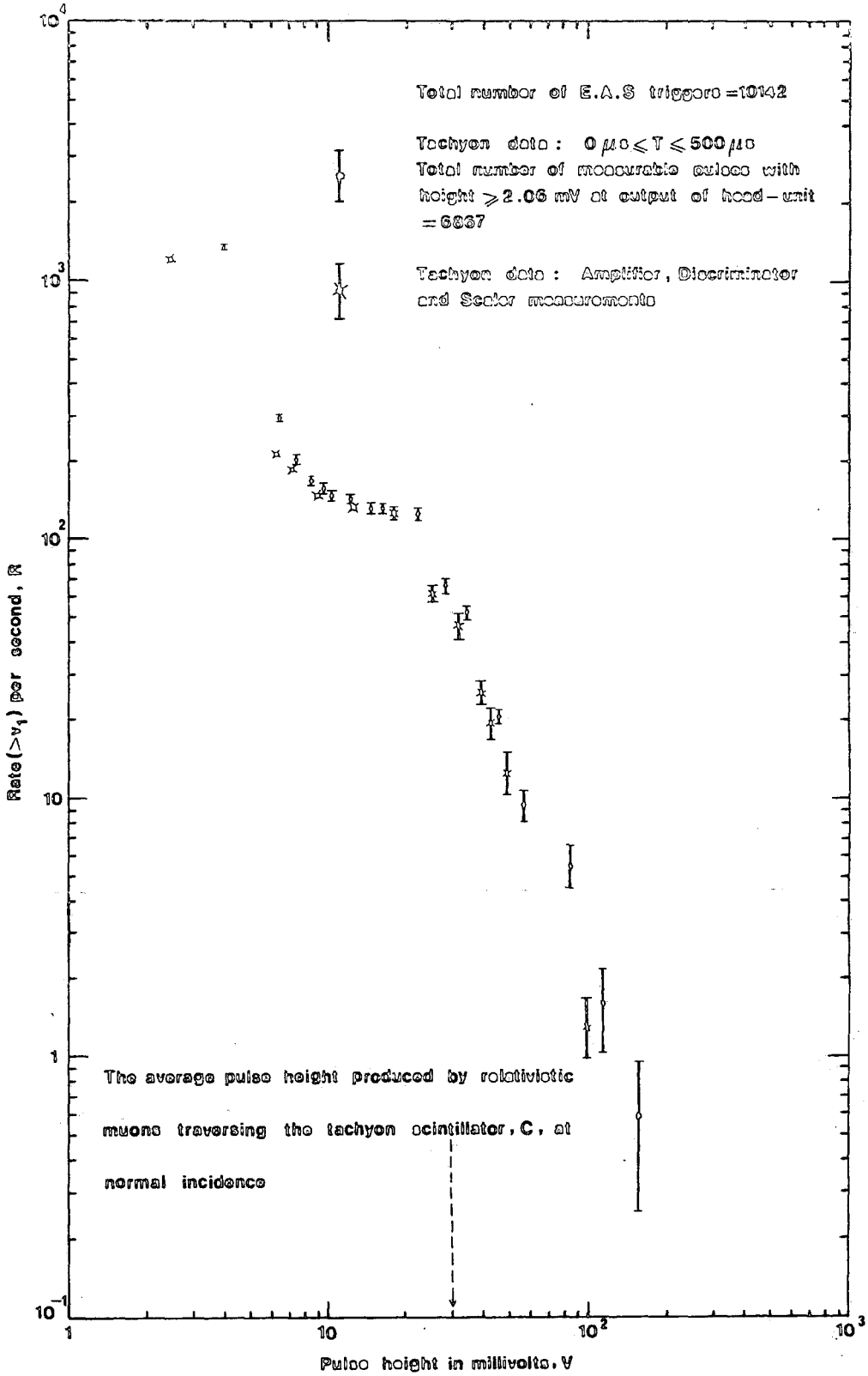

Figure 6.11 Response of the tachyon detector to the total cosmic ray flux. Integral rate of pulse of height > V millivolts (measured at the output of head-unit) versus pulse height, V. The average pulse height produced by relativistic muons traversing the detector at normal incidence is 30 mV and is indicated on the graph by arrow.

there is reasonable agreement between the two methods of obtaining the absolute integral pulse height distribution at the output of the head-unit.

6.7) EFFECT OF EXPERIMENTAL BIAS ON THE DISTRIBUTION IN HEIGHT OF PULSES OCCURRING IN THE 265 μS TIME DOMAIN BEFORE AND THE 235 μS AFTER THE ARRIVAL OF THE E.A.S SHOWER FRONT

Bias arises because large shower front pulses saturate the recording electronic instruments and time domains occur in which small pulses would not be recorded even if present. The calculated correction factor, f, which was shown in figure 6.6, was applied to pulse heights in the size range 0.5-2mv recorded before the shower front and to pulses in the size range 0.5 – 20mv after the occurrence of the shower front pulses. The effect of experimental bias on the distribution in height of pulses occurring in the 265 μs time domain before and the 235μs after the arrival of E.A.S shower front pulses was investigated and the result is presented in the table 6.9. By using the data in the table, the differential and integral pulse height distributions for the different time domains were calculated and the consequences are evaluated in the tables 6.10a , 6.10b and 6.10c as described previously. These results are separately ploted in figures 6.12a, 6.12b , 6.12c , 6.13a , 6.13b , 6.13c, 6.14a and 6.14b for the differential and integral rate of pulses respectively which refer to the two time domains (i.e; 265 μs before and 235 μs after the arrival of shower front pulses) and to the total time of sweep. All these figures are

Pulse height range, $v_1 \rightarrow v_2$, on oscilloscope in millivolts	Pulse height range at output of head-unit in millivolts	N(< 265μs) after correction factor	N(> 265μs) after correction factor	N(0 - 500μs) after correction factor
0.5- 2	2.06- 4.08	2195	1850	4045
2- 4	4.08- 5.75	943	1333	2276
4- 6	5.75- 7.02	175	363	538
6- 8	7.02- 8.08	45	183	228
8- 10	8.08- 9.02	11	63	74
10- 12	9.02- 9.87	4	46	50
12- 14	9.87- 10.65	3	29	32
14- 16	10.54- 11.37	3	14	17
16- 18	11.37- 12.05	1	16	17
18- 20	12.05- 12.69	0	10	10
20- 22	12.69- 13.30	0	9	9
22- 24	13.30- 13.89	3	6	9
24- 26	13.89- 14.45	1	5	6
26- 28	14.45- 14.98	0	2	2
28- 30	14.98- 15.50	3	17	20
30- 32	15.50- 16.00	0	0	0
32- 34	16.00- 16.49	0	0	0
34- 36	16.49- 16.96	0	0	0
36- 38	16.96- 17.42	0	0	0
38- 40	17.42- 17.86	15	65	80
40- 42	17.86- 18.30	0	0	0
42- 44	18.30- 18.72	0	0	0
44- 46	18.72- 19.13	0	0	0
46- 48	19.13- 19.54	0	0	0
48- 50	19.54- 19.94	3	24	27
50- 100	19.94- 28.05	115	154	269
100- 150	28.05- 34.25	39	49	88
150- 200	34.25- 39.47	35	36	71
200- 300	39.47- 48.19	34	23	57
300- 400	48.19- 61.56	10	10	20
400- 500	61.56- 72.45	4	2	6
500- 600	72.45- 82.76	2	2	4
600- 700	82.76- 92.61	3	3	6
700- 800	92.61-102.09	0	4	4
800- 900	102.09-111.26	1	1	2
900-1000	111.26-120.15	2	0	2
1000-1100	120.15-128.81	0	1	1
1100-1200	128.81-146.26	1	0	1
1200-1400	146.26-170.00	2	0	2
> 1400	> 170.00	0	0	0
		Σ=3653	Σ=4320	Σ=7973

Table 6.9 Tachyon data. Pulse height distribution obtained from a sample of 10142 extensive air shower triggers after application of correction factor, f. N(< 265μs) is the number of events observed in the first 265 μs of the oscilloscope sweep of 500 μs and N(> 265μs) is the number of events observed in the final 235 μs.

N(0-500 μs) = N(< 265 μs) + N(> 265 μs).

Pulse heights range on oscilloscope in millivolts	Pulse heights range, $v_1 \rightarrow v_2$, at output of head-unit in millivolts	$\Delta v = v_2 - v_1$ in millivolts	mean $\bar{v} = \frac{v_2 + v_1}{2}$ in millivolts	No. of events with pulse height in range: $v_1 \rightarrow v_2$ $N_1(v_1, v_2)$	No. of events with pulse height in range, $\frac{N_1(v_1, v_2)}{\Delta v}$ i.e. differential frequency per millivolt, N_2	$N(>v_1)$	Integral rate $>v_1$ per second
0.5- 4	2.06- 5.75	3.69	3.91	6321 ± 79	1713 ± 21	7973	1573 ± 18
4- 6	5.75- 7.02	1.27	6.39	538 ± 23	424 ± 18	1652	326.2 ± 8.0
6- 8	7.02- 8.08	1.06	7.55	228 ± 15	215 ± 14	1114	220.0 ± 6.6
8- 10	8.08- 9.02	0.94	8.55	74.0 ± 8.6	79.0 ± 9.2	886	175.0 ± 5.9
10- 12	9.02- 9.87	0.85	9.45	50.0 ± 7.1	59.5 ± 8.4	812	160.4 ± 5.6
12- 14	9.87- 10.65	0.78	10.26	32.0 ± 5.7	41.5 ± 7.3	762.64	150.4 ± 5.4
14- 24	10.65- 13.89	3.24	12.27	62.0 ± 7.9	19.2 ± 2.4	730.23	144.0 ± 5.3
24- 28	13.89- 14.98	1.09	14.44	8.0 ± 2.8	7.3 ± 2.6	668	131.7 ± 5.1
28- 38	14.98- 17.42	2.44	16.20	20.0 ± 4.5	8.2 ± 1.8	660	130.1 ± 5.1
38- 90	17.42- 26.63	9.21	22.03	305 ± 17	33.1 ± 1.9	640	126.2 ± 5.0
90- 100	26.63- 28.05	1.42	27.34	71.0 ± 8.4	50.0 ± 5.9	335	66.1 ± 3.6
100- 200	28.05- 39.47	11.42	33.76	159 ± 13	13.9 ± 1.1	264	52.1 ± 3.2
200- 300	39.47- 48.19	8.72	43.83	57.0 ± 7.5	6.54 ± 0.87	105	20.7 ± 2.0
300- 400	48.19- 61.56	13.37	54.88	20.0 ± 4.5	1.50 ± 0.33	48	9.5 ± 1.4
400- 800	61.56-102-09	40.53	81.83	20.0 ± 4.5	0.49 ± 0.11	28	5.5 ± 1.0
800-1000	102.09-120.15	18.06	111.12	4.0 ± 2.0	0.22 ± 0.11	8	1.58 ± 0.56
1000-1100	120.15-128.81	8.66	124.48	1.0 ± 1.0	0.11 ± 0.11	4	0.79 ± 0.39
1100-1400	128.81-170.00	41.19	149.41	3.0 ± 1.7	0.07 ± 0.04	3	0.59 ± 0.34
> 1400	> 170.00	-	-	-	-	-	

Table 6.10c The measured pulse height distribution of pulses observed in the 265 μs period before and the 235 μs period after the arrival of the shower front pulse after application of correction factor, f, and determination of their differential size distribution and their integral rate distribution.

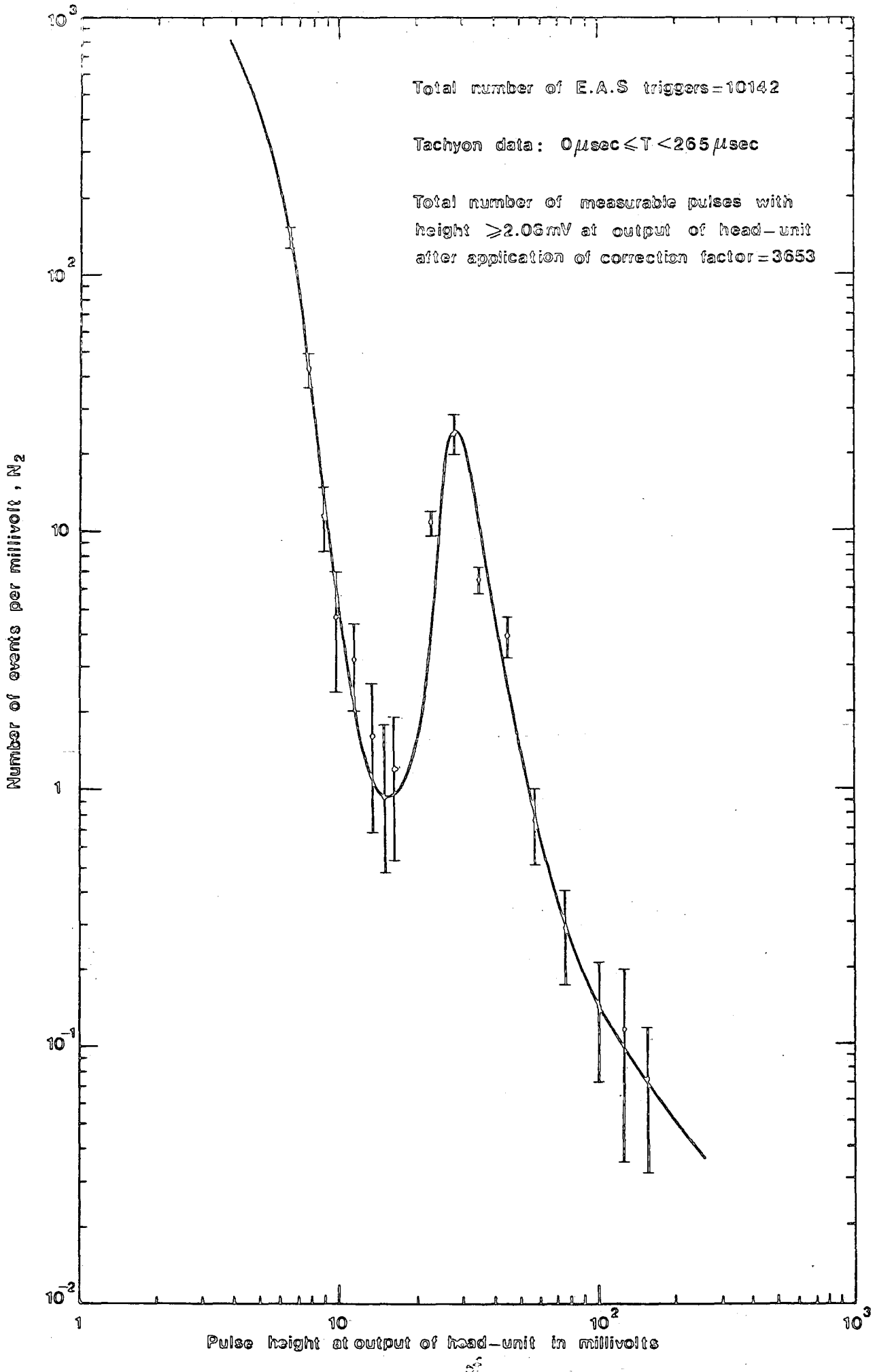

Figure 6.12a The differential distribution/pulse height occurring in the 265μs period before the arrival of the shower front pulse after application of correction factor, f, at the output of head-unit for the sample of 10142 shower triggers.

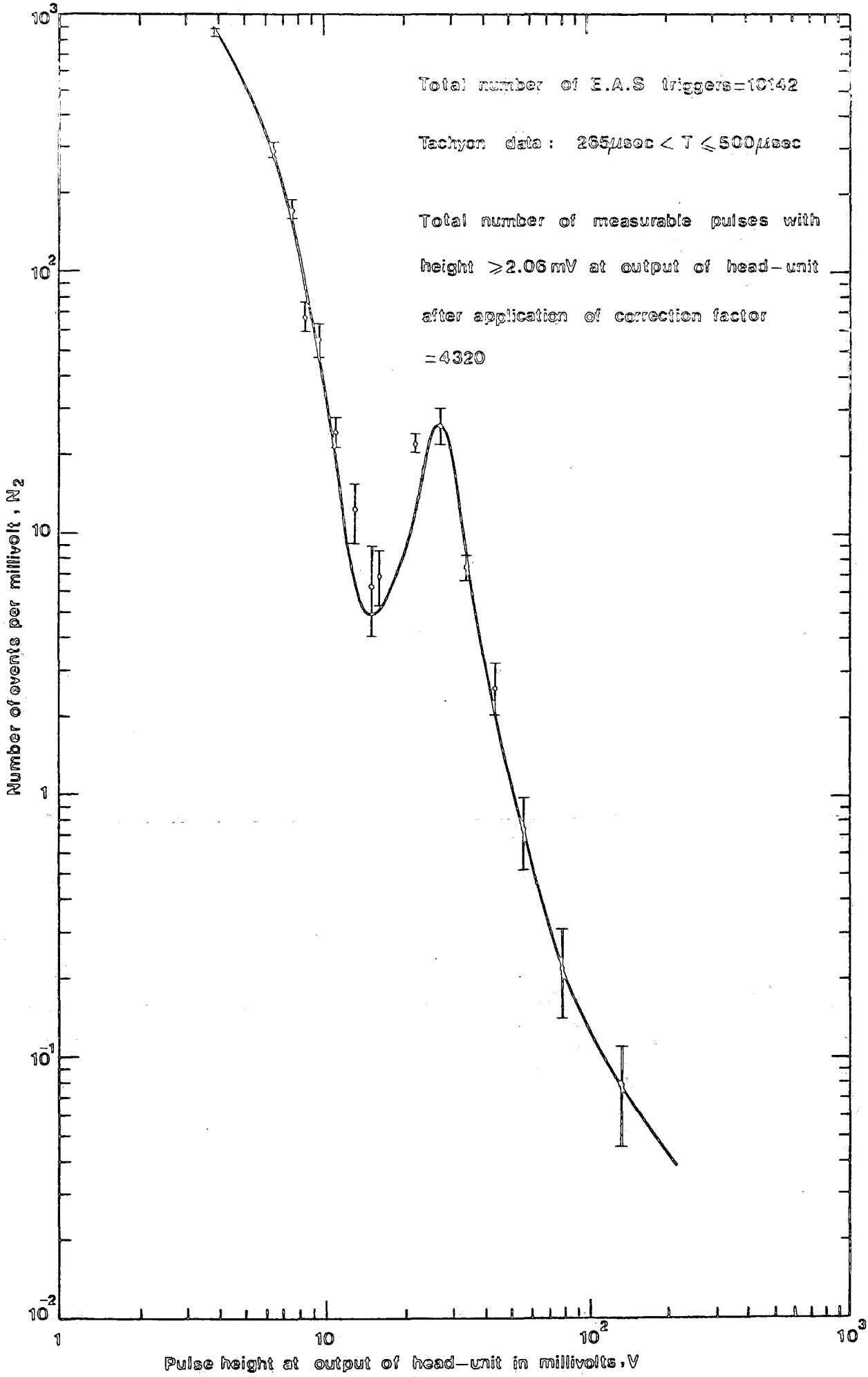

Figure 6.12b The differential distribution of pulse height occurring in the 235μs period after the arrival of the shower front pulse after application of correction factor, f, at the output of head-unit for the sample of 10142 shower triggers.

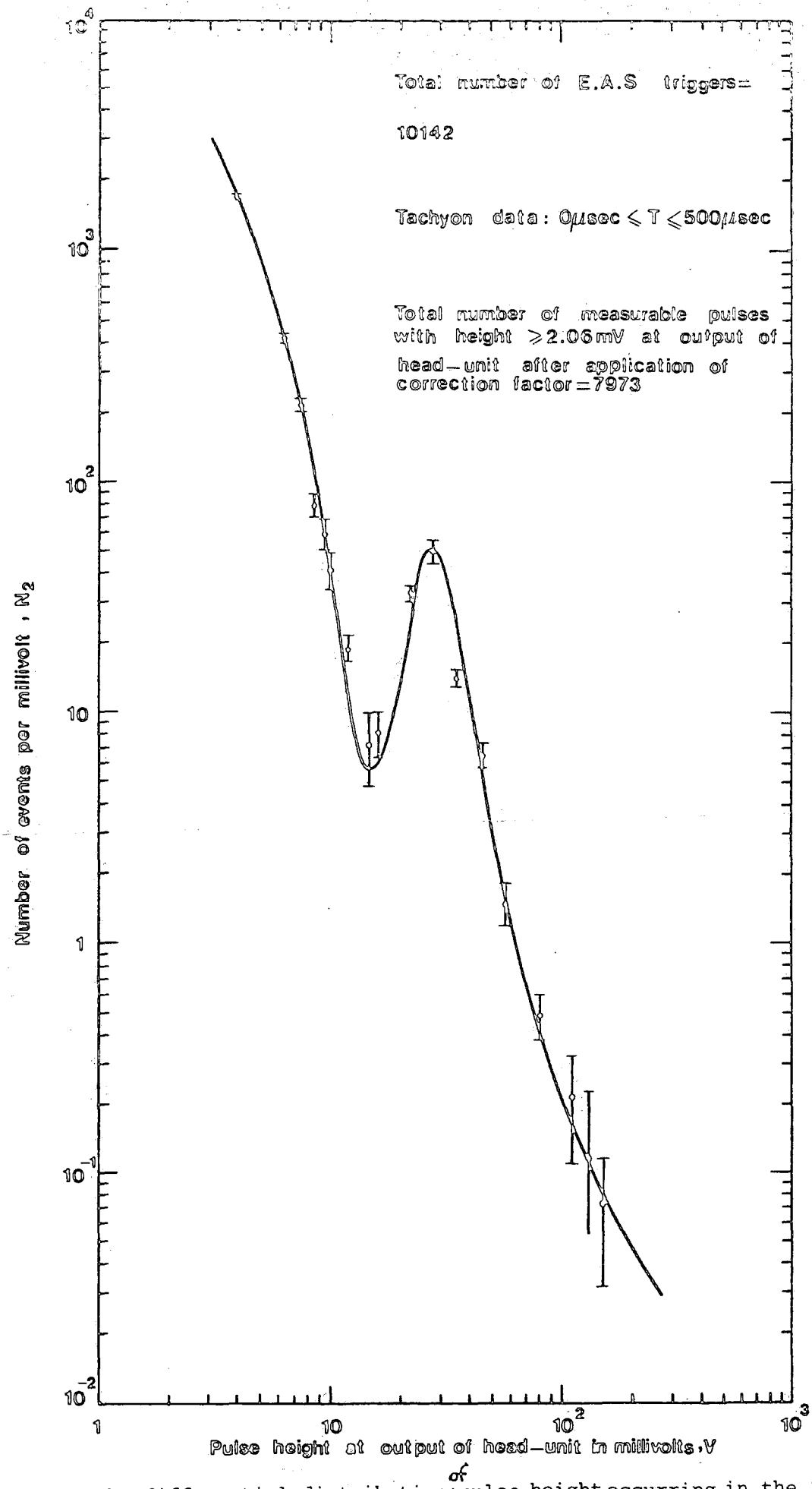

Figure 6.12c The differential distribution of pulse height occurring in the 265μs period before shower front and the 235μs period after the arrival of the shower front pulse after application of correction factor, f, at the output of head-unit for a sample of 10142 shower triggers.

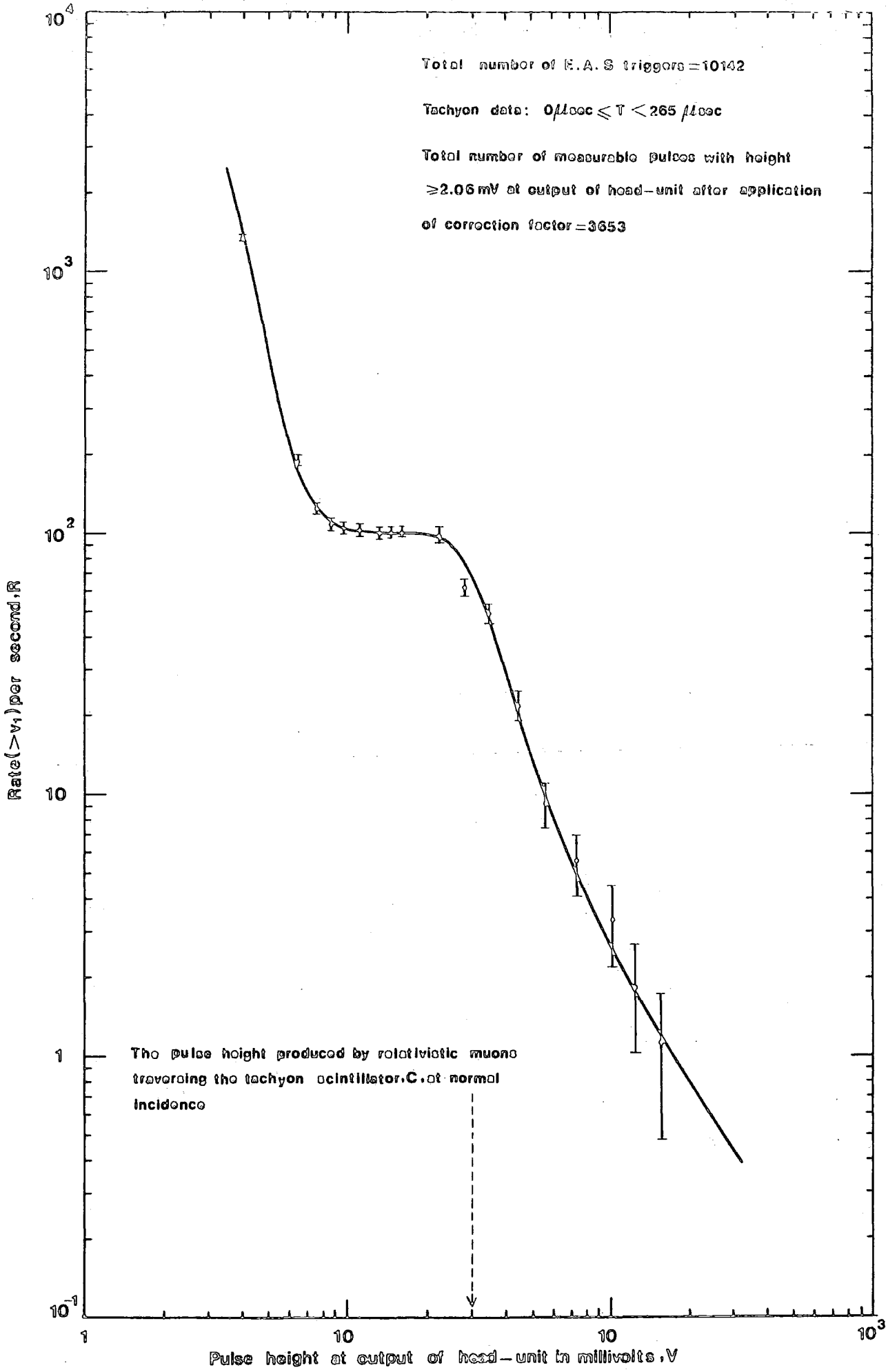

Figure 6.13a The integral rate of pulses of size > V at the output of head-unit as a function of V determined from pulses observed in the 265μs period before the arrival of the shower front pulse after application of correction factor, f, for a sample of 10142 shower triggers.

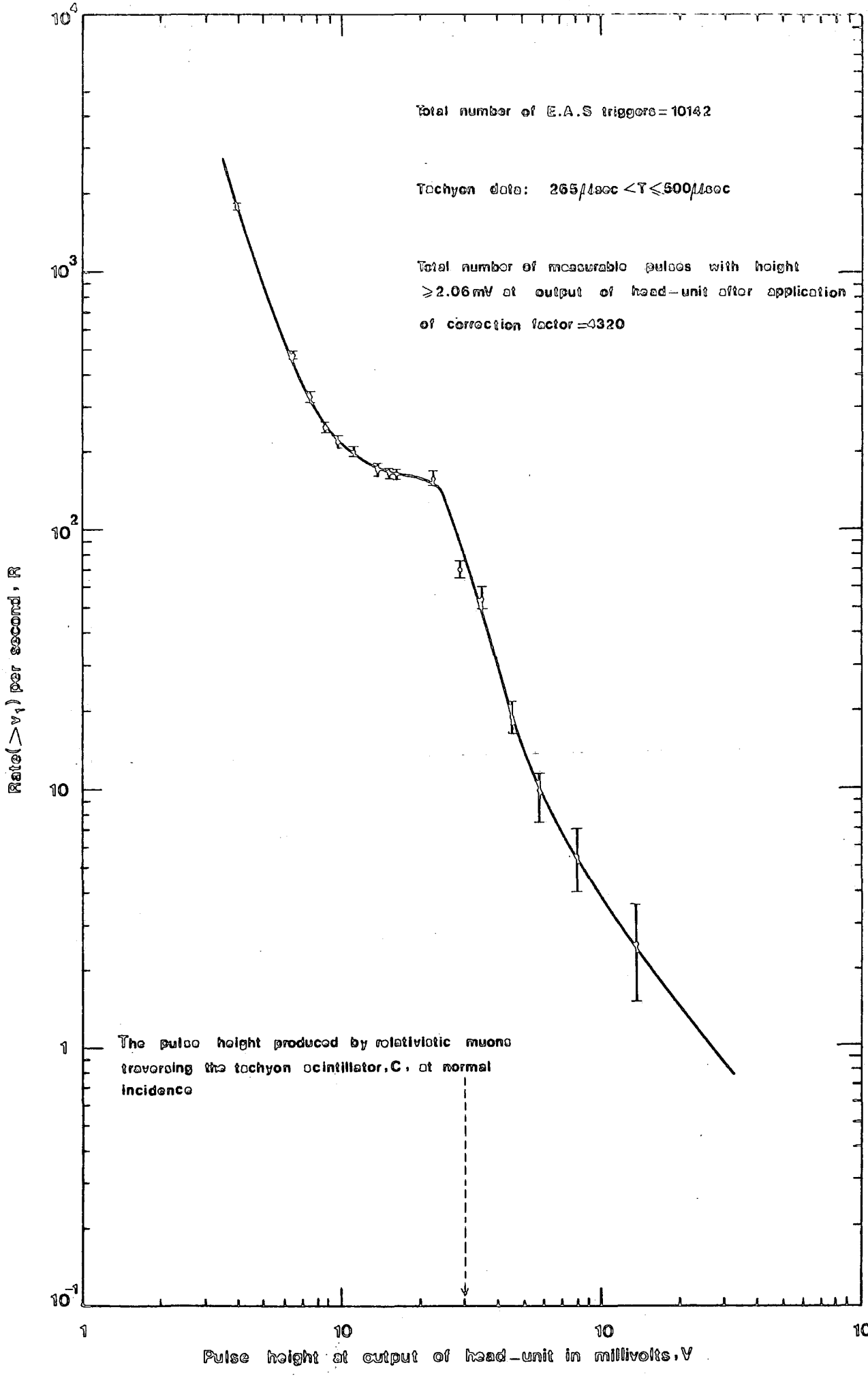

Figure 6.13b The integral rate of pulses of size > V at the output of head-unit as a function of V determined from pulses observed in the 235μs period after the arrival of the shower front pulse after application of correction factor, f, for a sample of 10142 shower triggers.

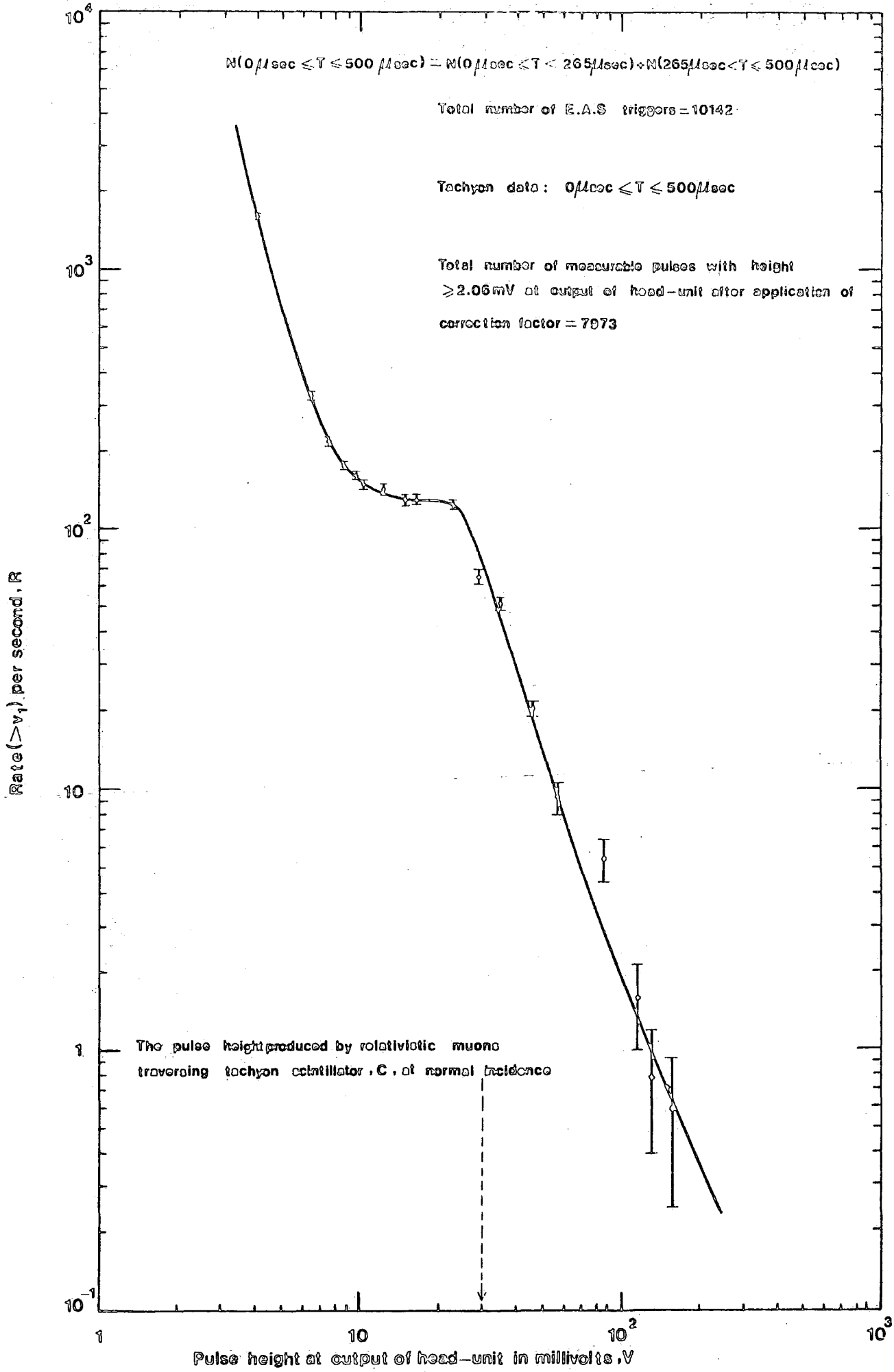

Figure 6.13c The integral rate of pulses of size > V at the output of the head-unit as a function of V determined from pulses observed in the 265μs period before the arrival of shower front and the 235μs period after the arrival of shower front pulse after application of correction factor, f, for a sample of 10142 shower triggers.

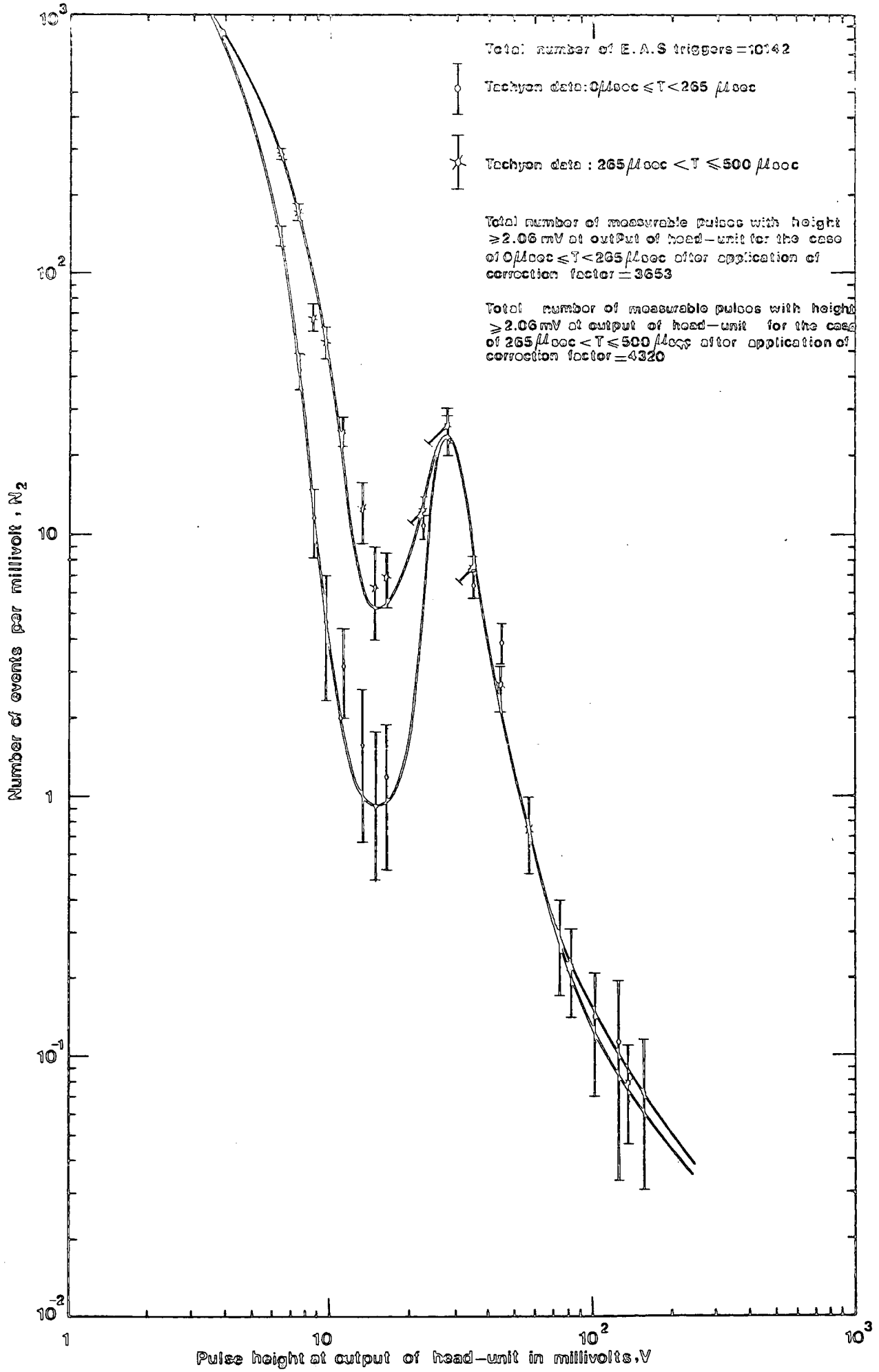

Figure 6.14a The comparison between the differential distributions of pulse occurring in the 265μs period before shower front and the 235μs period after the arrival of the shower front pulse after application of correction factor, f, at the output of head-unit for a sample of 10142 shower triggers.

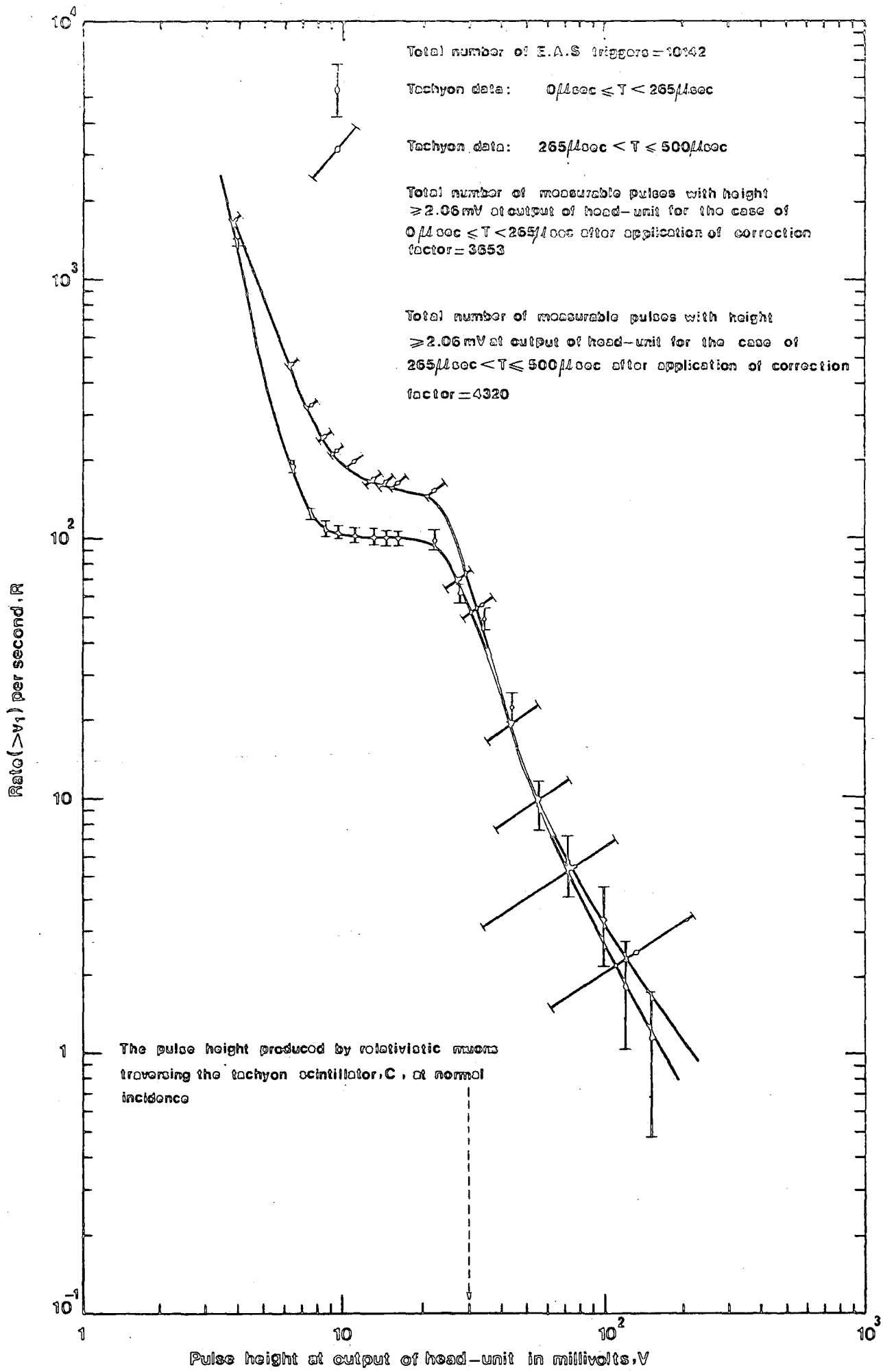

Figure 6.14b The comparison between the integral rate of pulses of size > V at the output of head-unit as a function of V determined from pulses observed in the 265μs period before the arrival of the shower front and in the 235μs period after the arrival of the shower front pulse after application of correction factor, f, for a sample of 10142 shower triggers.

only slightly different from the corresponding figures where no effect of experimental bias was applied.

6.8) RANDOM TRIGGER DATA

This work was done to establish the true background and the data has been analysed in exactly the same way as for the extensive air shower trigger data. The time distribution (time measured from the start of the oscilloscope time base) of pulses occurring in six different ranges of pulse height measured on the oscilloscope are shown in table 6.11 and figure 6.15. Figure 6.15 also shows the corresponding range of energy deposition in the tachyon scintillator of thickness 5cm in terms of 'e' where 'e' is the energy loss (10MeV) produced by a relativistic muon traversing the scintillator at normal incidence. In the analysis the "DATABIN" program was used twice with the following requirements:

Maximum time = 530 μs	Maximum time = 530 μs
Number of time bins = 2	Number of time bins = 2
Maximum pulse height = 31.5 mV	Maximum pulse height = 1455 mV
Number of pulse height bins = 15	Number of pulse height bins = 29

Table 6.12 shows the distribution in pulse height of the observed background pulses over the whole 500 μs time range of the oscilloscope sweep, and also the distribution in the first 265 μs and the final 235 μs. The latter distributions were measured so as to give a direct comparison with those of the tachyon data. By using the data in the present table, the differential and integral pulse height distributions for the

Time range on oscilloscope in μs	NUMBER OF PULSES					
	0.5mv≤v≤2mv	2mv<v≤4mv	4mv<v≤30mv	30mv<v≤120mv	v>120mv	v≥700mv
0- 10	2	7	1	0	0	0
10- 20	5	2	3	1	0	0
20- 30	4	3	0	1	2	0
30- 40	9	9	3	0	1	0
40- 50	3	5	2	2	0	0
50- 60	0	7	1	1	2	0
60- 70	5	4	2	4	0	0
70- 80	3	10	3	0	4	0
80- 90	15	7	2	0	0	0
90-100	3	5	1	1	0	0
100-110	6	12	1	1	0	0
110-120	9	6	0	1	1	0
120-130	8	5	1	0	1	0
130-140	13	9	0	1	0	0
140-150	3	5	2	2	1	0
150-160	6	4	4	1	1	0
160-170	6	4	2	2	0	0
170-180	8	9	0	2	1	0
180-190	3	9	2	1	1	0
190-200	9	7	0	1	0	0
200-210	7	5	2	0	2	0
210-220	7	5	1	1	1	1
220-230	7	8	3	1	3	0
230-240	6	2	2	0	1	0
240-250	8	6	0	1	1	0
250-260	10	8	2	0	3	0
260-270	11	8	1	0	0	0
270-280	6	3	1	0	0	0
280-290	6	4	2	1	0	0
290-300	7	6	0	2	0	0
300-310	2	7	1	1	0	0
310-320	12	7	1	0	0	0
320-330	6	5	1	1	0	0
330-340	9	6	2	2	0	0
340-350	9	8	1	2	0	0
350-360	6	14	2	3	0	0
360-370	7	7	4	1	2	0
370-380	5	6	2	0	1	0
380-390	10	3	2	0	0	0
390-400	4	6	3	0	1	0
400-410	14	9	0	0	2	0
410-420	5	10	2	3	0	0
420-430	6	9	2	0	0	0
430-440	2	5	0	0	1	0
440-450	3	4	1	1	1	0
450-460	4	7	1	2	2	0
460-470	4	6	0	1	0	0
470-480	6	5	2	2	0	0
480-490	6	5	2	0	0	0
490-500	3	4	0	1	1	0
	Σ= 318	Σ= 317	Σ= 73	Σ= 48	Σ= 37	Σ= 1

Table 6.11 Random trigger data. Time distribution of events in different ranges of pulse height (measured on the oscilloscope) from a sample of 508 random triggers.

Pulse heights range on oscilloscope in millivolts	Pulse height range, $v_1 \rightarrow v_2$, at output of head-unit in millivolts	$\Delta v = v_2 - v_1$ in millivolts	mean $\bar{v} = \frac{v_2+v_1}{2}$ in millivolts	No.of events with pulse height in range; $v_1 \rightarrow v_2$ $N_1(v_1, v_2)$	No.of events with pulse height in range $\frac{N_1(v_1,v_2)}{\Delta v}$ i.e. differential frequency per millivolt, N_2	$N(>v_1)$	Integral Rate $>v_1$ per sec.
0.5- 4	2.06- 5.75	3.69	3.91	635 ± 25	172.1 ± 6.8	792	3118 ± 111
4- 6	5.75- 7.02	1.27	6.39	51 ± 7.1	40.2 ± 5.6	157	618 ± 49
6- 8	7.02- 8.08	1.06	7.55	10 ± 3.2	9.4 ± 3.0	106	417 ± 40
8- 10	8.08- 9.02	0.94	8.55	3 ± 1.7	3.2 ± 1.8	96	378 ± 39
10- 12	9.02- 9.87	0.85	9.45	2 ± 1.4	2.3 ± 1.7	93	366 ± 38
12- 20	9.87- 12.69	2.82	11.28	4 ± 2.0	1.42 ± 0.71	91	358 ± 38
20- 28	12.69- 14.98	2.29	13.84	2 ± 1.4	0.87 ± 0.62	87	342 ± 37
28- 38	14.98- 17.42	2.44	16.20	1 ± 1.0	0.41 ± 0.41	85	335 ± 36
38- 90	17.42- 26.63	9.21	22.03	30 ± 5.5	3.26 ± 0.60	84	331 ± 36
90- 100	26.63- 28.05	1.42	27.34	8 ± 2.8	5.6 ± 2.0	54	213 ± 29
100- 150	28.05- 34.25	6.20	31.15	18 ± 4.2	2.90 ± 0.68	46	181 ± 27
150- 200	34.25- 39.47	5.22	36.86	11 ± 3.3	2.11 ± 0.63	28	110 ± 21
200- 300	39.47- 48.19	8.72	43.83	8 ± 2.8	0.92 ± 0.32	17	67 ± 16
300- 400	48.19- 61.56	13.37	54.88	4 ± 2.0	0.30 ± 0.15	9	35 ± 12
400-1000	61.56-120.15	58.59	90.86	4 ± 2.0	0.07 ± 0.03	5	19.7 ± 8.8
1000-1400	120.15-170.00	49.85	145.08	1 ± 1.0	0.02 ± 0.02	1	3.9 ± 3.9
> 1400	> 170.00	-	-	-	-	-	-

Table 6.13 Random trigger data. Basic data obtained from a sample of 508 random triggers of the measuring oscilloscope time base of length 500 μs and calculation of the differential and integral spectra of the measured pulse heights.

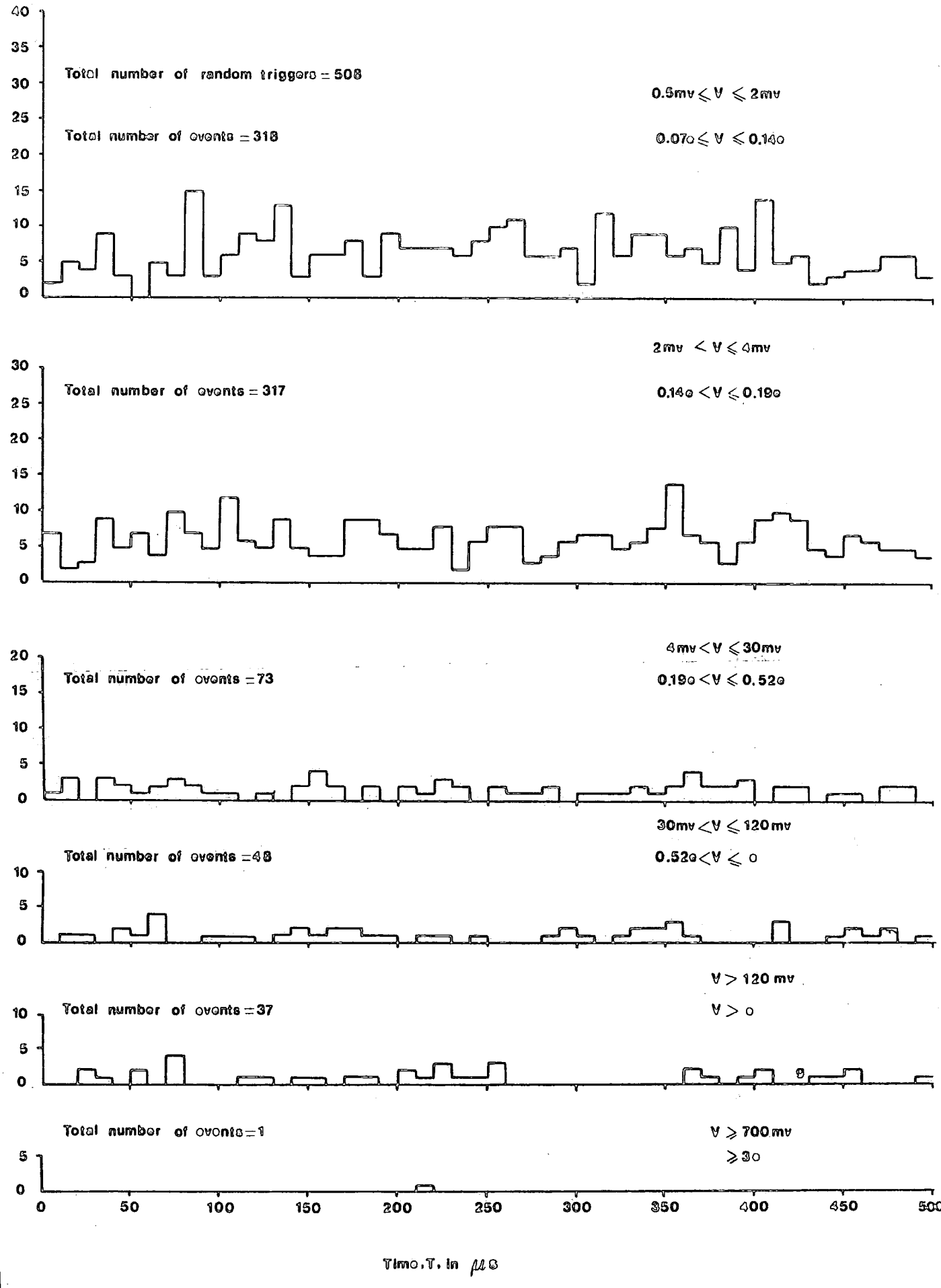

Figure 6.15 Time distribution of pulse heights between two limits of threshold energy loss in the tachyon detection scintillator C for 508 random triggers of oscilloscope time base.

Pulse height range $v_1 \rightarrow v_2$ on oscilloscope in millivolts	Pulse height range at output of head-unit in millivolts	N(< 265μs)	N(> 265μs)	N(0 - 500μs)
0.5- 2	2.06- 4.08	176	142	318
2- 4	4.08- 5.75	171	146	317
4- 6	5.75- 7.02	27	24	51
6- 8	7.02- 8.08	7	3	10
8- 10	8.08- 9.02	2	1	3
10- 12	9.02- 9.87	1	1	2
12- 14	9.87- 10.65	1	0	1
14- 16	10.54- 11.37	0	0	0
16- 18	11.37- 12.05	1	0	1
18- 20	12.05- 12.69	1	1	2
20- 22	12.69- 13.30	0	0	0
22- 24	13.30- 13.89	1	1	2
24- 26	13.89- 14.45	0	0	0
26- 28	14.45- 14.98	0	0	0
28- 30	14.98- 15.50	0	1	1
30- 32	15.50- 16.00	0	0	0
32- 34	16.00- 16.49	0	0	0
34- 36	16.49- 16.96	0	0	0
36- 38	16.96- 17.42	0	0	0
38- 40	17.42- 17.86	1	1	2
40- 42	17.86- 18.30	0	0	0
42- 44	18.30- 18.72	0	0	0
44- 46	18.72- 19.13	0	0	0
46- 48	19.13- 19.54	0	0	0
48- 50	19.54- 19.94	2	3	5
50- 100	19.94- 28.05	17	14	31
100- 150	28.05- 34.25	11	7	18
150- 200	34.25- 39.47	8	3	11
200- 300	39.47- 48.19	4	4	8
300- 400	48.19- 61.56	2	2	4
400- 500	61.56- 72.45	3	0	3
500- 600	72.45- 82.76	1	0	1
600- 700	82.76- 92.61	1	0	0
700- 800	92.61-102.09	0	0	0
800- 900	102.09-111.26	0	0	0
900-1000	111.26-120.15	0	0	0
1000-1100	120.15-128.81	1	0	1
1100-1200	128.81-146.26	0	0	0
1200-1400	146.26-170.00	0	0	0
> 1400	> 170.00	0	0	0
		Σ=439	Σ=354	Σ=792

Table 6.12 Random trigger data. Pulse height distribution obtained from a sample of 508 random triggers. N(< 265μs) is the number of events observed in the first 265 μs of the oscilloscope sweep of 500 μs and N(> 265μs) is the number observed in the final 235 μs.

N(0-500 μs) = N(< 265μs) + N(> 265μs).

whole 500μs time range of the oscilloscope sweep was calculated and the result is shown in table 6.13 and corresponding graphs are shown in figures 6.16a and 6.16b respectively. Figure 6.17 shows the comparison between the differential pulse height distribution at the output of the head – unit which was measured from the photographs of 508 random triggers with that obtained by differentiating the integral rate distribution determined using an amplifier , discriminator and scaler. It shows a well resolved peak produced by the passage of single relativistic patricles through the scintillator and the peak occurs at a pulse height of 30mv measured at the output of the head – unit which agrees with the value found from the analysis of the tachyon data film for pulses occurring in the time range before and after the shower front pulse. Figures 6.18a , 6.18b and 6.18c give the integral pulse height distributions, which are relevant in comparing the tachyon data and random trigger data. The differences between the two sets of data are believed to be due to:

a) Sampling fluctuations.
b) Meteorological changes which affect the low energy cosmic radiation flux at sea level.
c) They are integral plots so all the points are not statistically independent.

Figures 6.19a, 6.19b and 6.19c give the integral pulse height distributions obtained from the tachyon data after application of the correction factor for experimental bias to compare with the random triggering data.

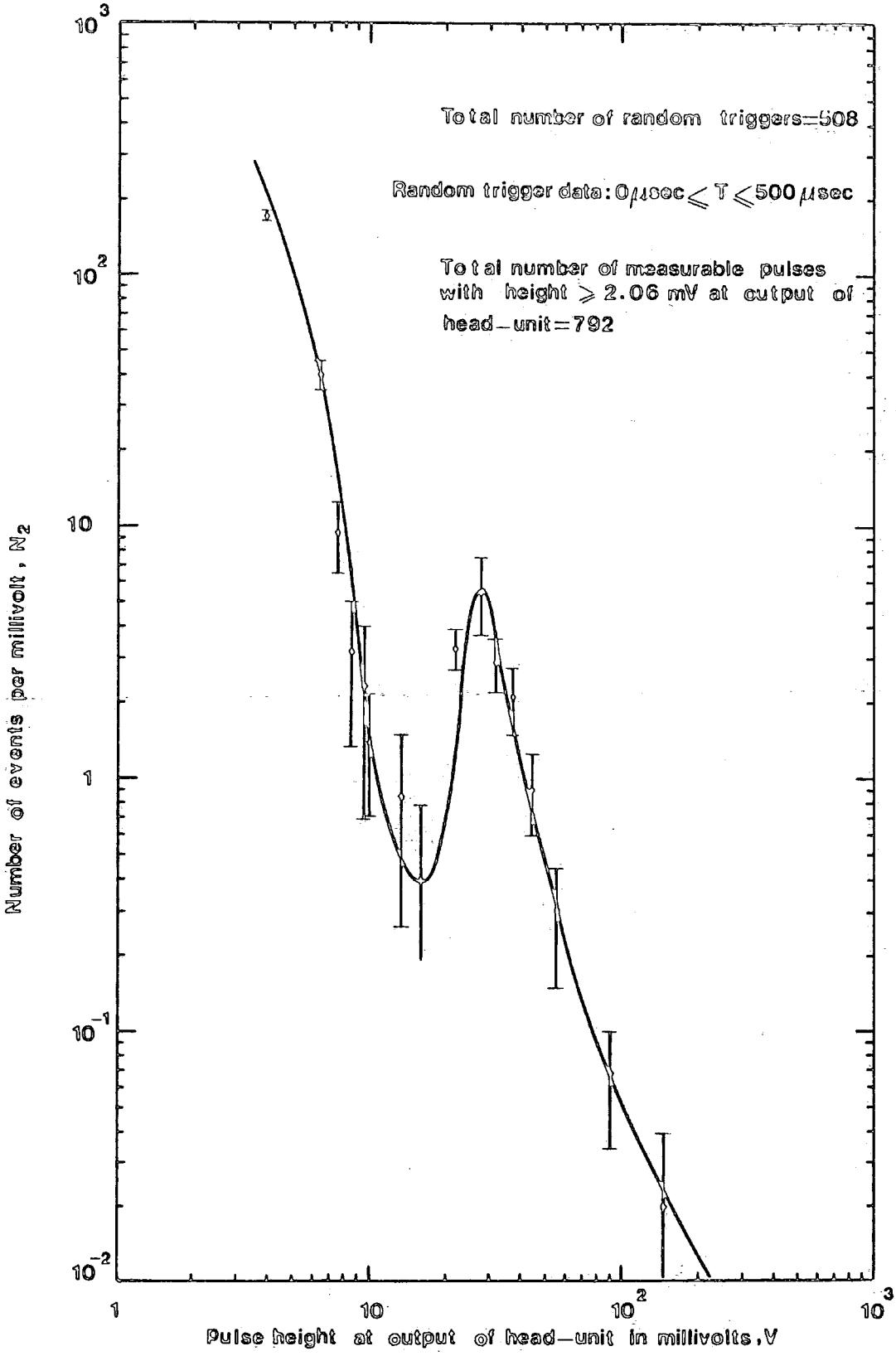

Figure 6.16a The differential distribution of background pulses determined from a sample of 508 random triggers of the oscilloscope time base.

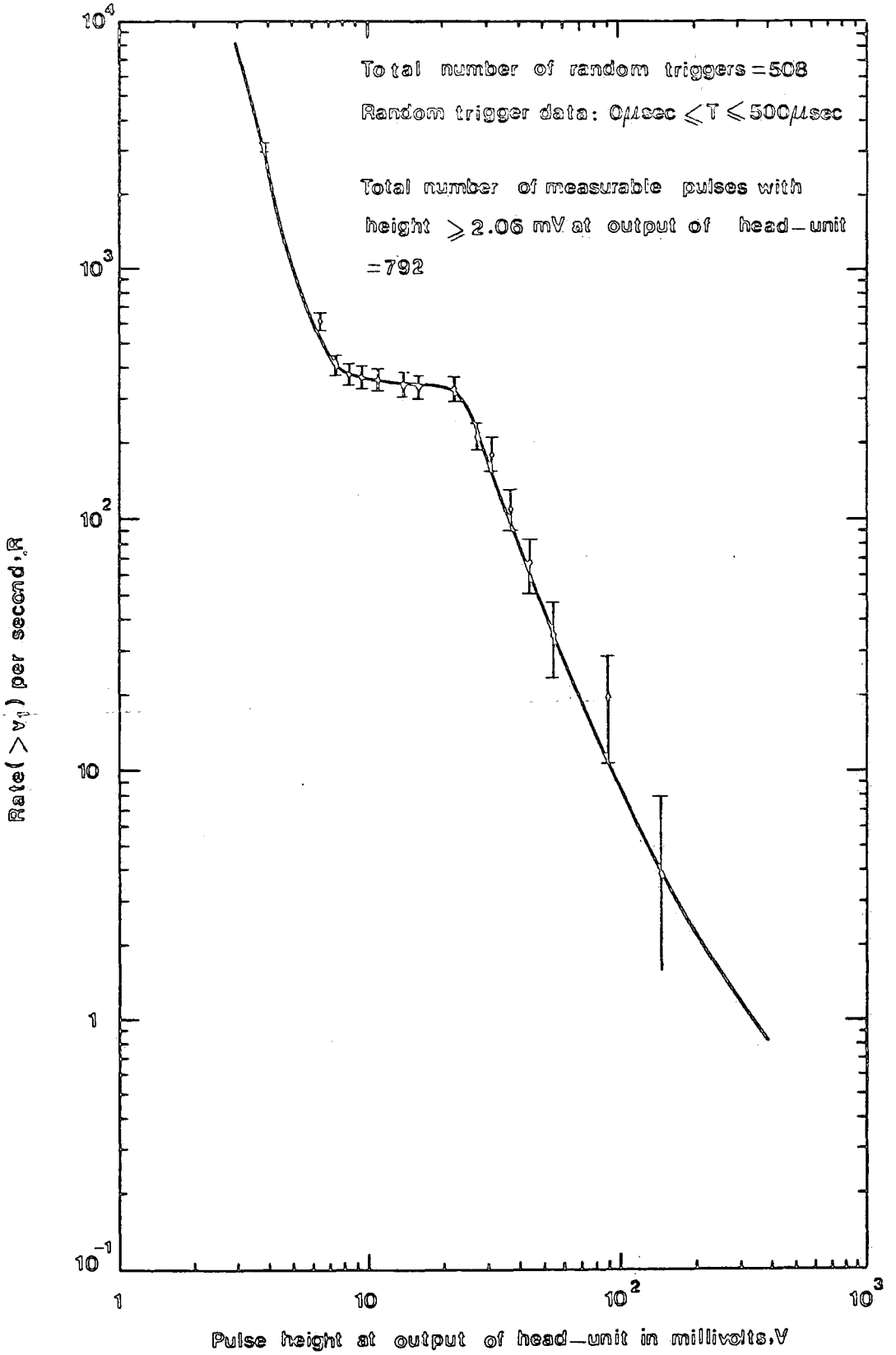

Figure 6.16b The integral rate of background pulses determined from a sample of 508 random triggers of the oscilloscope time base.

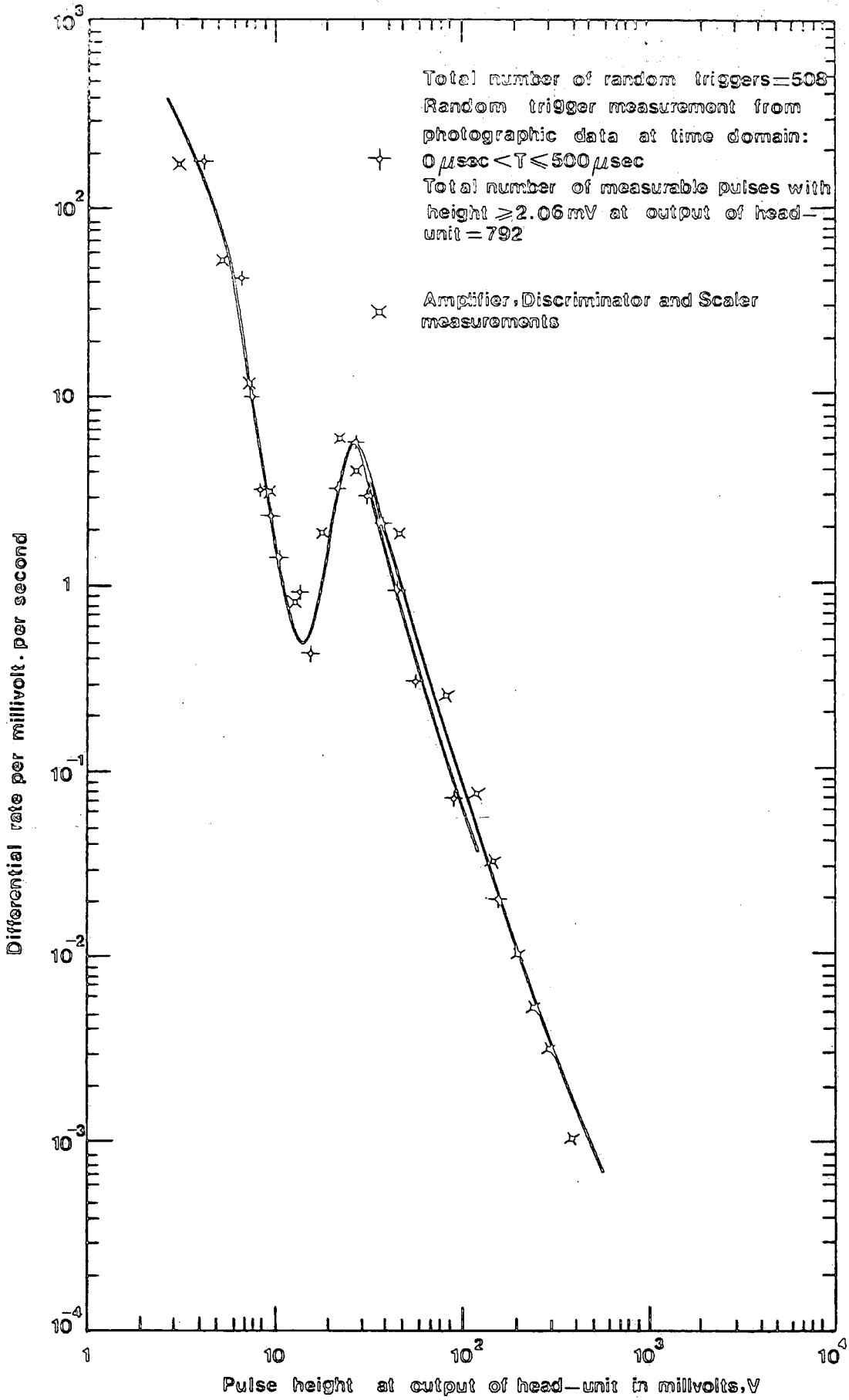

Figure 6.17 Comparison of the differential pulse height distribution at the output of the head-unit as determined from:

(a) measurements on the photographs of 508 random triggers, ✦

(b) By differentiating the integral rate distribution determined using an amplifier, discriminator and scaler, ✕

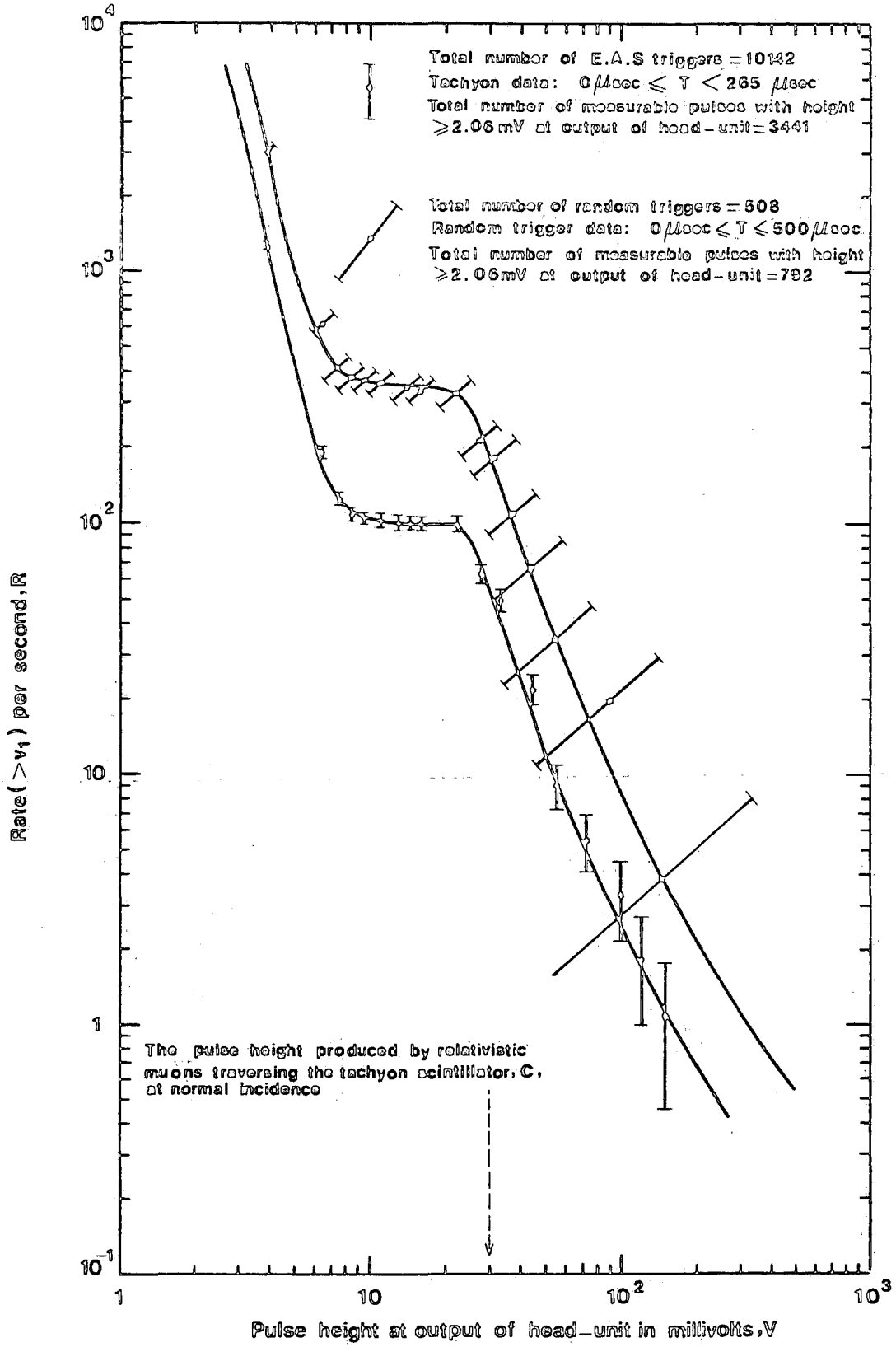

Figure 6.18a The integral rate of pulses occurring in the 265μs period before the arrival of the shower front pulse in the tachyon experiment and comparison with the integral rate of background pulses determined from a sample of 508 random triggers of the oscilloscope time base.

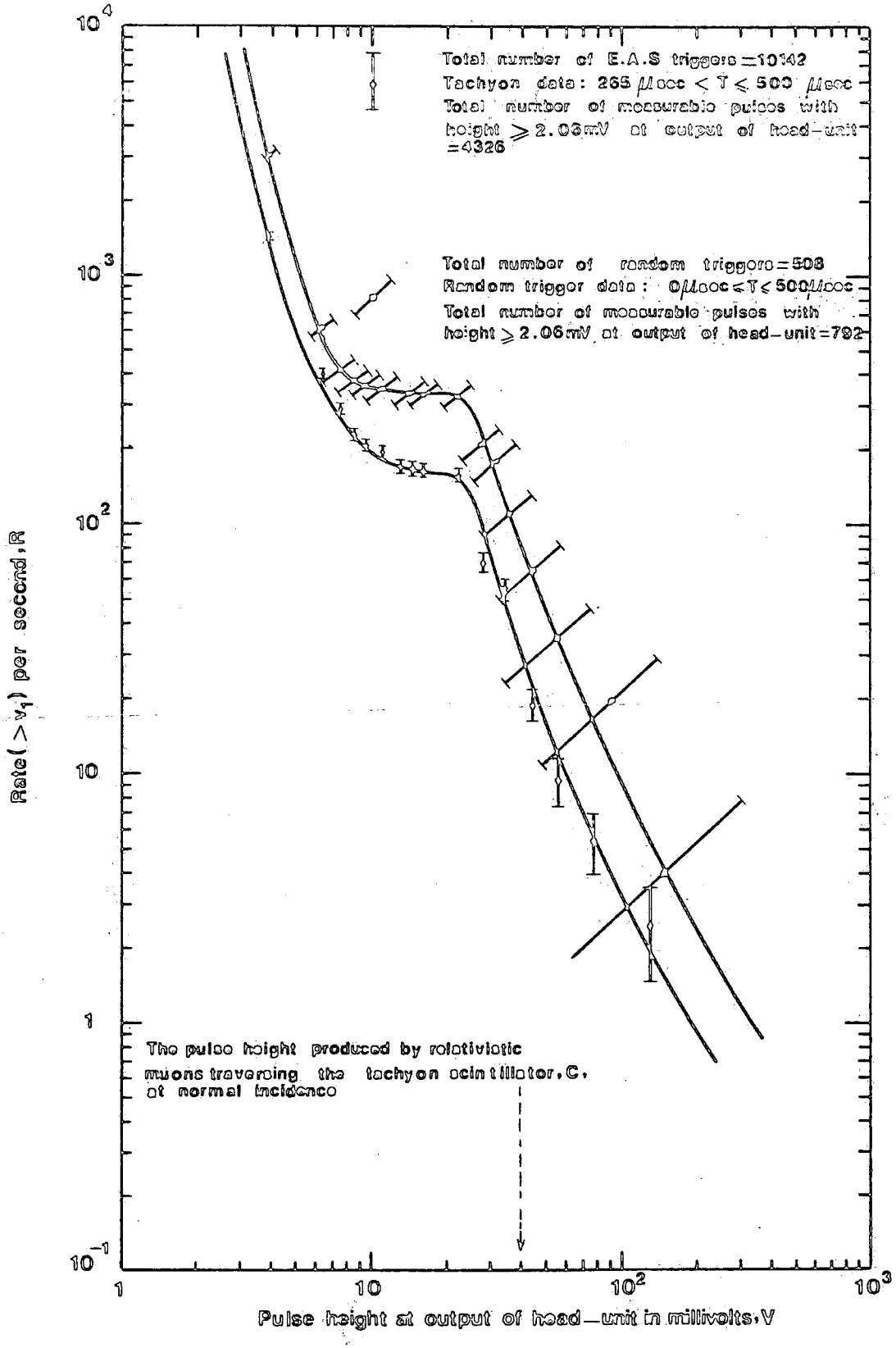

Figure 6.18b The integral rate of pulses occurring in the 235μs period after the arrival of the shower front pulse in the tachyon experiment and comparison with the integral rate of background pulses determined from a sample of 508 random triggers of the oscilloscope time base.

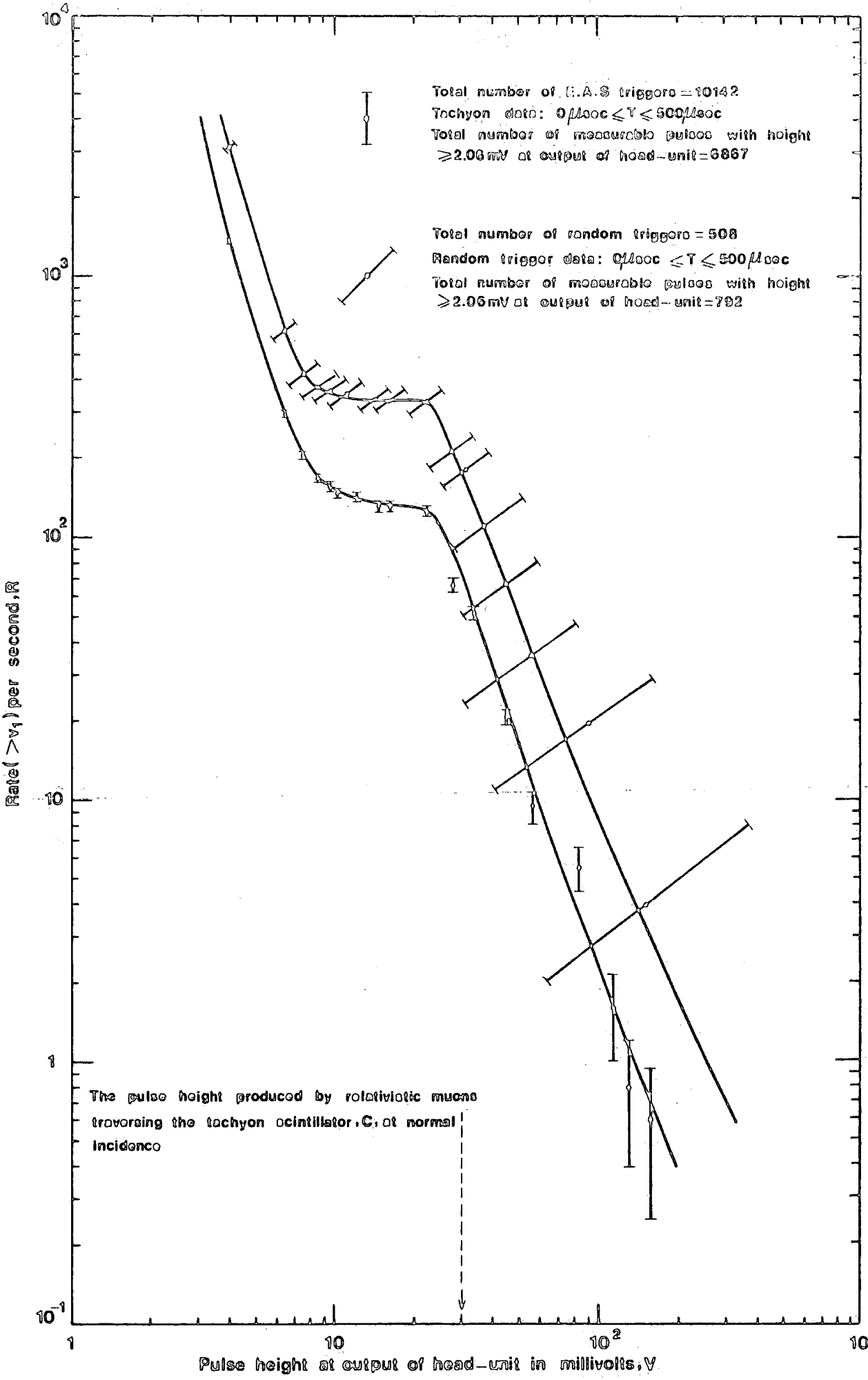

Figure 6.18c The integral rate of pulses occurring in the 265μs period before and the 235μs period after the arrival of the shower front pulse and comparison with the integral rate of background pulses determined from a sample of 508 random triggers of the oscilloscope time base.

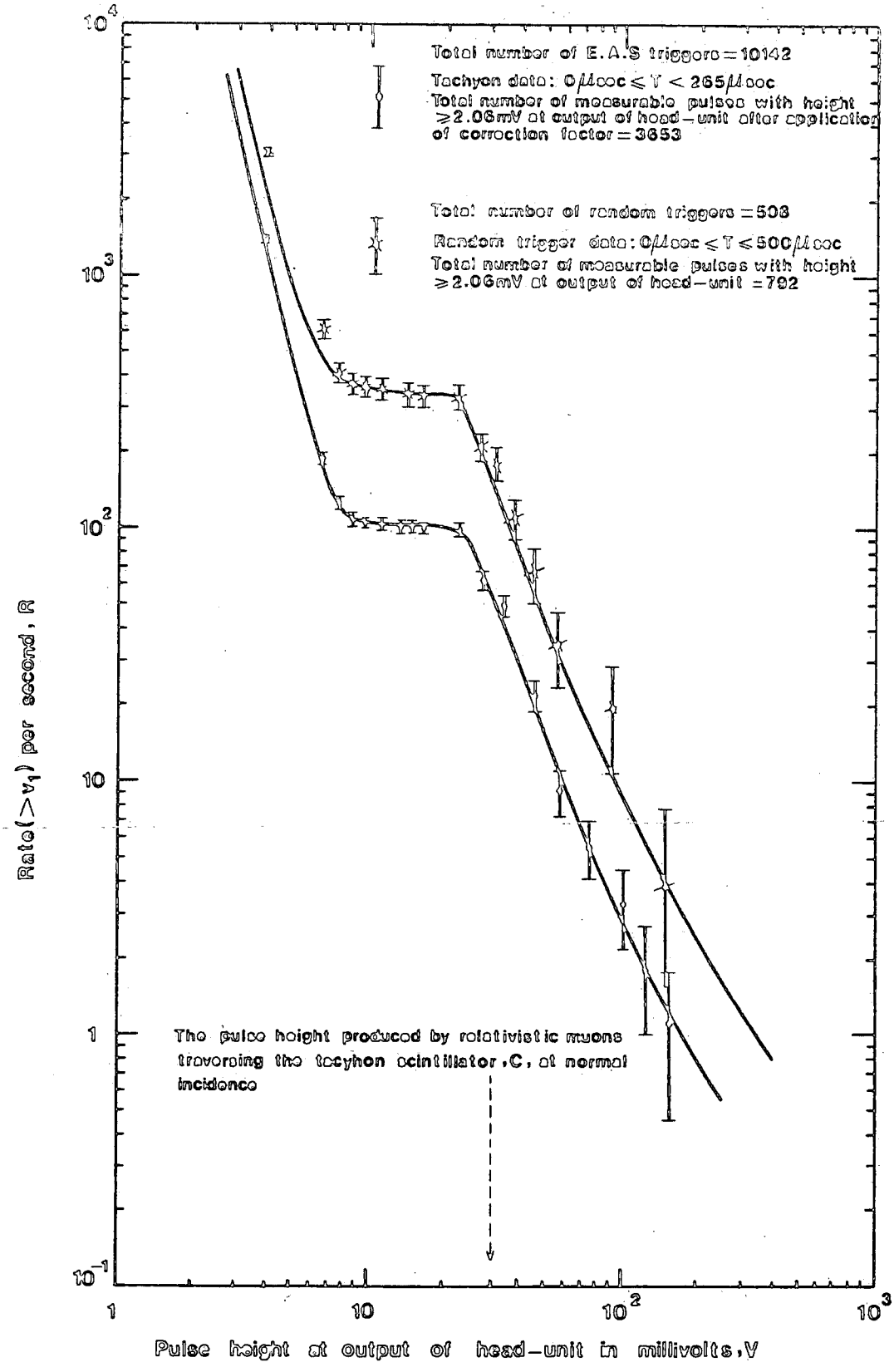

Figure 6.19a The integral rate of pulses occurring in the 265μs period before the arrival of the shower front pulse in the tachyon experiment after application of correction factor, f, and comparison with the integral rate of background pulses determined from a sample of 508 random triggers of the oscilloscope time base.

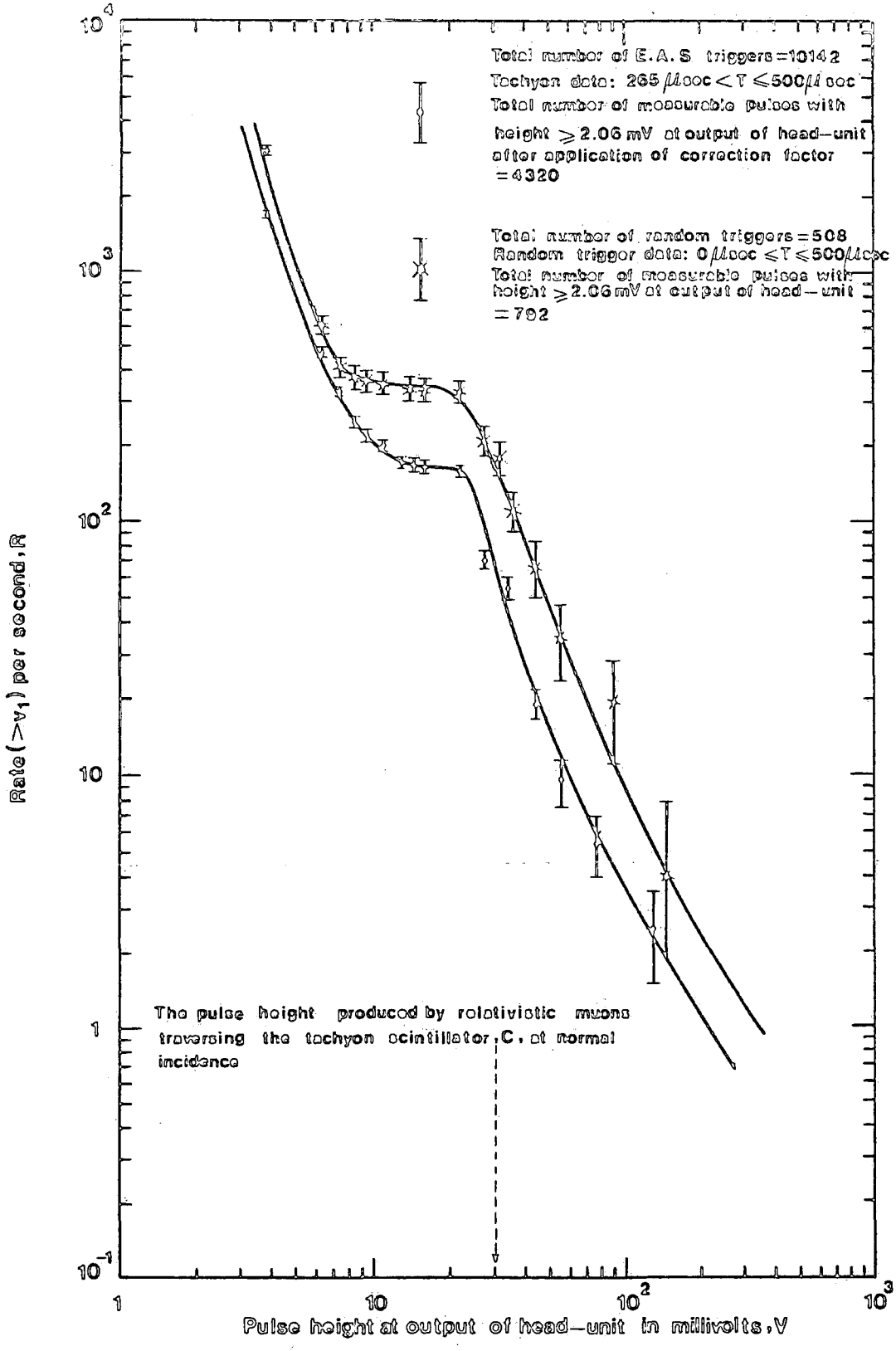

Figure 6.19b The integral rate of pulses occurring in the 235μs period after the arrival of the shower front pulse in the tachyon experiment after application of correction factor, f, and comparison with the integral rate of background pulses determined from a sample of 508 random triggers of the oscilloscope time base.

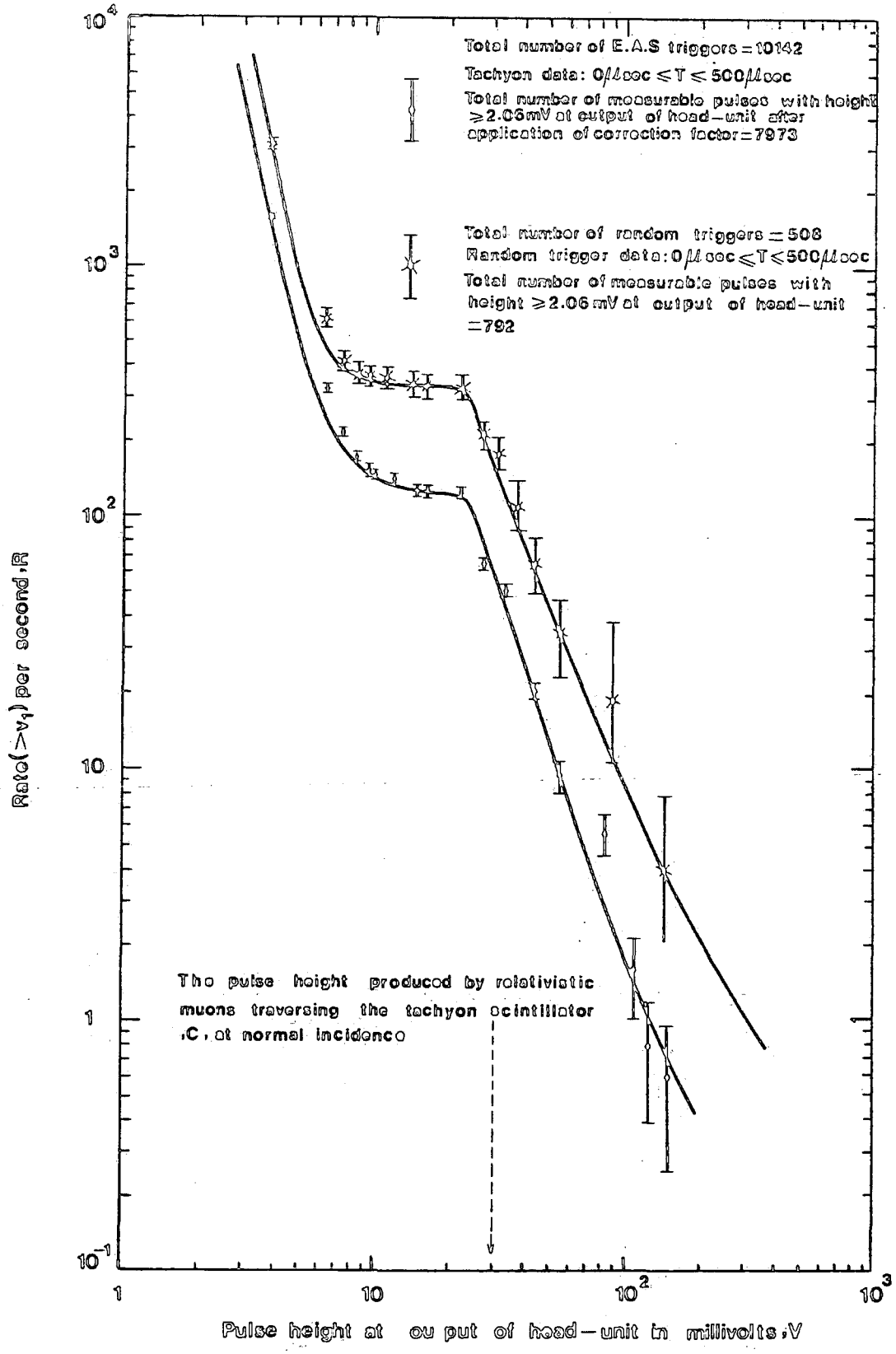

Figure 6.19c The integral rate of pulses in the 265μs period before and the 235μs period after the arrival of the shower front pulse after application of correction factor, f, and comparison with the integral rate of background pulses determined from a sample of 508 random triggers of the oscilloscope time base.

6.9) MULTIPLE PULSE EVENTS

Since the fact that in the both the tachyon data and the random trigger data, a significant number of multiple pulse events were observed it is necessary to investigate them. In fact, the multiple pulse events observed in the time domain before the arrival of the shower front pulse in the tachyon data are of particular interest as they could in principle provide evidence for or against a significant tachyon flux. Therefore, if a tachyon signal is present in the data then an excess of observed events having two early pulses can be expected as a real early tachyon pulse associated with some showers would mean that both early pulses are not randomly related with respect to the shower front pulse. Roughly speaking, if multiple pulses have a significant non-random origin (this would be single tachyon pulses occurring in the 150 μs preceding the shower front pulse in the present experiment) then a broad difference between the expected (n_e) and observed (n_o) numbers should be obtained. The expected number of multiple pulse events is expected to obey the Poisson distribution provided that they are all randomly related. If for a given threshold energy loss the average number of pulses observed is z, then the probability of observing r is: $P(r)= \frac{e^{-z}.z^{r}}{r!}$. Table 6.14 shows the frequency distribution of observed multiple pulses in the tachyon data which are compared with the expected number for different threshold values of energy loss in the tachyon detector. The number of events with n=0 increases with threshold energy loss because the rate of the background pulses decreases rapidly with increasing

$t < 265\,\mu s$				$t > 265\,\mu s$			
Threshold Energy ≥ 0.5mv				Threshold Energy ≥ 0.5mv			
n	n_o	n_e	$n_o - n_e$	n	n_o	n_e	$n_o - n_e$
0	7139	7167.91	-28.91	0	7355	7235.36	+119.64
1	2547	2487.78	+59.22	1	2252	2443.42	-191.42
2	404	431.71	-27.71	2	449	412.58	+36.42
3	44	49.95	- 5.95	3	72	46.45	+25.55
4	7	4.33	+ 2.67	4	11	3.92	+ 7.08
5	1	0.30	+ 0.70	5	3	0.26	+ 2.74
6	0	0.02	- 0.02	6	0	0.01	- 0.01
	10142				10142		

$t < 265\,\mu s$				$t > 265\,\mu s$			
Threshold Energy ≥ 2mv				Threshold Energy ≥ 2mv			
n	n_o	n_e	$n_o - n_e$	n	n_o	n_e	$n_o - n_e$
0	8590	8581.07	+ 8.93	0	8323	8230.53	+ 92.47
1	1418	1434.13	- 16.13	1	1570	1718.82	-148.82
2	126	119.84	+ 6.16	2	208	179.48	+ 28.52
3	7	6.68	+ 0.32	3	33	12.49	+ 20.51
4	1	0.28	+ 0.72	4	7	0.65	+ 6.35
5	0	0	0	5	1	0.03	+ 0.97
6	0	0	0	6	0	0	0
	10142				10142		

Table 6.14 Tachyon data. Number of triggers showing n pulses in the tachyon detector in the 265 μs time domain (indicated by $t < 265\,\mu s$ in the table) prior to the arrival of an EAS shower front pulse and the 235 μs time domain (indicated by $t > 265\,\mu s$ in the table) after the shower front pulse. n_o is the observed number of events and n_e is the expected number assuming the expected number obeys a Poisson distribution.

$t < 265\,\mu s$				$t > 265\,\mu s$			
Threshold Energy ≥ 4mv				Threshold Energy ≥ 4mv			
n	n_o	n_e	$n_o - n_e$	n	n_o	n_e	$n_o - n_e$
0	9688	9684.63	+ 3.37	0	9348	9322.97	+ 25.03
1	441	446.89	- 5.89	1	743	785.03	- 42.03
2	12	10.32	+ 1.68	2	44	33.05	+ 10.95
3	1	0.16	+ 0.84	3	5	0.93	+ 4.07
4	0	0	0	4	2	0.02	+ 1.98
5	0	0	0	5	0	0	0
6	0	0	0	6	0	0	0
	10142				10142		

$t < 265\,\mu s$				$t > 265\,\mu s$			
Threshold Energy ≥ 30mv				Threshold Energy ≥ 30mv			
n	n_o	n_e	$n_o - n_e$	n	n_o	n_e	$n_o - n_e$
0	9924	9921.43	+ 2.57	0	9806	9792.18	+ 13.82
1	213	218.15	- 5.15	1	318	343.72	- 25.72
2	5	2.40	+ 2.6	2	16	6.03	+ 9.97
3	0	0.02	- 0.02	3	2	0.07	+ 1.93
4	0	0	0	4	0	0	0
5	0	0	0	5	0	0	0
6	0	0	0	6	0	0	0
	10142				10142		

Table 6.14 (continued)

$t < 265\,\mu s$				$t > 265\,\mu s$			
Threshold Energy > 120 mv				Threshold Energy > 120 mv			
n	n_o	n_e	$n_o - n_e$	n	n_o	n_e	$n_o - n_e$
0	10052	10051.41	+ 0.59	0	10050	10050.42	- 0.42
1	89	90.19	- 1.19	1	92	91.17	+ 0.83
2	1	0.40	+ 0.60	2	0	0.41	- 0.41
3	0	0	0	3	0	0	0
4	0	0	0	4	0	0	0
5	0	0	0	5	0	0	0
6	0	0	0	6	0	0	0
	10142				10142		

$t < 265\,\mu s$				$t > 265\,\mu s$			
Threshold Energy ≥ 700 mv				Threshold Energy ≥ 700 mv			
n	n_o	n_e	$n_o - n_e$	n	n_o	n_e	$n_o - n_e$
0	10136	10136	0	0	10136	10136	0
1	6	6	0	1	6	6	0
2	0	0	0	2	0	0	0
3	0	0	0	3	0	0	0
4	0	0	0	4	0	0	0
5	0	0	0	5	0	0	0
6	0	0	0	6	0	0	0
	10142				10142		

Table 6.14 (continued)

threshold energy loss. It is seen from table 6.14 that an excess is observed for small threshold energy losses ($\gtrsim$0.5mv or $\gtrsim$0.07e) in the detector before the arrival of shower front pulse, but the excess is not statistically significant. For larger threshold energy losses the agreement between the observed and expected number of multiple pulse events is reasonable. Moreover, the same calculations were carried out for the background data and the result is represented in table 6.15. These calculations indicate that there is no evidence for a real tachyon signal.

6.10) TIME SEPARATION DISTRIBUTION OF SUCCESSIVE E.A.S TRIGGERS

A method for the checking the correct functioning of the extensive air shower selection trigger during the experiment is the calculation of the differential and integral time separation distribution of successively recorded events. If a sample of N events are observed in a time T, the mean time separation of events is $\overline{T} = \frac{N}{T}$. Moreover, assuming the successive events are unrelated then the number expected with time separation in the range t to t+dt (i.e; differential time separation distribution) is given by:

$$n(t)dt = N e^{-\frac{t}{\overline{T}}} \times \frac{dt}{\overline{T}} \qquad 6.3$$

and the number expected with time separation greater than t (i.e; integral time separation distribution) is given by:

$$n(>t) = N e^{-\frac{t}{\overline{T}}} \qquad 6.4$$

$t < 265\,\mu s$				$t > 265\,\mu s$			
Threshold Energy ≥ 0.5 mv				Threshold Energy ≥ 0.5 mv			
n	n_o	n_e	$n_o - n_o$	n	n_o	n_e	$n_o - n_e$
0	178	223.11	- 45.11	0	209	252.07	- 43.07
1	259	183.58	+ 75.42	1	248	176.65	+ 71.35
2	55	75.53	- 20.53	2	45	61.90	- 16.90
3	15	20.72	- 5.72	3	6	14.46	- 8.46
4	1	4.26	- 3.26	4	0	2.53	- 2.53
5	0	0.70	- 0.70	5	0	0.35	- 0.35
6	0	0.10	- 0.10	6	0	0.04	- 0.04
	508				508		

$t < 265\,\mu s$				$t > 265\,\mu s$			
Threshold Energy ≥ 2 mv				Threshold Energy ≥ 2 mv			
n	n_o	n_e	$n_o - n_o$	n	n_o	n_e	$n_o - n_e$
0	241	273.79	- 32.79	0	273	300.92	- 27.92
1	227	169.23	+ 57.77	1	206	157.57	+ 48.43
2	33	52.30	- 19.30	2	27	41.26	- 14.26
3	7	10.78	- 3.78	3	2	7.21	- 5.21
4	0	1.67	- 1.67	4	0	0.94	- 0.94
5	0	0.21	- 0.21	5	0	0.10	- 0.10
6	0	0.02	- 0.02	6	0	0	0
	508				508		

Table 6.15 Background data. Similar table to table 6.13 except that this table refers to the background data measurements.

$t < 265\,\mu s$				$t > 265\,\mu s$			
Threshold Energy $\geq$ 4mv				Threshold Energy $\geq$ 4mv			
n	n_o	n_e	$n_o - n_e$	n	n_o	n_e	$n_o - n_e$
0	434	436.55	- 2.55	0	452	454.08	- 2.08
1	71	66.17	+ 4.83	1	55	50.95	+ 4.05
2	3	5.01	- 2.01	2	1	2.86	- 1.86
3	0	0.26	- 0.26	3	0	0.11	- 0.11
4	0	0.01	- 0.01	4	0	0	0
5	0	0	0	5	0	0	0
6	0	0	0	6	0	0	0
	508				508		

$t < 265\,\mu s$				$t > 265\,\mu s$			
Threshold Energy $\geq$ 30mv				Threshold Energy $\geq$ 30mv			
n	n_o	n_e	$n_o - n_e$	n	n_o	n_e	$n_o - n_e$
0	469	470.46	- 1.46	0	480	480.76	- 0.76
1	39	36.12	+ 2.88	1	28	26.50	+ 1.50
2	0	1.38	- 1.38	2	0	0.73	- 0.73
3	0	0.04	- 0.04	3	0	0.01	- 0.01
4	0	0	0	4	0	0	0
5	0	0	0	5	0	0	0
6	0	0	0	6	0	0	0
	508				508		

Table 6.15 (continued)

$t < 265\,\mu s$				$t > 265\,\mu s$			
Threshold Energy > 120 mv				Threshold Energy > 120 mv			
n	n_o	n_e	$n_o - n_e$	n	n_o	n_e	$n_o - n_e$
0	490	490.32	- 0.32	0	498	498.10	- 0.10
1	18	17.37	+ 0.63	1	10	9.80	+ 0.20
2	0	0.31	- 0.31	2	0	0.10	- 0.10
3	0	0	0	3	0	0	0
4	0	0	0	4	0	0	0
5	0	0	0	5	0	0	0
6	0	0	0	6	0	0	0
	508				508		

$t < 265\,\mu s$				$t > 265\,\mu s$			
Threshold Energy ≥ 700 mv				Threshold Energy ≥ 700 mv			
n	n_o	n_e	$n_o - n_e$	n	n_o	n_e	$n_o - n_e$
0	507	507	0	0	508	508	0
1	1	1.0	0	1	0	0	0
2	0	0	0	2	0	0	0
3	0	0	0	3	0	0	0
4	0	0	0	4	0	0	0
5	0	0	0	5	0	0	0
6	0	0	0	6	0	0	0
	508				508		

Table 6.15 (continued)

Using a program called "TIME SEPARATION" in conjunction with a Commodore PET computer (see appendix D) the time separation distribution of 10,142 extensive air shower triggers was calculated and the results is shown in table 6.16. Using this table, the measured differential and integral time separation distributions along with the best fit lines representing the above expressions (i.e; equations 6.3 and 6.4) are shown in the figures 6.20a and 6.20b respectively. The mean time separation of both distributions was calculated and the results are summarised in the table 6.17. Obviously, the results obtained for the trigger rate in this way should be consistent with the trigger rate which is determined directly by using the fact that 10,142 extensive air shower triggers in a total period of 839hr 46min 40sec gives a trigger rate of 12.08 ± 0.12 per hour. In comparing this rate with the figures in table 6.17, it can be seen that the differential time separation distribution gives a closer agreement with this figure than the integral distribution. The reason for this is due to the fact that in experimental data plotted as a differential distribution, all the experimental points are statistically independent whereas this is not the case for an integral distribution.

6.11) DELAYED IONIZING EVENTS OBSERVED IN REGIONS OF EXTENSIVE AIR SHOWERS OF LOCAL ELECTRON DENSITY $>25m^{-2}$

As noted earlier , figure 6.3 shows the observed time distribution of pulses occurring in the tachyon detector (i.e; scintillator C of area $1.05m^2$) in the 260 μs time domain prior to the arrival of an extensive air shower and also in the 230μs

Time Separation in Minutes	Frequency	Integral
0- 2	3298 ± 57	10142 ± 101
2- 4	2412 ± 49	6844 ± 83
4- 6	1473 ± 38	4432 ± 67
6- 8	985 ± 31	2959 ± 54
8-10	669 ± 26	1974 ± 44
10-12	423 ± 21	1305 ± 36
12-14	289 ± 17	882 ± 30
14-16	192 ± 14	593 ± 24
16-18	124 ± 11	401 ± 20
18-20	86.0 ± 9.3	277 ± 17
20-22	62.0 ± 7.9	191 ± 14
22-24	39.0 ± 6.2	129 ± 11
24-26	31.0 ± 5.6	90.0 ± 9.5
26-28	14.0 ± 3.7	59.0 ± 7.7
28-30	11.0 ± 3.3	45.0 ± 6.7
30-32	10.0 ± 3.2	34.0 ± 5.8
32-34	5.0 ± 2.2	24.0 ± 4.9
34-36	5.0 ± 2.2	19.0 ± 4.4
36-38	3.0 ± 1.7	14.0 ± 3.7
38-40	6.0 ± 2.4	11.0 ± 3.3
40-42	1.0 ± 1.0	5.0 ± 2.2
42-44	3.0 ± 1.7	4.0 ± 2.0
44-46	0.0 ± 0.0	1.0 ± 1.0
46-48	1.0 ± 1.0	1.0 ± 1.0

Table 6.16 Frequency and integral distribution of time separation in minutes for 10142 shower triggers.

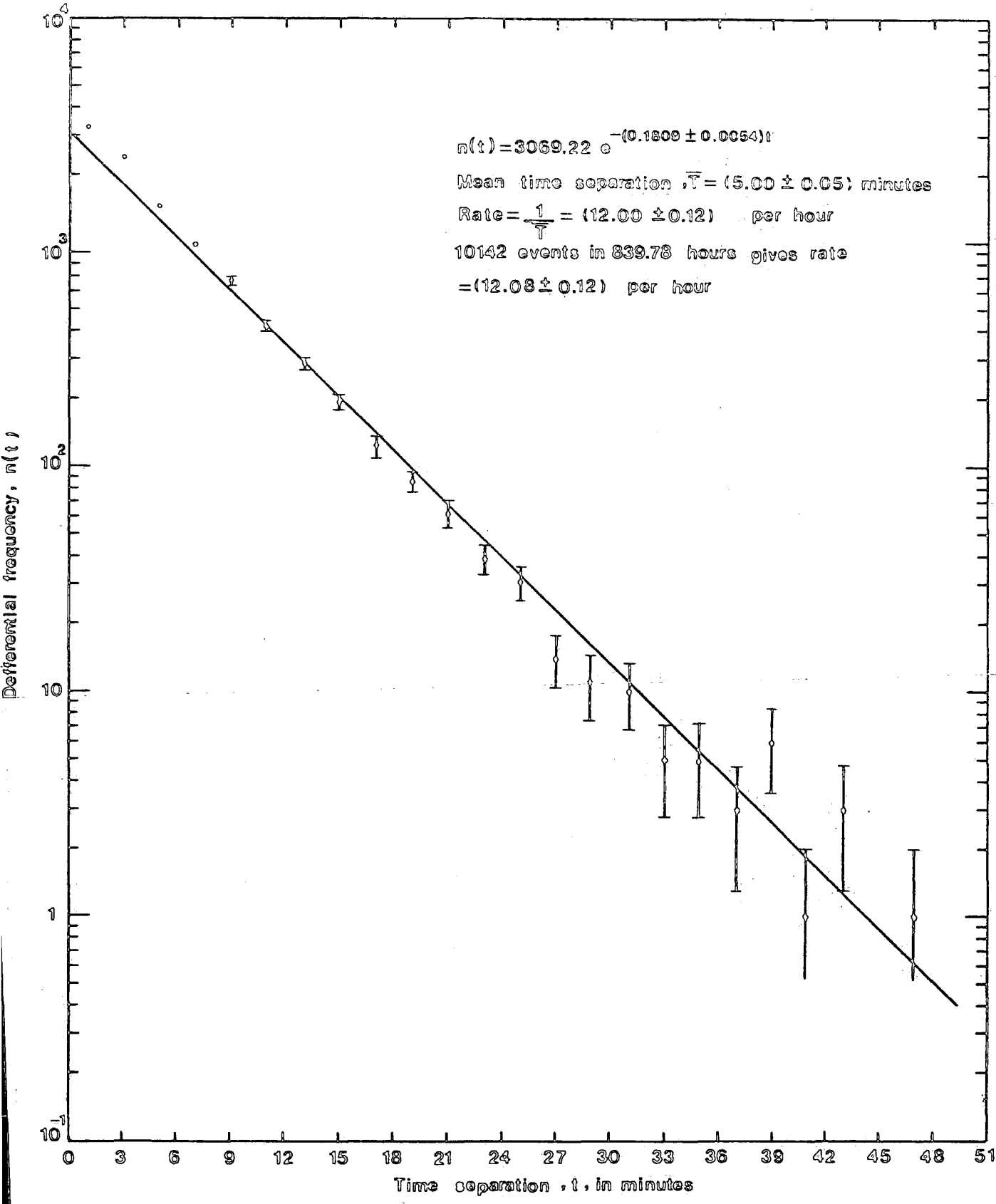

Figure 6.20a Differential distribution of time separation of 10142 extensive air shower triggers observed in a running time of 839.75 hours corresponding to a mean time separation, $\bar{T} = (5.00 \pm 0.05)$ minutes.

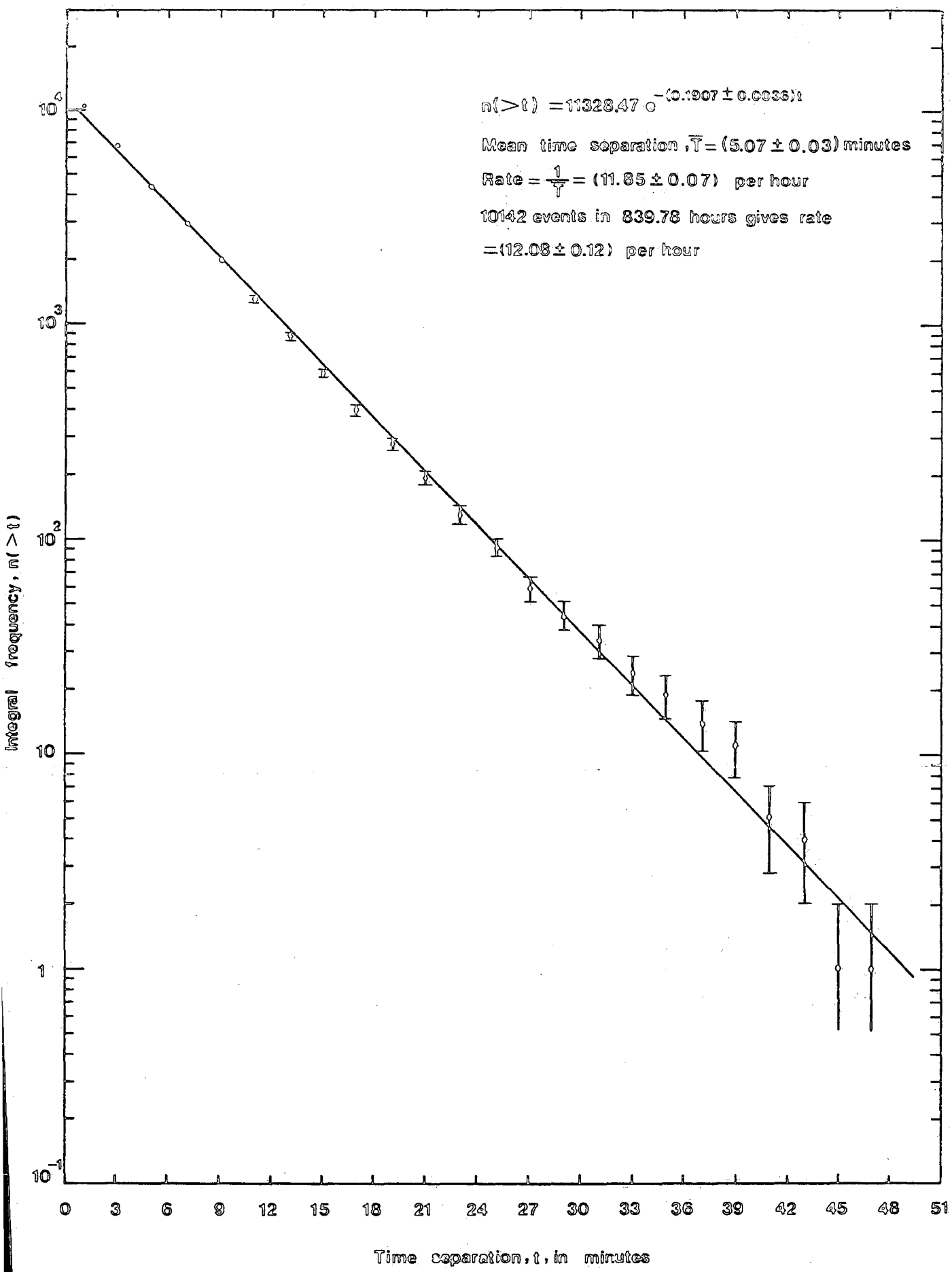

Figure 6.20b Integral plot of time separation of 10142 extensive air shower triggers observed in a running time 839.78 hours corresponding to a mean time separation, $\bar{T}$ = (5.07 ± 0.03) minutes.

	Mean time separation, $\bar{T}$, in minutes	Trigger rate = $\frac{1}{\bar{T}}$ per hour
Differential time separation distribution	(5.00 ± 0.05) min	$(12.00 \pm 0.12)\ hr^{-1}$
Integral time separation distribution	(5.07 ± 0.03) min	$(11.85 \pm 0.07)\ hr^{-1}$

Table 6.17 Summary of results obtained concerning mean time separation, $\bar{T}$, for differential and integral distributions.

after the arrival of the extensive air shower. It is clear from figures 6.3 and 6.7 that there is evidence of significant excess of events occurring after the arrival of the shower front pulse, at least for some ranges of energy deposition in the tachyon detection scintillator. With the aid of previous tables (e.g; table 6.2), the excess (i.e; $\Delta N = N_2 - N_1$) has been found quantitatively by subtracting the number of events N_1 occurring in a given time range before the arrival of the shower front from N_2 where N_2 is the number of events occurring in the same time range after the arrival of the shower front pulse. The consequences of such calculations for various ranges of energy deposition in tachyon detection scintillator (i.e; scintillator C) are shown in table 6.18. In these tables, the sum of events in the 230 μs period after and before the arrival of the shower front pulse are shown at the bottom of respective columns. The excess was plotted as a function of the time after the occurrence of the shower front pulse as measured on the oscilloscope time base and the result is given in figure 6.21. In this figure the shower front occurs at a time of 265 μs. The effect of experimental bias (see section 6.5) for certain ranges of energy deposition in the detector is also shown in the figure. It is obvious from figure 6.21 that the excess of events is greatest for pulse heights observed in the tachyon detection scintillator in the ranges 0.14e – 0.19e and 0.19e-0.52e where e=10MeV is the energy deposit produced by a muon traversing the scintillator at normal incidence. Also, the events are approximately uniformly distributed over the 270 – 500 μs time ranges covered by the measurements. In table 6.19

$0.5mv \leqslant v \leqslant 2mv$

$0.07e \leqslant v \leqslant 0.14e$

Δt_2 in μs	N_2	Δt_1 in μs	N_1	$\Delta N = N_2 - N_1$
270-280	33 (63)	250-260	52 (92)	-19 ± 9(-29 ± 17)
280-290	57 (81)	240-250	57 (93)	0 ± 11(-12 ± 16)
290-300	69 (98)	230-240	63 (96)	6 ± 11(2 ± 17)
300-310	51 (72)	220-230	68 (95)	-17 ± 11(-23 ± 15)
310-320	71 (101)	210-220	65 (83)	6 ± 12(18 ± 16)
320-330	63 (89)	200-210	75 (91)	-12 ± 12(-2 ± 15)
330-340	55 (78)	190-200	60 (70)	- 5 ± 8(8 ± 14)
340-350	53 (75)	180-190	89 (102)	-36 ± 12(-27 ± 15)
350-360	43 (59)	170-180	59 (65)	-16 ± 10(- 6 ± 13)
360-370	70 (95)	160-170	65 (66)	5 ± 12(29 ± 14)
370-380	68 (90)	150-160	97 (98)	-29 ± 13(-8 ± 15)
380-390	56 (73)	140-150	85 (86)	-29 ± 12(-13 ± 13)
390-400	50 (64)	130-140	86 (87)	-36 ± 12(-23 ± 13)
400-410	66 (83)	120-130	87 (88)	-21 ± 12(- 5 ± 14)
410-420	54 (68)	110-120	89 (90)	-35 ± 12(-22 ± 13)
420-430	71 (87)	100-110	68 (69)	3 ± 12(18 ± 13)
430-440	65 (79)	90-100	81 (82)	-16 ± 12(-3 ± 13)
440-450	83 (99)	80- 90	76 (77)	7 ± 13(22 ± 14)
450-460	62 (73)	70- 80	75 (76)	-13 ± 12(-3 ± 13)
460-470	85 (99)	60- 70	80 (81)	5 ± 13(18 ± 14)
470-480	55 (64)	50- 60	88 (89)	-33 ± 12(-25 ± 13)
480-490	56 (64)	40- 50	94 (95)	-38 ± 12(-31 ± 13)
490-500	85 (97)	30- 40	96 (97)	-11 ± 13(0 ± 14)
	1421(1851)		1755(1968)	-334 ± 56(-117± 67)

Table 6.18 Determination of the excess of events N_2-N_1 occurring in given time intervals Δt_2 after the arrival of the shower front over the number N_1 occurring in a similar time interval Δt_1 before the arrival of the shower front. N_2 is the number of events occurring in the time interval Δt_2. Times in the table are measured from the start of the oscilloscope time base with the shower front occurring at 265 μs. The figures in brackets are the number of events corrected for experimental bias. Total number of shower triggers = 10142.

$2mv < v \leq 4mv$
$0.14e < v \leq 0.19e$

Δt_2 in µs	N_2	Δt_1 in µs	N_1	$\Delta N = N_2 - N_1$
270-280	20 (38)	250-260	17	3 ± 6 (21 ± 9)
280-290	29 (41)	240-250	29	0 ± 8 (12 ± 9)
290-300	40 (57)	230-240	34	6 ± 9 (23 ± 11)
300-310	33 (47)	220-230	52	-19 ± 9 (-5 ± 11)
310-320	36 (51)	210-220	42	- 6 ± 9 (9 ± 11)
320-330	51 (72)	200-210	29	22 ± 9 (43 ± 11)
330-340	39 (55)	190-200	20	19 ± 8 (35 ± 10)
340-350	40 (56)	180-190	43	- 3 ± 9 (13 ± 11)
350-360	34 (47)	170-180	46	-12 ± 9 (1 ± 11)
360-370	39 (53)	160-170	45	- 6 ± 9 (8 ± 11)
370-380	74 (98)	150-160	33	41 ± 10 (65 ± 13)
380-390	52 (68)	140-150	31	21 ± 9 (37 ± 11)
390-400	47 (60)	130-140	39	8 ± 9 (21 ± 11)
400-410	46 (58)	120-130	45	1 ± 10 (13 ± 11)
410-420	52 (65)	110-120	33	19 ± 9 (32 ± 11)
420-430	44 (54)	100-110	28	16 ± 8 (26 ± 10)
430-440	47 (57)	90-100	40	7 ± 9 (17 ± 10)
440-450	46 (55)	80- 90	36	10 ± 9 (19 ± 10)
450-460	47 (55)	70- 80	39	8 ± 9 (16 ± 10)
460-470	51 (60)	60- 70	39	12 ± 9 (21 ± 11)
470-480	48 (56)	50- 60	38	10 ± 9 (18 ± 10)
480-490	48 (55)	40- 50	33	15 ± 9 (22 ± 10)
490-500	67 (76)	30- 40	48	19 ± 11 (28 ± 11)
	1030 (1334)		839	191 ± 43 (495 ± 51)

Table 6.18 (continued)

4mv < v ⩽ 30mv
0.19e < v ⩽ 0.52e

Δt_2 in μs	N_2	Δt_1 in μs	N_1	$\Delta N = N_2 - N_1$
270-280	13 (25)	250-260	6	7 ± 4 (19 ± 7)
280-290	19 (26)	240-250	6	13 ± 5 (20 ± 7)
290-300	13 (18)	230-240	6	7 ± 4 (12 ± 6)
300-310	19 (27)	220-230	9	10 ± 5 (18 ± 7)
310-320	11 (15)	210-220	11	0 ± 5 (4 ± 6)
320-330	24 (33)	200-210	7	17 ± 6 (26 ± 7)
330-340	20 (28)	190-200	7	13 ± 5 (21 ± 7)
340-350	28 (39)	180-190	13	15 ± 6 (26 ± 8)
350-360	22 (30)	170-180	10	12 ± 6 (20 ± 7)
360-370	37 (49)	160-170	12	25 ± 7 (37 ± 9)
370-380	33 (42)	150-160	9	24 ± 6 (33 ± 8)
380-390	27 (35)	140-150	3	24 ± 5 (32 ± 7)
390-400	29 (37)	130-140	8	21 ± 6 (29 ± 8)
400-410	34 (43)	120-130	15	19 ± 7 (28 ± 9)
410-420	29 (36)	110-120	10	19 ± 6 (26 ± 7)
420-430	38 (46)	100-110	7	31 ± 7 (39 ± 8)
430-440	20 (24)	90-100	12	8 ± 6 (12 ± 6)
440-450	37 (44)	80- 90	11	26 ± 7 (33 ± 8)
450-460	26 (30)	70- 80	10	16 ± 6 (20 ± 7)
460-470	27 (31)	60- 70	7	10 ± 6 (24 ± 6)
470-480	35 (40)	50- 60	15	20 ± 7 (25 ± 8)
480-490	28 (32)	40- 50	10	18 ± 6 (22 ± 7)
490-500	32 (36)	30- 40	7	25 ± 6 (29 ± 7)
	601 (766)		211	390 ± 28 (555 ± 35)

Table 6.18 (continued)

30mv < v ⩽ 120 mv
0.52e < v ⩽ e

Δt_2 in μs	N_2	Δt_1 in μs	N_1	$\Delta N = N_2 - N_1$
270-280	3	250-260	4	-1 ± 3
280-290	3	240-250	7	-4 ± 3
290-300	5	230-240	9	-4 ± 4
300-310	9	220-230	4	5 ± 4
310-320	8	210-220	10	-2 ± 4
320-330	6	200-210	8	-2 ± 4
330-340	3	190-200	2	1 ± 2
340-350	8	180-190	5	3 ± 4
350-360	16	170-180	3	13 ± 4
360-370	8	160-170	6	2 ± 4
370-380	14	150-160	11	3 ± 5
380-390	17	140-150	7	10 ± 5
390-400	8	130-140	4	4 ± 3
400-410	17	120-130	8	9 ± 5
410-420	14	110-120	8	6 ± 5
420-430	20	100-110	6	14 ± 5
430-440	15	90-100	5	10 ± 4
440-450	14	80- 90	7	7 ± 5
450-460	14	70- 80	3	11 ± 4
460-470	19	60- 70	5	14 ± 5
470-480	15	50- 60	11	4 ± 5
480-490	17	40- 50	6	11 ± 5
490-500	17	30- 40	3	14 ± 4
	270		142	128 ± 20

Table 6.18 (continued)

v > 120 mv
v > e

Δt_2 in µs	N_2	Δt_1 in µs	N_1	$\Delta N = N_2 - N_1$
270-280	4	250-260	5	-1 ± 3
280-290	2	240-250	7	-5 ± 3
290-300	2	230-240	3	-1 ± 2
300-310	5	220-230	2	3 ± 3
310-320	3	210-220	4	-1 ± 3
320-330	3	200-210	8	-5 ± 3
330-340	2	190-200	5	-3 ± 3
340-350	5	180-190	6	-1 ± 3
350-360	5	170-180	5	0 ± 3
360-370	3	160-170	4	-1 ± 3
370-380	2	150-160	2	0 ± 2
380-390	2	140-150	5	-3 ± 3
390-400	4	130-140	4	0 ± 3
400-410	6	120-130	5	1 ± 3
410-420	5	110-120	4	1 ± 3
420-430	5	100-110	4	1 ± 3
430-440	5	90-100	4	1 ± 3
440-450	8	80- 90	2	6 ± 3
450-460	3	70- 80	1	2 ± 2
460-470	7	60- 70	5	2 ± 3
470-480	10	50- 60	6	4 ± 4
480-490	6	40- 50	2	4 ± 3
490-500	7	30- 40	5	2 ± 3
	104		98	6 ± 14

Table 6.18 (continued)

$V \geqslant 700$ mv
$v \geqslant 3e$

Δt_2 in μs	N_2	Δt_1 in μs	N_1	$\Delta N = N_2 - N_1$
270-280	0	250-260	0	0 ± 0
280-290	0	240-250	0	0 ± 0
290-300	0	230-240	0	0 ± 0
300-310	1	220-230	0	1 ± 1
310-320	0	210-220	2	-2 ± 1
320-330	0	200-210	0	0 ± 0
330-340	0	190-200	0	0 ± 0
340-350	0	180-190	0	0 ± 0
350-360	0	170-180	1	-1 ± 1
360-370	0	160-170	0	0 ± 0
370-380	0	150-160	0	0 ± 0
380-390	0	140-150	1	-1 ± 1
390-400	0	130-140	0	0 ± 0
400-410	1	120-130	1	0 ± 1
410-420	1	110-120	0	1 ± 1
420-430	0	100-110	1	-1 ± 1
430-440	0	90-100	0	0 ± 0
440-450	0	80- 90	0	0 ± 0
450-460	1	70- 80	0	1 ± 1
460-470	3	60- 70	0	3 ± 2
470-480	0	50- 60	0	0 ± 0
480-490	0	40- 50	0	0 ± 0
490-500	0	30- 40	0	0 ± 0
	7		6	1 ± 4

Table 6.18 (continued)

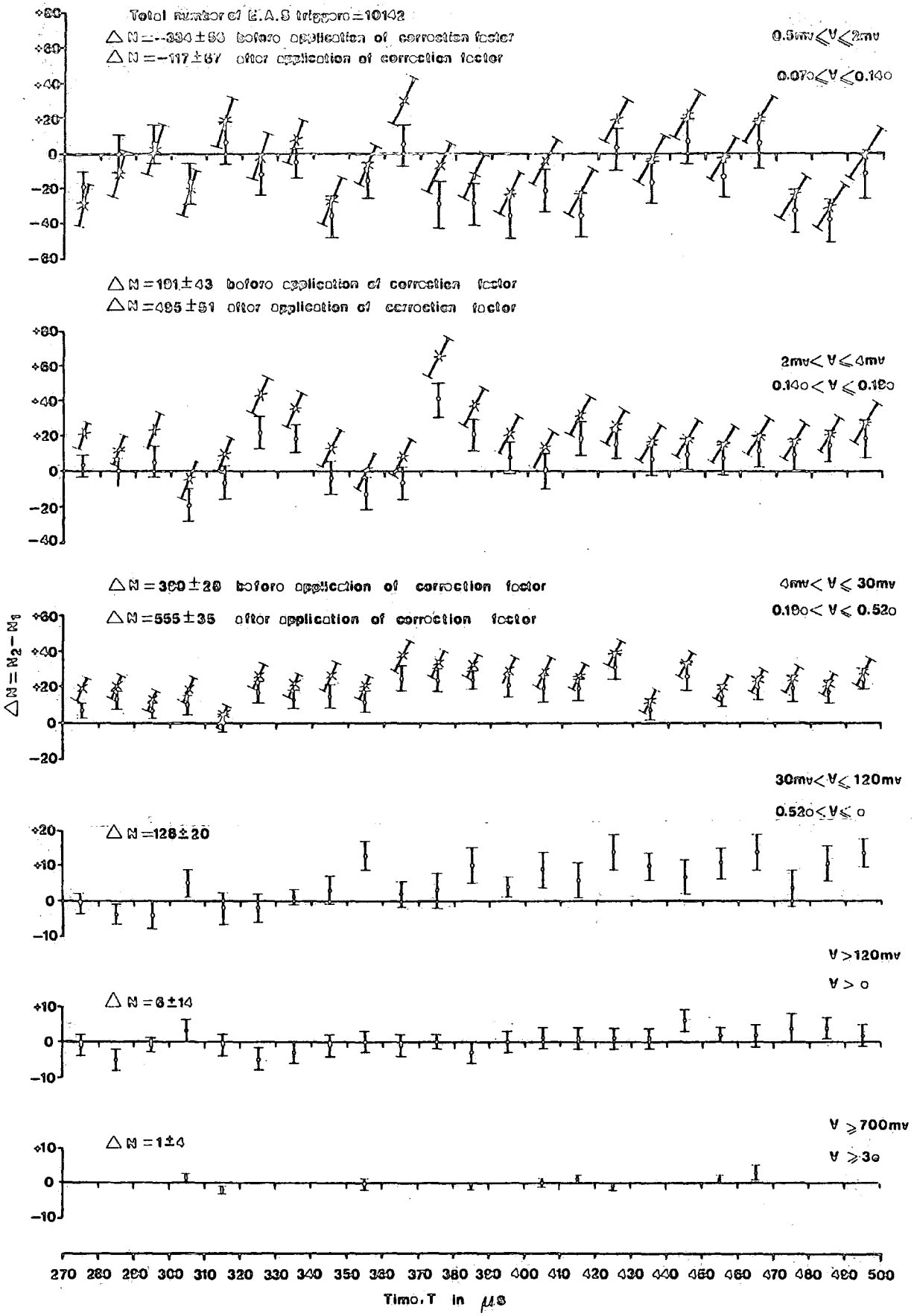

Figure 6.21 The excess events $\Delta N = N_2 - N_1$ observed to follow a shower front pulse where N_2 is the number of events observed in a given time interval after a shower and N_1 is the number of events observed in a similar time interval before the shower front. In the figure time is as measured from the start of the recording oscilloscope sweep with the shower front pulse occurring at a time of 265μs. $\Delta N = N_2(270\text{-}500) - N_1(30\text{-}260)$ is the total number of excess events in the 230μs period after the shower front compared to the 230μs period before the shower front after correction for experiental bias. Symbols o and X indicate before and after applying the correction factor for experimental bias respectively.

Range of pulse height	$\bar{e}$	Δe	Excess events $N_2(270-500) - N_1(30-260) = \Delta N$	Differential rate $= \frac{\Delta N}{\Delta e}$ per unit e
0.5mv$\leqslant$ v $\leqslant$ 2 mv 0.07e$\leqslant$ v $\leqslant$ 0.14e	0.105e	0.07e	-117 $\pm$ 67	-1671 $\pm$ 957/unit e
2mv< v $\leqslant$ 4mv 0.14e < v $\leqslant$ 0.19e	0.165e	0.05e	495 $\pm$ 51	9900 $\pm$ 1020/unit e
4mv < v $\leqslant$ 30mv 0.19e < v $\leqslant$ 0.52e	0.355e	0.33e	555 $\pm$ 35	1682 + 106/unit e
30mv < v $\leqslant$120mv 0.52e < v $\leqslant$ e	0.760e	0.48e	128 $\pm$ 20	267 $\pm$ 42/unit e
v > 120 mv v > e	-	-	6 $\pm$ 14	-
v $\geqslant$ 700 mv v $\geqslant$ 3e	-	-	1 $\pm$ 4	-
120mv < v $\leqslant$700mv e < v $\leqslant$ 3e	2e	2e	5 $\pm$ 15	2.5 $\pm$ 7.5/unit e

Table 6.19 Calculation of the differential pulse height distribution of all delayed events. $\Delta N = N_2(270-500) - N_1(30-260)$ is the total number of excess events in the 230μs period after the shower front compared to the 230μs period before the shower front after correction for experimental bias. e = 10MeV is the energy loss of a relativistic muon traversing the tachyon detector at normal incidence. Total number of EAS triggers = 10142.

the differential pulse height distribution of all delayed events is calculated and the result is plotted out in terms of e in figure 6.22. In fact, this figure indicates to the differential energy loss distribution of all delayed events occurring in the time domain 270 − 500 μs where time is as measured on the recording oscilloscope time base and the shower front pulse occurs at a time of 265 μs. The negative value for the differential rate at $\bar{e} = 0.105e$ of -117 ± 67 is attributed to a statistical fluctuation and means that for the corresponding range of energy deposition more events were observed to precede the shower front than to follow it. However, the excess of events found to trail the arrival of the air shower front could be due to low energy evaporation neutrons from air nuclei produced in the air shower hadron cascade which subsequently interact in the detection scintillator.

Assuming that the measured pulse heights are produced by relativistic particles that lose $2 MeV/g.cm^{-2}$ in the phosphor, the differential energy distribution of all delayed events was calculated and the result is given in table 6.20. This table is the same as table 6.19 except that the energy deposition in the tachyon detection scintillator is given in MeV. The resulting differential energy loss distribution is shown in figure 6.23. The number of events for a given energy deposition falls rapidly with increasing energy in the power − law form. It is noted that the peak of the pulse height distribution shown in figure 6.22 is close to the value of $(\frac{1}{3})^2 e = \frac{1}{9} e = 0.11e$ expected for relativistic charge e/3 quarks. However, the absence of a peak at $(\frac{2}{3})^2 e = \frac{4}{9} e = 0.44e$ corresponding to relativistic 2e/3

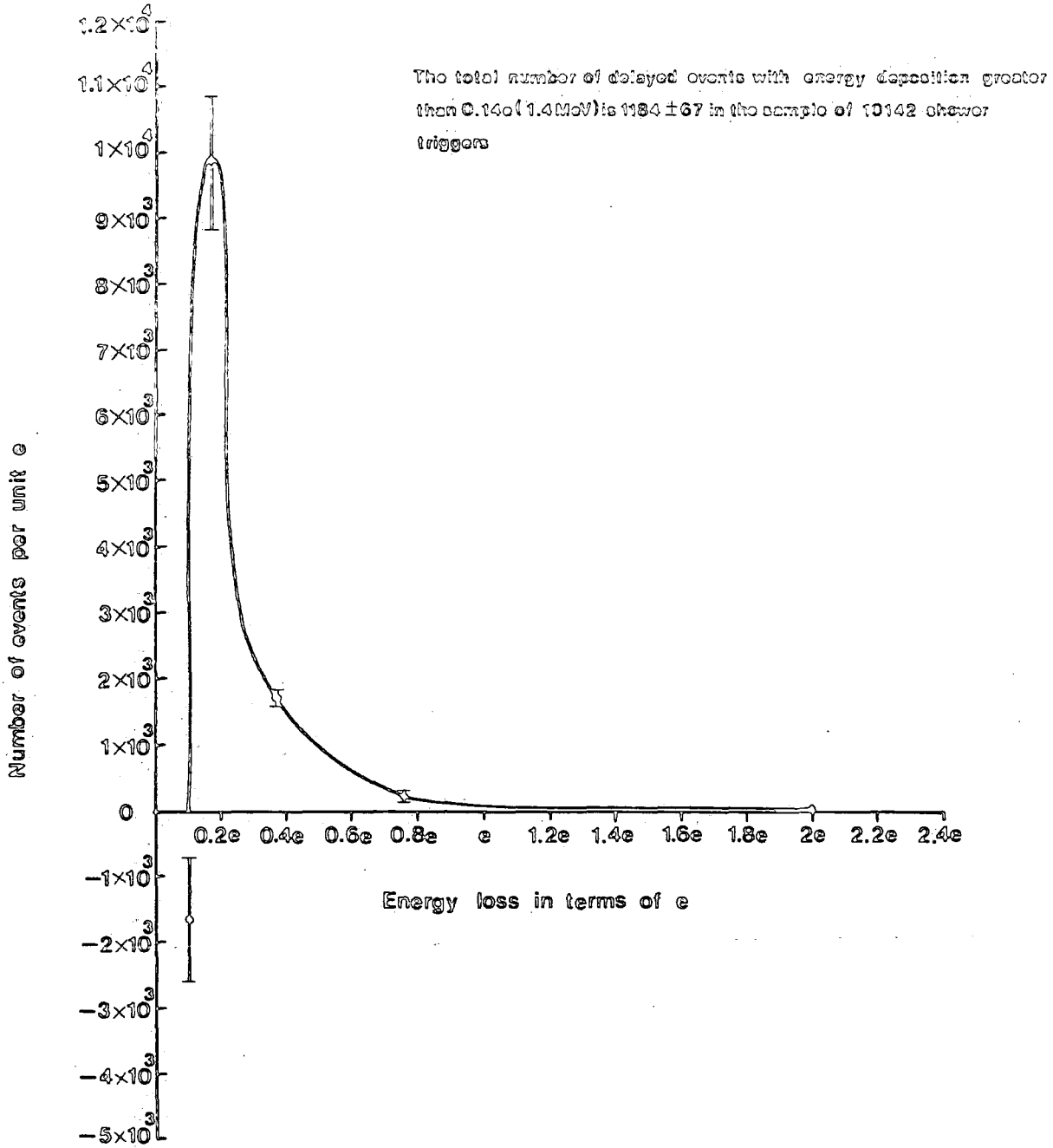

Figure 6.22 The differential energy loss distribution of all delayed events occurring in the time domain 270-500μs where time is as measured on the recording oscilloscope time base and the shower front pulse occurs at a time of 265μs. e = 10MeV is the energy loss of a relativisitic muon traversing the tachyon detection scintillator at normal incidence. The total number of delayed events with energy deposition > 0.14e (1.4MeV) = 1184 ± 67 in the sample of 10142 shower triggers.

Energy range in MeV	$\bar{E}$ in MeV	ΔE in MeV	Excess events $N_2(270-500) - N_1(30-260) = \Delta N$	Differential rate $= \frac{\Delta N}{\Delta E}$ per MeV
0.7 - 1.4	1.05	0.70	-117 ± 67	-167 ± 96
1.4 - 1.9	1.65	0.50	495 ± 51	990 ± 102
1.9 - 5.2	3.55	3.30	555 ± 35	168 ± 11
5.2 - 10	7.60	4.80	128 ± 20	27 ± 4
10 - 30	20	20	5 ± 15	0.25 ± 0.75

Table 6.20 Use of the basic data in table 6.19 to calculate the differential energy distribution of all delayed events assuming that the measured pulse heights are due to relativistic particles that lose 2 MeV/g.cm^{-2} in the phosphor.

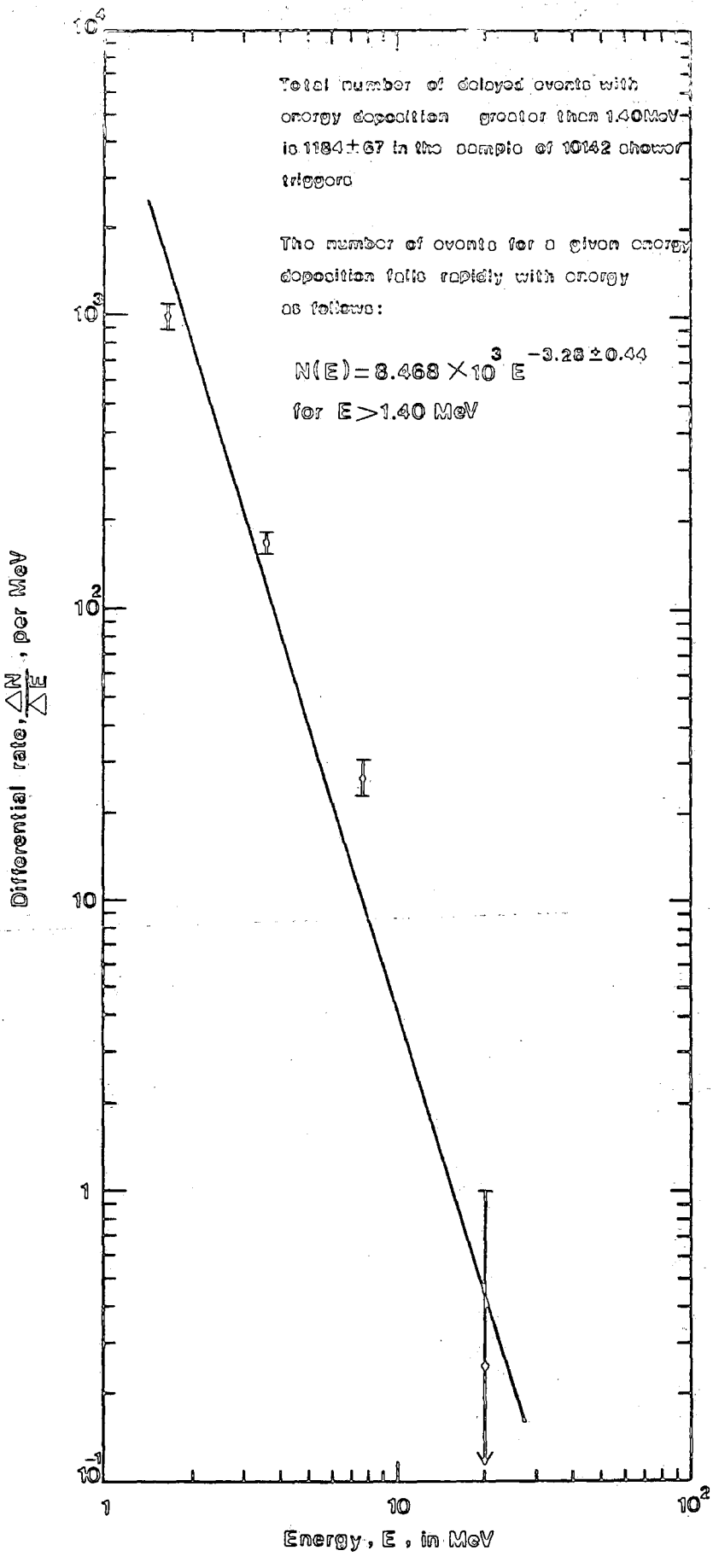

Figure 6.23 The differential energy distribution of all delayed events assuming that the measured pulse heights are produced by relativistic particles that lose 2 MeV/gcm^{-2} in the phosphor.

quarks would seem to rule out the possibility that a significant fraction of the events are due to this cause.

So far it has been assumed that the measured pulse heights are due to relativistic particles that traverse the phosphor. However, it is possible that the measured pulse heights are produced by low energy protons presumably knocked on by low energy neutrons incident on the phosphor. It is required to find the locus of corresponding electron and proton energies that produce the same amount of light output from the phosphor. This was carried out using data from Knoll (1979) for NE102A plastic scintillator and the result is shown in figure 6.24. By using the basic data in table 6.19 and also figure 6.24, the differential energy distribution of all delayed events for this case was calculated and the result is shown in table 6.21 and plotted in figure 6.25. A comparison of the differential energy distributions of all delayed events in which the measured pulse heights are produced either by relativistic particles or by low energy protons knocked-on by incident low energy neutrons is shown in figure 6.26. Also, another plot is shown in figure 6.27 in which the fitted power law was made only to the first three measured points. In both cases (i.e; the measured pulse heights produced either by relativistic particles or by low energy protons knocked on by incident low energy neutrons) the number of events for a given energy deposition falls rapidly with increasing energy in the power-law form, and this fall is somewhat more rapid in the case of low energy protons. The data shown in table 6.21 shows that if the delayed events are due to knock-on protons produced

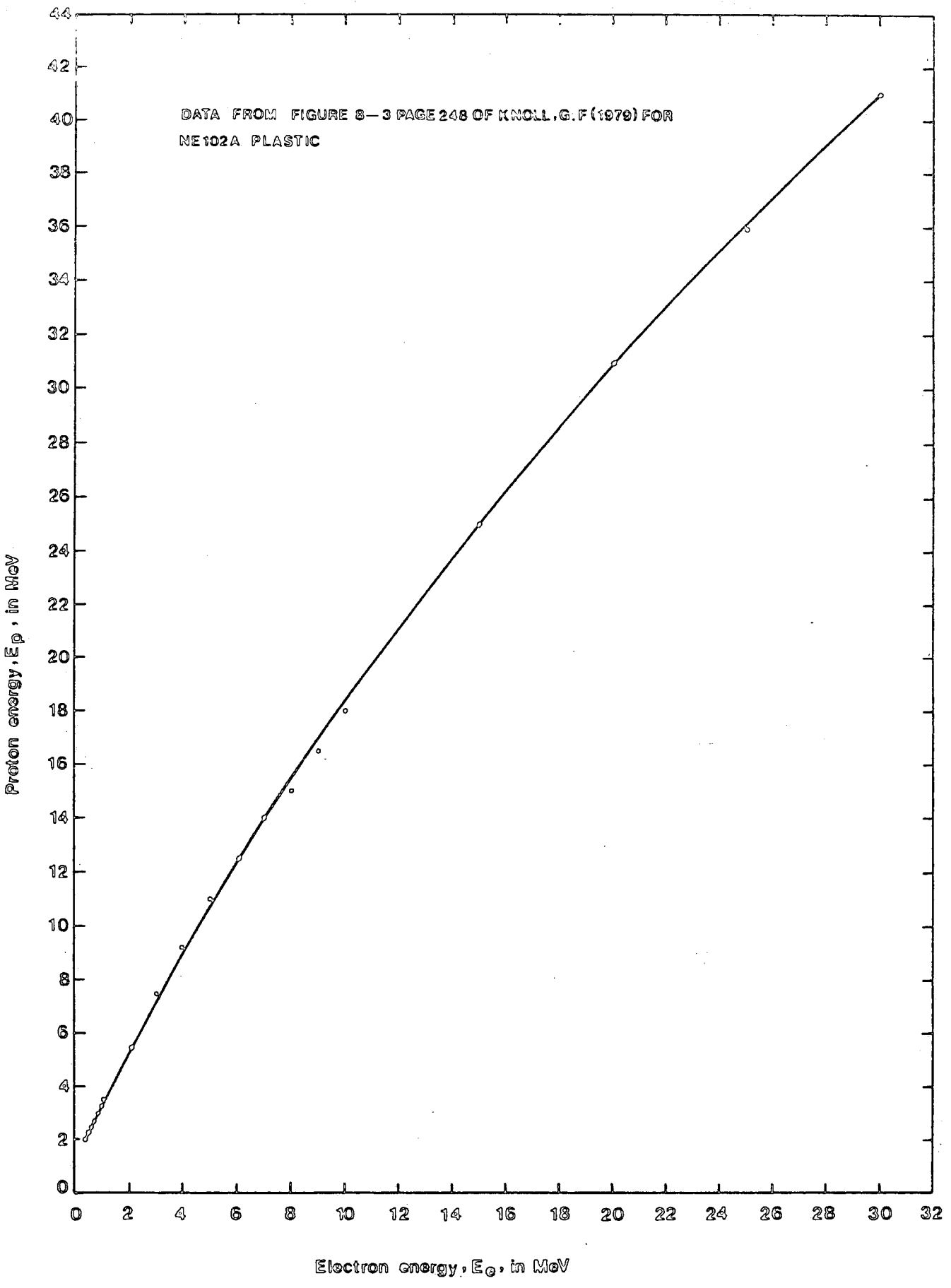

Figure 6.24 The curve is the locus of corresponding electron and proton energies that produce the same amount of light output from the phosphor. (Data from Figure 8-3 page 248 of Knoll (1979)).

Energy range in MeV	$\bar{E}$ in MeV	ΔE in MeV	Excess events $N_2(270-500) - N_1(30-260) = \Delta N$	Differential rate $= \frac{\Delta N}{\Delta E}$ per MeV
2.70 - 4.00	3.35	1.30	-117 ± 67	-90 ± 52
4.00 - 5.20	4.60	1.20	495 ± 51	413 ± 43
5.20 - 11.20	8.20	6.00	555 ± 35	93 ± 6
11.20 - 18.40	14.80	7.20	128 ± 20	18 ± 3
18.40 - 41.00	29.70	22.60	5 ± 15	0.22 ± 0.66

Table 6.21 Use of the basic data in Table 6.19 to calculate the differential energy distribution of all delayed events assuming that the measured pulse heights are due to low energy protons (presumably knocked on by low energy incident neutrons).

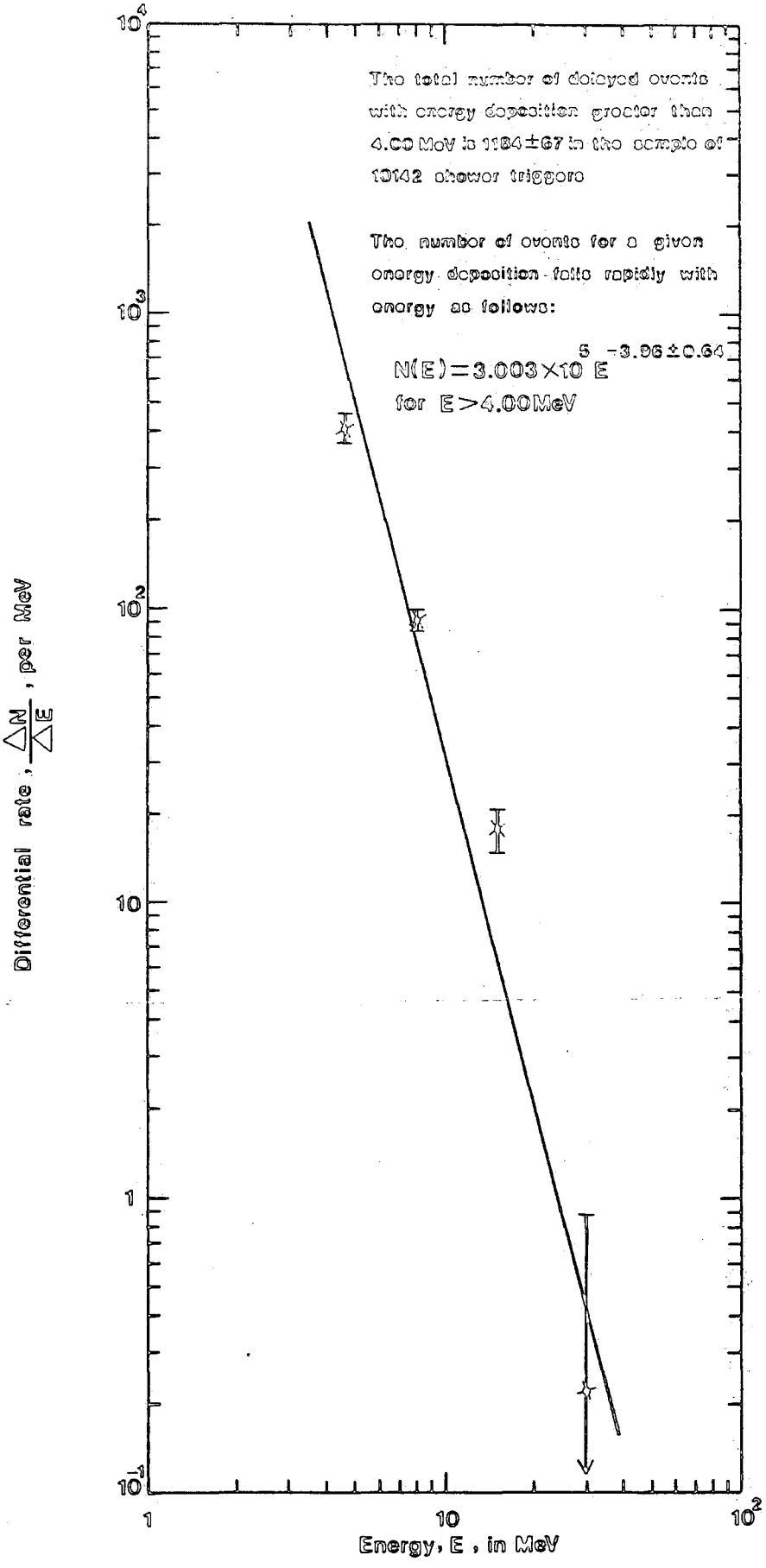

Figure 6.25 The differential energy distribution of all delayed events assuming that the measured pulse heights are produced by low energy protons knocked on by incident low energy neutrons.

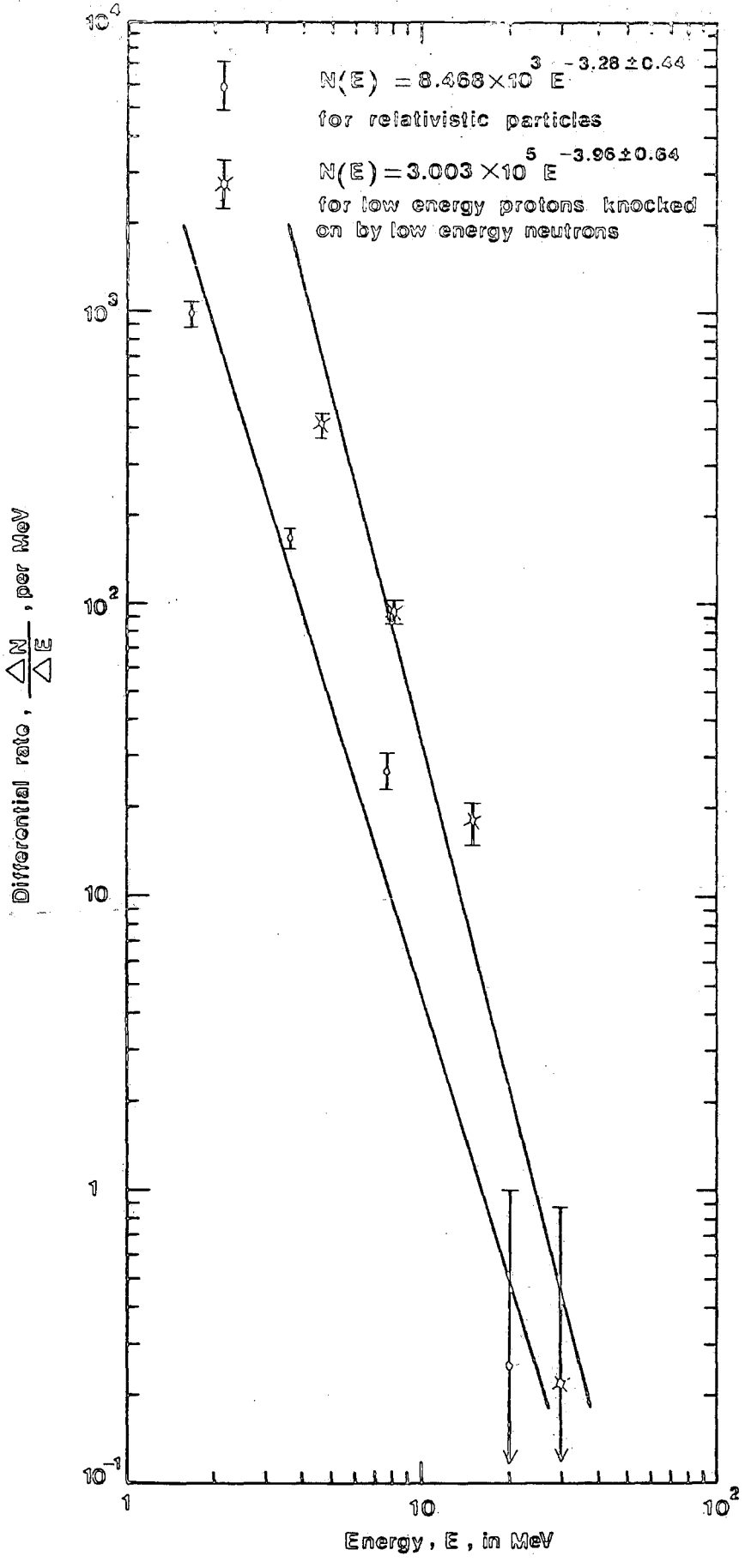

Figure 6.26 Comparison of the differential energy distributions of all delayed events assuming that the measured pulse heights are produced either by relativistic particles (denoted by o) or by low energy protons knocked on by incident low energy neutrons (denoted by X) respectively.

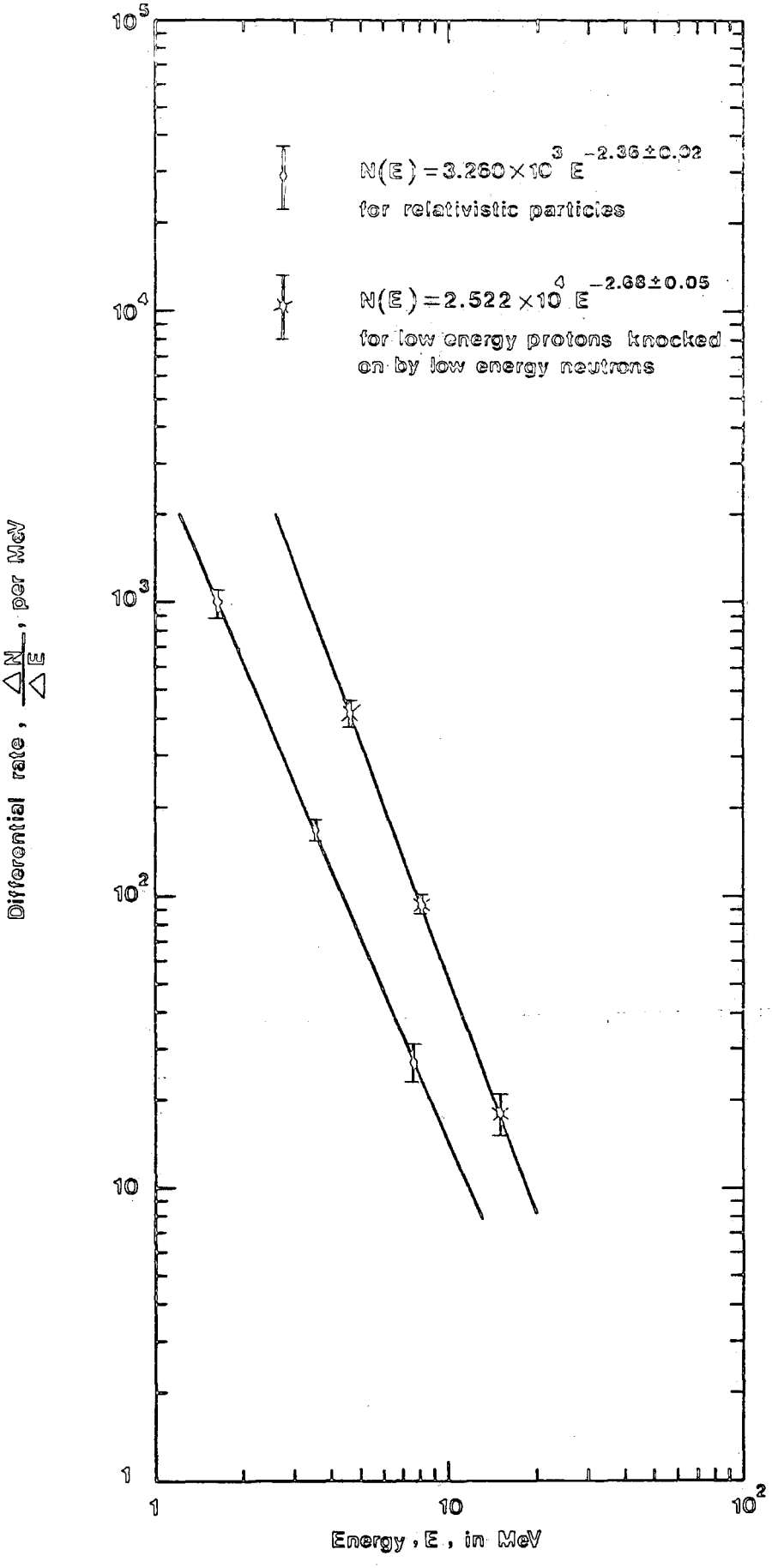

Figure 6.27 Comparison of the differential energy distributions of all delayed events assuming that the measured pulse heights are produced either by relativistic particles (denoted by o) or by low energy protons knocked on by incident low energy neutrons (denoted by X) respectively. The fitted power law is made only to the first three measured points.

in the scintillation counter phosphor then the knock-on protons predominantly have kinetic energies in the range 4.0 – 11.2MeV. Considering a representative proton energy of 7MeV it is likely that this would be generated by a neutron incident on the phosphor of kinetic energy 14MeV assuming the knock – on protons are produced by neutron – proton elastic scattering. Such a neutron has a velocity β given by:

$$K.E = \frac{1}{2} m_o v^2 = \frac{1}{2} m_o c^2 . \beta^2$$

$$14 = \frac{1}{2} 938 . \beta^2$$

$$\beta = 0.17$$

To produce a delay of 100 μs the required production height of 14MeV neutrons above the detector is:

$$0.17 . 3.10^8 . 100 . 10^{-6} \text{ metres} = 5.1 \text{ Km}$$

This is a reasonable value and indicates that all the delayed events possibly can be explained by the above mechanism.

6.12) SUMMARY

Since there is no comprehensive theory for the various properties of tachyonic objects in any type of experiment some initial assumptions are essential. In the extensive air shower method as used in the present work, it is assumed that tachyons are probably produced as particle – antiparticle pairs in interactions of the sort that occur when cosmic ray primary protons or nuclei of energy $\gg 10^{15}$ eV collide with a nucleus of air in the upper atmosphere. Furthermore, it is assumed that a tachyon will lose energy in a detection scintillator and give rise to photons or will be detectable by the production of

secondaries which can be detected.

In the present experiment, a total number of 10,142 extensive air shower triggers with local electron density $\geq 25 m^{-2}$ were recorded in a sensitive time of 839hr 46min 40sec. The time distribution of recorded pulse heights occurring in the 260 μs before and the 230μs after the arrival of the air shower front were measured for six different ranges of energy deposition in the tachyon detection scintillator of thickness 5cm. Analysis shows that the pulses recorded in the 260 μs before the arrival of the extensive air shower front pulse are due to thermal electrons emitted from the tachyon detector photomultiplier photocathodes and due to the passage of muons through the detector which are unassociated with the extensive air shower producing the master trigger for the experiment. No evidence is found for a finite flux of tachyons in this time domain.

Similar pulses are observed in the 230 μs time domain after the arrival of a shower front but also there is a finite flux of delayed ionizing events. The most likely explanation of the delayed events is that they are produced by low energy neutrons generated by hadrons in the atmospheric cascade interacting with air nuclei. The neutrons subsequently interact in the detector phosphor material and produce low energy knock on protons.

CHAPTER SEVEN

SUMMARY AND CONCLUSION

The work described in this thesis has been concerned mainly with the development of large area scintillation counters suitable for use in cosmic ray experiments and subsequently their use in an experiment to search for tachyons in the sea level cosmic radiation. The achievements attained and the conclusions reach will be discussed in turn.

SCINTILLATION COUNTER DEVELOPMENT

The type of scintillation counter described in Chapter four (of which nine were subsequently constructed) was found to be convenient to use from the point of view that it gives a single particle peak, well resolved from the noise, when its response to the global cosmic ray flux is recorded on a pulse height analyser. This is a considerable improvement on the detectors originally used in the Durham laboratory as all these had to be calibrated using a subsidiary cosmic ray telescope.

TACHYON EXPERIMENT

Two of the scintillation counters just described were used in two-fold coincidence to select extensive air showers with local electron density $\geqslant 25 m^{-2}$ in the tachyon experiment. In the tachyon experiment the 265 μs time period before and the 235 μs after the arrival of an extensive shower front was studied for 10,142 shower triggers. No evidence is found for a

finite flux of tachyons but a significant number of delayed ionizing events is observed. The most likely interpretation of these events is that they are produced by low energy neutrons interacting in the tachyon detector phosphor, the neutrons originating from the interaction of hadrons with air nuclei in the atmospheric hadron cascade.

APPENDICES

APPENDIX A

DATABIN PROGRAM

APPENDIX B

LIGHT EMITTING DIODES (L.E.D)

APPENDIX C

CHARACTERISTICS AND PROPERTIES OF FLASH TUBES AND MODIFICATIONS TO THE FLASH TUBE CHAMBER

APPENDIX D

TIME SEPARATION PROGRAM

APPENDIX A

DATABIN PROGRAM

The 35mm photographic film obtained in the tachyon experiment was analysed by using a photographic enlarger. The enlarged oscilloscope record of each event was traced on paper so as to secure a permanent record. The occurrence time (which was measured from the start of the 500 μs oscilloscope sweep) and pulse height of each pulse occurring on the trace was measured. Initially, the basic information for each event was:

a) The time and date that the event occurred.

b) Pairs of values of occurrence time and pulse height.

The problem in analysing the data was to determine the occurrence time distribution for pulses in a given range of pulse height in a given range of occurrence time. Namely, pre-shower front pulses $t<265$ μs , shower front pulses $t=265$ μs and post-shower front pulses $t>265$ μs. To obtain this information the "DATABIN" program in conjunction with a Commodore PET computer (CBM model 4032) was used. The program serves a dual purpose as it will:

a) Store input information on magnetic tape in a series of files to be specified by the user.

b) Read data from the files , histogram it as requested and display the result.

The data from the tachyon experiment (i.e; tachyon data and background data) was stored in discrete files on magnetic tape as a series of occurrence time , pulse height pairs. Then, the

histograms and tables presented in Chapter six were obtained using the program analysis routine. As an example, to obtain the pulse height distribution of the pre and post shower front pulses, the "DATABIN" program was run twice and requirements were set to:

Maximum time = 530 μs	Maximum time = 530 μs
Number of time bins = 2	Number of time bins = 2
Maximum pulse height = 31.5 mV	Maximum pulse height = 1455 mV
Number of pulse height bins = 15	Number of pulse height bins = 29

Also to acquire the pulse height distribution of shower front pulses which all occur at the same time of 265μs, the "DATABIN" program was run twice and the requirements were set to:

Maximum time = 265 μs	Maximum time = 265 μs
Number of time bins = 1	Number of time bins = 1
Maximum pulse heigh = 31.5 mV	Maximum pulse height = 1455 mV
Number of pulse height bins = 15	Number of pulse height bins = 29

DATABIN PROGRAM

```
READY.

 10 REM TACHYON DATA-BINNING PROGRAM
 20 DIMT(255),H(255),C(99,50)
 21 INPUT"MAX TIME ";MT
 22 INPUT"MAX HEIGHT";MH
 23 INPUT"# OF TIME BINS (MAX IS 100)";NT
 24 INPUT"# OF HEIGHT BINS (MAX IS 50)";NH
 25 IFNT>100ORNH>100THENGOTO23
 30 PRINT"WHAT OPTION IS REQUIRED?"
 40 PRINT:PRINT"  1  DATA FROM TAPE"
 50 PRINT"  2  DATA FROM KEYBOARD"
 60 PRINT:INPUT"OPTION #";OP
 70 IF OP<1 OR OP>2 THEN60
 80 INPUT"FILENAME FOR DATA INPUT/OUTPUT";F$
 90 IF OP=1 THEN 120
100 GOSUB300
110 GOTO130
120 GOSUB500
130 GOSUB800
140 STOP
150 END
300 REM KEYBOARD INPUT ROUTINE
310 PRINT"WIND TAPE TO A CLEAR AREA FOR LOADING"
320 PRINT"DATA":PRINT
330 K=1:E$=F$+STR$(K)
340 PRINT"INPUT TIME(MICROSECONDS),PULSE HEIGHT(MILLIVOLTS)"
350 PRINT"UPTO 256 VALUES PER FILE ALLOWED"
360 PRINT"IF THIS IS EXCEEDED A NEW FILE WILL BE STARTED"
370 PRINT"AT THE END OF DATA INPUT, ENTER 0,0"
380 FORI=0TO255
390 INPUTT(I),H(I)
400 IF T(I)> MT OR H(I)< 0 THEN 410
405 IFT(I)<0ORH(I)>MHTHEN410
406 GOTO420
410 PRINT"ERROR - REDO ENTRY":GOTO 390
420 IF H(I)=0 THEN 440
430 NEXT
440 NO=I
450 GOSUB700
451 OPEN1,1,1,E$
452 FORI=0TONO
453 PRINT#1,T(I)
454 PRINT#1,H(I)
455 NEXT
456 CLOSE1
460 IFI<255THEN490
470 PRINT"NEW FILE BEING STARTED, WAIT FOR PROMPT"
475 PRINT"BEFORE ENTERING FURTHER DATA"
480 K=K+1:E$=F$+STR$(K)
490 RETURN
500 REM TAPE INPUT ROUTINE
510 PRINT"WIND TAPE TO START OF DATA"
520 PRINT
540 PRINT:INPUT"HOW MANY FILES ARE REQUIRED";N
560 FORK=1TON
570 E$=F$+STR$(K)
580 PRINT"LOADING",E$
```

```
590 OPEN1,1,0,ES
600 FORI=0TO255
610 INPUT#1,T(I)
615 INPUT#1,H(I)
620 IFH(I)=0GOTO640
630 NEXT
640 NO=I
650 GOSUB700
660 NEXTK
670 RETURN
700 REM BINNING ROUTINE
710 FORI=0TONO-1
720 X=INT(T(I)/(MT/NT))
730 Y=INT(H(I)/(MH/NH))
735 IFX<0ORY<0THENPRINT"ERROR":STOP
740 IFX>NT  THENX=NT
750 IFY>NHTHENY=NH+1
760 C(X,Y)=C(X,Y)+1
770 NEXT
780 RETURN
800 REM OUTPUT ROUTINE
810 FORI=0TONT-1
815 XX=MT/NT:YY=MH/NH
820 PRINT"TIME RANGE IS"I*XX"-"I*XX+XX
830 PRINT:PRINT"HEIGHT RANGE":PRINT
840 FORJ=0TONH
845 IFJ<NH+1THEN850
846 PRINT">"J*YY TAB(20)C(I,J)
847 GOTO860
850 PRINTJ*YY "-"(J+1)*YY TAB(20)C(I,J)
851 IFJ=0THEN860
852 IFJ/14<>INT(J/14)THEN860
853 PRINT"PRESS ANY KEY TO CONTINUE"
854 GETA$:IFA$=""THEN854
860 NEXTJ
870 PRINT"PRESS ANY KEY TO CONTINUE"
880 GETA$:IF A$=""THEN880
890 NEXTI
900 RETURN
```

APPENDIX B

LIGHT EMITTING DIODES(L.E.D)

Small light emitting diodes based on GaAS that produce yellow , green and red light, are now readily available commercially and the use of pulsed light emitting diodes is the most convenient way of testing photomultiplier tubes.

Using a light tight box containing a light emitting diode and photomultiplier tube (see figure 4.2), the variation of photomultiplier output pulse height with the voltage applied to the tube can be rapidly measured. Moreover, using the same light emitting diode as a light source, the relative sensitivities of a number of photomultiplier tubes can be found and hence the voltage at which each should be operated to have the same sensitivity is determined. From a practical point of view, one needs to know how large and how wide the voltage and current pulse applied to the diode must be in order to generate a sufficient amount of light to be readily detected. These problems have been investigated for three different light emitting diodes (emitting yellow , green and red light) and the results are shown in figures B.1 , B.2 , B.3 , B.4 and B.5. It must be noted that all the measurements refer to the use of a Philips 53 AVP photomultiplier tube employed as a detector. From these figures, it is concluded that for photomultiplier tubes of this type (i.e; with an S11 photocathode response) light emitting diodes which produce yellow light are the most satisfactory to use.

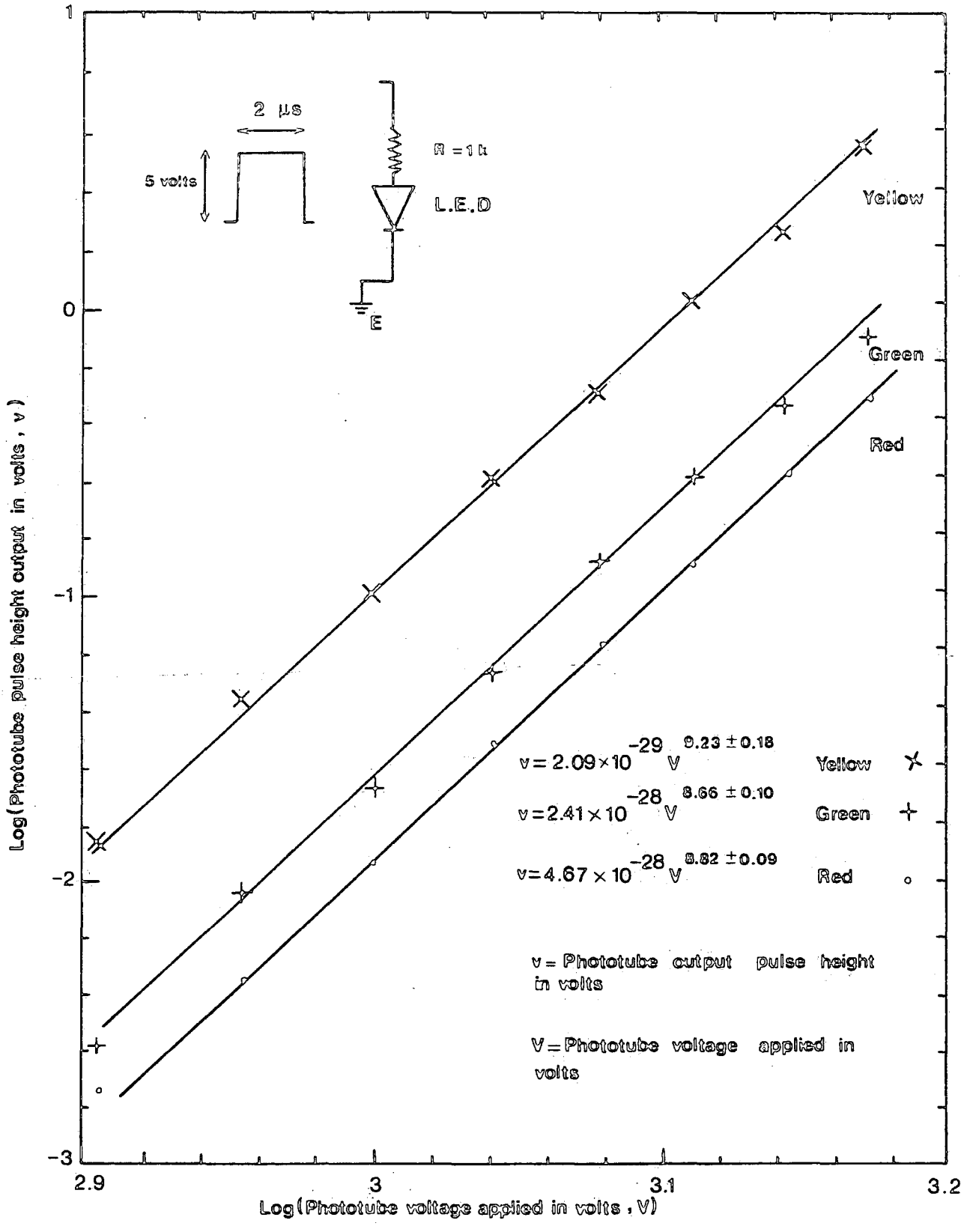

Figure B.1 Comparison of variation of photomultiplier tube output pulse height, v, with voltage applied, V, in volts. Different colour light emitting diodes used as light source.

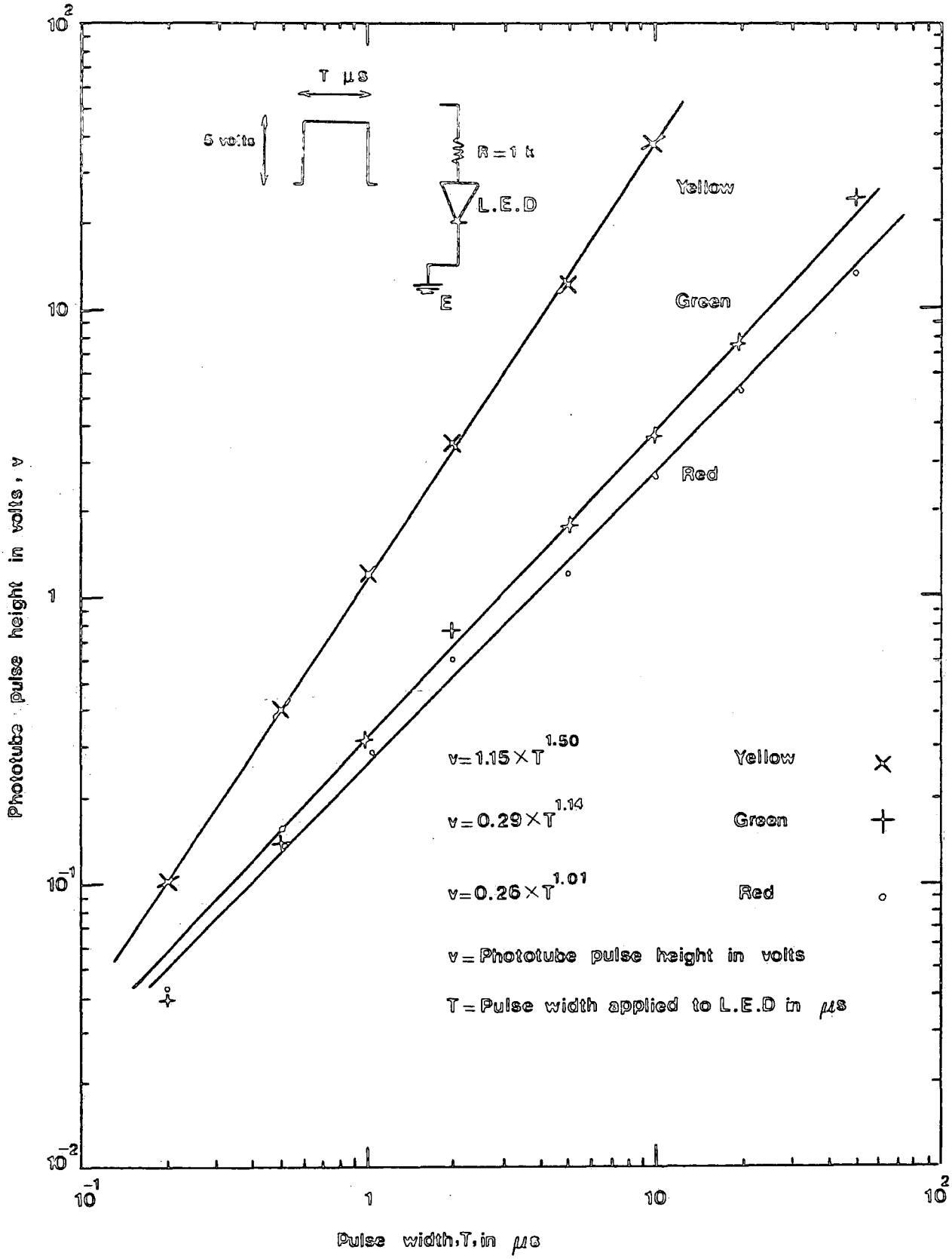

Figure B.2 Comparison of variation of photomultiplier tube pulse height, v, in volts with pulse width applied to light emitting diode, T, in microseconds for different colours.

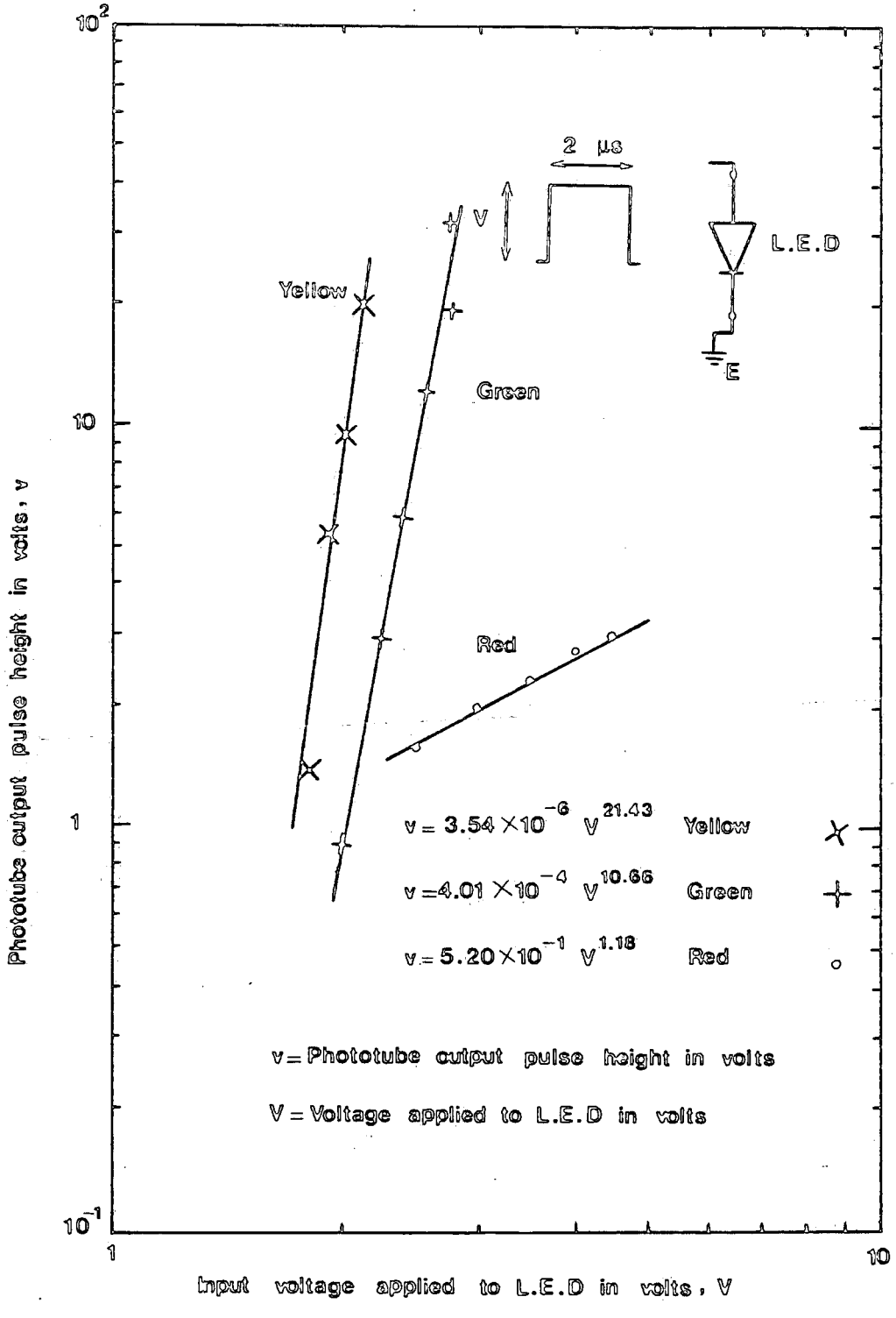

Figure B.3 Comparison of variation of photomultiplier tube output pulse height, v, in volts with voltage applied to light emitting diode, V, in volts for different colours.

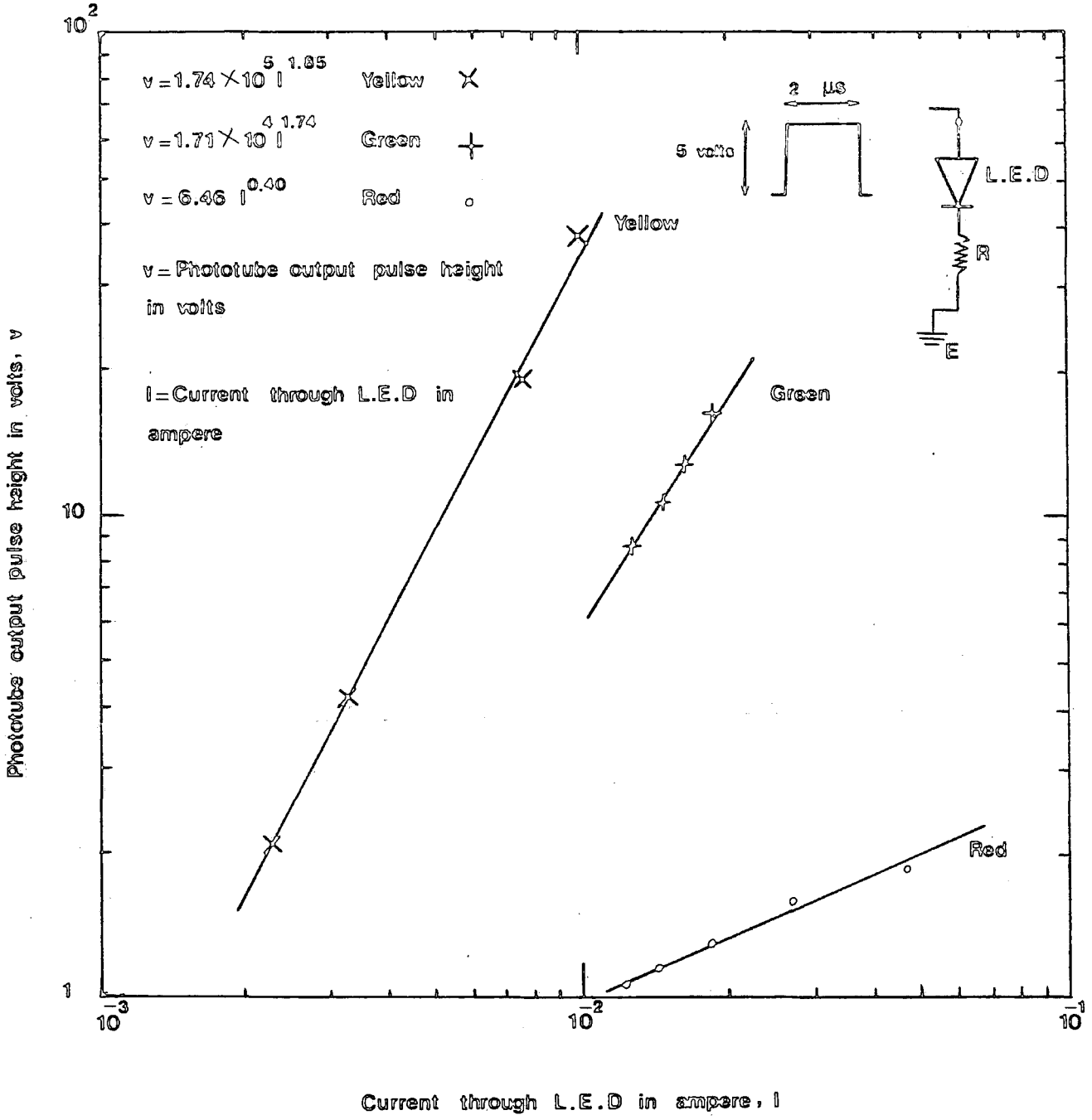

Figure B.4 Comparison of the variation of photomultiplier tube pulse height, v, in volts with current applied to the light emitting diode, I, in amperes for different colours.

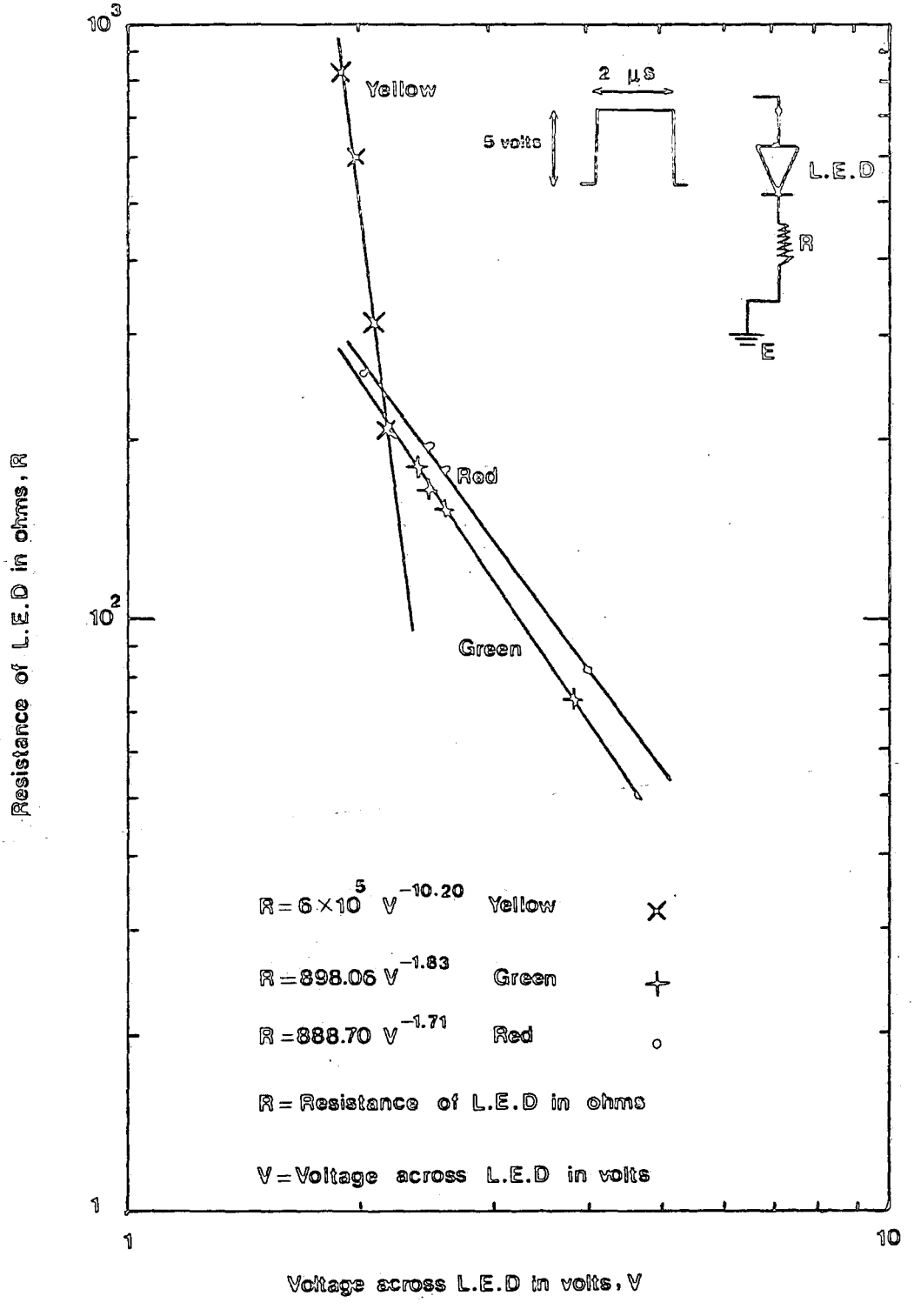

Figure B.5 Comparison of the variation of the resistance of the light emitting diode, R, in ohms with voltage applied across the light emitting diode, V, in volts for different colours.

APPENDIX C

CHARACTERISTICS AND PROPERTIES OF FLASH TUBES AND MODIFICATIONS TO THE FLASH TUBE CHAMBER

C.1) INTRODUCTION

The neon flash tube chamber is a large visual detector mainly used to observe the tracks of cosmic ray particles. Hadrons interacting in the lead or iron absorbers on top of the flash tube chamber (see figure 5.1), enable an investigation to be made of the energy and lateral distribution of them in extensive air showers. Unlike bubble chambers or spark chambers, which are often used in accelerator experiments, flash tubes, since their introduction in 1955 by Conversi and Gozzini have been used in many cosmic radiation experiments. One of the main reasons for this is that flash tubes are made of glass which is a relatively strong material, so they have a long life time and are an ideal detector for long experiments , and moreover their characteristics remain unchanged in a wide range of temperature, pressure and humidity conditions.

C.2) CHARACTERISTIC AND PROPERTIES OF FLASH TUBES

C.2.1) DISCHARGE MECHANISM

The flash tubes used in the flash tube chamber are cylindrical and 2 metres in length with mean external diameter 1.78cm and an internal diameter of 1.58cm. They are made of soda glass filled with neon gas (98%) and helium gas (2%) to a pressure of 60 cm of mercury. Each tube is covered with black

polythene sleeving to inhibit light passing to neighbouring tubes. The flash tubes are distributed in layers such that between every two layers of tubes is an aluminium electrode, 0.122cm thick and with area $2.95m^2$.

When a charged particle passes through a flash tube , it ionizes the gas and leaves a trial of positive ions , electrons and excited atoms along its track. On applying a high voltage pulse to the electrode plates the electrons left by the primary ionizing particle are accelerated towards the anode plate and gain sufficient energy to produce secondary electrons via collisions with gas atoms. The avalanches generated, produce luminous discharges which may be photographed. The problem of ionization and what causes the discharged has been discussed theoretically in detail by Lloyd (1960). He concluded that the positive ions and the secondary electrons released by the collision of metastable neon atoms are usually small in number and can be neglected as far as the basic discharge mechanism is concerned. Although the actual numbers will depend on gas composition and pressure, it is normal to expect up to 30 electrons to be produced in a flash tube by the passage of an ionizing particle through it.

C.2.2) EFFICIENCY

The most important and convenient parameter specifying the performance of a flash tube is its efficiency, or the probability that it will discharge after the passage of an ionizing particle through it. Because of inherent insensitive material present in a flash tube array, two efficiency

parameters have been defined. These are the internal efficiency , τ , which is defined as the probability of a tube flashing if an ionizing particle passes through the gas of the tube, and the layer efficiency , τ_L , which represents the probability of a tube flashing and hence registering the passage of an ionizing particle through a layer of tubes. The layer efficiencies of tubes are normally measured experimentally from which the internal efficiencies can be obtained by using the relation:

$$\tau = \tau_L \frac{r}{d} \qquad (C.1)$$

where r is the distance between flash tube centres and d is the internal diameter of the flash tubes. The efficiency of flash tubes is a function of many factors. Factors include high voltage pulse characteristics , such as rise time , width and delay, gas mixtures, temperature and spurious flashing rates.

C.2.3) SENSITIVE TIME, T_s

Another important flash tube parameter is sensitive time, T_s , which is defined as the time delay between the passage of an ionizing particle and the application of high electric field to the tube such that the internal efficiency of the flash tubes falls to 50%. Lloyd set up diffusion equations for the electrons produced in the tube and solved them. The solution gave the probability of a discharged occurring (i.e; internal efficiency), when a high voltage pulse is applied to the tube in a time T_s μs after the passage of a charged particle. He expressed it as a function of $\frac{D \cdot T_s}{a^2}$ and in terms

of a parameter apq , where D is the diffusion coefficient of thermal electrons , a is the internal radius of the tube , p is the probability that a single electron is capable of producing a flash when a high voltage pulse is applied and q is the probability per unit track length that the primary charged particle produces an electron – ion pair. The only parameter dependent on the charge of the particle is q and is related to the ionization loss of the charged particle in the gas which is a function of the square of the electric charge. Using the calculations of Lloyd , the internal efficiency of the flash tube as a function of time delay for different values of the apq parameter has been calculated and are shown in figure C.1. It is seen that the efficiency of the flash tube falls off as the time delay increases. This is due to the fact that the initial number of electrons in the gas will decrease due to diffusion to the glass tube walls where they stick. It is clear from the work of Lloyd that the efficiency of flash tubes depends strongly on the charge of the primary ionizing particle. In other words; with a fixed delay time , the higher the charge of a passing particle the larger the number of tubes on a particle trajectory will flash.

C.3) MODIFICATIONS TO THE FLASH TUBE CHAMBER

In the design of the previous chamber , all neon flash tubes were mounted with their axes parallel to one another. Obviously with this geometry , only projected spatial information in one view was available and no visual information was accessible concerning the spatial position of tracks in the

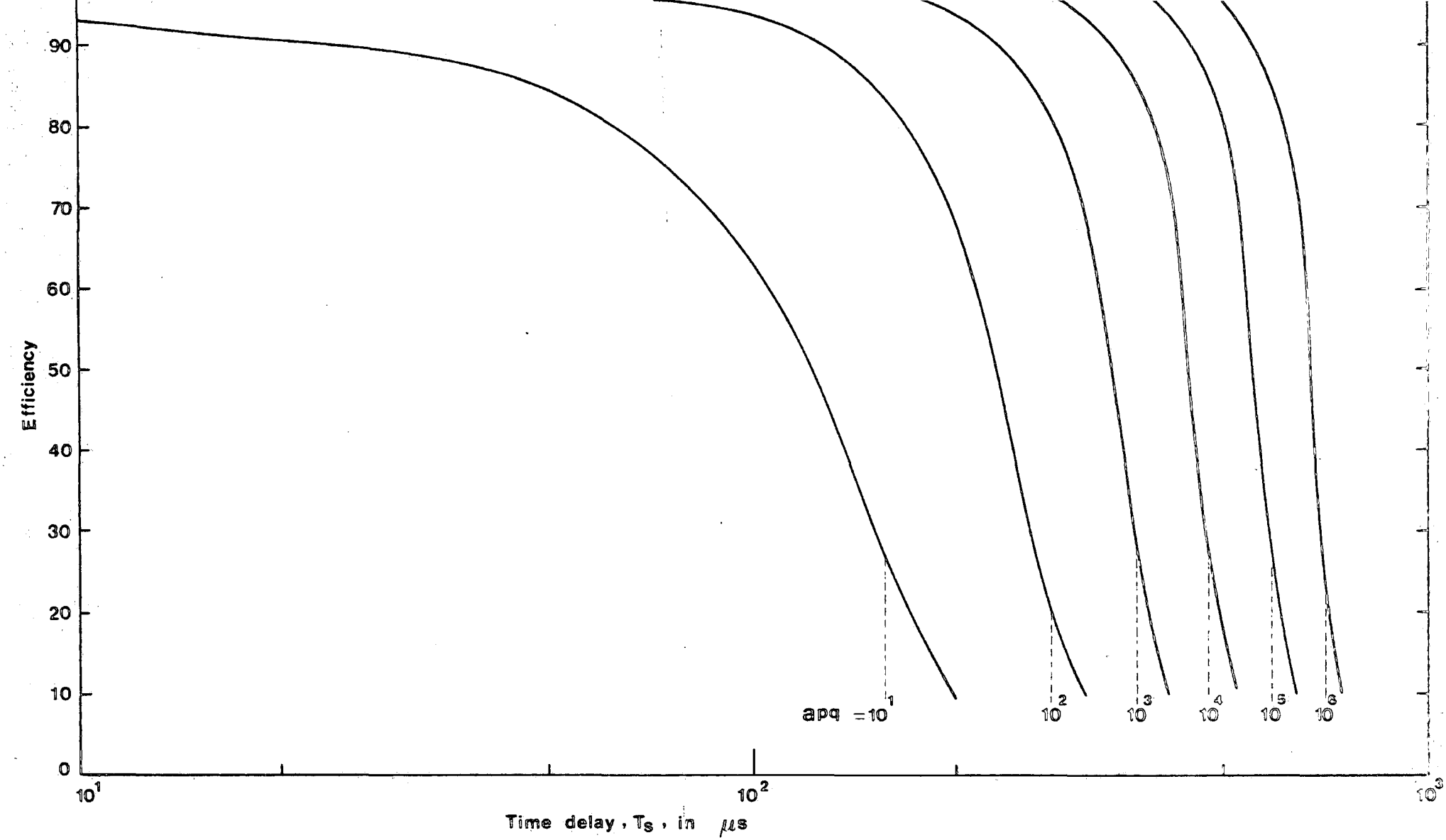

Figure C.1 Predicted variation between the internal efficiency of the flash tubes and the high voltage pulse time delay for different values of the parameter apq. apq=10 gives a good fit to the measured efficiency versus time delay curve for relativistic muons traversing the chamber.

"back plane".

A scale diagram of the present neon flash tube chamber is shown in figure C.2. A total number of 11,825 neon flash tubes are used in the chamber and their characteristics were explained in section C.2. As described in chapter five, the two extensive air shower selection scintillators A and B used in the tachyon experiment were mounted above the flash tube chamber while the tachyon detection scintillator C was inserted inside the chamber. The shielding materials of the chamber are the 15cm of lead situated on the top which absorb the soft components (i.e; electrons and photons) of extensive air showers and let more penetrating particles (mainly; muons) to be clearly studied in the chamber and also act as a target for nuclear interactions of hadrons. The 15cm of iron absorber allows electromagnetic bursts to be investigated in the chamber. The improvement made was to stack the neon flash tubes in successive double layers of tubes such that the tube axes in successive double layers were orthogonal to one another. Thus a penetrating particle traversing the chamber is expected to produce a track as illustrated in figure C.2. Figure C.3 shows the mirror system used to simultaneously photograph the front and side views of the chamber so that the views appear side by side on 35mm film and figure C.4 shows a photograph which was taken in this way. During the time that the experiment runs , the chamber must remain in the dark and photographs are taken by a camera without a shutter. This means that the camera is continuously sensitive to an event and it winds on automatically by one frame after each event. Because of high

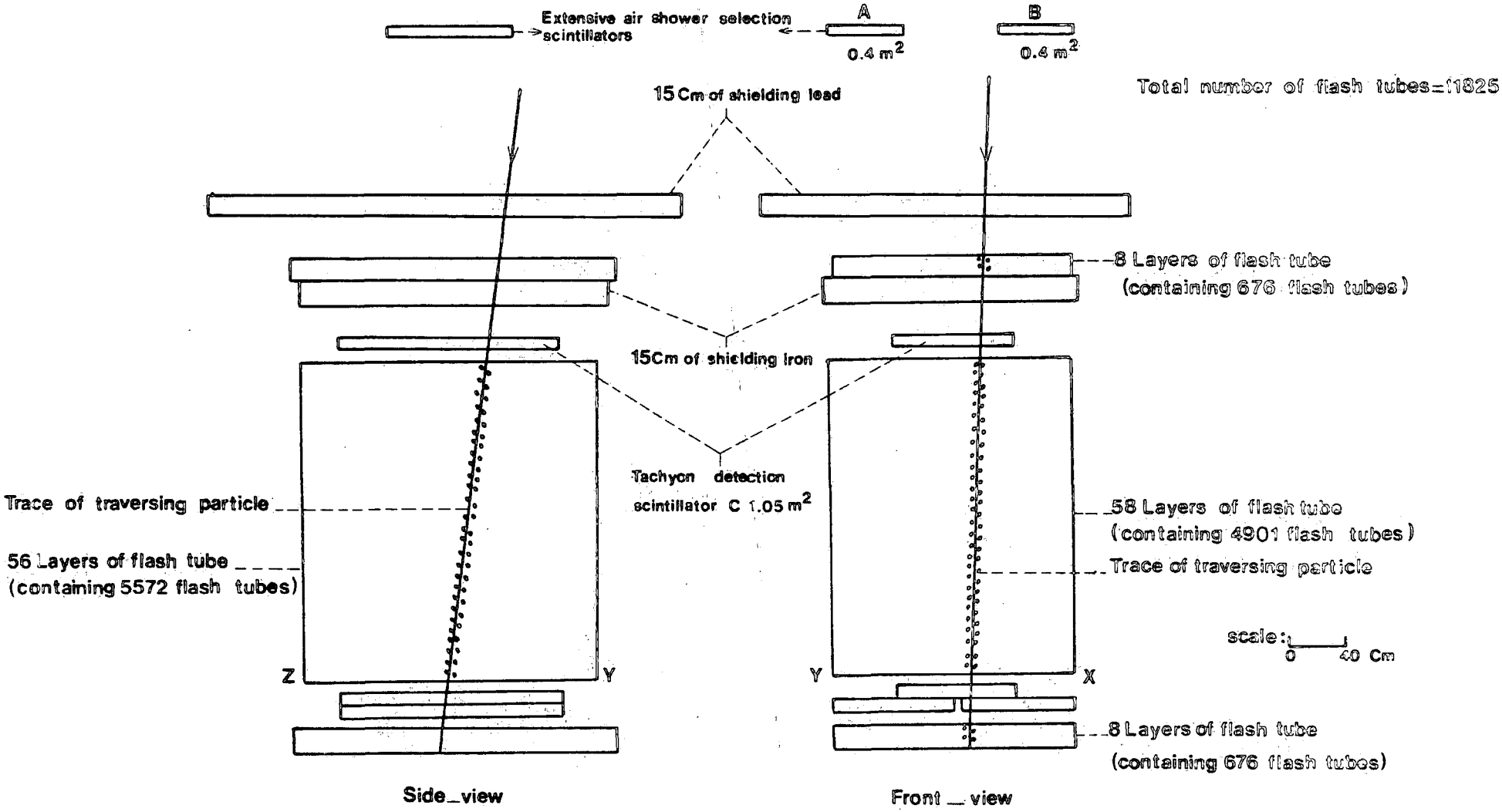

Figure C.2 Scale diagram of the improved flash tube chamber. A and B are the scintillation counters used to select extensive air shower and C is the tachyon detection scintillator. The track of a single penetrating charged particle (mainly muons) through the chamber is added to clarify the positions of the flash tubes.

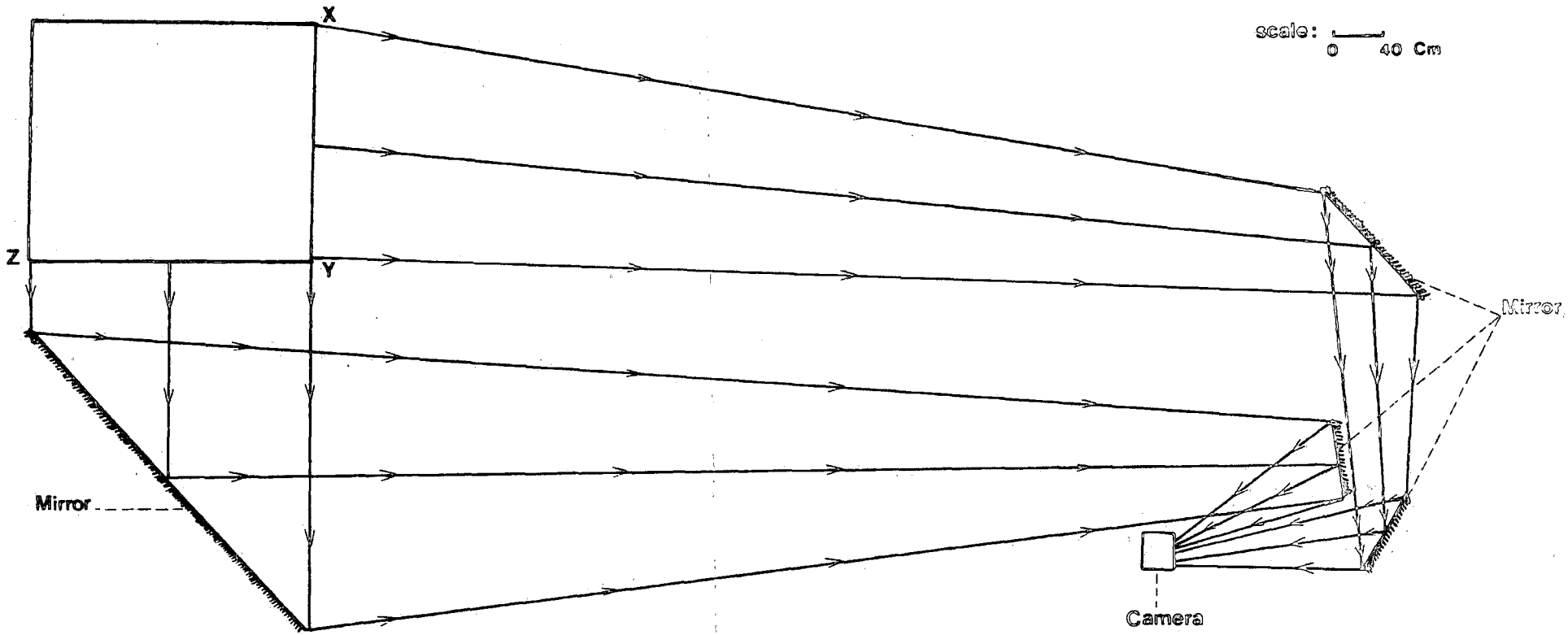

Figure C.3 The mirror system used to simultaneously photograph the front and side views of the flash tube chamber shown in Figure C.2. The points X, Y and Z in this figure (which is a plan view) corresponds to the points marked X, Y and Z in Figure C.2.

voltage pick up problems, the chamber was not operated during the exploratory tachyon experiment. To operate it the chamber has to be pulsed with a high voltage pulse (≃10kv lasting 10μs) while in the tachyon experiment pulses as small as 0.5mv were measured. If the pick up problems can be solved then an obvious improvement to the tachyon experiment would be to operate in conjunction with the flash tube chamber.

APPENDIX D

TIME SEPARATION PROGRAM

```
READY.

 1 PRINT"□"
 3 INPUT "INTIAL TIME ";T$
 4 GOTO 20
 5 PRINT "□"
 6 PRINT "PRIVIUS TIME = ";T$
 7 PRINT:PRINT
 10 INPUT" TIME ";T$
 15 IF T$ ="END" GOTO 200
 20 A$=LEFT$(T$,2)
 30 B$=MID$(T$,3,2)
 40 C$=MID$(T$,5,2)
 50 A=VAL(A$)
 51 B=VAL(B$)
 52 C=VAL(C$)
 70 A2=A*60*60
 72 B2=B*60
 74 T=A2+B2+C
 80 D=T-T9
 81 PRINT:PRINT:PRINT
 84 X(N)=D
 85 IF N<>0 THEN PRINT "DELTA =";D;" SEC'S"
 86 T9=T
 87 N=N+1
 90 GET A$: IF A$="" THEN GOTO 90
 100 GOTO 5
 200 B=N-1
 210 PRINT "□"
 215 PRINT "DO YOU WANT "
 220 PRINT "          [1] SEE DELTA"
 230 PRINT "          [2] EDIT "
 240 PRINT "          [3] SAVE IT"
 250 INPUT "          ";V
 260 ON V GOTO 300,400,500
 300 PRINT "□"
 310 FOR G=1 TO B
 320 PRINT G;"___";X(G)
 330 S=G/10 : S%=G/10
 340 IF S<>S% GOTO360
 350 GET A$: IF A$="" GOTO 350
 360 NEXT G
 370 PRINT "**********"
 380 GET A$: IF A$ <>"" GOTO 380
 390 GOTO 210
 400 PRINT "□"
 410 PRINT " WRITE THE ELEMENT NUMBER"
 415 INPUT J
 420 PRINT X(J)
 430 PRINT " WRITE THE CORRECTION"
 440 INPUT X(J)
 450 GOTO 210
 500 INPUT " FILE NAME";NF$
 510 OPEN 5,1,1,NF$
 520 FOR I=1 TO B
 530 PRINT#5,X(I)
 540 NEXT I
 545 CLOSE 5
 550 PRINT " DATA SAVED"
 560 GET A$: IF A$="" GOTO 560
 570 GOTO 210
```

REFERENCES

(PICCR=Proceedings of the International Conference on Cosmic Rays)

Aarons, M.E., et al (1968), Phys.Rev., 173, 1622.

Aguilar-Benitez, M., et al (1982), Phys.Lett., 111B, (April).

Allen, J.S., (1953), Los Alamos Sci.Lab.Rept., LA-1613.

Alvager, T., et al (1968), Phys.Rev., 171, 1357.

Alvager, T., et al (1969), Phys.Rev., 183, 1132.

Andreyev, Yu.M., et al (1979), PICCR, Kyoto, 10, 184.

Antippa, A.F., et al (1971), Phys.Rev., D4, 2198.

Antippa, A.F. (1972), Nuov.Cim., 10A, 389.

Antippa, A.F., et al (1973), Phys.Rev., D8, 2352.

Ashton, F., et al (1965), PICCR, London, 2, 1079.

Ashton, F., et al (1970), Acta.Phys.Hung., 29, Suppl., 3, 29.

Ashton, F., et al (1977), PICCR, Plovdiv, 7, 370.

Ashton, F., et al (1979), PICCR, Kyoto, 13, 238.

Baltay, C., et al (1970), Phys.Rev., D1, 759.

Bartlett, D.F., et al (1972), Phys.Rev., D6, 1817.

Bartlett, D.F., et al (1978), Phys.Rev., D18, 2253.

Bassi, P., et al (1953), Phys.Rev., 92, 441.

Bell, C.J., et al (1974), J.Phys.A:Math.Nucli.Gen., 7, 990.

Bhabha, H.J. (1936), Proc.Roy.Soc., 154A, 195.

Bhabha, H.J. (1938), Proc.Roy.Soc., 164A, 257.

Bhat, P.N., et al (1979), J.Phys.G., 5, L13.

Bilaniuk, O.M.P., et al (1962), Am.J.Phys., 30, 718.

Birks, J.B. (1951), Proc.Phys.Soc., 64A, 874.

Birks, J.B. (1964), "The Theory and Practice of Scintillation Counting", Pergamon Press, Oxford.

Blandford, R.D., et al (1977), Nature, 267, 211.

Bohr, N., (1915), Phil.Mag., 30, 581.

Bothe, W. and Kolhorster, W. (1928), Naturwiss, 16, 1044.

Caro, D.E., et al (1950), Austral.J.Sci.Res., A4, 16.

Clay, J., (1927), Proc.Roy.Acad.Amsterdam, 30, 1115.

Clay, R.W. and Crouch, P.C. (1974), Nature, 248, 28.

Cohen, M.H., et al (1977), Nature, 268, 405.

Compton, A.H. (1933), Phys.Rev., 43, 387.

Corben, H.C., et al (1939), Proc.Camb.Phil.Soc., 35, 463.

Crispin, A., et al (1964), Proc.Phys.Soc., 83, 1051.

Csonka, P.L. (1970), Nucl.Phys., B21, 436.

Danburg, J.S., et al (1971), Phys.Rev., D4, 53.

Danburg, J.S., et al (1972), Phys.Rev., D5, 1575.

Dattoli, G., et al (1978), Lett.Nuov.Cim., 22, 65.

Davison, P.W. (1952), Nucleonics, 19, 33.

Dhar, J., et al (1968), Phys.Rev., 174, 1808.

Dirac, P.A.M. (1931), Proc.Roy.Soc., A133, 60.

Dirac, P.A.M. (1948), Phys.Rev., 74, 817.

Earl, J.A. (1961), Phys.Rev.Lett., 6, 125.

Edge, D.M., et al (1973), J.Phys.A:Math.Nucl.Gen, 6 1612.

Elster, J. and Geitel, H. (1899), Physik., Z, 1, 11.

Emery, M.W., et al (1975), PICCR, Munich, 7, 2480.

Engstrom, R.W., et al (1952), Nucleonics, 10, 58.

Ettinger, G.M. (1955), Rev.Sci.Instr., 26, 763.

Everett, A.E. (1976), Phys.Rev., D13, 795.

Ey, C.M. and Hurst, C.A. (1977), Nuov.Cim., 39B, 76.

Fegan, D.J., et al (1975), PICCR, Munich, 7, 2480.

Fegan, D.J. (1981), PICCR, Paris, 5, 55.

Feinberg, G. (1967), Phys.Rev., 159, 1089.

Feinberg, E.L. (1972), Phys.Rep., 5, 237.

Feinberg, G. (1978), Phys.Rev., D17, 1651.

Feldman, L.M. (1974), Am.J.Phys., 42, 179.

Fermi, E. (1940), Phys.Rev., 57, 445.

Feynman, R.P. (1949), Phys.Rev., 76, 749.

Filosofo, I., et al (1954), Nuov.Cim., 12, 809.

Fowler, G.N., et al (1961), Handbuch der Physik, 46, 272.

Fowler, P.H., et al (1967), Proc.Roy.Soc., A301, 39.

Giacconi, R., et al (1962), Phys.Rev.Lett., 9, 439.

Gluck, M. (1970), Nuov.Cim., 67A, 658.

Gockel, A. (1911), Physik., Z, 12, 295.

Goldoni, R. (1972), Lett.Nuov.Cim., 5, 495.

Goldoni, R. (1973), Il Nuov.Cim., 14A, 501.

Gooding, T.J., et al (1960), Nucl.Instr.and Meth., 7, 189.

Greisen, K. (1942), Phys.Rev., 61, 212.

Greisen, K. (1960), Ann.Rev.Nucl.phys., 10, 63.

Greisen, K. (1965), PICCR, London, 9, 609.

Hazen, W.E., et al (1975), Nucl.Phys., B96, 401.

Hess, V.F (1912) Physik., Z, 13, 1084.

Hillas, A.M. (1981), PICCR, Paris, 6, 244.

Hopkins, J.I. (1951), Rev.Sci.Instr., 22, 29.

Jelly, J.V. (1958), "Cerenkov Radiation", published by Pergamon Press page 279.

Johnson, T.H. (1938), Rev.Mod.Phys., 10, 193.

Juliusson, E. (1975), PICCR, Munich, 8, 2689.

Karakula, S., et al (1974), J.Phys.A:Math.Nucl.Gen., 7, 437.

Kempa, J., et al (1974), J.Phys., A, 7, 1213.

Knoll, G.F. (1979), "Radiation Detection and Measurement", published by John Wiley and Sons, page 248.

Kraushaar, W., et al (1968), A.P.J., 153, L203.

Landau, L. (1944), J.Phys.U.S.S.R., 8, 201.

Lemke, H. (1975), Nuov.Cim., 27A, 141.

Lemke, H. (1976), Nuov.Cim., 32A, 169.

Lemke, H. (1976a), Nuov.Cim., 35A, 181.

Lemke, H. (1976b), Lett.Nuov.Cim., 17, 209.

Lloyd, J.L. (1960), Proc.Phys.Soc., 75, 387.

Maccabee, H.D., et al (1968), Phys.Rev., 165, 469.

Marchildon, L., et al (1979), Il Nuov.Cim., 53B, 253.

Mariwalla, K.H. (1969), Am.J.Phys., 37, 1281.

Meyer, P., et al (1974), Phys.Today, 27, 23.

Mignani, R., et al (1972), Lett.Nuov.Cim., 4, 144.

Mignani, R., et al (1973), Lett.Nuov.Cim., 7, 388.

Mignani, R., et al (1973a), Lett.Nuov.Cim., 8, 110.

Mignani, R., et al (1973b), Nuov.Cim., 14A, 169.

Mignani, R., et al (1973c), Lett.Nuov.Cim., 8, 780.

Mignani, R., et al (1974), Lett.Nuov.Cim., 9, 362.

Mignani, R., et al (1974a), Lett.Nuov.Cim., 9, 367.

Mignani, R., et al (1975), Nuov.Cim., 30A, 533.

Mignani, R., et al (1976), Lett.Nuov.Cim., 16, 449.

Millikan, R.A. and Bowen, I.S. (1936), Phys.Rev., 43, 695.

Moller, C. (1932), Annalen d.Phys., 14, 531.

Moroney, J.R., et al (1954), Austral.J.Phys., 7, 423.

Mrowczynski, St. (1983), Lett.Nuov.Cim., 38, 247.

Narlikar, J.V., et al (1976), Mon.Not.R.Astron.Soc., 175, 105.

Negi, O.P.S. and Rajput, B.S. (1982), J.Math.Phys., 23, 1964.

Newton, R.G. (1967), Phys.Rev., 162, 1274.

Newton, R.G. (1970), Science, 167, 1569.

Nuclear Enterprises Catalogue, 1980, February

Oppenheimer, J.R., et al (1940), Phys.Rev., 57, 75.

Owen, B.G., et al (1951), Proc.Phys.Soc., London, A64, 417.

Parker, L. (1969), Phys.Rev., 188, 2287.

Pathak, K.M., et al (1981), PICCR, Paris, 7, 11.

Pavlopoulus, T.G. (1967), Phys.Rev., 159, 1106.

Prescott, J.R. (1975), PICCR, Munich, 7, 2474.

Raffle, J.F., et al (1952), Proc.Phys.Soc., 65B, 320.

Ramana Murthy, P.V. (1971), Lett.Nuov.Cim., 1, 908.

Robinett, L. (1978), Phys.Rev., D18, 3610.

Rodgers, A.L. (1957), Ph.D. Thesis, Manchester University.

Rossi, B. (1952), "High-Energy Particles", Prentice-Hall Physics Series.

Ryan, M.J., et al (1972), Phys.Rev.Lett., 28, 985.

Schroer, B. (1971), Phys.Rev., D3, 1764.

Schwartz, C. (1982), Phys.Rev., D25, 356.

Smith, A.C. (1976), Ph.D. Thesis, Durham University.

Smith, G.R., et al (1977), Can.J.Phys., 55, 1280.

Srivastava, S.K. (1983), J.Math.Phys., 24, 996.

Srivastava, S.K. (1984), J.Math.Phys., 25, 693.

Sternheimer, R.M. (1952), Phys.Rev., 88, 851.

Sternheimer, R.M. (1953), Phys.Rev., 91, 256.

Sternheimer, R.M. (1956), Phys.Rev., 103, 511.

Sternheimer, R.M. (1966), Phys.Rev., 145, 247.

Sternheimer, R.M. (1967), Phys.Rev., 164, 349.

Symon, K.R. (1948), Ph.D. Thesis, Harvard University.

Tanaka, S. (1960), Progr.Theoret.Phys., 24, 171.

Terletskii, Ya.P. (1960), Soviet Physics, Doklady, 5, 782.

Van Allen, J.A., et al (1950), Phys.Rev., 78, 819, correction, 80, 116

Vavilov, P.V. (1957), J.Exp.Theoret.Phys., 5, 749.

Vysin, V. (1978), Lett.Nuov.Cim., 22, 76.

Walske, M.C. (1952), Phys.Rev., 88, 1283.

Walske, M.C. (1956), Phys.Rev., 101, 940.

Wilson, C.T.R. (1901), Proc.Roy.Soc., 68A, 151.

Wolfendale, A.W. (1963), "Cosmic Rays", published by George Newness Limited, London, page 142.

Wolfendale, A.W. (1973), "Cosmic Rays at Ground Level", published by the Institute of Physics., London.

Wright, G.T. (1953), Phys.Rev., 91, 1282.